Advances in Green Extraction and Isolation Methods

Dissertation

zur Erlangung des Doktorgrades der Naturwissenschaften (Dr. rer. nat.)

der Fakultät für Chemie und Pharmazie

der Universität Regensburg

vorgelegt von

Verena Huber

aus Stammham am Inn

2022

This doctoral thesis is based on the data collected between November 2019 and September 2022 at the Institute of Physical and Theoretical Chemistry, Faculty IV (Chemistry and Pharmacy), University of Regensburg, Germany, under the supervision of Prof. Dr. Werner Kunz.

Dissertation Submission: 04.10.2022

Dissertation Defense: 24.11.2022

Ph.D. Supervisor	Prof. Dr. Werner Kunz
Ph.D. Committee	
1st Chair	Prof. Dr. Werner Kunz
2nd Chair	Prof. Dr. Hubert Motschmann
3rd Chair	Prof. Dr. Ruth M. Gschwind
Committee Chairperson	Prof. Dr. Oliver Tepner

Acknowledgments

The realization of this work was made possible by the contributions and support of many people to whom I want to express my deepest gratitude.

At the very first, I want to express my warmest thankfulness to **Prof. Dr. Werner Kunz**, who gave me the opportunity and trust to work on this interesting topic at his working group. With his advice and support, I was able to learn a lot and got the chance to present my work to colleagues at various conferences.

Likewise, I want to thank **Prof. Dr. Hubert Motschmann** and **Prof. Dr. Ruth M. Gschwind**, the second and third referees, and **Prof. Dr. Oliver Tepner**, the committee chairman, for their time and valuable comments.

My deepest appreciation goes to my supervisor, and I dare say, friend **Dr. Didier Touraud**. Thank you for raising many precious points, for giving me an endless load of ideas and advice, for discussing and brainstorming, and for passing by my lab or office to simply chat, which never ceased to amuse the both of us.

I am also grateful to our secretaries **Rosi** and **Bianca**, to our **technicians**, to **Dr. Johnny Hioe**, and to **Prof. Dr. Rainer Müller**, who could always help me no matter the task. As well, I want to acknowledge **Prof. Dr. Heilmann** and his working group for allowing me to use their facilities and equipment. I also want to acknowledge **SKH GmbH**.

Additionally, I want to express my gratefulness to all my colleagues at our working group, especially **Dr. Pierre Degot**, who helped me shape my topic and taught me how to be a scientist, **Nadja Ulmann**, my awesome lab partner, and to my interns, especially **Laurie Muller** and **Michi Schmidt**, who conducted their master theses under my supervision, as well as **Kasia**, **Vanessa**, **Lea**, **Lena**, **Katharina**, **Lukas**, **Katharina**, and **Maximilian**.

Passing the time during my dissertation not only required academic support, but also the love and open ears of my beloved friends. I want to show them my sincere gratitude. A special thank you goes to my colleagues turned friends **Fadi**, **Manu** and **Lea**, with whom I spent not only my lunch breaks, destressing and talking about everything work and non-work related, but also memorable evenings out or in. I really cherish the times we spent and will spend together and am happy to have gotten to know you during my time at the university.

I also want to appreciate **Franzi**, who makes the best pigs in blankets and cocktails and shares my sense of humor. Thank you for all the late nights just talking or bingeing TV shows. As well, thanks to **Goethe**, who always knows the right time for cuddles.

For her unwavering support, I want to thank my best friend and neighbor **Nina**, who is always there for me with either some sassy comments, funny stories, or a place on her couch with a glass of wine. I will miss having you as the coolest neighbor ever.

None of this could have happened without the wonderful support of my family. My deepest gratitude goes to my sister and her sons, my aunt and cousin, and my grandparents, especially my grandpa **Adi**, who was my greatest shoulder to lean on but passed before he could see the finished result. But I know he would be proud.

I also want to thank my lovely girlfriend **Vera** for all the patience she had with me and her steady support and comfort. Thank you for being my favorite distraction, taking your time, motivating me, and making me laugh. I love you dearly, thank you for always being there for me.

Last, and most importantly, I want to show my love and appreciation to my parents **Sabine** and **Hans**. They have always been my greatest supporters since I started university. Even through my doubts and the times I felt like quitting, they continue being there for me and building me back up again to reach my goals. I cannot thank you enough for that.

A great thank you to all of you!

Verena Huber

Danksagungen

Diese Arbeit konnte nur durch die starke Mithilfe und Unterstützung meiner Familie verwirklicht werden. In diesen paar Zeilen möchte ich ihnen nochmals ausdrücklich dafür danken.

Vielen Dank an meine Großeltern **Anneliese**, **Johann** und **Annemarie**, die immer für mich da waren und sich über Bilder und Geschichten aus der Uni gefreut haben. Außerdem gilt mein Dank auch meinem verstorbenem Großvater **Adi**, der mir immer die größte Stütze war und sich mit mir über all meine Erfolge am meisten gefreut hat.

Darüber hinaus gilt mein Dank auch meiner Schwester **Franziska** und ihren Söhnen, **Michael** und **Andreas**, sowie meiner Tante **Renate** und meinem Cousin **Michael**, denen man immer eine Freude bereiten konnte, wenn man zu Besuch kam.

Zuletzt möchte ich mich aufrichtig bei meinen Eltern **Sabine** und **Hans** bedanken, die immer an mich geglaubt haben und mir über alle Zweifel hinweggeholfen haben. Worte reichen für ihre Unterstützung nicht aus.

Vielen Dank an euch alle!

Verena Huber

Remerciements

En surplus, je voudrais dire un grand merci à **Professeur Kunz** pour me donner l’opportunité d’apprendre le français pendant ma thèse de doctorat.

Avec ces cours j’ai pu améliorer ma compréhension culturelle et participer à des projets avec notre collègues et stagiaires de France. Ainsi, je voudrais exprimer mes remerciements pour eux en leur langue.

Merci beaucoup à **Didier Touraud**, qui m’a donné l’appui possible et avec qui on s’est amusés toujours. Tu vas me manquer !

Aussi, merci à **Pierre Degot**, qui m’a aidé toujours et qui m’a montré la façon de travailler scientifiquement. Je savourais notre temps ensemble dans le laboratoire.

Enfin, je voudrais dire merci à **Laurie Muller**, ma stagiaire du mastère, pour son aval et travaille extraordinaire. J’ai hâte de te voir tôt.

Un grand merci à tous !

Verena Huber

Abstract

Three plants of interest and their active ingredients were examined throughout this thesis: γ-irone of *Iris germanica* L., the curcuminoids of *Curcuma longa* L., and cinnamaldehyde of *Cinnamomum cassia*. They also dictate the structure of the presented study.

Chapter 3 deals with the extraction and concentration of the odiferous γ-irone from Iris Barbata-Elatior, a cultivar of *Iris germanica* L. The dried and ground rhizomes were extracted in four different approaches with solvents based on myristic acid. The best result with a γ-irone yield of ~ 66% was achieved through the extraction of rhizomes soaked in water with pure myristic acid. This model extraction was scaled up in order to obtain enough extract to successively perform molecular distillation for concentration purposes. The optimum distillation method was developed beforehand by taking the Clausius-Clapeyron relation as a theoretical basis and validating it with experiments using structural analogues of γ-irone. Eventually, the γ-irone content could be concentrated 18-fold after two molecular distillation cycles.

The curcuminoids of *Curcuma longa* L. were the molecules of interest throughout Chapters 4 and 5. A screening of different natural deep eutectic solvents in terms of curcumin solubility was performed. The most promising ones were the mixtures of choline chloride with lactic and levulinic acid. They were chosen to replace the aqueous phase in ternary mixtures with ethanol and triacetin. Successively, the phase behavior of these ternary mixtures was examined while also mapping the solubility of curcumin depending on the weight ratios of these ternary mixtures. In the domains of highest solubility, extraction experiments were performed. It was possible to achieve curcuminoid extraction yields of up to 79% (lactic acid) and 84% (levulinic acid). Consecutively, cycle extractions were investigated, showing that the solvents could be concentrated through repeated extraction of fresh rhizomes. The change of the solvent during these cycle extractions was monitored and determined to be the limiting factor of cycles.

After determining the natural deep eutectics' capability to solve and extract curcuminoids, the mechanism of solubility was investigated. Nine different eutectics based on the quaternary ammonium compounds choline chloride, betaine, and carnitine mixed with lactic, levulinic, and pyruvic acid were examined. UV/Vis

spectroscopy was used to monitor the eutectics' capability to solve curcumin. The underlying intermolecular interactions were assessed theoretically by using COSMO-RS predictions of the chemical potential and experimentally backing those with ^{1}H and NOESY NMR measurements. Different additional functionalities of the quaternary ammonium compounds did not influence the solubility of curcumin in ethanolic solutions, while functionalities had a significant effect when regarding ethanolic solutions of the acids. The natural deep eutectics containing levulinic acid yielded the highest curcumin solubilities based on a solubility synergy between the acid and the quaternary ammonium compounds. Non-specific and directed intermolecular interactions were identified as the driving force behind the strong solubility increase.

In the last part, Chapter 6, the curcumin solubility in ethanolic solutions of natural aromas was examined. A series of natural aromas with different functionalities were screened experimentally with UV/Vis spectroscopy and theoretically with COSMO-RS, yielding cinnamaldehyde as the molecule of highest solving ability. Natural essential cinnamon oils of *Cinnamomum cassia* and *Cinnamomum verum*, high in cinnamaldehyde, were examined in view of composition and solving capability. The phase behavior of ternary mixtures of the best cinnamon essential oil (*Cinnamomum cassia* oil), water, and ethanol was characterized, and the curcumin solubility was mapped. Cycle extraction experiments showed that rather the loss of solvent was the limiting factor of cycles than the solvent change over time. A theoretical model for cycle extractions was developed.

Zusammenfassung

Drei Pflanzen sowie deren Inhaltsstoffe waren von besonderer Bedeutung für diese Arbeit und wurden untersucht: γ-Iron aus *Iris germanica* L, die Curcuminoide von *Curcuma longa* L und Zimtaldehyd aus *Cinnamomum verum*. Diese geben auch die Struktur der Arbeit vor.

Kapitel 3 beschäftigt sich mit der Extraktion und Aufkonzentrierung des Duftstoffes γ-Iron aus der Pflanze *Iris Barbata-Elatior*, einem Kultivar der Spezies *Iris germanica* L. Die getrockneten und gemahlenen Rhizome wurden auf vier unterschiedliche Arten mit myristinsäurebasierten Lösemitteln extrahiert. Das beste Ergebnis mit einer Ausbeute von ~ 66% γ-Iron wurde durch die Extraktion von zuvor in Wasser eingelegten Rhizomen mit reiner Myristinsäure erreicht. Um genügend Extrakt für eine darauffolgende Aufarbeitung mittels einer Molekulardestillationsanlage zu erhalten, wurde ein Upscaling dieser Modellextraktion vorgenommen. Die optimale Destillationsmethode wurde theoretisch anhand der Clausius-Clapeyron-Beziehung entwickelt und mit Experimenten zu γ-Iron strukturellen Analoga validiert. Somit wurde nach zwei Destillationszyklen eine 18-fache Aufkonzentrierung von γ-Iron ermöglicht.

Die Curcuminoide von *Curcuma longa* L. werden in den Kapiteln 4 und 5 behandelt. Ein Screening verschiedener natürlicher Eutektika mit Blick auf die Löslichkeit von Curcumin wurde durchgeführt. Am vielversprechendsten waren die Mischungen aus Cholinchlorid mit Milch- und Lävulinsäure, die ausgewählt wurden, um die wässrige Phase in ternären Mischungen mit Ethanol und Triacetin zu ersetzen. Das Phasenverhalten dieser ternären Mischungen wurde charakterisiert und die Curcuminlöslichkeit in Abhängigkeit von den ternären Zusammensetzungen kartographiert. In den Bereichen der höchsten Löslichkeit wurden Extraktionsexperimente durchgeführt. So war es möglich, Extraktionsausbeuten von 79% (mit Milchsäure) und 84% (mit Lävulinsäure) zu erreichen. Daraufhin wurden die besten Lösemittelmischungen im Hinblick auf zyklische Extraktionen untersucht. Bei wiederholten Extraktionen von frischem Rohmaterial konnten die Lösemittel wiederverwendet und aufkonzentriert werden. Die Veränderung des Lösemittels während der Zyklen wurde als limitierender Faktor der Zyklen festgestellt.

Nachdem die Curcumin-Lösungs- und Extraktionsfähigkeit der natürlichen tiefen Eutektika-Mischungen gezeigt werden konnten, wurde der diesbezügliche Mechanismus untersucht. Neun verschiedene Eutektika auf der Basis der quaternären Ammoniumverbindungen Cholinchlorid, Betain und Carnitin gemischt mit Milch-, Lävulin- und Brenztraubensäure wurden betrachtet. Mittels UV/Vis Spektroskopie wurde die Löslichkeit von Curcumin beobachtet. Die zugrundeliegenden intermolekularen Interaktionen wurden theoretisch durch die Vorhersage des chemischen Potentials mittels COSMO-RS bemessen und durch ^{1}H- und NOESY-NMR-Messungen bekräftigt. Funktionelle Gruppen hatten kaum Einfluss auf die Löslichkeit von Curcumin in ethanolischen Lösungen der quaternären Ammoniumverbindungen, während ihr Einfluss im Hinblick auf die Säuren nicht zu vernachlässigen war. Die höchsten Curcuminlöslichkeiten wurden in ethanolischen Lösungen mit natürlichen tiefen Eutektika mit Lävulinsäure als Bestandteil erreicht, was auf eine Synergie zwischen den quaternären Ammoniumverbindungen und der Säure zurückzuführen war. Unspezifische und direkte intermolekulare Wechselwirkungen wurden als treibende Kraft hinter der starken Löslichkeitserhöhung identifiziert.

Im letzten Teil, Kapitel 6, wurde die Curcuminlöslichkeit in ethanolischen Lösungen von natürlichen Aromastoffen erforscht. Eine Reihe natürlicher Aromen mit verschiedenen Funktionalitäten wurde experimentell mittels UV/Vis-Spektroskopie und theoretisch mittels COSMO-RS-Rechnungen untersucht. Zimtaldehyd wurde als Verbindung mit der höchsten Löslichkeitskraft identifiziert. Natürliche ätherische Öle von *Cinnamomum cassia* mit hohem Zimtaldehydanteil wurden mit Blick auf ihre Zusammensetzung und Löslichkeitskraft untersucht. Das Phasenverhalten des besten Öls in der Mischung mit Wasser und Ethanol wurde untersucht sowie die Curcuminlöslichkeit in Abhängigkeit der Zusammensetzung. Zyklische Extraktionen zeigten, dass weniger die Veränderung des Lösemittels als der Lösemittelverlust der limitierende Faktor der Zyklen war. Ein theoretisches Modell für zyklische Extraktionen wurde entwickelt.

Abbreviations

+M	Positive mesomeric effect
2D	Two-dimensional
2Φ	Two-phase, biphase
Aba	4-Acetylbutyric acid
AcCh	Acetylcholine
ACN	Acetonitrile
ACS	American Chemical Society
BDC	Bisdemethoxycurcumin
Bet	Betaine
Car	Carnitine
ChCl	Choline chloride
COSMO-RS	Conductor-like screening model for real solvents
CP	Critical point
Cur	Curcumin
DC	Demethoxycurcumin
DES	Deep eutectic solvents
DLS	Dynamic light scattering
DMSO-*d6*	Hexadeuterodimethylsulfoxid
EtOH	Ethanol
FCC	Food Chemicals Codex
FG	Food Grade
FID	Flame ionization detector
GC	Gas chromatography
HAc	Acetic acid
HBA	Hydrogen bond acceptor
HBD	Hydrogen bond donor
HETP	Height equivalent of a theoretical plate
Hex	Hexanoic acid
HMyr	Myristic acid
HPLC	High-performance liquid chromatography
HSP	Hansen Solubility Parameter
IUPAC	International Union of Pure and Applied Chemistry

Lac	Lactic acid
Lev	Levulinic acid
LLE	Liquid-liquid-equilibrium
Mal	Malic acid
Man	Mandelic acid
MeOD	Tetradeuteromethanol
MeOH	Methanol
MS	Mass spectrometry
n/n	Molar ratio
$N_{3333}Br$	Tetrapropylammonium bromide
NADES	Natural deep eutectic solvents
NaMyr	Sodium myristate
NaOH	Sodium hydroxide
NIST	National institute of standards and technology
NMR	Nuclear magnetic resonance
NOESY	Nuclear Overhauser enhancement spectroscopy
Ova	2-Oxavaleric acid
Oxa	2-Oxabutyric acid
p.a.	Pro analysis
PMI	Process mass intensity
Pro	Proline
PTFE	Polytetrafluoroethylene
Pyr	Pyruvic acid
QA	Quaternary ammonium cation
RCP	Reminiscent critical point
SFME	Surfactant-free microemulsion
TriA	Triacetin
UCST	Upper critical solution temperature
UV/Vis	Ultraviolet and visible spectroscopy
w/w	Mass ratio

Symbols

$+z$	Parallel orientation to the magnetic field's direction
$-z$	Antiparallel orientation to the magnetic field's direction
$\propto$	Proportionality
A	Absorbance
A_0	Arrhenius parameter
A_A-C_A	Fitting parameters of the Antoine equation
A_C-C_C	Causes of peak broadening in chromatography
a^{eff}	Effective contact area between two surface segments
a_{Index}	Area of index
A_W-F_W	Fitting parameters of the Wagner equation
B_0	Magnetic field
c	Concentration
c_0	Speed of light in vacuum
d	Molecular diameter
dp	Change of pressure
dT	Change of temperature
E_{Index}	Energy of Index
f	Response factor of 0.935 a.u.
G	Gibbs free energy
h	Plack's constant
H	Enthalpy
I	Remaining light intensity
I_0	Initial light intensity
i and j	Arbitrary compound and state variables
k_B	Boltzmann constant
k_{evap}	Evaporation rate constant
l	Illuminated layer thickness
m_{Index}	Mass of index
m^s	Magnetic quantum number of the nucleus
n	Number of cycles
N_0	Ground state
N_1	Excited state

N_A	Avogadro constant
P	Spin angular momentum
$p^i(\sigma)$	σ-profile
p_{Index}	Pressure of index
q_i	Probability of state i
R	Gas constant
s	Spin quantum number of the nucleus
S	Entropy
T_{Index}	Temperature of index
u	linear velocity
v_{Index}	Molar volume of index
V	Solvent volume
V_2	Solvent volume loss
x_{Index}	Mole fraction
y_{Index}	Vapor mole fraction
α	Adjustable parameter
γ	Gyromagnetic ratio
Δ	Change/Difference
δ_{Index}	Index Solubility Parameter
ε	Molar extinction coefficient
ζ_i	Activity coefficient of i
λ	Wavelength
λ_{max}	Wavelength of maximum absorption
$<\lambda>$	Collision-free mean pathway
$\mu_{c,s}^i$	Combinatorial term considering the size and shape differences of the molecules in question
$\mu_s(\sigma)$	σ-potential
μ_s^i	Chemical potential of i
μ_M	Magnetic moment
ν	Frequency
σ	Charge density
τ	Transmittance

Contents

ACKNOWLEDGMENTS II

DANKSAGUNGEN IV

REMERCIEMENTS V

ABSTRACT VI

ZUSAMMENFASSUNG VIII

ABBREVIATIONS X

SYMBOLS XII

CONTENTS XIV

1 INTRODUCTION 3

2 GENERAL INFORMATION 7

2.1 PHYTOCHEMICALS 7
2.2 EXTRACTION OF PHYTOCHEMICALS 11
2.2.1 Soxhlet Extraction 13
2.2.2 Maceration 14
2.2.3 Nonconventional Extraction Methods 15
2.3 GREEN EXTRACTION AND GREEN SOLVENTS 16
2.4 NATURAL DEEP EUTECTIC SOLVENTS 18
2.5 UV/VIS SPECTROSCOPY 21
2.6 NUCLEAR MAGNETIC RESONANCE SPECTROSCOPY – NMR 24
2.6.1 Introduction to Nuclear Magnetic Resonance Spectroscopy 24
2.6.2 Nuclear Overhauser Enhancement Spectroscopy – NOESY 27
2.7 CHROMATOGRAPHY 27
2.7.1 High-Performance Liquid Chromatography – HPLC 29
2.7.2 Gas Chromatography – GC 32
2.8 SOLUBILITY AND ITS PREDICTIONS 34
2.8.1 Hansen Solubility Parameters 34
2.8.2 Conductor-Like Screening Model for Real Solvents – COSMO-RS 36

3 ISOLATION OF IRONES VIA SHORT-PATH DISTILLATION 41

3.1 INTRODUCTION 41
3.2 EXPERIMENTAL 44
3.2.1 Chemicals 44
3.2.2 Methods and Techniques 44
3.2.2.1 Fatty Acid Extraction of γ-Irone from Iris Barbata-Elatior Rhizomes 44
3.2.2.2 Short-Path Distillation 46
3.2.2.3 GC-FID Analysis 47

3.3 RESULTS AND DISCUSSION 48

3.3.1 Extraction of γ-Irone from the Rhizomes of Iris Barbata-Elatior 48

3.3.2 Molecular Distillation 50

3.4 CONCLUSION 56

4 SOLUBILITY AND EXTRACTION OF CURCUMIN IN NADES SYSTEMS 61

4.1 INTRODUCTION 61

4.2 EXPERIMENTAL 63

4.2.1 Chemicals 63

4.2.2 Methods and Techniques 64

4.2.2.1 NADES Preparation 64

4.2.2.2 Determination of Ternary Phase Diagrams 64

4.2.2.3 Solubility Examination via Optical Density Measurements 65

4.2.2.4 Dynamic Light Scattering 65

4.2.2.5 Liquid-Liquid-Equilibrium (LLE) Simulation 66

4.2.2.6 Curcuminoid Extraction 66

4.2.2.7 HPLC Method 68

4.2.2.8 ^{13}C-NMR Analysis 69

4.2.2.9 Conductivity Measurements 69

4.3 RESULTS AND DISCUSSION 69

4.3.1 Curcumin Solubility in Different NADES Systems 69

4.3.2 Phase Diagrams and Solubility Maps 72

4.3.3 Extraction Ability 77

4.4 CONCLUSION 85

5 UNCOVERING THE CURCUMIN SOLUBILIZATION ABILITY OF NADES 91

5.1 INTRODUCTION 91

5.2 EXPERIMENTAL 91

5.2.1 Chemicals 91

5.2.2 Methods and Techniques 92

5.2.2.1 Sample Preparation 92

5.2.2.2 Solubility Examination via Optical Density Measurements 92

5.2.2.3 NMR Analysis 93

5.2.2.4 COSMO-RS Calculations 93

5.2.2.5 NADES Preparation 93

5.2.2.6 Karl-Fischer Measurements 93

5.3 RESULTS AND DISCUSSION 94

5.3.1 Influence of Quaternary Ammonium Compounds 94

5.3.2 Influence of Acids 98

5.3.3 Influence of NADES 104

5.4 CONCLUSION 108

6 *CINNAMOMUM CASSIA* ESSENTIAL OIL AS GREEN SOLVENT 113

6.1 INTRODUCTION 113
6.2 EXPERIMENTAL 115
6.2.1 Chemicals 115
6.2.2 Methods and Techniques 116
6.2.2.1 Sample Preparation 116
6.2.2.2 Optical Density Measurements 116
6.2.2.3 COSMO-RS Calculations 116
6.2.2.4 NMR Analysis 116
6.2.2.5 GC-FID Analysis 117
6.2.2.6 GC-MS Analysis 117
6.2.2.7 Determination of Ternary Phase Diagrams 117
6.2.2.8 Determination of the Critical Point 118
6.2.2.9 Cyclic Solvent Extraction of Curcuma Longa L. 118
6.3 RESULTS AND DISCUSSION 118
6.3.1 Screening of Natural Aromas 118
6.3.2 Preparation for Extraction Experiments – A Proof of Concept 126
6.4 CONCLUSION 129

7 COLLECTIVE CONCLUSION 133

8 BIBLIOGRAPHY 137

9 APPENDIX 157

9.1 IMPORTANT CHEMICALS AND THEIR STRUCTURES 157
9.2 SUPPLEMENTARY INFORMATION OF CHAPTER 2 161
9.2.1 The 12 Principles of Green Chemistry [6] 161
9.2.2 Comparison of Ionic Liquids and Deep Eutectic Solvents 162
9.3 SUPPLEMENTARY INFORMATION OF CHAPTER 3 163
9.3.1 GC Chromatogram of the Technical Mixture of Irone Isomers 163
9.3.2 Clausius-Clapeyron Calculations 164
9.3.3 Distillation Results 164
9.4 SUPPLEMENTARY INFORMATION OF CHAPTER 4 165
9.4.1 Curcumin Solubility in Binary Mixtures of Water with ChCl and NADES 165
9.4.2 Dynamic Light Scattering Examination 166
9.4.3 Prediction of the Ethanol/Triacetin Phase Diagram 168
9.4.4 HPLC Calibration Curves 168
9.4.5 Extraction Yields in Numbers 169
9.4.6 Curcuminoid Content after Every Cycle of Extraction 170
9.4.7 Curcuminoid Concentration after Different Extraction Cycles 171
9.4.8 NMR Spectra of the Extraction Solvent over Time 172
9.5 SUPPLEMENTARY INFORMATION OF CHAPTER 5 174
9.5.1 Curcumin Solubility in EtOH Depending on Additive Content in mol% 174
9.5.2 ^{1}H-NMR spectra of Curcumin and the QAs 175

9.5.3 Determination of the Keto-Enol-Ratio 183

9.5.4 NOESY Spectra of Curcumin and the QAs 185

9.5.5 Curcumin Solubility in EtOH Depending on the Acid Content in mol% 187

9.5.6 Hansen Space 188

9.5.7 Chemical Potential of Curcumin Solubility via COSMO-RS 189

9.5.8 Curcumin Solubility in EtOH Depending on the Acid Content in wt% 190

9.6 SUPPLEMENTARY INFORMATION OF CHAPTER 6 191

9.6.1 Screening of Natural Aromas in wt% 191

9.6.2 ^{1}H and NOESY NMR spectra of Curcumin with Cin and HCi 192

9.6.3 Screening of Cinnamaldehyde Derivatives 196

9.6.4 GC-FID Chromatograms 197

9.6.5 GC-MS Data of the Cinnamomum Oils 201

9.6.5.1 Cinnamaldehyde Reference 202

9.6.5.2 Cinnamomum Cassia Oil by PCW 202

9.6.5.3 Cinnamomum Zeylanicum Oil by Jean Pütz 204

9.6.5.4 Cinnamomum Verum Oil by PCW 208

9.6.6 Characterization of the Ternary Phase Diagram 212

9.6.7 Calibration Curves of Curcumin in Ethanol and Acetone 213

LIST OF FIGURES 214

LIST OF TABLES 226

SCIENTIFIC CONTRIBUTIONS 228

POSTER PRESENTATIONS 228

ORAL PRESENTATIONS 229

PUBLICATIONS 230

DECLARATION 232

EIDESSTATTLICHE ERKLÄRUNG 232

STATUTORY DECLARATION 233

CHAPTER 1

INTRODUCTION

1 Introduction

The kingdom of plantae and its use for humanity will be the main concern in this thesis. It comprises a multitude of different species which are abundant throughout the whole world and are capable of sustaining life. Plants provide active ingredients, which can be nutritional but are also of high interest in terms of their other properties like scent, color, and health promoting effects. Due to these peculiarities, which have been known for ages, many plants have earned their due significance [1].

To obtain these natural molecules in their pure form, separated from their plant matrix, extraction is the method of choice. It is a ubiquitous method that has been known for centuries and anyone who has ever brewed a cup of tea or coffee has performed an extraction. Through infusion of the ground natural product with boiling hot water, the molecules responsible for the flavor and color impressions in the respective drinks will be removed from their matrix and transferred to the solvent, water. Putting this in a more scientific perspective, extraction is a method to remove the active ingredients from the inactive plant tissues using some sort of solvent [1–4].

Especially nowadays, consumers take an interest in the ingredients of their products and many environmental factors aid the demand for natural products’ increase. Particularly the food and beverage industry as well as the personal care industry can profit of the growing natural extracts market [5].

Extraction may seem like an easy process, but plenty of research and time is spent to improve this topic. Keeping in mind the principles of green chemistry and green extraction, popularized by P. Anastas and F. Chemat respectively, the challenges which need to be tackled include increasing processes’ efficacies with regard to yield and selectivity while employing alternative solvents [6,7]. Instead of continuing using conventional, petroleum-based, organic solvents, sustainable and environmentally friendly alternatives with lower health risks upon exposure need to be developed. In the pursuit of finding green alternatives, once again, the plant kingdom can serve as an example, as nature may already contain what can be used as a solvent. Especially noteworthy in this case is so-called natural deep eutectic solvents (NADES). They are mixtures of natural (often solid) molecules which depress their respective melting points at an ideal molar ratio through intermolecular interactions, yielding liquid solvents. Sometimes, they are embraced as a new type of liquid phase inside living organisms [8]. Apart from these, lipids and essential oils contained in plants also exhibit agreeable solvent characteristics and can be employed as alternatives to conventional ones [9,10]. Thus, nature already provides the necessary solvents to use for extraction, which only have to be examined further.

Motivated by the vast abundance of natural solvent sources, this study deals with the development of sustainable extractions. The focus was put on the extraction of irones from *Iris germanica* L. using a fatty acid, which was already part of the plant, and curcuminoids from *Curcuma longa* L., employing different natural deep eutectic solvents and natural aromas as extraction solvents.

CHAPTER 2

GENERAL INFORMATION

CONTENTS

In this chapter the theoretical background about phytochemicals, the concept of extraction, green chemistry, analysis methods, and solvents will be presented.

2 General Information

This chapter will give an overview of the theoretical backgrounds of the methods and solvents in question and will introduce the necessary and important concepts.

2.1 Phytochemicals

According to rough estimations, 400’000 species of plants currently populate the earth. In a way, they can be seen as nature’s chemists as they possess the ability to produce countless metabolites of high versatility [1,11–18]. Chemically active compounds produced in plants are called phytochemicals. Their name is derived from the Greek word φυτόν (*phyton*), meaning *plant*, indicating their origin. In this study, three plants and their ingredients were investigated:

- Iris *Barbata Elatior* as a source of γ-irone (cf. 3 Isolation of Irones via Short-Path Distillation)
- *Curcuma longa* L., containing the three major curcuminoids curcumin, demethoxycurcumin, and bisdemethoxycurcumin (cf. 4 Solubility and Extraction of Curcumin in NADES Systems, 5 Uncovering the Curcumin Solubili, and 6 *Cinnamomum Cassia* Essential Oil as Green Solvent)
- *Cinnamomum Cassia* providing cinnamaldehyde (cf. 6 *Cinnamomum Cassia* Essential Oil as Green Solvent)

A more precise definition of these will be given in their respective chapters and their molecular structures can be viewed in Section 9.1 Important Chemicals and their Structures. Here, however, only a general description of phytochemicals will be presented.

As already assessed above, phytochemicals arise in plants. They can accumulate in different parts like the roots, stems, leaves, flowers, fruit, or seeds [16]. In total, they can be divided into three classes: hormones as well as primary and secondary metabolites [19]. But in this study, the focus will be placed solely on primary and secondary metabolites. An overview of these is given in Figure 2-1.

As their name says, primary metabolites can be derived from the primary or central metabolism, which is responsible for the survival of an organism. This means these compounds can be found in almost every cell of every living organism. Prominent representatives of primary metabolites are products of glycolysis, the citric acid cycle, or any metabolic pathway producing precursors of essential chemicals necessary for everyday life, like essential amino acids. These are the key compounds and are, therefore, placed in the center of Figure 2-1. These primary metabolites often act as precursors for the synthesis of secondary metabolites, which are also called specialized metabolites or natural products. In the case of the second class, the variety of molecules is vast, as they can serve different purposes apart from basal functionality, growth, development, or reproduction. Thus, neither every organism nor every cell of an organism is necessarily able to produce these specialized metabolites [20]. Besides, as they do not sustain life, the mechanisms behind their synthesis are less regulated inside the cells, which would also explain their manifoldness. Some examples of these natural products are given in Figure 2-1. Of course, breaking down this huge class of natural molecules into three categories seems somewhat reductive and while skimming through the literature, one might find even more refined categorizations. However, these three main groups of alkaloids, terpenes, and phenolic compounds make up the majority of secondary metabolites that are known so far [21]. Most of the extra classifications can be included in the presented three.

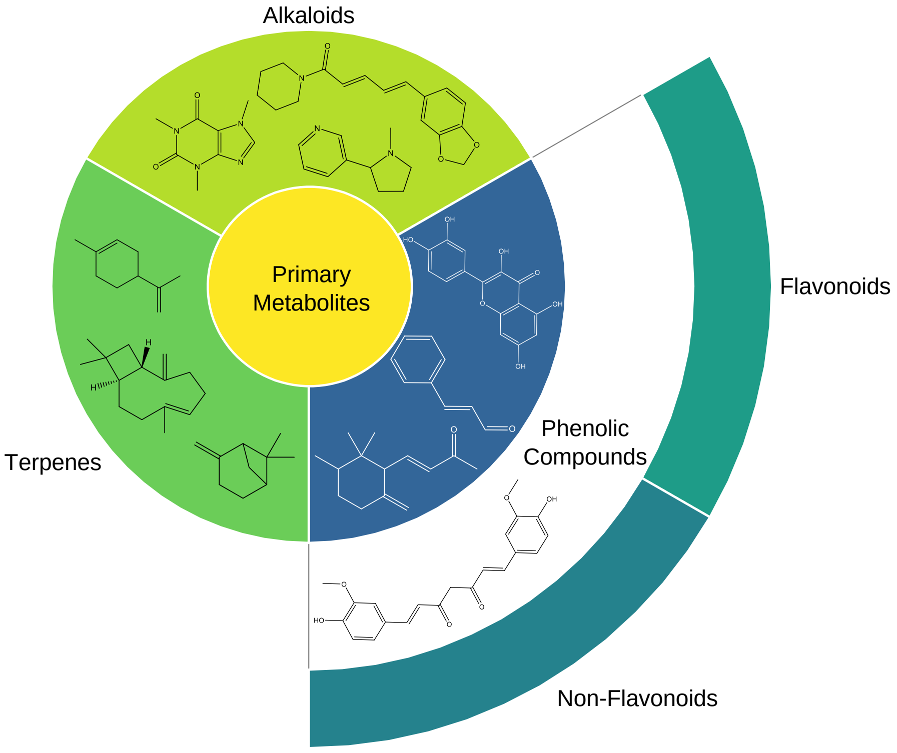

Figure 2-1: Overview of the two kinds of plant metabolites inspired by [22–24]. *The primary metabolites (yellow) in the center are the basic molecules necessary for the functionality of organisms. They are the source materials from which the secondary metabolites (outer ring) can be synthesized. These secondary metabolites are divided into three groups: alkaloids (bright green; represented by caffeine, nicotine, and piperine), terpenes (dark green; represented by limonene, caryophyllene, and pinene), and phenolic compounds (blue; represented by quercetin, cinnamaldehyde, γ-irone, and curcumin. The last three can also be viewed in Section 9.1.*

The sorting usually follows the components' metabolic pathway [25]. However, as a rule of thumb, the classes can be characterized as follows [16,21]:

- Alkaloids usually are derived from amino acids and possess at least one nitrogen atom in heterocycles. They are often of a basic nature.
- Terpenes are liposoluble molecules based on isoprene, which can occur at a random number. They are often polycyclic and are known for their flavor. In plants, they can usually be found as essential oils.
- Phenolic compounds have at least one hydroxy group attached to one or more aromatic rings. They are the largest category of secondary metabolites [1,16,26]. The phytochemicals investigated in this study, γ-irone, curcumin, and cinnamaldehyde, fall into the category of non-flavonoid phenolic compounds. Their structures are also included in Figure 2-1 and can be viewed as well in Tables 9-1 and 9-3 of the Appendix.

In terms of chemical ecology, however, nature would not waste energy for the synthesis of secondary metabolites without getting some benefits in return. This opens the question of why they are even produced. It is assumed that the development of the secondary metabolites was provoked evolutionarily, though, to this day, the driving force behind it is unclear [13]. There are many theories claiming that those natural products have an adaptive purpose making plants competitive when interacting with their environment as a way of ensuring their dominance and ability to survive and reproduce. These theories also explore the possibility that mixtures of secondary metabolites can create efficacy synergies, prevent accelerated adaption of predators, or create means of communication. On the other hand, there is also a possibility that phytonutrients stem from screening processes of plants searching for advantages. However, which theories are true is hard to prove [13].

Since one can still only speculate about the purpose of secondary metabolites' existence, there are only some palpable explanations for their functions so far. Two key roles have been identified: attraction and protection. As plants are static organisms, they rely on external help to reproduce. Thus, the attraction of dispersers like bees, who transport the pollen, is of great importance. In this case, the secondary metabolites can act as so-called attractants that lure in the dispersers. This can be achieved through pleasant smells or colors. At the same time, some creatures may also act predatory, feeding on the plants. To combat this behavior, plants protect themselves, which can also be achieved with secondary metabolites. The phytochemicals can act in a harmful way as bitterns or toxins preventing active feeding. For example, many essential oils are known to be good insecticides [27,28]. Bright colors as well can send warning signals shooing away unwanted company [13].

In addition to these two functions specialized in active interactions with the environment, the metabolites can also act in a conserving matter. Through extended π-systems and antioxidative properties, the chemicals are also capable to prevent oxidative stress and stress induced through UV radiation to keep the host plant healthy [29].

Exactly these features that are in place to ensure the well-being of the plants make the secondary metabolites so interesting for humans. For centuries, plants have been a source of healing and the empirical knowledge about that has been passed on over generations. The discovery of secondary metabolites has been the starting point of phytochemistry, the field of plant compounds and their properties, dealing with their identification, quantification, and purification [21]. Extensive research has been conducted to identify phytochemicals that can augment human life. There are many application fields, like the cosmetic industry, using the natural products' olfactory properties. Some secondary metabolites are very popular in the food industry as they bring flavor and color. Also, in the attempt of finding new drugs or pharmaceutically active compounds, the medicinal characteristics of phytochemicals are very important [1]. However, not all pharmaceutically active ingredients are suitable as medication. Active effects for curing diseases may not be observed in all phytonutrients. Yet, through antioxidative, anti-microbial, anti-viral, anti-cancer, and many more advantageous effects [16,30,31], they serve as excellent supplements in a daily diet.

Regardless of their application field, the demand for natural products is on a rise due to consumers' increasing health awareness. Thus, attention is placed on the origin and manufacture of products, increasing the demand for wholesome, natural, and health-promoting products and ingredients [32,33]. Especially the market of polyphenols (in the United States) is predicted to grow at a rate of > 7% during the next decade, which is conjectured to be driven by their health benefitting effects [34]. To exploit the whole potential of these natural products and to do the increasing demand justice, the pure phytochemicals have to be extracted and separated from their matrix to obtain them in their pure form for analysis and their use in modern formulations [21].

2.2 Extraction of Phytochemicals

As mentioned above, to obtain the natural products in their pure form, extractions are performed. The word *extraction* has a Latin origin, *extrahere*, which means *pull out* or *remove*, which is exactly what happens during an extraction process. The so-called extractant is removed from its matrix, often with the purpose of purifying and quantifying it [35].

Four different types of extraction can be distinguished: mechanical expression, distillation, sublimation, and solvent extraction [2,36,37]. The process of mechanical expression is also called pressing. This method is used on plants high in oil content like citrus fruits or nuts yielding extracts free of solvent residues with a similar quality to the pure oil in the plants [38,39]. Volatile organic compounds can be extracted via distillation methods, with or without water or steam. They can have different sensory characteristics compared to the whole plant, as solely the volatile compounds are removed from the raw material [37]. Lastly, solvent extraction is the most widely applied method of extracting natural products by using a solvent. This study focuses on the extraction of natural compounds using solvents. Therefore, only this method will be described more thoroughly.

Solvent extraction is a thermodynamically driven process of solvation following the equation of Gibbs free energy ΔG [4]:

$$\Delta G = \Delta H_{tot} - T\Delta S \tag{2-1}$$

$$\Delta H_{tot} = \Delta H_{Solute} + \Delta H_{Solvent} + \Delta H_{Mix} \tag{2-2}$$

with ΔH_{tot} = total enthalpy of the system, T = temperature, ΔS = entropy, ΔH_{Solute} = enthalpy between solute molecules, $\Delta H_{Solvent}$ = enthalpy between solvent molecules, and ΔH_{Mix} = enthalpy between solute and solvent molecules.

Only if ΔG reaches a negative value, the extraction will take place spontaneously. The entropic term is always a positive one, weighing in favor of the spontaneous process as forming solutions increases the entropy in any case. Increasing temperatures as well are auxiliary [1]. However, the spontaneity of an extraction depends on the enthalpy between the solvent and solute molecules. The attractive energy between the solvent and the solute molecules ΔH_{Mix} has to outweigh the energy necessary to break the interaction between the solute ΔH_{Solute} and solvent $\Delta H_{Solvent}$ molecules themselves. Therefore, the choice of solvent is vital [4].

In general, the principle of similarity and intermiscibility commonly known as “like dissolves like” can be applied to have the extractants preferably solve or partition in the used solvent. This means that solvent and solute of similar polarity will yield satisfactory results [2,40,41] while also the pH, surface tension, vapor pressure, and melting and boiling point have to be considered [4,42]. However, the right solvent for an extraction process still needs to meet more requirements. Ideally, the menstruum is highly selective with respect to the target material to avoid coextractions of unwanted compounds. In addition, the solvent should be cheap and easily manageable in terms of viscosity and reactivity. The quality of the extraction can suffer greatly if the solvent reacts with the extractants, or the extraction is hindered through slow mass transfer. Most importantly, the solvent must be safe. Nonvolatility, nonflammability, and nontoxicity are preferred characteristics to ensure a safe work environment [3]. For the incorporation of the extracts into foodstuffs, food-grade (FG) solvents must be used to ensure the safety of consumption. These solvents are often water, ethanol, and mixtures thereof. In a finished product, functional food, or beverages, the content of ethanol, however, has to be lower than 1.2% to avoid any health claims through EU legislation. Any other organic solvent, e.g. methanol or acetone, must be removed completely to allow the incorporation of the respective extract into food products [1].

Before being able to start the extractions, the natural product samples have to be prepared adequately. The preservation of the plant matrix is crucial as pre-treatments can have an influence on the quality of the extract. Thus, samples can be dry or fresh. Nevertheless, plants have to be washed, dried or sifted, and homogenized. Homogenization via grinding yields powders, which are perfect raw materials for extraction. Powders have a big surface, which is necessary to achieve good extraction results, as it promotes solvent penetration and diffusion of solutes. This also leads to shortened extraction times. If the particle size, however, is too small, the extraction efficiency will decrease due to filtration difficulties caused by excessive sorption of the menstruum into the plant material. Therefore, a compromise must be found [1,2,42]. When these starting criteria are met, the extraction can begin advancing through the following steps: The biological matrix is penetrated by the solvent. Successively, the target compound partitions into the menstruum and will be transported out of the plant matrix. Then, the solvent fractions containing the solute are collected and filtered if necessary. The extraction efficiency can always be improved by increasing the diffusion and solubility of the target by means of elevated temperatures. Also, the extraction time and powder-to-solvent ratio play an important role [1,2,4]. Thus, the right extraction method has to be chosen.

There is a multitude of extraction techniques suited for the extraction of natural products from their plant matrix, which can either be inexhaustive or exhaustive, i.e., they are able to drain the raw material of their target. Exhaustion can be achieved through repeated extraction or strongly elevated partition coefficients. Exhaustive methods are often applied to characterize the phytochemical profile of raw materials as they can be extended as much as necessary to obtain the total of a targeted compound. In contrast, inexhaustive methods are not designed for the recovery of the total amount of a target. However, these methods are faster and need less solvent. In the following, a more detailed description of Soxhlet and maceration extraction will be presented and an overview of some important extraction techniques will be given in Table 2-1 at the end of the chapter [2–4,29,36,41–44].

2.2.1 Soxhlet Extraction

Soxhlet extraction, also known as continuous extraction, was developed in the last century by Franz von Soxhlet to analyze the fat content in dried food [35]. It is a method to remove target compounds exhaustively from their matrix through repeated solvent extraction. Thus, it can be used as a reference to evaluate the quality of other extraction methods. The apparatus can be described as a closed solvent circuit comprised of a round bottom flask serving as a solvent reservoir, an extraction chamber, a siphon tube, and a reflux condenser. A porous container called a thimble, which is usually made of strong filter paper, holds the sample (cf. Figure 2-2). Through refluxing and condensing, the extraction solvent can pass through the sample, continuously extracting it. When the extraction chamber is filled to capacity, the solvent with the extracted material is drained through the siphon and returned to the solvent reservoir, which consequently gets enriched in extractant. The process is repeated until the raw material is completely depleted of the extractant. Extracting with a Soxhlet apparatus yields highly concentrated extracts while using moderate amounts of solvents. On the other hand, long extraction periods of up to 24 h and thermal degradation of temperature-sensitive compounds are its main drawbacks [2–4,35,43].

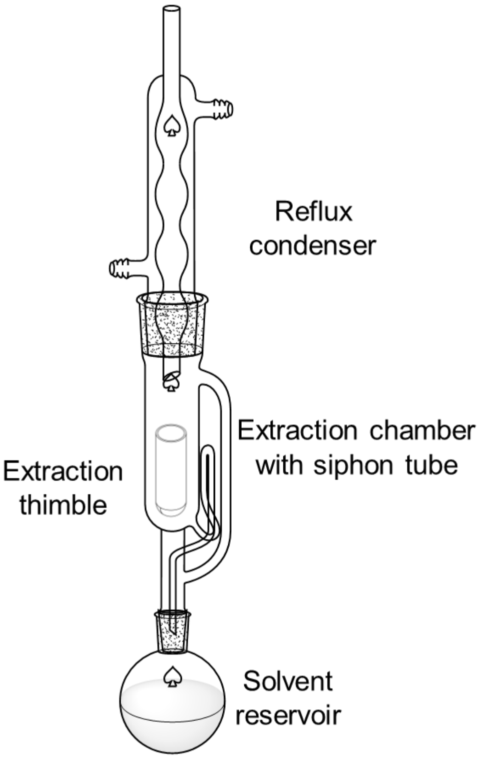

Figure 2-2: Laboratory diagram of a Soxhlet apparatus. The templates of the glassware were provided via ChemDraw 18.1 by PerkinElmer.

2.2.2 Maceration

Maceration or soaking is a very simple and cheap extraction method without high applicational effort. Commonly, this extraction procedure is performed at room temperature, making it a suitable method to extract thermolabile compounds. However, depending on the desired results, the temperature can be adjusted [2–4,35,43,45].

The extraction is performed by putting the sample in a container, immersing it in the solvent, which is usually of organic nature, and leaving it for one to three days, depending on the extracted material and the literature, to ensure that the soluble matter has dissolved in the solvent. Agitation can either be applied continuously or sporadically to increase the mass transfer and diffusion while avoiding supersaturation in the solvent surrounding the sample particles. Also, motion in the sample prevents bed compression of the raw material, which would slow down the extraction efficiency. After the extraction, the remaining marc has to be separated from the solvent, which is achieved through pressing, decantation, filtration, or clarification. To obtain the pure extract in a final step, the solvent has to be removed, e.g. through evaporation [1,3,4,29,43–45].

Through repeated maceration of the raw material with control percolation at the end, this extraction method can be made exhaustive [46]. Its big versatility still makes it a very popular process. However, the huge consumption of solvent and the long extraction periods are the grave disadvantages of maceration extraction [1,3,4,29,43,44].

2.2.3 Nonconventional Extraction Methods

Apart from the classical methods (Soxhlet Extraction and Maceration), the scientific community thrives in developing alternatives that are able to improve the extraction yields while minimizing the practical efforts, solvent consumption, and extraction durations. These ameliorations can either refer to the progress made on new techniques and apparatus or novel solvents.

Amongst others, microwave-assisted (MAE) and ultrasound-assisted (UAE) extraction methods have been on the rise. Both techniques increase the applicational efforts only slightly, with the benefit of reducing the necessary amount of solvent and the time of extraction. This is achieved through elevated solvent penetration and diffusion promoted by interactions of the microwaves and ultrasonic soundwaves with the plant material. Microwaves act through localized internal superheating, leading the plant cells to explode and ultrasonic waves in a frequency range of 20-200 kHz cause cavitation in the cell walls yielding extraction results [3,29,43].

Several attempts were made to replace conventional solvents with more effective alternatives. Their value either comes from reducing the necessary purification steps after the extractions or improving the extraction yields. One very prominent example is the extraction using supercritical fluids. Carbon dioxide in this state of matter has extraordinary solvent properties while not leaving solvent traces behind in the end. However, the necessary equipment is very expensive and complicated [1]. Another effort was made by P. Degot *et al.*, who used a ternary mixture of water, ethanol, and triacetin, with a superior solubility to enhance the extraction yields of curcumin. This solvent could be reused several times to extract fresh rhizomes, reducing the necessary amount of solvent [47,48].

These discussed techniques are all in accordance with the six principles of green extraction as proposed by F. Chemat *et al.* [7], which will be discussed in the next chapter.

Table 2-1: Overview of various extraction techniques, conventional and nonconventional [2–4,29,36,41–44].

Method	Solvent	Time	Temperature
Maceration	Aqueous and organic	Long	Room temperature or under heat
Percolation	Aqueous and organic	Long	Room temperature or under heat
Decoction	Water	Moderate	Under heat
Soxhlet	Volatile, organic	Moderate	Under heat
Microwave- and Ultrasound-assisted	Aqueous and organic	Short	Room temperature or under heat
Supercritical fluid	Supercritical fluids plus additives	Short	Close to room temperature

2.3 Green Extraction and Green Solvents

The concept of green chemistry came into being already throughout the 1960s triggered by R. Carson and her book *Silent Spring* criticizing the neglect of the environment by the industry and politics [49]. This piece of writing forged a new awareness for environmental care and can be seen as an inspiration for the modern environmental movement [50]. Successively, several ideas to improve the chemical synthesis in terms of atom efficiency and catalysis to tackle the wastefulness of some processes developed. Pioneered by P. Anastas and J. Warner in 1998, they postulated the so-called *12 Principles of Green Chemistry*, which are described in more detail in Section 9.2, to draw attention to chemical pollution and resource depletion in an attempt to lead the way to a greener future [6,51]. Green chemistry got a name and became a movement. Also known as sustainable, clean, benign, or environmental chemistry, the name *green chemistry* stuck due to its colorful language, alluding to nature and being associated with peace, life, and nature [52].

Green chemistry has to be understood in its entirety. The twelve principles cannot be seen as isolated accomplishments that can be reached separately. Processes advertising greenness by only taking into account single points are “green bait” and can be seen as nothing more than marketing ploys. Of course, change takes little steps and greenness is a relative concept. However, only the interplay of all presented ideas will lead to the goal of improved interaction with the world and its resources. This is why innovation is key. Instead of seeing these proposed ideas as restrictions of what cannot be done, they should be seen as motivation to find alternative solutions, fostering new ideas and competition [53,54].

In the case of extraction, F. Chemat refined the principles of green chemistry to fit the needs for sustainable procedures in his 6 Principles of Green Extraction [7]:

- Renewable resources and variety should be the driving force of innovation and selection.
- Alternative solvents, preferably water and solvents from agricultural resources, should be used.
- The energy consumption should be reduced by recovery processes or innovative technologies.
- Waste production should be avoided by producing co-products for the bio-refining industry.
- Conventional unit operations should be replaced with safer, more robust, and controlled processes.
- Non-denatured and biodegradable extracts without contaminants should be the aim of any extraction process.

These six principles are a guide for the industry and researchers alike to develop sustainable extraction processes. In easier terms, these principles give the input to improve established procedures, especially in terms of rethinking the use of equipment and examining new solvents [7].

Solvent selection in general is a broadly discussed topic of vested interest. The demand for solvents is high, constituting approximately 80-90% of the total volume of chemicals [55]. Of course, solvents are ubiquitous in chemistry thinking synthesis, extraction, and purification. Thus, the sustainability of these processes and the resulting products are mainly defined by the sustainability of the employed solvent [6,7,55]. Different approaches on how to pick the optimum solvents have been introduced, among others, companies like Pfizer, AstraZeneca, and GSK as well as the Innovative Medicines Initiative proposed selection guidelines [54]. The common question these guides have to answer is [56]: “What is a green solvent?”

The difficulty in answering this question lies in the fact that the definition of greenness is relative and that no solvent is the best alternative to any solvent [57]. However, the points on which all of them can agree are that the environmental, health, and safety properties have to be the focus while toxic and harmful solvents must be replaced [56]. The ranking systems of these proposed guidelines are very similar and usually come to comparable results. Considerations are often placed on the exposure limit values, boiling and flash point, and the solvents’ origin [58,59]. Apart from the conventional solvents some guidelines also consider neoteric and renewable ones. However, these guidelines only regard the greenness of a solvent but not its performance, which makes sense, of course. How could they also pay attention to the countless processes where solvents are needed? Naturally, neoteric solvents like ionic liquids, deep eutectic solvents (DES), and supercritical solvents seem to be greener than the established ones. Yet, the whole lifecycle of any given process has to be regarded to be able to decide whether the replacement of the conventional solvent is really a step towards greenness [54,60]. But progress sometimes comes from trial and error or from taking risks, thus, the research concerning novel solvents continues. Especially the investigation of aqueous solvent systems, ionic liquids, DES, bio-based, and switchable solvents have been in vogue in recent years [61,62]. This study mainly focused on the examination of natural deep eutectic solvents (NADES) as innovative alternatives. A more detailed overview of NADES will be given in the following chapter 2.4.

2.4 Natural Deep Eutectic Solvents

Deep eutectic solvents commonly abbreviated as DES are a relatively novel class of solvents, which has been mentioned first in 2001 [63]. Their name, a contraction of ευ (*eu*) and Τήξις (*teksis*), which means *easy melting*, finds its origin also in the Greek language [64,65]. Without going too deep into the history of their nascency, it has to be mentioned that DES can be seen as successors of ionic liquids. Ionic liquids were in their prime during the beginning of this century as they were deemed the new and green alternative to conventional organic solvents. They are described as solvents solely consisting of ions with a melting point lower than the arbitrary temperature of 100 °C. Nowadays when talking about ionic liquids, the discussion centers on discrete ions like organic cations such as quaternary ammonium ions (QAs), mostly imidazolium-based but not limited to it, and tetrafluoroborate or acetate anions. They are mostly robust against ambient conditions and can be tuned towards their field of application. However, they do not fully comply with the principles of green chemistry in terms of their health and environmental effects or their way of synthesis. Thus, the discovery of DES seemed to be the more promising solution [66–68]. For a more thorough description and more information on the history and application of ionic liquids, the work of N. Plechkova and K. Seddon [69] can be recommended and a comparison between ionic liquids and DES is given in Table 9-4 of the Appendix.

Coming back to A. Abbot *et al.* [63], deep eutectic solvents were described as mixtures of at least two Lewis or Brønsted-Lowry acids and bases. In their ideal eutectic molar ratio, these mixtures yield the lowest melting point T_ε relative to the melting temperatures of their initial components [67] (cf. Figure 2-3). In easy terms, a melting point depression upon mixing of the components occurred. Above the round phase borders, the unified liquid medium can be found, while below crystallization of one or all compounds takes place.

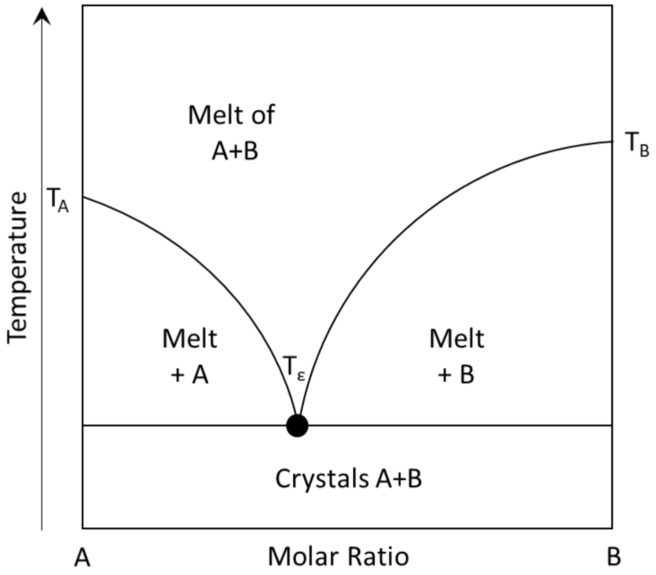

Figure 2-3: Typical phase diagram of a binary eutectic mixture of compounds A and B, with their single melting temperatures T_A and T_B and the eutectic melting temperature T_ε at the eutectic molar ratio [65,66,70].

The strong melting point depression is caused by intermolecular interactions, mostly hydrogen bonding interactions between a hydrogen bond donor (HBD) and a hydrogen bond acceptor (HBA). Also, Van der Waals forces can contribute to a small extent. The decrease in lattice energy of the single molecular units through these intermolecular interactions is the driving force behind the DES formation while the extent of melting point depression in a eutectic mixture is influenced by the interactions' strength [71]. Nuclear magnetic resonance (NMR) as well as infrared spectroscopy and mass spectrometry combined with computational models like the conductor-like screening model for real solvents (COSMO-RS) are used to monitor the interactions, but suitable mixtures have still to be found through trial and error as predictions about the necessary intermolecular interactions are difficult [68,71]. However, the most common molar ratios of binary DES are 1:1, 1:2, and 1:3 (*n/n*) with 44%, 20%, and 9% respectively [72].

In contrast to ionic liquids, which are molecular entities bound by ionic forces, the intramolecular interactions of DES are of low thermodynamic stability which makes them susceptible to changes in their chemical environment. This can lead the DES to dissociate [72,73].

To be able to differentiate possible deep eutectics depending on their complexing agent and to navigate their fields of application, they can be divided into four classes [65,66,73]:

- **Organic Salt + Metal Salt:** Often quaternary ammonium salts, e.g., imidazolium-based ones, are complexed with metal halides to form low melting mixtures, but the range is limited.
- **Organic Salt + Metal Salt Hydrate:** The DES with hydrates as complexing agents are a derivative of the first type of DES. They are relatively cheap and air/moisture insensitive, which makes them interesting for industrial purposes.
- **Organic Salt + HBD:** These eutectics are often based on choline chloride. Amino acids are possible as well, mixed with hydrogen bond donors such as alcohols, organic acids, amides, or carbohydrates. Combinations of various carbohydrates also fall in this category. This third type of DES builds the basis of natural deep eutectic solvents (NADES), which are DES made exclusively of natural ingredients. The focus of this study is put on this type of DES, which will be described more thoroughly in the following.
- **Metal salt + HBD:** The last class of DES is a derivative of the previous one, replacing the organic salt with an inorganic one, which proved useful in plating applications.

NADES are a subclass of DES. They are characterized, as mentioned above, by their ingredients, which are completely derived from nature and, therefore, count as sustainable. Mostly, primary metabolites with high abundance throughout all living cells are the building blocks of NADES. In their first mention by Y. Choi *et al.* in 2011 [8], it was hypothesized that NADES are a third class of liquid phase in organisms aside from water and lipids. This hypothesis could not be proven yet, still, there is some circumstantial evidence. According to the study, NADES serve as solubilizers as well as solvents in the biosynthesis, transport, and storage of molecules that are poorly soluble in both water and lipid environments. Besides, some plants are able to survive extreme temperature conditions, either hot, as the NADES can supposedly stabilize membranes and enzymes while water is scarce, or cold, as they can avert the rupture of cells through crystallization by preventing water from freezing [74].

Since they are abundant in nature, NADES can be seen as green solvents like mentioned above. However, like most DES, they usually have high viscosities, which limit their application fields. Though, the viscosity of any given (NA)DES can be adjusted by the water content or the temperature of a given process, as a positive linear correlation with higher water contents and temperatures exists [72]. On the plus side, NADES are easy to prepare, usually unreactive with water, relatively low cost, and often biodegradable. Their ability to solve a wide range of molecules, either inorganic or organic, makes them interesting alternatives to conventional organic solvents in a multitude of industrial processes. The choice of possible HBDs is estimated to surpass 10^6, leading to an uncountable number of possible NADES mixtures. Through this enormous variety, each NADES can be tuned to suit the desired application [60,66,71]. Apart from serving as solvents for chemical synthesis or plating procedures, they have been investigated as extraction solvents for secondary plant metabolites, like polyphenols [31]. The application as an extraction solvent and solubilizing agent of polyphenols was also the aspect of the investigation in this study [60].

2.5 UV/Vis Spectroscopy

A simple way to assess the quality of a product, either extract or any processed food, is by looking at the color. To put this in an analytical perspective, optical spectroscopy in the ultraviolet and visible spectral regions (UV/Vis) is the method of choice. This technique is widely used in research, production, quality control, and the examination of new substances as the spectrum can give information about the target substance [75].

The basis of optical spectroscopy is the interaction of radiation with matter. This radiation can be described as an electromagnetic wave traveling through time, which can be characterized by its energy defined through its wavelength or frequency by which it propagates. An overview of the electromagnetic spectrum is given in Figure 2-4.

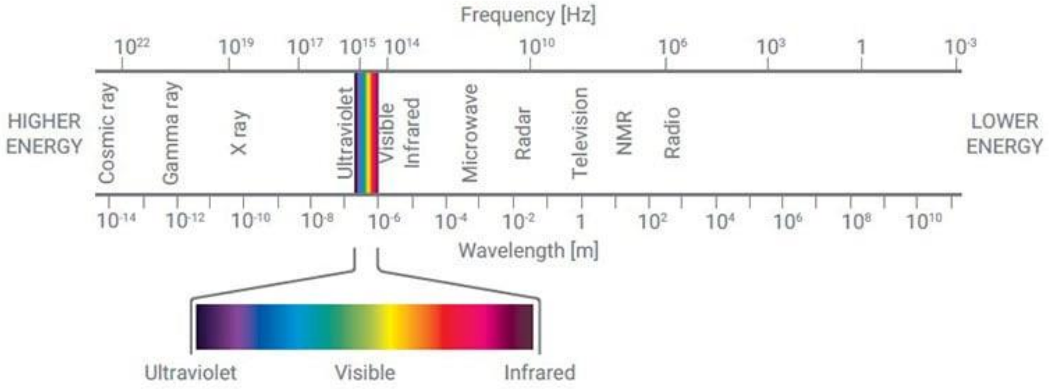
Frequency [Hz]
10²²
10¹⁹
10¹⁷
10¹⁵
10¹⁴
10¹⁰
10⁶
10³
1
10⁻³
HIGHER ENERGY
Cosmic ray
Gamma ray
X ray
Ultraviolet
Visible
Infrared
Microwave
Radar
Television
NMR
Radio
LOWER ENERGY
10⁻¹⁴
10⁻¹²
10⁻¹⁰
10⁻⁸
10⁻⁶
10⁻⁴
10⁻²
1
10²
10⁴
10⁶
10⁸
10¹⁰
Wavelength [m]
Ultraviolet
Visible
Infrared

Figure 2-4: Electromagnetic spectrum with expanded visible (Vis) spectrum of 350-700 nm followed by the ultraviolet (UV) spectrum in a range of 200-350 nm. The picture was taken from Agilent [76].

Depending on the literature, ultraviolet light is defined to cover the spectral region of 200-400 nm, while visible light can be observed from 400-700 nm [77,78]. Like in Figure 2-4, the human eye can detect these rays by means of color, giving the visible spectral region its name. The spectroscopic analysis of samples in both regions of energy is known as UV/Vis spectroscopy. Radiation of higher (X-ray) or lower (infrared) energy can be used for other analysis methods, often in terms of structure determination [78].

Light can interact with matter in different ways, either through scattering, optical rotation, and, in the case of spectroscopy, absorption and emission. Absorption and emission can only take place for discrete amounts of energy, which can be described by the Bohr-Einstein frequency relationship (2-3) [35,78]:

$$\Delta E = h \cdot \nu = \frac{h \cdot c_0}{\lambda} \tag{2-3}$$

with ΔE = absorbed energy, h = Planck's constant, ν = frequency, c_0 = speed of light in vacuum, and λ = wavelength.

When light is absorbed, it can excite electrons (usually valence electrons) of a molecule's energetic ground state into an excited state. Through emission in terms of radiationless or radiating emission, either spontaneous or stimulated, the energy can be released, returning the molecule to its ground state. If this discrete energy in both cases falls in the visible region of the spectrum, a color impression can be observed [35,79–81].

The wavelength range a molecule can absorb depends on the electronic structure of the molecule, which dictates the energetic position of its ground and excited states. Structure elements with delocalized electrons, like conjugated systems or lone pairs, are able to interact with UV/Vis radiation. The bigger the extended conjugation is, the lower is the necessary excitation energy. Mesomeric and inductive effects can also have an influence on the necessary energy. After absorption, only the reflected part of the light causes the color impression an observer gets to behold, which is why only the complementary color of the absorbed spectrum can be perceived [79].

Absorption spectra are graphical depictions of absorbance as a function of wavelength, which can give qualitative (wavelength of maximum absorbance λ_{max}) and quantitative information about any target molecule. The spectra can be recorded in all states of matter, however, solutions of an approximate concentration of 10^{-4} mol/L in optically pure solvents are preferred [78]. This means that the used solvents must not absorb on their own in the spectral region of interest and cannot have strong interactions with the solvent, which can lead to alterations of the spectrum. When these criteria are met, the target can be measured. To this purpose, the samples are irradiated by light, which is partially absorbed when passing through the sample cuvette. The remaining light intensity is recorded by a suitable detector. The relation between absorbance and light intensity is given in (2-4) [35,78–80]:

$$A = -\log \tau = -\log\left(\frac{I}{I_0}\right) \tag{2-4}$$

with A = absorbance, τ = transmittance, I = remaining light intensity, and I_0 = initial light intensity.

Using the unitless quantity of absorbance is comfortable for the quantitative analysis according to Lambert-Beer’s law which is given in (2-5), as it is related linearly to the concentration of the analyte [35,78–80]:

$$A = \varepsilon \cdot l \cdot c \tag{2-5}$$

with ε = molar extinction coefficient, l = illuminated layer thickness, and c = concentration.

The measurements of UV/Vis can either be performed on a single or double-beam spectrophotometer. A model of the latter is given in Figure 2-5. As the names imply, the devices differ from each other in the number of light beams. With the single beam photometer, the same light beam is used to measure the blank and analyte samples successively on one detector. With the double beam device, the light of one source is split into two identical light beams, which measure the reference and the analyte samples simultaneously on two separate detectors. The biggest advantage of this setup is the elimination of signal distortion by fluctuations of the light source in real-time. Since absorbance is an additive property, the signal of the blank sample is subtracted from the signal given by the analyte sample, resulting in the sole signal coming from the pure analyte [35,80].

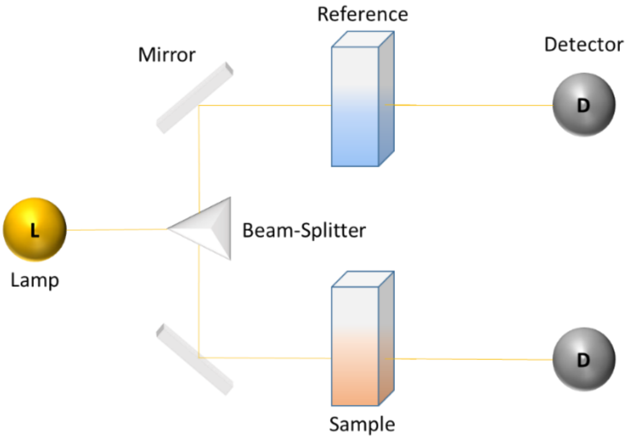

Figure 2-5: Model of a double beam photometer for optical density measurements.

2.6 Nuclear Magnetic Resonance Spectroscopy – NMR

2.6.1 Introduction to Nuclear Magnetic Resonance Spectroscopy

Nuclear magnetic resonance spectroscopy (NMR) is one of the most vital and impactful analytic methods of identification and structural characterization of molecules. It studies the energetic behavior of molecules, in particular of their nuclei, in an electromagnetic field subjected to radiofrequency, which was first discovered by P. Zeeman in the 19th century [80,82]. Regarding Figure 2-4, the radiofrequency can be found at the low energy end of the known electromagnetic spectrum, possessing low frequencies ($> 10^{10}$ Hz) and large wavelengths ($< 3 \cdot 10^7$ nm). In contrast to electrons, nuclei are far heavier, which is why additionally to the irradiation a strong magnetic field B_0 with frequencies of 300-900 MHz is necessary to excite them [35].

Most nuclei possess a spin angular momentum P, also called nuclear spin, which is disparate to zero. A prerequisite for the existence of this spin is that either the number of protons, the nucleon number, or both of a certain nucleus are uneven. If this condition is fulfilled, the nuclear spin will also have a corresponding magnetic moment μ_M (cf. Equation (2-9)) [78,82,83]:

$$\mu = \frac{\gamma \cdot h \cdot \sqrt{s(s+1)}}{2\pi} = \gamma \cdot P \qquad (2\text{-}6)$$

with γ = gyromagnetic ratio, h = Planck's constant, and S = spin quantum number of the nucleus.

In this case, γ is a proportionality constant, which is characteristic of each isotope of any element. It is an indicator of the abundance and the sensitivity of detection of a certain nucleus as it is directly proportional to the magnetic momentum [80].

In the ground state, all nuclei possess the same level of magnetic energy E. When applying a strong external magnetic field, this energy level can degenerate into $2S+1$ quantized levels of different magnetic energy, which is called the Zeeman effect. These different states of energy correspond to the orientation of the magnetic moment in relation to the direction z of the magnetic field B_0. The energy can be described according to the following relation (2-7) [82]:

$$E = -\mu \cdot B_0 = -\frac{m_S \cdot \gamma \cdot h \cdot B_0}{2\pi} \qquad (2\text{-}7)$$

with m_S = magnetic quantum number of the nucleus.

The most common nuclei to examine are ^{1}H and ^{13}C, which possess a spin quantum number of 0.5, resulting in a degeneration into only two different states. The difference in energy ΔE between the two energetic states is directly proportional to the strength of the magnetic field. It can be overcome by absorption of radiation. As mentioned above, only discrete energies of electromagnetic waves can be absorbed (cf. Equation (2-3)). The amount of absorbed energy depends on many factors, amongst others the strength of the external magnetic field, the nucleus' interactions with its surroundings, like additional nuclei or the electron shell, and the effective magnetic environment of the molecule itself [80]. The low energy state is oriented parallel along the magnetic field's direction ($+z$), while the state of high energy will align itself antiparallel to the magnetic field ($-z$). Because of the spin angular momentum, the magnetic moment cannot adjust itself perfectly parallel to the magnetic field. The effect of the magnetic field on the nuclei, thus, is rather a deviation of the spin resulting in a complex rotational pattern. This can be described as a wobbling motion of some sort, which is called precession [84].

When subjecting the nuclei to a radiofrequency of adequate energy (Larmor frequency) perpendicular to the magnetic field, absorbance can take place, leading to a “flip” from the $+z$ to the energetically higher $-z$ state. Through relaxation phenomena, the nuclei can return to their ground state. An equilibrium between the population of the ground N_0 and excited states N_1 is established, which can be described via the Boltzmann equation [82]:

$$\frac{N_1}{N_0} = e^{-\frac{\Delta E}{k_B T}} \tag{2-8}$$

with ΔE = difference in Energy, k_B = Boltzmann constant and T = temperature.

A slight excess of the species in the ground state, which is of course dependent on the system’s energy, prevails in equilibrium. This uneven distribution of relaxed and excited nuclei provides the signal that can be measured in NMR [82].

Coming back to the influence of a nucleus’ environment, there are two major effects on the signals that have to be discussed. The first effect is the chemical shift. The nucleus in question is shielded from the external magnetic field by its surrounding electron shell as well as other nuclei. Thus, the effective magnetic field of the nuclei will always be smaller than the external one. Depending on the distance of the electrons to the nucleus, the shift can be larger with close electrons or smaller due to electrons being far away from the nucleus. The chemical shift is a relative number given in ppm referring to an internal standard, which is usually the signal of tetramethyl silane at 0 ppm [35,78,80].

The second effect is the so-called spin-spin coupling. A fine structure of signals can be obtained through interactions with the effective magnetic field of neighboring, non-equivalent nuclei, either of the same kind (homonuclear) or a different kind (heteronuclear). Through the effective magnetic field of a nucleus’ neighbors, it may also orient itself alongside its neighbors’ magnetic fields, leading to a split of the signals. Depending on the number of bands of a peak, it can be characterized as a singlet, doublet, triplet, etc., or commonly as multiplets [78,80]. Couplings can occur between direct neighboring nuclei, but also between nuclei that are separated by two to three bonds. The complexity of coupling patterns, of course, becomes more complicated, the more nuclei participate. For more information confer to M. Hesse, H. Meier, and B. Zeeh [78].

2.6.2 Nuclear Overhauser Enhancement Spectroscopy – NOESY

The nuclear Overhauser enhancement spectroscopy (NOESY) deals with the interaction of nuclear dipoles coupling throughout space. Cross-relaxation and chemical exchange processes can be examined [85]. The basis of this method is built on the nuclear Overhauser effect, which describes the overall intensity change of one resonance while in close proximity to a saturated one. The system will be brought out of equilibrium through the oversaturation of one nucleus. To return to an equilibrium state, the probability of zero- or double quantum relaxation transitions will increase. The relaxation follows a dipolar mechanism, which also explains the spatial dependence as dipolar interactions depend on the distance to the sixth power. Thus, interactions in a distance of less than 4-5 Å between two spins can be examined [83,86].

For homonuclear proton-proton examinations, the frequency labeling of the magnetization, the nuclear Overhauser effect through cross-relaxation between interacting dipoles, and the measurement of the induced signals of the exchanged magnetic moments are achieved through a series of three non-selective 90° pulses. Through Fourier transformation, the spectrum is produced [85,87]. On both axes, the chemical shifts of the protons are shown. The correlations of the single peaks themselves yield the dots filling the diagonal. Off-diagonal signals which occur symmetrically to the diagonal indicate exchange processes transferring magnetization after the second pulse. The location of these signals then identifies the interacting protons [78,87].

2.7 Chromatography

The word chromatography finds its origin in the Greek language, coming from the words χρῶμα (*chroma*) and γράφειν (*graphein*), which translates to *color writing*. The phenomenon with its name was first described at the beginning of the 20th century by M. Tsvett, who tried to separate colorful plant pigments on a glass column of chalk. However, one cannot only grant M. Tsvett praise for developing this technique which is now known as chromatography. Adsorption experiments for separation on paper have far preceded him. Yet, the research that made the method the versatile tool that it is, was mostly based on M. Tsvett’s observations, making him the father of chromatography [88,89].

Chromatographic processes are the principal tools to separate plant extracts with a subsequent concentration determination of the target compounds. Different categories can be distinguished by regarding the mechanical setup with the most popular being thin layer, column, and gas chromatography. The separation for all techniques relies on the interaction of the analytes in the mobile phase with the stationary phase. The mobile phase, which can be a liquid, gas, or in newer technologies a supercritical fluid, is the carrier of the analyte, which moves past the stationary phase, which is either an immobile solid or liquid film. Both phases need to be able to interact with the analytes either physically or chemically. Differential partitioning of the analyte between the two phases is responsible for the retention time differences and subsequent separation of several analytes. Analytes with a stronger interaction with the stationary phase spend more time passing it by, i.e., they have a longer retention time. Analytes with a weaker interaction, on the other hand, pass by faster, leading to a shorter retention time [81].

Looking at column and gas chromatography, separation with successive detection yields so-called chromatograms, which are graphical depictions of a certain signal impulse intensity of the detector on the ordinate and the retention time on the abscissa. The area under the signal peaks can be used as an indication of the concentration. In an ideal experiment, the obtained signals are sharp, symmetric Gaussian peaks, which are clearly separated. The height and area of the signals can give quantitative information about the analytes in the sample, while the retention time may give qualitative information. However, real live samples may deviate from the perfect peak shape in terms of broadening, asymmetry, or tailing. These distortions are caused by three different physicochemical phenomena, which were summarized by J. Van Deemter *et al.* [35,89–92]:

- **A – Multi-path dispersion:** This effect is also known as Eddy-diffusion. It is caused by uneven particle movement through the stationary phase as not all particles move along the same way and do not have a uniform flow velocity. Thus, an irregular and broadened retention occurs, which can be described by the constant term in the Van Deemter equation (cf. Equation (2-9)).
- **B – Longitudinal diffusion:** Particles not only move through transport along the separation axis but also passively through diffusion. Diffusion can go in any direction, independent of the separation axis, leading to peak broadening,

which is described by the B-term of the Van Deemter equation (cf. Equation (2-9)). However, it has to be noted that this effect only contributes significantly at low flow rates.

- **C – Mass transfer phenomena:** The resistance of mass transfer in the mobile and stationary phases, especially at the beginning and the end of a sample zone, is caused by varying progression velocities of the sample around the stationary phase and pools of trapped mobile phase in the pores of the packing material. The concentration at the edges of a sample zone changes more drastically so that only local equilibria can be established, which are different at the beginning and at the end of the zone. This broadening phenomenon can be described by the linear term of the Van Deemter equation (cf. Equation (2-9)) and becomes prominent within columns packed with large particles and at high flow rates.

These three causes of peak broadening can be used to calculate the ideal height equivalents to a theoretical plate of a chromatographic column according to the Van Deemter equation (2-9). In a combination of the terms described above, *HETP* must reach a minimum to guarantee a most effective separation [35].

$$HETP = A_C \cdot \frac{B_C}{u} \cdot C_C \cdot u \tag{2-9}$$

with $HETP$ = height equivalent of a theoretical plate, A_C = multi-path dispersion, B_C = longitudinal diffusion, C_C = mass transfer phenomena, and u = linear velocity.

In the following chapters, two particular column chromatography setups, namely high-performance liquid chromatography (HPLC) and gas chromatography (GC), will be introduced in more detail.

2.7.1 High-Performance Liquid Chromatography – HPLC

High-performance liquid chromatography (HPLC) is the most widely used analytical technique for separating mixtures like plant extracts with subsequent analysis of compounds [88] as it can be used for 60-80% of all known compounds [89]. It is especially useful for thermolabile analytes or analytes which are not volatile or too hard to derivatize [89]. A schematic depiction of an HPLC system is given in Figure 2-6 and the single components will be explained in the following.

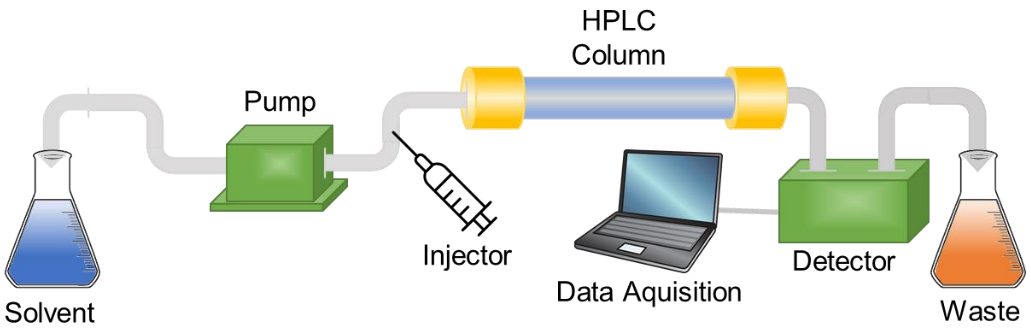

Figure 2-6: Schematic set-up of an HPLC system. The picture was inspired by bionity.com [93].

The device consists of a solvent transport system that is liquid and can be a mixture of one or more solvents, called eluent. Ideally, the solvents are of high purity, of low cost and viscosity, as well as non-toxic and non-corrosive towards the entire HPLC system, and have a high solubility for the analytes [89]. The solvent flow can be applied in two different modes, either the isocratic mode, in which the solvent remains unchanged throughout the whole elution, or the gradient mode, in which the solvent can change its composition over time. A gradient is used to improve the separation of similar compounds, yielding a higher resolution of the chromatograms. The pumps keep the mobile phase afloat throughout the whole system. The pressure can be adjusted to be constant or to change over time. An eluent flow rate of 0.1-5 cm/s, translating to 0.7-1.5 ml/min, yielding system pressures of 10-400 bar is ideal for good separations [80].

The injector is the point of the HPLC arrangement where the sample is introduced into the system. The injection is automated to obtain quantitatively reproducible results, which is most precise at high pressures. The samples must not contain any solids, as this could clog the column. Ideally, solid analytes are solved in the eluent. Successively, the sample solutions are filtered, which is an essential step before injection. Sample volumes of 1-2000 µL are advisable, depending on the amount of analyte in the samples. In this thesis, 10 µL was the volume of choice. An overload with sample leads to the broadening of peaks through tailing or fronting. Depending on the column, 1-100 µg of sample component per gram column material can be loaded on the column [35,80].

The columns can have a dimension in the mm to cm area with a diameter of conventionally 2-4.6 mm [35]. They are made of steel, glass, or polymers and are the heart of any HPLC apparatus. They contain the stationary phase, made of silica or polymers with particle sizes in the range of µm [35,77,80]. Depending on the process and the analytes, the stationary phases can be varied. Amongst others, exclusion, salting out, partition, affinity, and ion chromatography are some options for specialized applications. For more information about the kinds of chromatography, it is advised to consult M. Dong [89]. A more basic and common kind of chromatography is adsorption chromatography, which can be subdivided into normal- and reversed-phase chromatography. In the case of adsorption chromatography, the retention of the analytes is linked to their preferential adsorption to the stationary phase. In the normal phase chromatography, polar stationary phases with active surfaces, like free silanol groups, are used. Molecules with free electrons, functional groups, or double bonds may interact with the stationary phase and can be eluted with non-polar solvents like hexane. However, there are some drawbacks to performing normal phase chromatography, like the water content of the solvents. The content of water has to be monitored closely, as it can have a big influence on the separation. Additionally, the big surface of the silica material is prone to irreversible adsorption and is sensitive to pH changes [81,89].

To tackle these problems, chemical modifications through alkyl substitution on the free silanol groups of the stationary phase's surface can be made, reversing the polarity of the latter. Usually, C8 or C18 moieties – but also nitrogen and oxygen-containing ones are possible – are linked to the silica surface to create the desired polarity. Though, not all free silanol groups can be connected to the alkyl bodies due to steric reasons. To prevent unsought adsorption, like in the normal phase, the silanol groups can be *end-capped*, e.g., with trimethylsilyl chloride. Since the polarity of the stationary phase is altered in the reversed-phase mode, also the polarity of the mobile phase has to change. Thus, preferably, water, methanol, acetonitrile, or mixtures thereof are used, especially in gradient mode to improve the resolution. Flushing the column with pure organic solvent after each elution can remove hydrophobic residues [35].

After passing the column, the separated analytes are monitored by a detection system of high sensitivity. During the detection process, the analytes may be analyzed qualitatively and quantitatively. The retention time, volume, and factor can be examined in terms of qualitative analysis, while the peak height and area give quantitative information. The peak area, however, is more precise, even though the height can be used if the resolution is poor [77]. In any case, calibration is necessary, either internal, through the addition of an internal standard, or external, by preparing a calibration curve. Most detection systems following HPLC are non-destructive and can be used independently or in series for a more thorough examination. Commonly, UV/Vis or refraction detectors are employed, but also fluorescence, electrochemical, and mass spectrometric detection is an option. The key element of every detector is its measuring cell. It possesses a special Z shape with a diameter of 0.15-0.5 mm, a length of 1 cm, and a volume of 10 µL [35] to facilitate the detection. In the case of UV/Vis, this Z-shaped cell makes use of Lambert-Beer's law (cf. Equation (2-5)), increasing the illuminated path length, leading to a higher sensitivity. The signals of any detector are then sent to the corresponding software generating the chromatograms while the passed eluent is discarded in the waste [89].

2.7.2 Gas Chromatography – GC

Gas chromatography (GC) is the second most important separation tool, following HPLC, to examine especially organic, volatile compounds. It was introduced in 1952 by Martin and James [35]. Approximately 15-20% of all known compounds can be investigated using this method [35,89] as it is limited to molecules that can be vaporized without degradation.

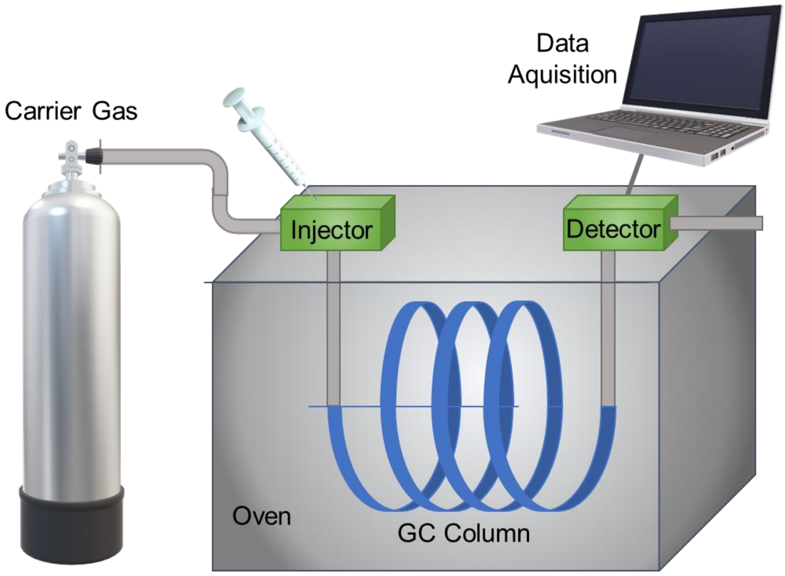

Figure 2-7: Schematic setup of a GC apparatus. The image was inspired by D. Hage [77].

In contrast to HPLC presented before, GC does not use liquid mobile phases but inert gasses like nitrogen, helium, argon, carbon dioxide, or hydrogen to transport the gaseous samples through the column. In Figure 2-7 a schematic setup of a GC apparatus is presented. The arrangement of a GC system does not differ too much from an HPLC device (cf. Figure 2-6). After all, the principle of separation is the same: After injection, the eluent, in this case the carrier gas, transports the sample through the column with the stationary phase for separation and successive detection. The particularities of the GC constituents will be illustrated in the following.

The gas, as mentioned above, acts as the carrier for the analyzable substances. It has to be inert so as to prevent any undesired reactions with either the analytes or the packing material. Additionally, the gas should be of high purity as contaminants like water or oxygen may harm the column, have an influence on the detector, and affect the measurements. Molecular sieve beds and inline traps on the gas sources are used for purification before having the gas enter the GC system. The gas is provided by a standard gas cylinder, but a gas generator is also an option. Controlling the pressure, mostly done by simple pressure regulators, is of utmost importance to ensure a well-defined carrier gas flow. This is necessary for reproducible elution and to maintain column efficiency. Flow rates of 10-60 mL/min and 1-2 mL/min are typical for packed and capillary columns respectively [35,77,80].

The introduction of the sample into the GC circulation has to be accomplished without disrupting the column’s gas flow. While gaseous samples can be administered with the gas flow, liquid samples are evaporated before being injected. If samples are not volatile or thermostable enough by themselves, derivatization can offer relief. Commonly, 0.5-10 µL samples are necessary for an adequate load of the injector. Split/splitless injectors, which separate the gas stream, are used particularly for capillary columns to avoid overloading them. With a split injector, volumes as small as 0.001 µL can be applied to the column [35,77,80].

There are two types of columns for GC, packed columns made of steel or glass with a diameter of 3-6 mm and a length of 1-3 m and capillary columns of fused silica with 100-800 µm diameter and lengths up to 100 m. The focus will only be placed on the capillary columns. Because of their dimensions, capillary columns are more efficient in terms of separation and resolution, which is why they are the most common type of GC columns [77]. They are coated with a thin layer of polyimide for protection and flexibility on the outside. On the inside, the stationary phase is attached or coated on the surface. Liquid stationary phases are an option, just like solid particles or particles coated with a liquid, which offer a variety of applications. In addition to the column, the separation is also driven by temperature effects, which can be controlled via the oven. With isothermal temperature programs, the application of GC is restricted as low boiling compounds evaporate fast one after another resulting in overlapping peaks, while compounds with a high boiling point evaporate, if they do so, slowly and yield flat and broad peaks. These problems can be bypassed by temperature programming. At higher temperatures, compounds with low boiling points and interactions with the stationary phase will elute first. The thermal stability of the stationary phase is the limiting factor for temperature programming [35,77,80].

After separation, there are many options for the detection of the separated samples after the column. Most popular is the detection by flame ionization (FID), with which the calculation of the percentile ratio of all compounds is possible, or mass spectrometry (MS) for compound identification [35,77,80].

2.8 Solubility and its Predictions

The solubility of any substance in another substance or a solvent is an intricate phenomenon captivating scientists and non-scientists alike. It seems like some sort of magic to have two or more different substances vanishing into one another and reappearing depending on the temperature. This magic, however, is how solubility is defined: as the quantity of dissolved and undissolved solute in a solvent in equilibrium at a distinct temperature and pressure. Scientifically speaking, this definition of how much solute is indeed soluble in a solvent is helpful when looking at industrial processes, biological processes like oxygen transport, or extraction. Hence, the prediction of solubilities is indispensable. The principle of like dissolves like is a good rule of thumb, of course [40]. Therefore, there are already a lot of passable solvents on the market. However, the prediction is an aid in the pursuit of solvents that are more effective and in accordance with green chemistry [62]. Many models are dealing with the prediction of solutes in certain solvents. Some of the most famous representatives, which will also be discussed in this thesis, are the Hansen Solubility Parameters (HSPs), and the conductor-like screening model for real solvents (COSMO-RS).

2.8.1 Hansen Solubility Parameters

The Hansen model was developed by C. Hansen as an evolution of the Hildebrand parameter. The solubility parameter δ was described as the cohesion energy density according to Equation (2-10) [94,95].

$$\delta^2 = \frac{E}{v} \tag{2-10}$$

with δ = solubility parameter E = (measurable) energy of vaporization and v = molar volume of the pure solvent.

The interactions of a solvent molecule with another solvent molecule are the origin of cohesion energy. This energy is considered to be equal to the vaporization energy and can, therefore, be measured by evaporation of the liquid as evaporation will break all cohesive bonds. While Hildebrand's work was limited to relatively non-polar and non-hydrogen-bonding molecules, Hansen extended this model by taking the multiple parts into account that add up to the energy of vaporization. The three contributions of the Hansen parameters are made up by dispersion (London) forces (E_D), polar interactions, like dipole-dipole interactions, either permanent or induced (E_P), as well as hydrogen bonding (E_H) (Equation (2-12)).

$$E_T = E_D + E_P + E_H \tag{2-11}$$

with E_T = total cohesion/vaporization energy

Dividing the energies by the molar volume like above, the square of the solubility parameter can be obtained (Equation (2-12)).

$$\delta_T^2 = \delta_D^2 + \delta_P^2 + \delta_H^2 \tag{2-12}$$

with $\delta^2{}_T$ = total solubility parameter, $\delta^2{}_D$ = dispersion cohesion (solubility) parameter, $\delta^2{}_H$ = hydrogen bonding cohesion (solubility) parameter, and $\delta^2{}_P$ = polar cohesion (solubility) parameter.

The total solubility parameter, in this case, should be identical to the one determined by Hildebrand. This, however, cannot always be guaranteed, especially for materials with specific interactions, as these parameters rely on heavy predictions and may, therefore, not be completely accurate [62,95,96].

To predict the possibility of solvation, the distance between two molecules, a solute *i* and solvent *j*, in a so-called Hansen three-dimensional space is of great importance. The further the two components of interest are apart, the more unlikely it is for them to be soluble. The distance is calculated as follows:

$$Distance = \sqrt{4\left(\delta_{D,i} - \delta_{D,j}\right)^2 + \left(\delta_{P,i} - \delta_{P,j}\right)^2 + \left(\delta_{H,i} - \delta_{H,j}\right)^2} \tag{2-13}$$

The equation was developed according to experimental data, which showed that the factor 4 was convenient to present the solubility data as a sphere in the three-dimensional space [62,95].

Since their development, the HSPs have been used in many fields of application. They are highly versatile and opened new possibilities when working with solvents, as almost all molecules and sample probes, like pigments, DNA, and even skin can be described in HSP terms. The prediction of solubility can be done in such an easy way and can be applied to various problems [97].

2.8.2 Conductor-Like Screening Model for Real Solvents – COSMO-RS

A. Klamt developed the conductor-like screening model in the 90s as a tool able to predict chemical potentials μ in liquids. The basis for this development were dielectric continuum solvation models, which could include solvent effects in quantum chemical calculations [100–102]. However, these models were not satisfactory as the theory of the dielectric continuum is a linear response theory. In reality, however, polar molecules possess strong electric fields on their surface, leading to a deviation from the linear behavior of the polarizable continuum [98,99,101].

Then, COSMO-RS was developed successively as an extension to these models. It starts at the surface of a molecule, which can be computed by quantum chemical methods. Presenting the whole theory here would extend the scope of this work. But it can be read up in A. Klamt, 2005 [100]. When breaking it down, COSMO-RS links fast statistical thermodynamics, electrostatic surface interactions, and dielectric continuum models with quantum chemistry [99,102,103], allowing for the prediction of a great variety of physicochemical properties.

Essentially, a discrete surface of a molecule localized in a virtual conductor with an infinite dielectric as a new reference state can be characterized by quantum mechanical COSMO calculations. This surface is identified by its charge density σ and can be imagined as a cavity surrounding the molecule. COSMO-RS can split this surface into smaller segments with individual screening charge densities, considering the electrostatic screening by its surroundings and its back-polarization [47,102]. Considering a solute in a solvent, the solute is tightly packed in the ensemble of closely packed and screened molecules. To have an ideal packing, the whole system is compressed, leading to slight deformations of the surface cavities. This spatial arrangement leads to local pairwise interactions of conducting COSMO surface segments. These interactions in real systems lead to a misfit energy E_{misfit} between two non-identical screening charge densities [100,102].

$$E_{misfit}(\sigma,\sigma') = a^{eff} \cdot \frac{\alpha}{2}(\sigma + \sigma')^2 \tag{2-14}$$

with a_{eff} = effective contact area between two surface segments and α = adjustable parameter.

Calculating the probability distribution of a molecule's COSMO surface segments of a specific polarity results in the so-called σ-profile $p^i(\sigma)$, a histogram of charge intensities, which is a characteristic identifier of the molecule. This solute's affinity to surface segments of a distinct polarity of a solvent is given by the σ-potential $\mu_s(\sigma)$. Combining these two variables, the chemical potential $\mu_s{}^i$ of a solute in a solvent can be calculated according to the following Equation (2-15) [47,62,98–100]:

$$\mu_s^i = \int p^i(\sigma)\mu_s(\sigma) + \mu_{c,s}^i \tag{2-15}$$

with $\mu_{c,s}{}^i$ = combinatorial term considering the size and shape differences of the molecules in question.

Based on this theory, COSMO-RS finds its application in many different fields of physical chemistry. It is a strong tool with high accuracy that relies solely on theoretical data without the necessity of experimental input. With far fewer approximations than HSP, it presents an elegant way to predict and elucidate dissolving mechanisms in liquids [62].

CHAPTER 3

ISOLATION OF IRONES VIA SHORT-PATH DISTILLATION

CONTENTS

The advances of the extraction and concentration of γ-irone, the odiferous compound from the rhizomes of *Iris Barbata-Elatior*, will be presented.

3 Isolation of Irones via Short-Path Distillation

The **SKH GmbH** has contributed to the creation of this section by providing the ground rhizomes of *Iris Barbata-Elatior* and by sharing their knowledge. The goal of this study was to extract γ-irone using myristic acid (HMyr) as the extraction solvent and successively concentrating the fatty acid extract via short-path distillation.

3.1 Introduction

Iris Barbata-Elatior is a cultivar of bearded iris. This species, also known as orris or *Iris germanica* L., is ranked among the *Iris* L. genus, which counts roughly 260-300 different species in total [104–106] and belongs to the *Iridaceae* family. The name iris (ίρις) has a Greek origin and means *rainbow*, which is possibly an allusion to the vast diversity of the genus' inflorescence showy colors [105–108].

Experts suppose that the species of *Iris germanica* L. was derived through hybridization and is native to the eastern Mediterranean region [105,109]. It can, however, also be cultivated throughout the Eurasian continent and in the far East [107,108]. The plants are perennial and can grow to a size of 30-100 cm upon flowering. Typical of the species of bearded irises apart from the color variety of the blossoms are the thick hairs on the throat of the flowers leading to the pollen [105,106,110]. Even though the aerial parts have a nice appearance, the plants are not only ornamental. Their rhizomes, which can grow up to 10 cm in length and 3-4 cm in diameter, can be used for propagation/planting and contain the active ingredients [105,106,109].

The rhizomes of *Iris germanica* L. have been studied most extensively [107] as they are a rich source of phytochemicals. Flavonoids, benzene derivatives, and triterpenes can be found [106,108]. These triterpenes are usually called iridals and are the main group of molecules found in freshly harvested rhizomes [104]. They are known to possess pharmacological activities, like antioxidative, anti-inflammatory, and many more properties. To obtain the desired sensory characteristics, resembling the smell of violet flowers, as well, the rhizomes have to be stored for a period of 2-5 years. During this time, the iridals will undergo oxidative degradation, resulting in the fragrant molecules, the irones. Due to the long storage period, which is necessary to obtain these odiferous compounds naturally, they are very valuable. The content of the different regioisomers α, β, and γ (cf. Figure 3-1) varies from species to species of *Iris* and depends on the different iridals present in the rhizomes before oxidation, yielding not only a single irone isomer but usually mixtures [105–107,111]. The cultivar used in this thesis only contained the cis-γ-isomer.

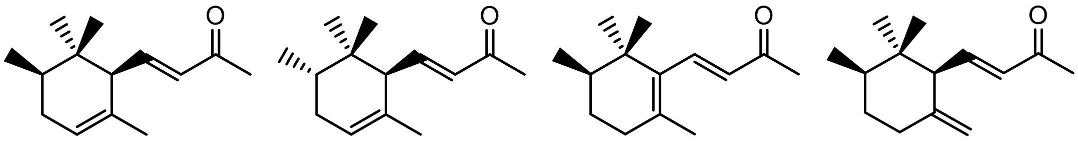
cis-α-irone *trans*-α-irone β-irone ***cis*-γ-irone**

Figure 3-1: List of irone regioisomers. γ-irone is marked in bold as it is the molecule of interest throughout this study and the only irone present in the used cultivar.

To separate the fragrances from the plant, the dried rhizomes in their powdered form with an essential oil content of up to 0.2% [109] are steam distilled. The result in this case is the so-called orris butter, a creamy to waxy solid of mostly myristic acid (up to 85%) and other fatty acids loaded with the irones (~ 15%). Through further processing, orris absolute with higher irone and lower fatty acid contents can be obtained. Both extracts find their application in the cosmetic industry as additives to luxury perfumes, e.g., Chanel *No 19*. [104,105,112].

Looking for green alternatives when extracting is vital in a step towards a greener future [7], especially if the extraction is, like in the case of the irones, very time consuming and elaborate. Thus, an alternative based on a fatty acid extraction with successive short-path distillation, which had specialized in the separation of vitamins from oils [113], was proposed in this chapter. The benefit in this case is that myristic acid, the solvent, is already part of the plant [105].

A liquid boils as soon as its vapor pressure equals the atmospheric pressure. The relation between pressure and temperature has been defined by the Clausius-Clapeyron relation (cf. Equation (3-1)) [114]:

$$\frac{dp}{dT} = \frac{\Delta_{vap}H}{\Delta_{vap}v \cdot T} \tag{3-1}$$

with dp = first derivative of pressure, dT = first derivative of the temperature, $\Delta_{vap}H$ = molar evaporation enthalpy, and $\Delta_{vap}v$ = change of the molar volume of the gaseous (v_{gas}) and liquid (v_{liquid}) phase.

Distillation itself is a simple process of separating liquid mixtures depending on their boiling points. In a binary mixture, the vapor phase is enriched in the more volatile component. The process of distillation exploits this by a sequence of vapor condensation while successively setting a new boiling equilibrium [115].

The separation process of two liquids can be refined by introducing a pressure regulator into a distillation system. Especially problems in terms of selectivity, reactivity, and sensitivity can be bypassed by evacuating the apparatus [116,117].

The short-path or molecular distillation device is an improvement of a conventional vacuum distillation. It is characterized by a short time of heat exposure, low operating temperature, and characteristic mass transfer between evaporator and condenser [113,116,118]. It is deemed as one of the safest methods in terms of separation and purification of thermolabile or low-volatile compounds. Even separations of mixtures with close boiling points or azeotropes should be feasible due to the theoretical basis of the method taking into account the molecular diameter d. Supposedly, molecules of a smaller diameter should be more volatile than larger ones. The collision-free mean path $\langle\lambda\rangle$ of the molecules is described by Equation (3-2) [115,116,118,119]:

$$\langle\lambda\rangle = \frac{RT}{\sqrt{2}\pi d^2 N_A p} \qquad (3\text{-}2)$$

with R = gas constant, T = temperature, N_A = Avogadro constant, and p = pressure.

For practical purposes, it is advisable that the gap between condenser and evaporator is in a similar order of magnitude. High vacuum conditions (10^{-1}-10^{-3} mbar), which are typical for molecular distillation, will yield a necessary free mean path of only a few centimeters [115,118].

Separation of the desired mixtures takes place in the evaporation chamber. The chamber is connected to the pressure regulation, enabling the monitoring of the pressure in the system. Regarding a short-path evaporator, the condenser is located in the middle of the heated evaporator. After introducing the feed into the evaporation chamber, it is agitated by rotor-wipers, spreading it on the walls of the evaporator. This leads to a big surface film of constant thickness and motion, from which the target compounds can evaporate easily. The film thickness depends on the rotor velocity and can range from 0.1-1 mm. No nucleate boiling is necessary for evaporation in this case. After vaporization, the gaseous molecules only have to overcome a short pathway before reaching the condenser and finishing the separation process. Devices equipped with this kind of evaporator chamber are called *molecular distillation* and are able to withstand pressures of ~ 10^{-3} mbar [115,116,118].

3.2 Experimental

3.2.1 Chemicals

All chemicals with their abbreviations, purities, and vendors which were used in this section can be found in the following Table 3-1.

Table 3-1: Chemicals used in Section 3.

Chemical	Abbreviation	Purity	Vendor
Ground Rhizomes of *Iris Barbata-Elatior*	-	-	SKH GmbH, Ortenburg, Germany
α-Ionone	-	> 90%	TCI, Eschborn, Germany
Irone isomers (mostly α-Irone)[a]	-	> 90%	Sigma Aldrich, Darmstadt, Germany
Myristic Acid	HMyr	> 95%, FCC, FG	Sigma Aldrich, Darmstadt, Germany
Methanol	MeOH	> 99.9%	Merck, Darmstadt, Germany
Hexane	-	> 95%	
Sodium Hydroxide	NaOH	p. a.	VWR, Darmstadt, Germany

[a] GC analysis showed a distribution of 49% *trans*-α-irone and 51% *cis*-α-irone (cf. Section 9.3.1).

A special thank you goes to the SKH GmbH for providing the ground rhizomes with a γ-irone content of ~ 1 mg/g free of charge. NaMyr was made in-house by neutralization of myristic acid (HMyr) with sodium hydroxide and successive filtration and drying. Using a Millipore Milli-Q purification system (Merck Millipore, Billerica, Massachusetts, USA), water was deionized. All chemicals were used without further purification.

3.2.2 Methods and Techniques

3.2.2.1 Fatty Acid Extraction of γ-Irone from Iris Barbata-Elatior Rhizomes

3.2.2.1.1 Laboratory-Scale Pre-Tests

To identify the best way of extraction, four different scenarios were examined: extraction of soaked and dry rhizomes with pure HMyr or HMyr with 1 wt% of sodium myristate (NaMyr). All samples were made in triplicates and the extractions were performed in 15 mL centrifuge tubes by VWR (Darmstadt, Germany).

The soaked rhizomes were prepared by macerating 2 g of ground iris rhizomes for 1 h in 10 g Millipore water at room temperature. To remove the excess water, the samples were centrifuged at 4’000 G for 5 min. After taking away the water, the rhizomes were pressed manually in order to remove even more water.

The extraction of both, the soaked and the dry rhizomes, commenced by mixing 2 g (dry weight) of rhizomes with 8 g of the melted extraction solvent (HMyr or HMyr + 1 wt% NaMyr). The mixtures were put into a temperature-controlled ultrasound bath and kept at 60 °C. Every hour the extraction mixtures were sonicated for 20 min and were kept in the bath for 24 h. After this period of time, the extraction was assumed to be completed and the solvent was removed from the rhizomes.

For a quantitative examination, 500 mg of the solidified fatty acid extraction solvent was solved in 10 mL hexane. The same was done for α-ionone. Then 2 mL of the extract solution and 1 mL of the α-ionone stock solution were mixed and topped off to 10 mL with hexane. The samples were filtered into GC vials using 0.2 µm PTFE (polytetrafluoroethylene) filters. Then, the samples were examined via GC-FID.

3.2.2.1.2 Upscaling of the Extraction Process

After determining the best procedure through the pre-tests, the extraction of soaked ground iris rhizomes with HMyr was scaled up in order to successively be able to perform re-extraction of γ-irone from HMyr via short-path distillation.

Thus, 200 g of the rhizomes were soaked in 1 L of Millipore water for 1 h at room temperature and gently shook by hand every 15 min. The excess water was removed by filtrating the mixture through a Büchner funnel applying the suction of a water pump jet. To assist the sucking and drying process, the rhizomes in the funnel were also pressed manually. The process was finished when all excess water was sucked through the funnel and no visible trace of water remained among the rhizomes. The water was discarded as it contained no other molecules of interest. The pressing left a dense and moist mass, which was loosened before further treatment.

The damp rhizomes were transferred quantitatively into 1 L Schott flasks (Schott AG, Mainz, Germany). 600 mL of melted HMyr were added and the mixture was put into a temperature-controlled ultrasound bath at 60 °C for the first round of extraction.

During the first 4 h of extraction, the mixture was sonicated for 20 min every hour. Then it was left to macerate for 48 h. The fatty acid was saved in another flask and the rhizomes were again extracted with 200 g of fresh fatty acid, sonicated as described above, and macerated for 24 h in total with successive removal of the extraction solvent. This procedure was performed twice to ensure an extraction as exhaustive as possible. The extraction solvent of all three extraction steps was collected in one flask and homogenized by melting and pivoting. The extraction was performed in triplicate. The γ-irone content was determined via GC-FID. The samples were prepared the same way as described in Section 3.2.2.1.1 Laboratory-Scale Pre-Tests above.

3.2.2.2 Short-Path Distillation

3.2.2.2.1 Method Development

Samples of 200 g HMyr with 0.2% α-ionone were prepared and homogenized by melting the mixture at a temperature of 60 °C. A screening of different distillation parameters was performed to find the optimum conditions to separate the odoriphore from the fatty acid matrix using a short path distillation apparatus KDL 5 by UIC (Alzenau-Hörnstein, Germany). The conditions can be viewed in the following table:

Table 3-2: Distillation conditions tested for the screening.

$T_{Evaporator}$ (°C)	117			120				123			126	
p (mbar)	2.4	1.8	1.3	2.4	1.8	1.3	0.9	1.8	1.3	0.9	1.3	0.9

These tests were performed in singlets since they only served to get an overview of the distillation behavior. The more promising conditions at temperatures of 123 °C and 126 °C were screened again using a technical mixture of α-irones by Sigma applying the same sample preparation as described above. The irone screening was performed using α-isomers instead of the γ-isomer, as they were available at reasonable prices. The second screening run was necessary to determine if the tested conditions were applicable to irones as they differ structurally and could, therefore, show different thermal behavior, even though the vaporization enthalpies are similar (cf. Table 9-6). To get a statistically significant understanding, the α-irone screening was performed in triplicates.

The intake of the starting materials into the distillation apparatus was controlled by a gear pump with a continuous feeding rate set to 150 rpm, translating to an intake of 270 mL/h. A condenser temperature of 60 °C was held constant for all screening tests to avoid spontaneous freezing of the distillate in the outlet valve. To avoid sputtering of the starting material onto the condenser, as could happen at high rotation speeds, the stirrer velocity on the evaporator wall was kept at 375 rpm.

For the samples containing α-irones, the preparation was carried out analogous to Section 3.2.2.1.1 Laboratory-Scale Pre-Tests. 100 mg of the distillate were solved in 10 mL MeOH. An α-ionone stock solution was prepared in the same way. Then, 2 mL of the distillate solution and 1 mL of the α-ionone stock were mixed and topped off to 10 mL with MeOH. After filtration into GC vials with 0.2 µm PTFE filters, the samples were examined via GC.

3.2.2.2.2 Isolation of γ-Irone from the Fatty Acid Extract

The live sample of extracted iris rhizomes containing γ-irone was re-extracted using the optimum distillation parameters, which were determined in Section 3.2.2.2.1 to be 123 °C evaporator temperature and 1.3 mbar system pressure.

The fatty acid extract was melted and transferred quantitatively into the supply part of the short-path distillation apparatus and distilled according to the parameters mentioned above. The distillate was collected and homogenized by melting. Qualitative analysis was performed according to the sample preparation described in Section 3.2.2.1.1 Laboratory-Scale Pre-Tests. The distillate was then again distilled a second time using the same distillation conditions as before. The new distillate was collected and homogenized yielding the finished product before quantitative analysis via GC-FID.

3.2.2.3 GC-FID Analysis

The quantitative analysis of the odiferous compounds was performed by elution of the samples using a GC-FID 7890A system by Agilent (Santa Clara, USA) with a VF-5ms column (30 m × 250 µm × 0.25 µm) and detection through flame ionization at 300 °C. 1 µL of the sample was injected with a 1:80 split at an injector temperature of 300 °C and eluted with a constant gas flow of 1.5 mL/min with helium as the carrier. The following temperature profile was used: heating from 100-250 °C at a heating rate of 8 °C/min followed by a heating rate of 50 °C/min to 300 °C.

The fragrances α-ionone, α-irone, and γ-irone were analyzed through their retention times and peak areas. The quantitative analysis of the irones was realized through internal calibration using α-ionone. The response factor $f = 0.935$ a.u. between α-ionone and the irones was kindly provided by the SKH GmbH. The mass of the irones (both α and γ) was calculated according to equation (3-3), where *m* represents the mass and *a* the area of the irones and ionone:

$$m_{irone} = f \cdot \frac{a_{irone}}{a_{ionone}} \cdot m_{ionone} \tag{3-3}$$

3.3 Results and Discussion

3.3.1 Extraction of γ-Irone from the Rhizomes of *Iris Barbata*-Elatior

Following the principles of green chemistry, the extraction of the odiferous compound γ-irone of ground iris rhizomes was carried out by using HMyr, a compound naturally produced in the plant, as the main extractant.

The total γ-irone content of 1 mg/g rhizomes, which was determined through repeated solvent extraction in diethyl ether, was given by the SKH GmbH. This result was set as a yield of 100% as this repeated solvent extraction is gentle and exhaustive.

Four different approaches of fatty acid solvent extraction were examined to extract γ-irone from the rhizomes: Soaking the ground, dried rhizomes in water as a pre-treatment, or using untreated, dried rhizomes before extracting with HMyr or HMyr + 1% NaMyr. The results of extractions are presented in Figure 3-2.

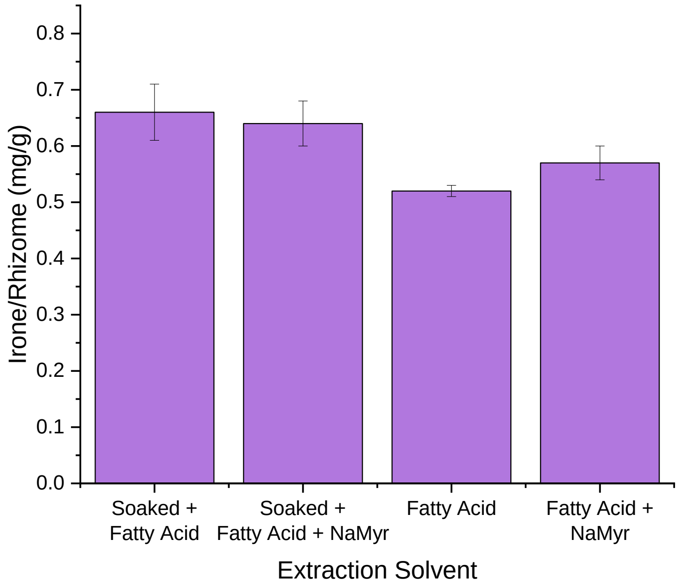

Figure 3-2: Extraction yields of γ-irone in mg/g rhizome with different extraction solvents according to the process described in Section 3.2.2.1.1 Laboratory-Scale Pre-Tests.

The extractions were performed with a powder (dry weight) to solvent ratio of 1:4. The high melting point of HMyr at 53.9 °C [120], however, was a problem throughout all extractions. It was difficult to maintain a high enough temperature of 60 °C to avoid spontaneous freezing of the fatty acid, keeping the extraction medium homogeneous.

The experiments with the soaked rhizomes yield better results (up to 0.66 mg/g) than the extractions with the untreated rhizomes (down to 0.51 mg/g). Through the elevated temperature of 60 °C during the extraction, the mass transfer was enhanced, which is the reason for the rather small yield difference between the untreated and soaked rhizomes. The increase of the γ-irone content of the extract of the soaked rhizomes, however, can be explained by the function of water. It can be assumed that water helped swell the plant cells and burst them during the process [121]. The opened and destroyed plant matrix in turn could be penetrated better by the liquid fatty acid. This allows for a better transfer of the molecule of interest from the plant matrix into the extraction medium. Since the soaked rhizomes were not completely dried before extraction in the fatty acid, the water content in the soaked rhizomes might have been an obstacle. Some water may have still been encased inside the treated cells, retaining the penetration of the fatty acid due to the unfavorable mixing of water and HMyr.

Interestingly, the addition of NaMyr to HMyr had only a small influence when used with the pre-treated rhizomes. The extraction yield from the soaked rhizomes with and without NaMyr regarding the error bars as well was similar. This would indicate that the influence of NaMyr was negligible or even unfavorable with rhizomes soaked in water before the extraction. The addition of NaMyr to the untreated rhizomes, however, did have an influence. Regarding Figure 3-2, the yield was significantly increased through the addition of NaMyr in comparison to the extraction with only the fatty acid. NaMyr in contrast to pure HMyr is more hydrophilic. Compared to the negative influence when using the wet rhizomes, it can be assumed that NaMyr might simulate the hydrophilic swelling effect of the cells. Of course, the 1% of NaMyr is not able to let the cells swell and burst like water is, which is why the yield was lower. However, it is possible that this surfactant can interact with the cells. If this is the case, the ability of the fatty acid to penetrate the cells in contact with NaMyr can be enhanced [122] without being held back by strong lipophobic repulsion.

Considering the results presented in Figure 3-2, soaking the rhizomes in water for 1 h and successive extraction in pure HMyr was the best method to extract γ-irone from the iris rhizomes with a rather low practical effort. The extraction yield in total was unfortunately rather low, only ~ 66%. Therefore, when scaling up, it was decided to extract the iris raw material three times instead of only once, to be able to increase the extraction yield even more. Of course, it is hardly possible to exhaustively extract the raw material in one go [4]. Yet, by repeating the extraction three times, a total extraction yield of 88% could be achieved in the collected extraction medium of the upscaled version. This extract with a γ-irone content of 0.02% ± 0.003% was used as the starting material for the molecular distillation.

3.3.2 Molecular Distillation

Before the extract could be processed further, a method for distilling γ-irone from HMyr had to be developed. For economic reasons, the first screening of the distillation conditions was performed using α-ionone as the target compound. Ionone is structurally similar to the irones found in the plant – for a comparison of the structures see Table 9-1 of the Appendix – but easier to synthesize and, therefore, cheaper (0.47 €/mL from TCI, Eschborn, Germany) than a technical mixture of irones (33.20 €/mL from Sigma Aldrich, Darmstadt, Germany). This mixture was used to assess the thermal behavior of irones instead of using γ-irone itself as no γ-irone samples were available to buy at a reasonable price.

Two restrictions were given before examining the best distillation conditions:

- The temperature of the condenser, which is connected to the outlet valve, had to be at least 60 °C to be able to collect the distillate, high in HMyr, without spontaneous freezing. Solidification of the distillate at a room temperature environment was possible as HMyr, which was inexorably distilled along γ-irone, has a melting point of 53.9 °C according to PubChem [120].
- According to the manual given by UIC [123], the best separation results can be achieved with a temperature difference of at least 50 °C between the evaporator and condenser, ensuring that the distillate will not reevaporate from the condenser.

By using the integrated Clausius-Clapeyron relation [114] (cf. Equation (3-4)), a starting point for the screening was calculated using a 60 °C temperature difference between the condenser and evaporator ($T_{Evaporator} = 120\,°C$). The vaporization enthalpy $\Delta_{vap}H$ of $51.16\,\frac{\mathrm{kJ}}{\mathrm{mol}}$ of α-ionone, determined at standard conditions ($0\,°C = 273.15\,K$ and $1\,bar$), was provided via Cheméo [124].The calculation can be seen in the following equations (3-4 to 3-6):

$$\ln\frac{p_1}{p_2} = \frac{\Delta_{vap}H}{R}\cdot\left(\frac{1}{T_1}-\frac{1}{T_2}\right) \tag{3-4}$$

$$p_2 = \frac{e^{\frac{\Delta_{vap}H}{R}\cdot\left(\frac{1}{T_1}-\frac{1}{T_2}\right)}}{p_1} \tag{3-5}$$

$$p_2 = \frac{e^{\frac{51.16\,\frac{kJ}{mol}}{8.314\cdot 10^{-3}\,\frac{kJ}{mol\cdot K}}\cdot\left(\frac{1}{273.15\,K}-\frac{1}{393.15\,K}\right)}}{1000\,mbar} \approx \mathbf{0.97\,mbar} \tag{3-6}$$

The result of 0.97 mbar for an evaporator temperature of 120 °C had to be taken with a grain of salt, of course, due to mathematical approximations as well as an approximation about ideal gas behavior [114]. Especially the ideal gas approximation can lead to errors since α-ionone is a rather bulky and big molecule (cf. Table 9-1 of the Appendix), which does not meet the model standards of an ideal gas. However, it provided some necessary insight on how to start. From this calculation on, the different distillation conditions, as described in Section 3.2.2.2.1 Method Development, were developed and the corresponding results can be viewed in Figure 3-3. The condenser temperature for all distillations was kept at 60 °C.

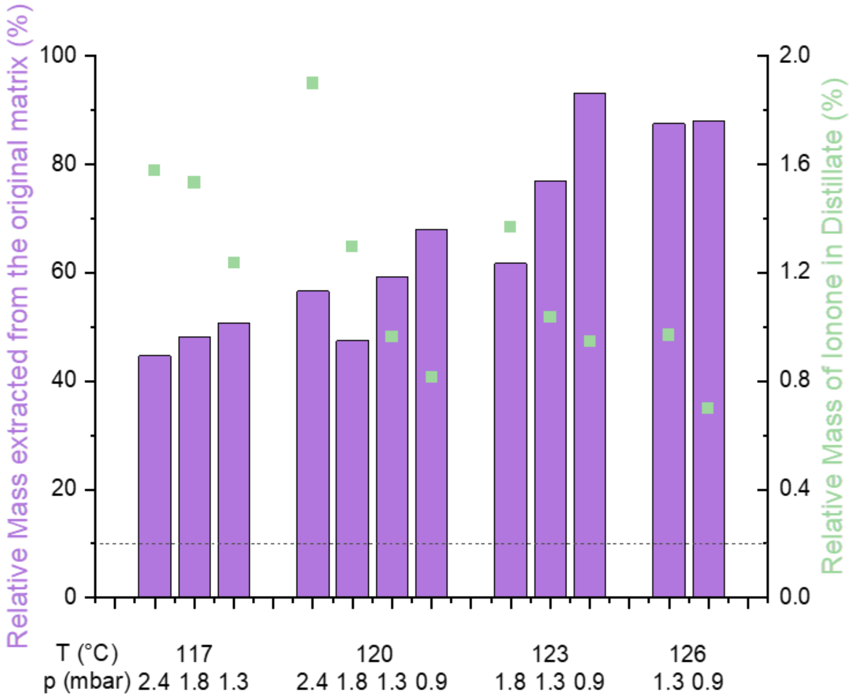

Figure 3-3: Extraction results of the first screening of the molecular distillation. The purple bars indicate the relative mass of α-ionone that was extracted from the original matrix containing 0.2% of α-ionone and the green squares indicate the relative mass of α-ionone in the distillate. The dotted line represents the α-ionone content of 0.2% in the original matrix.

The dotted line represents the original α-ionone content of 0.2% in the sample. With every distillation of the presented conditions, it was possible to remove at least 44% of α-ionone from the fatty acid matrix (represented by the purple bars). The results of the starting conditions around 120 °C were mediocre, with too low distillation yields of only ~ 60%. Thus, distillations at higher evaporator temperatures were investigated resulting in a higher relative extraction of the odoriphore. The optimum pressure settings for the temperatures of 123 °C and 126 °C were also calculated via the Clausius-Clapeyron equation. The results can be viewed in Table 9-6. Statistically speaking, higher temperatures lead to higher distillation results as more molecules reach the necessary energy (E) to perform a phase transition. This phenomenon can be expressed via the Boltzmann distribution (3-7) in which the proportionality ($\propto$) of q_i, the probability of the system being in state i, to the energy E_i of the respective state, the temperature T, and the Boltzmann constant k_B is described.

$$q_i \propto e^{-\frac{E_i}{k_B T}} \qquad (3\text{-}7)$$

The Boltzmann distribution finds application in the Arrhenius equation (3-8), describing the kinetic dependence of the evaporation rate constant k_{evap} on the activation energy E_A and temperature T of reactions or phase transitions [125].

$$k_{evap} = A_0 \cdot e^{-\frac{E_A}{RT}} \qquad (3\text{-}8)$$

with k_{evap} = evaporation rate constant, A_0 = Arrhenius parameter, E_A = activation energy, R = gas constant, and T = temperature.

Through the higher evaporation probability, the temperatures of 123 °C and 126 °C were advantageous to almost exhaustively extract the α-ionone (up to 97% yield) from the HMyr matrix. An increase in temperature, however, also caused more HMyr molecules to evaporate. Hence, the relative mass of α-ionone (signified by the green squares) in the distillate decreased at higher temperatures. Considering equations (3-7) and (3-8), the probability of distilling HMyr along with α-ionone increased with the elevated temperatures, leading to a lower α-ionone content in total.

To determine a significant trend, distillation at an evaporator temperature of 117 °C and gentle pressure conditions were examined. In these cases, it was visible that the extraction yield decreased while the relative mass in the distillate increased. Regarding all temperature settings, a trend in distillate content as well as in extraction yield was indeed to be observed. Mild distillation conditions were favorable to obtain extracts richer in odoriphore, while harsher settings (123-126 °C) achieved higher distillation yields with lower α-ionone content. Likewise, a trend in pressure could be observed. The higher, or rather milder, the pressure (2.4 mbar) of distillation was, the higher was the relative distilled amount (1.5-1.9%), while it was the contrary for lower pressures (0.7-0.9% at 0.9 mbar).

It was necessary to find a compromise between yield and content. Ultimately, it was decided that a nearly complete distillation was more important as the target compounds are too valuable to get lost in the sump. Hence, the second screening was performed at high temperatures and low pressures, investigating a technical mixture of α-irones. The α-irones are structurally similar to α-ionone and γ-irone and, therefore, were a perfect option to reassess the examined conditions as no pure γ-irone was available at a reasonable price. Reevaluation was necessary to review if the thermal behavior, though the vaporization enthalpies are similar (cf. Table 9-6), would change drastically with a small structural change from ionone to irone (cf. Table 9-1 of the Appendix). Hence, it was tested if the pressure and temperature settings of α-ionone were applicable for γ-irone. The results are presented in Figure 3-4:

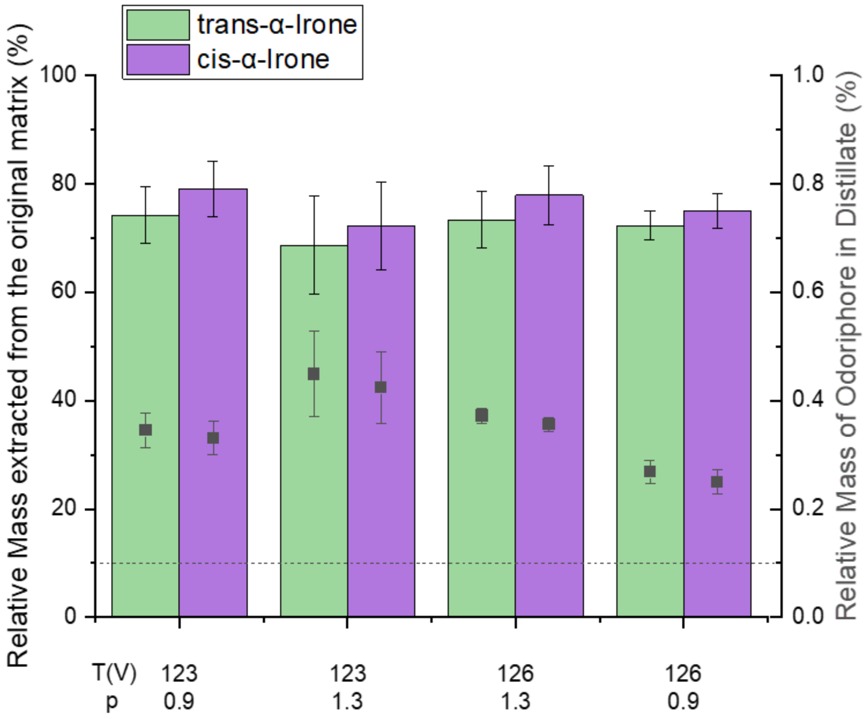

Figure 3-4: Extraction results of the molecular distillation screening using the technical mixture of irone isomers. The green and purple bars represent the relative amount of trans- and cis-α-irone extracted from the original matrix and the grey squares indicate the relative mass of the odoriphores in the distillate. The dotted line represents the odoriphore content (~ 0.1% of each, trans-α-irone and cis-α-irone) in the original matrix.

According to gas chromatographic analysis coupled with flame ionization detection (GC-FID), the technical mixture of α-irones consisted of approximately 49% *trans*-α-irone and 51% *cis*-α-irone (cf. Figure 9-1). The original relative content of 0.1% each in the fatty acid matrix is represented by the black dotted line. The extraction conditions of 123 °C and 126 °C at 0.9 mbar and 1.3 mbar were investigated, as before with α-ionone. The pressure settings were also checked by calculations using the Clausius-Clapeyron relation (Equation (3-6)) and presented in Table 9-6. Considering the calculations, softer pressure settings would have been enough for the distillation of α-irones due to a higher evaporation enthalpy. Overall, the results of this screening were rather similar to the results of the α-ionone screening before and changing between the four conditions only had small effects. With regard to the error bars, the extraction yield at every pair of varieties leveled off at around 74%. Since the initial content of the *trans*-isomer (represented by the green bars) was slightly lower than of the *cis*-isomer (purple bars), the relative extraction yields were lower as well.

The grey squares indicated the content of the odoriphore in the distillate. As expected, the lower the adjusted pressure was, the lower were the relative contents of the odoriphores in the distillate. The lowest relative irone content after distillation was attained by employing the harshest conditions of 126 °C and 0.9 bar, amounting to a relative odoriphore content of only 0.5%. When easing the pressure to 1.3 mbar, higher irone contents (> 0.8%) were achieved for both temperature settings. Factoring in the error bars, the obtained contents at 1.3 mbar resided in the same range, quadrupling the original total fragrance content. Eventually, it was decided that the optimum distillation settings for retrieving α-irones, serving as examples for the class of irones, from HMyr were **123 °C** at **1.3 mbar**. Using the lower temperature was beneficial as well from the economic point of view. A lower temperature means lower energy costs when running the short-path distillation apparatus. Likewise, the possibility of destroying the slightly thermolabile irones in the process was reduced [115,116]. Additionally, the distillation parameters were reviewed via the Clausius-Clapeyron relation (Equation (3-6), presented in Table 9-6). According to the calculations, the combination of 123 °C and 1.3 mbar were perfect for the distillation of γ-irone in theory. Hence, these settings were selected when handling the true extract. Figure 3-5 gives the results of the extract as prepared in Section 3.3.1 Extraction of γ-Irone from the Rhizomes of *Iris Barbata-Elatior* and the two distillation cycles.

Through every distillation cycle the γ-irone content inside the HMyr matrix, characterized by the purple bars, could be improved significantly. No linear trend between the γ-irone content and the number of distillations was found.

The starting point for the first distillation was the HMyr extract of γ-irone from the iris rhizomes. Even though through the repeated extraction of the rhizomes a γ-irone yield of 88% in the fatty acid was achieved, only a total fragrance content of ~ 0.02% was reached (confer to Table 9-7 for the accurate numbers). This fivefold difference in concentration had a strong influence on the quality of the first distillation cycle. A threefold increase of the γ-irone content was realized by distilling the extract once. However, when regarding the yield of the distillation (represented by the grey squares), only ~ 51% were removed from the matrix, leaving approximately half of the target molecules behind in the sump. Considering the screening results with the α-irones before (cf. Figure 3-4) accomplishing yields of ~ 74%, such a big loss was not expected. Nevertheless, this loss could also be explained via the Boltzmann distribution. With fewer molecules in the system, the probability of recovery in the distillate decreased as well. The γ-irone molecules that remained in the sump were eventually declared lost since distilling the sump a second time would only yield even worse results. In retrospect, the screening of the optimum distillation conditions should have considered the deviation of the starting content of the fragrance as this result was not satisfactory.

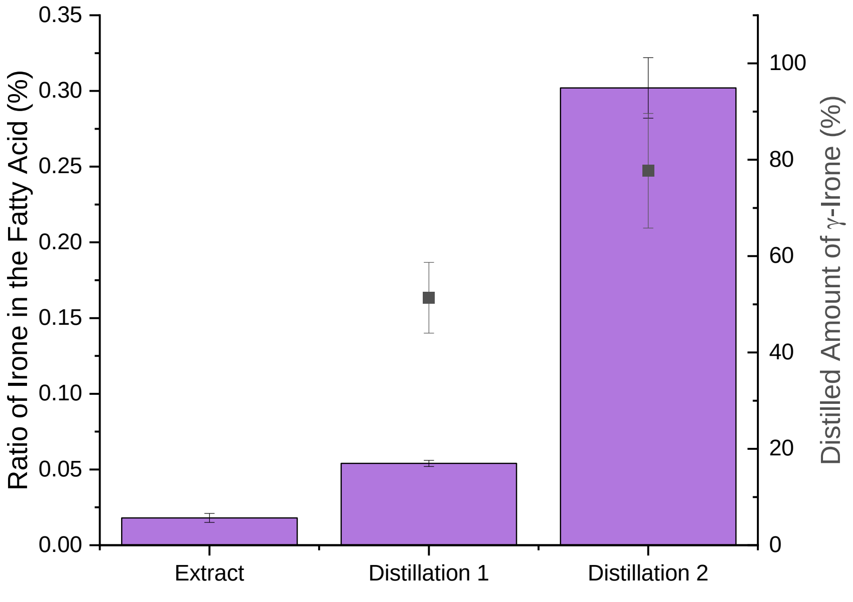

Figure 3-5: Comparison of the γ-irone content in the myristic acid matrix after different extraction steps, represented by the purple bars. The grey squares indicate the relative amount of γ-irone that was extracted from the source material, either the rhizomes (Extract) or the extracts (Distillation 1 and 2).

The second distillation cycle though was more promising. This extraction used the distillate of the first cycle as the feed. In this case, a sixfold increase of the γ-irone content from the first distillate was reached, yielding a total fragrance content of 0.3%. This amounted to an 18-fold increase in the rhizome extract. A distillation yield of ~ 78% was achieved in this case. Although the γ-irone content in the first distillate was only half the amount examined in the method development with α-irone, the distillation yield was in the same order. This implied that the screening with the α-irones was successful and gave confirmation about the good quality of the selected temperature and pressure conditions. One could now speculate that the distillation process was only somewhat dependent on the starting concentration of the target molecules as a factor of 2 did not make a significant difference in the extraction yield. On the other hand, it is also possible that through the structural differences between α-ionone, the α-irones, and γ-irone the thermal behavior of the compounds differed, and conditions were best suited for distillation of γ-irone.

3.4 Conclusion

The aim of this study was to find an environmentally friendly and simple extraction and concentration method for γ-irone from iris rhizomes. To this purpose, four extraction methods based on HMyr as the solvent were examined to extract the target compound from the plant matrix. Successively, the extracts were distilled to obtain a product, enriched in γ-irone.

Through pre-tests, it was determined that the most promising way to extract γ-irone was soaking the iris rhizomes in water for 1 h before extracting them with pure HMyr. Employing these parameters, a scaled-up, repeated batch extraction was performed. The scale-up was necessary to obtain enough extract to feed the short-path distillation apparatus. While the extraction process was easy and required only few active steps, it was also time-consuming, taking four days in total. In particular, the manual pressing of the water-soaked rhizomes was labor-intensive. Here, it would be necessary to find an automated alternative to speed up the process while also being able to dry the rhizomes more properly. The extraction with a 1:5 rhizome to solvent ratio was adequately green, as well as the solvent HMyr, especially since it was a compound that is found in the rhizomes themselves [105]. However, on a laboratory scale, it was difficult to maintain the necessary temperature of 60 °C during the solvent changes. Since HMyr has a melting temperature of 53.9 °C [120], spontaneous solidification occurred frequently, making it problematic to always maintain a homogeneous extraction solvent. Eventually, a satisfactory extraction yield of 88% γ-irone was achieved. This extract could be processed further via molecular distillation.

The optimum distillation parameters were found with the help of the Clausius-Clapeyron equation. Even with the necessary approximations, a very good prediction could be made, giving the right direction to find the optimum distillation conditions at 123 °C and 1.3 mbar. These settings were a compromise between a high distillation yield of γ-irone while also maintaining a relatively high content of odiferous compound in the distillates. However, more distillation cycles were necessary for good results.

With its ~0.3% of γ-irone, the second distillate already made a strong olfactory impression. Yet, the content in the HMyr matrix was still not high enough to be of industrial interest. A third cycle of distillation would have been necessary. Due to the big dead volume of the distillation apparatus, however, it was not possible to perform a third one. The raw material, which would have been the second distillate, was not enough. Based on the results so far, it could be expected that a third distillation should have been able to reach an interesting content of γ-irone in the fatty acid matrix. However, employing the distillation of the rhizome extract in an industrial context, with the option of better upscaling, the multiple extraction cycles should certainly be an option.

Still, the next step must be the optimization of the first distillation. The parameters would have to be adapted to the starting concentration of the extract. Of course, the optimum solution was to find temperature and pressure settings that make for a more selective separation of the odoriphore from the fatty acid. Though, it can be expected that in order to distillate more of γ-irone in the first cycle, harsher conditions have to be employed. This means in turn that an even higher amount of HMyr would be extracted alongside the target compounds, which was explained above (cf. Figure 3-3). The concentration process in total would be slower as the achievable concentration steps would be smaller, but the loss of the fragrance should be reduced as well.

CHAPTER 4

SOLUBILITY AND EXTRACTION OF CURCUMIN IN NADES SYSTEMS

CONTENTS

This chapter presents the advances in curcumin extraction by employing green solvents, based on natural deep eutectic solvents (NADES) in sustainable ternary solvent mixtures.

4 Solubility and Extraction of Curcumin in NADES Systems

The results presented in this Section have been published in 2021 in the three papers *Solubilization and extraction of curcumin from Curcuma Longa using green, sustainable, and food-approved surfactant-free microemulsions* by P. Degot *et al.* [47] and *NADES-based surfactant-free microemulsions for solubilization and extraction of curcumin from Curcuma Longa* as well as *Improvement of the Solubilization and Extraction of Curcumin in an Edible Ternary Solvent Mixture* by V. Huber *et al.* [70,126]. These studies will be summarized in this chapter; no licensing was necessary. The work was supported by **Laurie Muller**, who investigated the NADES and conducted the solubility tests, by **Katarzyna Krzemien**, recording the phase diagrams, by **Lena Schmauser**, performing the conductivity measurements, as well as by **Johnny Hioe**, performing the simulation calculations.

4.1 Introduction

The *Zingiberaceae* family is composed of roughly 1400 species of tropical, perennial herbs. One of the most important representatives is *Curcuma longa* L. or turmeric. Curcuma is the latinized version of the Arabic word كركم (*kourkoum*), meaning *saffron* [127]. Even though there is no definitive conclusion about the plant’s origin, experts assume it originated in Southeast Asia. There it is primarily cultivated, especially throughout India, which is the world’s largest producer, Pakistan, and Indonesia to name a few [128,129]. However, its cultivation is not limited to Asia, the tropical and subtropical conditions necessary are given elsewhere as well [130–133]. Turmeric has been known for centuries for its valuable characteristics as a preservative, colorant, and therapeutic agent [47].

Turmeric is an herbaceous, perennial plant of a size of 0.6-1.2 m. It possesses green, oblong, glabrous leaves of elliptical shape with a narrow base. They can become 45 cm long and 18 cm wide and are arranged helically around the base [128,129]. Its flowers sprout from 15-20 cm long stems surrounded by the leaves and can be of a yellow or crimson color [134]. The underground building blocks of the plant are the rhizomes, which are made up of two parts, the central “mother rhizome”, which can be of a size up to 4 cm, and its branches of a diameter of up to 1.5 cm. The main rhizome does not exhibit a uniform shape or size and can either be ovoid or almost round

[129,130,134,135]. These rhizomes are the source of turmeric's medically and nutritionally interesting phytochemicals.

Apart from containing 2-7% of essential oil, turmeric's most important and active ingredients are the so-called curcuminoids. They were isolated for the first time in 1815 [129] and make up 1-9% of the total dry weight content of the rhizomes. The large disparity in curcuminoid content can be explained by environmental factors like soil condition, nutrient availability, harvesting time, and genus diversity [128,133,135]. Predominantly, the class of curcuminoids consists of curcumin, which is the major compound with ~ 94%, curcumin II, also known as demethoxycurcumin, with ~ 6%, and curcumin III, bisdemethoxycurcumin, with a content of ~ 0.3%. The three of them can be distinguished from one another by the number of methoxy groups [136].

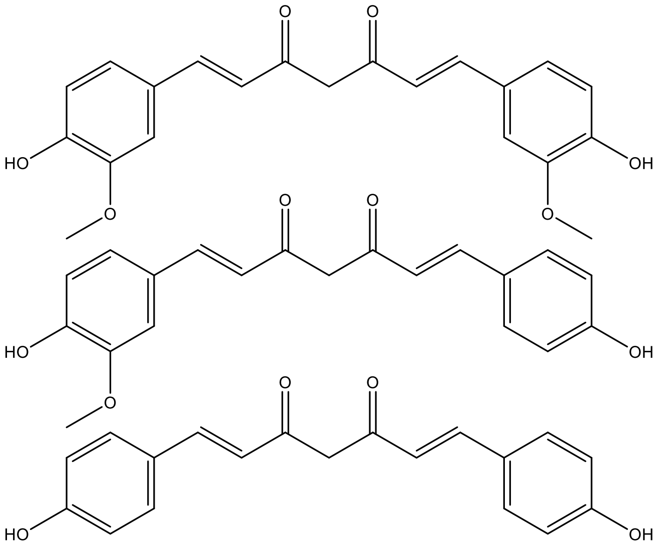

Figure 4-1: The three major curcuminoids, curcumin (top), demethoxycurcumin (middle), and bisdemethoxycurcumin (bottom).

Depending on the species and the cultivation, other diferoylmethane derivatives can occur as well, however, the three above are the most common ones [135,136]. Colloquially, the name curcumin is used synonymously to describe the lot of curcuminoids found in the rhizomes.

The main characteristic of the curcuminoids is their strong and bright yellow color, giving a color impression at concentrations as low as 5-200 ppm [128]. In addition to their dying properties, they exhibit beneficial effects on human health as well. This is the reason why *Curcuma longa* L. has been used for centuries in ayurvedic medicine. Nowadays, studies on the curcuminoids' health effects have been conducted, attesting them a plethora of valuable, therapeutic properties like antioxidant, anti-inflammatory, anti-microbial, anti-cancer, and even more activities [128,134,135,137]. In light of these discoveries, the global market size of trading curcumin is forecast to increase by ~ 16% until 2028 [138].

To harvest the natural pigments for applications in the pharmaceutical, food, and cosmetic industry, they have to be extracted and successively formulated. They are not soluble in water [128], which limits their area of applications, but are indeed soluble in alcohols, acetone, or petroleum-based solvents. The theory of extraction has been discussed in more detail above (cf. 2.2) as well as the basics of green chemistry (cf. 2.3). In the following chapter, an approach towards a greener and more effective extraction of curcuminoids in terms of sustainable solvents will be made. Based on the work of P. Degot *et al.* [47,48], an aqueous phase, limiting the solubility of curcumin, was replaced by NADES. They are indeed hydrophilic but show good solubility capabilities towards phytochemicals, and their mass transport limitations due to their high viscosity were bypassed by incorporating them into binary ethanol/triacetin solutions. Solubility and extraction experiments were performed to find potentially useful NADES mixtures in terms of extracting curcumin.

4.2 Experimental

4.2.1 Chemicals

All chemicals with their abbreviations, purities, and vendors which were used in this section can be found in the following Table 4-1.

Table 4-1: Chemicals used in Section 4.

Chemical	Abbreviation	Purity	Vendor
Curcumin	Cur	>97%	TCI (Eschborn, Germany)
Bisdemethoxy-curcumin	BDC	>98%	
Proline	Pro	>99%	
Rhizome Powder of *C. Longa*	-	-	Kwizda (Linz, Austria)
Demethoxy-curcumin	DC	>98%	Sigma Aldrich (Darmstadt, Germany)
Choline Chloride	ChCl	>99%	

Acetylcholine	AcCh	> 99%	
Lactic Acid	Lac	> 85%, FCC	
Levulinic Acid	Lev	> 98%	
Malic Acid	Mal	> 99%	Alfa Aesar (Kandel, Germany)
Oxalic Acid Dihydrate	Ox	> 99%	Merck (Darmstadt, Germany)
Ethanol	EtOH	> 99%	
Triacetin	TriA	> 99%, FG	
Acetone		> 99%	
Acetonitrile	ACN	> 99%, HPLC Grade	
Acetic Acid	HAc	> 99%	

Using a Millipore Milli-Q purification system (Merck Millipore, Billerica, Massachusetts), water was deionized. All chemicals were used without further purification. To see the chemical structures, confer to Section 9.1 of the Appendix.

4.2.2 Methods and Techniques

4.2.2.1 NADES Preparation

NADES of a 1:1 mole ratio based on the hydrogen bond acceptors (HBAs) acetyl choline (AcCh), choline chloride (ChCl), and proline (Pro) were prepared according to a heating method by Y. Dai, *et al.* [68]. The HBAs were mixed with the corresponding donors and different organic acids and heated to 80 °C for up to 90 min to obtain a clear liquid. Before use, the mixtures were left to cool to room temperature.

4.2.2.2 Determination of Ternary Phase Diagrams

To record the pseudo-ternary phase diagrams NADES/EtOH/TriA, 3 g samples of binary mixtures NADES/EtOH and EtOH/TriA were prepared in borosilicate tubes at different weight ratios. The corresponding third component, TriA, and NADES respectively, was added to the binary mixture in a dropwise manner until precipitation occurred or the mixture turned turbid. This was an indication of phase separation, which was judged by the bare eye. The exact weights of all components were recorded to determine the miscibility gap of the pseudo-ternary systems.

4.2.2.3 *Solubility Examination via Optical Density Measurements*

To determine the most promising NADES mixtures, a screening was performed. Thus, 5 g samples at a weight distribution of 50:20:30 of NADES/EtOH/TriA respectively were prepared and mixed until the mixture became homogeneous. This composition was chosen as the effects of the NADES at high shares mixed with the optimum binary mixture of EtOH/TriA (40:60) could be assessed. An excess of synthetic curcumin was added and stirred for 1 h at room temperature to saturate the samples.

The contour diagrams, giving an insight into the curcumin solubility in the monophasic domain of the ternary mixtures, were recorded for the two most promising NADES, ChCl+Lac and ChCl+Lev, mixed with EtOH and TriA. For a qualitative analysis of the monophasic regime, 5 g of binary (NADES/EtOH and ETOH/TriA) and ternary (NADES/EtOH/TriA) mixtures were prepared at different weight ratios throughout the monophasic region and saturated with synthetic curcumin.

The surplus of curcumin was removed by filtering the solutions through PTFE syringe filters of 0.45 µm pore size. UV/Vis analysis followed after adequately diluting the samples with EtOH by screening the whole visible spectrum of 350-700 nm on a Lambda 18 UV/Vis spectrometer by PerkinElmer (Waltham, Massachusetts, USA). The maximum absorbances at λ_{max} = 425 nm were compared to evaluate the results.

4.2.2.4 *Dynamic Light Scattering*

To examine the structuring of the ternary systems and to find the critical points in the binary and ternary, dynamic light scattering (DLS) experiments were conducted. A temperature-controlled CGS-3 goniometer by ALV (Langen, Germany), equipped with an ALV-7004/FAST Multiple Tau digital correlator and a vertically polarized 22 mW HeNe laser of a wavelength of λ = 632.8 nm was used. Using 0.2 µm PTFE filters, the samples were filtered into dust-free cylindrical light scattering cells with an outer diameter of 10 mm. Successively, the samples were thermostated in a toluene tub of 25 ± 0.1 °C and measured for 120 s. A qualitative analysis of the correlation curves was carried out based on the assumption consistent with T. Buchecker and S. Krickl that higher y-intercepts correspond to more time-stable structuring [139]. Thus, the critical points in the systems were determined accordingly.

4.2.2.5 Liquid-Liquid-Equilibrium (LLE) Simulation

No critical point in the binary system of EtOH/TriA could be determined via DLS experiments due to fast and hardly detectable fluctuations. Thus, a COSMO-RS formulation within the software package COSMOTherm 2021 was used to simulate a binary phase diagram consisting of TriA/EtOH. The LLE points were calculated with an increasing EtOH content of 0.05 wt% increments at a constant temperature.

Only three experimental data points were available and recommended for TriA at 284.24 K, 298.27 K, and 318.20 K. The Antoine equation (4-1) with three fitting coefficients (A_A-C_A) could be applied in this case, where T was the temperature.

$$\ln(p_i^0) = A_A - \frac{B_A}{T - C_A} \tag{4-1}$$

For EtOH instead, the more sophisticated Wagner equation (4-2) with six fitting coefficients (A_W-F_W) was employed as more experimental data points were known.

$$\ln(p_i^0) = \ln(A_W) - \frac{1}{1-\tau}(C_W\theta + D_W\theta^{1.5} + E_W\theta^3 + F_W\theta^6) \tag{4-2}$$

$$\text{with } \theta = 1 - \frac{T}{B_W}$$

According to Equation (4-3), the total vapor mole fraction y_i was calculated.

$$y_i = \frac{p_i^0 x_i \zeta_i}{p_{tot}} \tag{4-3}$$

With $p^0{}_i$ = vapor pressure of the pure substance i, x_i = mole fraction of i, ζ_i = activity coefficient of i.

4.2.2.6 Curcuminoid Extraction

4.2.2.6.1 Pressure- and Temperature-Controlled Soxhlet Extraction

An exhaustive Soxhlet extraction method was applied to determine the total curcuminoid content in the ground rhizomes. In order to avoid the thermal degradation of the thermolabile curcuminoids, the classical Soxhlet apparatus was enhanced with a pump to manually adjust the pressure. Through the reduction of the pressure to 234 mbar, a moderate temperature of 30 °C was sufficient to perform the extraction. With these conditions, 2 g of rhizomes were extracted with 70-80 mL acetone for ~ 5 h, translating to roughly 55-60 extraction cycles. The endpoint of the extraction was determined by the bare eye when the solvent surrounding the extraction thimble was visually transparent. Then the extract was transferred to a volumetric flask and topped off with acetone. Before elution via HPLC (cf. 4.2.2.7 HPLC Method), the extract solution was diluted 10-fold in ACN. This process was performed in triplicate.

4.2.2.6.2 Determination of the best Rhizome-to-Solvent Ratio for Extraction

The optimum powder to solvent ratio was determined by extracting 2 g of *Curcuma longa* L. using the solvent mixture ChCl+Lac/EtOH/TriA 35:27.5:37.5 at weight ratios of 1:6, 1:8, 1:10, and 1:12. The extractions were performed by stirring the mixtures for 1 h at 1300 rpm at room temperature. Centrifugation followed for 10 min at 4200 G. Successively, the extracts were topped off with ACN in volumetric flasks, diluted 25-fold in ACN/water 90:10 (*w/w*), and eluted via HPLC (cf. 4.2.2.7 HPLC Method). All samples were made in triplicates.

4.2.2.6.3 Solvent Extraction

With a 1:8 powder to solvent ratio, 2 g of turmeric powder were extracted with 16 g of different extraction mixtures. This was achieved by stirring the mixtures at 1300 rpm for 1 h at ambient temperatures. After the extraction, the samples were centrifuged for 10 min at 4200 G, the supernatant filtered into volumetric flasks, topped off with ACN, diluted 25-fold in ACN/water 90:10 (*w/w*) to avoid precipitation of the NADES, and eluted by HPLC (cf. 4.2.2.7 HPLC Method).

4.2.2.6.4 Cycle Extraction

To exploit the full solving capability of the pseudo-ternary NADES/EtOH/TriA systems, the solvent was reused in an attempt to enrich the solvent in curcuminoids. To this purpose, 2 g of ground rhizome powder was extracted with 32 g of the extraction solvents at their optimum compositions ChCl+Lac/EtOH/TriA 35:27.5:37.5 and ChCl+Lev/EtOH/TriA 30:40:30. To separate the supernatant from the rhizome remnants, the samples were centrifuged at 4700 G for 10 min. This process marked one cycle. 2 g of fresh rhizome powder was added to the collected supernatant for a further cycle and extracted again. After up to 12 cycles, the supernatant was filtered into volumetric flasks, topped off with EtOH, diluted 25-fold in ACN/water 90:10 (*w/w*), and eluted via HPLC (cf. 4.2.2.7 HPLC Method).

To evaluate if the solvent changed during the extraction cycles, the curcuminoid content after 7 cycles was imitated by solving the corresponding amounts of the synthetic chemicals curcumin or curcumin and demethoxycurcumin in the solvent mixture ChCl+Lev/EtOH/TriA 30:40:30. Then, one cycle of extraction was performed, topped off with EtOH in a volumetric flask, diluted 25-fold in ACN/water 90:10 (*w/w*), and eluted via HPLC (cf. 4.2.2.7 HPLC Method).

The preparation of all cycle samples was carried out in triplicates.

4.2.2.7 HPLC Method

All curcuminoid extracts of *Curcuma longa* L. were analyzed using a Waters HPLC system with two Waters 515 HPLC pumps, a Waters 717 autosampler, and a Waters 2487 UV/Vis detector. The separation of the extracted compounds was carried out on two different columns:

- An ACE Equivalent 3 C18-Column (300 Å, 150 × 2.1 mm) with a 5 µL injection volume and a 0.4 mL/min flow rate for the **lactic acid NADES** systems
- A Knauer Eurospher 5 C18-Column (100 Å, 250 × 4.6 mm) with a 10 µL injection volume and a flow rate of 1 mL/min for the **levulinic acid NADES** systems

All samples were eluted three times and prepared in triplicates. The elution was performed using a gradient method based on the works of P. Degot *et al.* [47] as described in Table 4-2 at a temperature of 40 °C. The mobile phase consisted of water with 0.3% acetic acid (A) and ACN (B).

Table 4-2: HPLC gradient method.

Time (min)	Solution A (%)	Solution B (%)
0-17	60-40	40-60
17-18	40-0	60-100
18-24	0	100
24-25	0-60	100-40
25-32	60	40

External calibration curves of the three curcuminoids in a concentration range of 0.04-0.2 mg/mL were recorded to quantify the curcuminoids extracted from the plant matrix. The elution was carried out as described before in both columns. The curves were obtained by plotting the concentration of the curcuminoids against the peak area.

4.2.2.8 ^{13}C-NMR Analysis

For the ^{13}C-NMR measurements, an Avance III 400 NMR-spectrometer by Bruker (Billerica, USA) operating at 400 MHz was used. Approximately 1 mL of the 30:40:30 (*w/w/w*) mixture ChCl+Lev/EtOH/TriA, serving as the extraction solvent, was filled into Norell 507-HP-7 High-Precision-NMR sample tubes (Norell Inc., Morganton, USA). The sample was measured three times: right after preparation, after one day, and three days after preparation. The NMR tube was not sealed, and the solvent was not changed in order to imitate normal conditions the solvent would have endured during the cycle extraction [126].

4.2.2.9 Conductivity Measurements

The measure of conductivity was used to determine a possible change in the solvent that can be linked to the extraction. The measurements were performed using a temperature-controlled measuring cell (25 ± 0.2 °C) of a low-frequency WTW inoLab Cond 730 conductivity meter, connected to a WTW TetraCon 325 electrode (Weilheim, Germany) under permanent stirring (~ 500 rpm) and manual mixing where necessary. Three different kinds of samples were examined [126]. No additional charge carriers were added to the examined mixtures as choline chloride served as the charged species.

- 20 g of the optimum ternary composition of 30:40:30 ChCl+Lev/EtOH/TriA was diluted in 0.5-2 g steps with 40:60 (*w/w*) EtOH/TriA.
- An imitation of the acidic hydrolysis of TriA was attempted by replacing parts of the TriA with the respective amounts of glycerol and acetic acid. The conductivities of the artificially hydrolyzed samples were measured in the range of 0-100% of TriA hydrolysis. Complete hydrolysis of TriA resulting in the basic species glycerol and acetic acid was presumed without regarding partially hydrolyzed species like diacetin or monoacetin for reasons of simplicity.
- After every cycle of extraction (up to 7 cycles), the conductivity of the solvent was monitored.

4.3 Results and Discussion

4.3.1 Curcumin Solubility in Different NADES Systems

P. Degot *et al.* introduced an edible surfactant-free microemulsion consisting of water, ethanol, and triacetin as a novel, green extraction medium. Characterizing this ternary mixture, a solubility synergy between the cosolvent ethanol and the oil phase triacetin, increasing the curcumin solubility by a factor of 3 and 5 respectively, was found. Extraction of ground *Curcuma longa* L. rhizomes with the optimum binary mixture, however, did lead to unsatisfactory extraction yields of only ~ 60%. Thus, water was added to the mixture, showing that with a to some extent aqueous solvent, the curcuminoid extraction yield could be increased. Yet, the addition of water to this binary system came at an expense of solubility [47,48].

The motivation for the following study was to replace water in the ternary mixture by another hydrophilic phase which still displayed a decent curcumin solubility. Thus, natural deep eutectic solvents (NADES) were chosen [140].

A screening of eleven different NADES already known in literature [141,142] was made to evaluate their ability to solve curcumin at ambient temperatures in a mixture with EtOH/TriA. The results are presented in Figure 4-2. The chosen NADES were based on acetylcholine (AcCh), choline chloride (ChCl), and proline (Pro), which are naturally produced in the body, mixed in a 1:1 molar ratio with citric acid (Cit), lactic acid (Lac), levulinic acid (Lev), and malic acid (Mal). To view the compounds' structures, confer to Table 9-2 of the Appendix. An investigation on the curcumin solubility in water with ChCl and the ChCl+Lac NADES as additives beforehand showed that the single compound and the NADES had a significant positive effect on the solubility of curcumin [70]. It can be viewed in Figure 9-2 of the Appendix. Since both ChCl and curcumin are soluble in the EtOH/TriA systems, it was assumed that the solubility synergy of the solvent mixed with the additives should yield even higher curcumin solubilities, initiating the following screening [70,126].

The screening of Figure 4-2 shows the qualitative UV/Vis results of the 50:20:30 (*w/w/w*) NADES/EtOH/TriA mixtures saturated in curcumin. The lines served as a representation of the references, the ternary mixture of water/EtOH/TriA at the same weight ratio of 50:20:30 in black, the optimum binary mixture of EtOH/TriA 40:60 (*w/w*) in red, and acetone in blue. All ternary mixtures containing NADES exhibited a superior curcumin solubility of at least a factor of 6 compared to the ternary mixtures with water. These results proved that curcumin was indeed more soluble in any tested NADES opposite to water. This find was expected, though, as curcumin is not soluble in water, whereas even hydrophilic NADES have been reported to be able to solve hydrophobic phytochemicals. Particularly phenols can be solved in NADES via hydrogen bonding [140,143]. Thus, to achieve a high solubility in a hydrophilic environment, NADES should replace water [70,126].

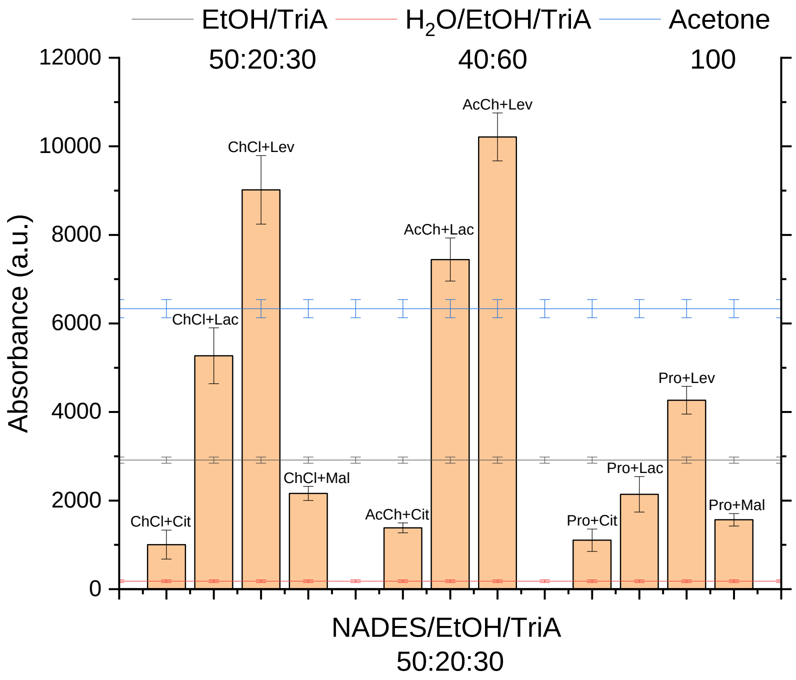

Figure 4-2: Qualitative screening of the curcumin solubility in eleven different NADES/EtOH/TriA 50:20:30 (w/w/w) mixtures determined via UV/Vis. The references, the ternary mixture of water/EtOH/TriA at the same weight ratio of 50:20:30 as the former mixtures in black on the bottom, the optimum binary mixture of EtOH/TriA 40:60 (w/w) in red, and pure acetone in blue at the top, are represented by the horizontal lines [126].

Only five of the eleven tested NADES in a ternary mixture, one based on Pro, two based on ChCl and AcCh each, could surpass the curcumin solubility in the optimum binary mixture of EtOH/TriA 40:60 (*w/w*). Thus, the power of the hydrogen bond acceptors could be ordered as follows: AcCh > ChCl > Pro. Looking at these molecules' structures (cf. Table 9-2), AcCh and ChCl share a positively charged nitrogen functionality, while Pro only possesses a non-charged secondary amine. Apparently, the quaternary ammonium ion had a positive influence on the curcumin solubility. It was speculated that cation-π interactions between the aromatic curcumin and the quaternary ammonium compounds (QAs) may be the reason. Even though these interactions are usually quite weak, they are powerful enough for favorable molecular recognition in proteins. Reports state that the quadrupole of conjugated π-systems of aromatic rings of amino acids can interact with the ions [144–147]. With this knowledge in mind, it was suspected that the interactions of AcCh and ChCl with curcumin were comparable to the interactions between ions and amino acids. This served as an explanation for the higher solubility of curcumin in the systems containing QAs in comparison to the systems containing Pro [70,126].

As a next step, the influence of the acids on the solubility of curcumin was ranked. Only three examined NADES could compete with acetone in terms of solubility, solving ~ 1.4 times more. Two of the best three ternary NADES/EtOH/TriA mixtures contained Lev, making it the best HBD of the examined ones, followed by Lac. Neither Mal nor Cit were able to create an environment suitable to enhance the solubility of curcumin in these pseudo-ternary mixtures. Successively, the acids could also be ranked according to their power in aiding the solubility of curcumin: Lev > Lac > Mal ≈ Cit [70,126].

The top NADES AcCh+Lev and ChCl+Lev show a similar solubility of curcumin with regard to their standard errors. AcCh, however, is a neurotransmitter and, therefore, not allowed as a food additive. ChCl on the other hand is a common additive in the food industry. Hence, all further experiments concerning the extraction of the curcuminoids from the ground roots of *Curcuma longa* L. for applications in the food sector were conducted using the runners-up ChCl+Lev and ChCl+Lac. No removal of the solvent was necessary when extracting with a food-approved solvent [70,126].

4.3.2 Phase Diagrams and Solubility Maps

To gather information about the phase behavior and the extent of the monophasic domains in the ternary mixtures of ChCl+Lev/EtOH/TriA and ChCl+Lac/EtOH/TriA, and water/EtOH/TriA, phase diagrams were recorded, which can be viewed in Figure 4-3. For complete accuracy in the following, it has to be noted that the regarded systems containing NADES were rather pseudo-ternary ones. Thermodynamically speaking, the examined NADES were two-component mixtures themselves, thus, the presented systems indeed were made of four components in total. For simplicity reasons, the NADES were regarded as a unit and the systems will continuously be referred to as ternary ones [70,126].

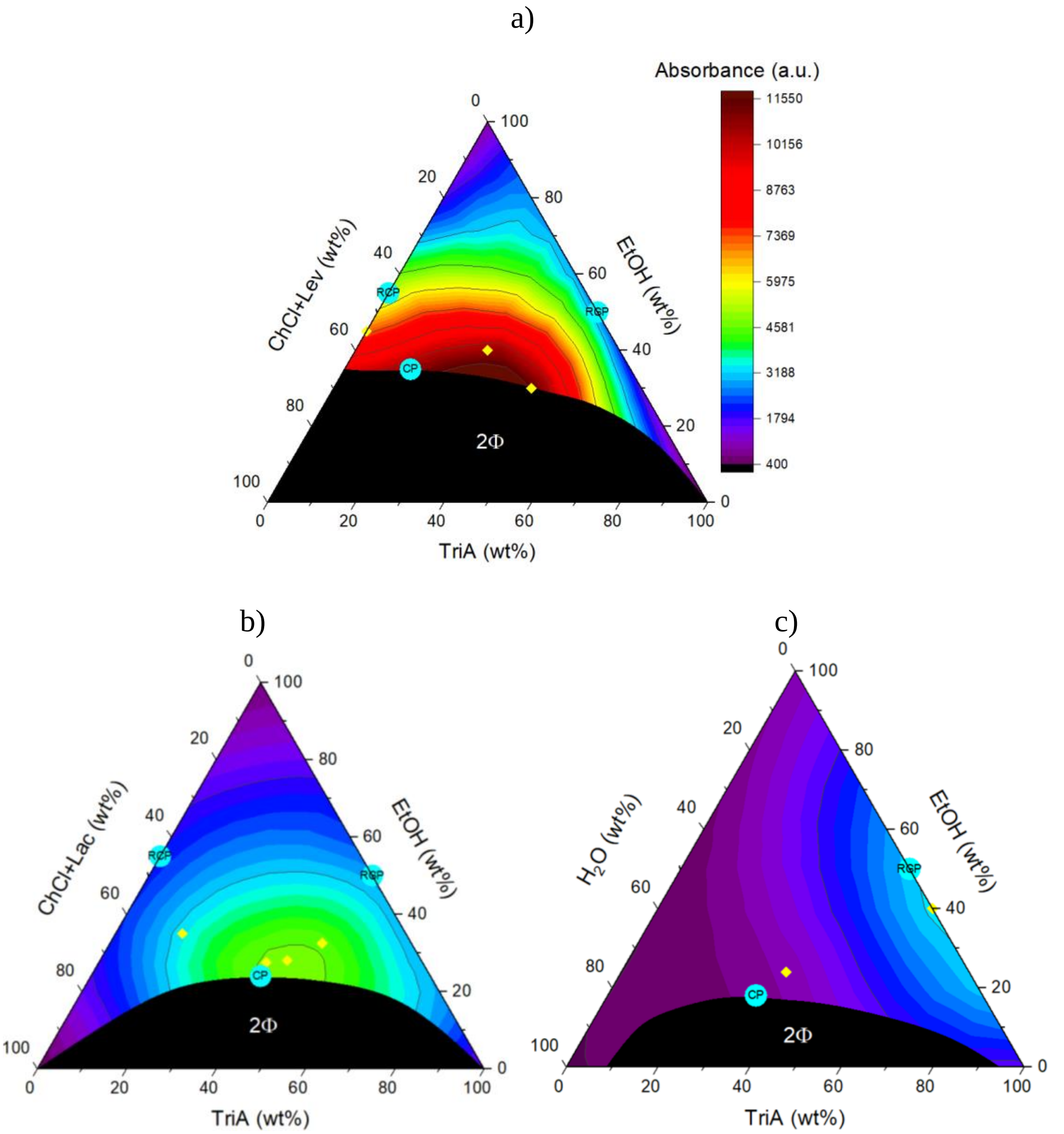
a)

b)

c)

Figure 4-3: Ternary phase diagrams with curcumin solubility maps consisting of EtOH as the cosolvent, TriA as the oil phase, and the hydrophilic component a) ChCl+Lev, b) ChCl+Lac, and c) water. The black areas labeled 2Φ represent the two phasic regions of immiscibility in the ternary systems. The heat maps in the monophasic parts indicate the curcumin solubility, where red shows a high solubility and purple a low one. The color scale of a) can be applied to all diagrams. The yellow diamonds indicate the points examined in the extraction experiments. The critical and reminiscent critical points are represented by the turquoise points labeled CP and RPC respectively [70,126].

All three phase diagrams look rather similar as the systems share each one two-phasic (2Φ) region between the hydrophilic and hydrophobic components. The major difference between the three of them was that both NADES were not miscible with TriA at all, whereas water and TriA were miscible to some extent (~ 10 wt%). This suggested that the NADES were even more polar than water. The largest 2Φ area was found in the system containing ChCl+Lev. 35 wt% of EtOH were necessary to achieve full miscibility of all three components, while 25 wt% and 20 wt% EtOH were enough in the systems with ChCl+Lac and water respectively. In these systems, in contrast to the former one, the binary mixtures of the hydrophilic and hydrophobic parts with the cosolvent EtOH were fully miscible. ChCl+Lev was only miscible to ~ 65 wt% with EtOH. This suggested that EtOH was not an ideally powerful cosolvent in this mixture. Based on this information, it can be speculated that a cosolvent, which is completely miscible with TriA and NADES, could decrease the biphasic region. Mixtures of water and EtOH come to mind as well as glycerol and polyethylene glycol. However, changing the cosolvent will also have an influence on the preferential solubility in the binary mixture of cosolvent and TriA as described by P. Degot *et al.* The monophasic domains obtainable with both NADES mixed with EtOH and TriA were large enough to arouse interest for successive extraction experiments [70,126].

P. Degot *et al.* reported structuring in the ternary water/EtOH/TriA mixture, which lead to a classification as a surfactant-free microemulsion (SFME) [47]. To justify a classification as SFME as well, dynamic light scattering experiments were conducted in the NADES systems. Through these examinations, the reminiscent critical points (RCPs) of the underlying binary mixtures of NADES/EtOH and EtOH/TriA and the ternary mixtures’ critical points (CPs) were determined. The CPs could be determined through scattering experiments by identifying the regions where the critical fluctuations were most pronounced. At these points, the correlation functions as indicators of structuring should reach their maximum [148,149]. RCPs were introduced here as descriptors of CPs of the binary mixtures, which can be observed at ambient temperatures. Since most examined binary solutions with EtOH are monophasic, talking about CPs is not totally precise as CPs imply a phase separation. Yet, fluctuations detected by light scattering indicated fluctuations and solving anomalies in these fully miscible solutions, suggesting a possible demixture of those binary solutions at certain conditions like temperature. The compositions where demixing would occur first would mark the CP. Projections of these critical compositions where fluctuations were detected to ambient temperatures were titled RCPs [126].

Samples above the 2Φ regions of all three ternary systems were inspected using DLS. The respective correlation functions are presented in Figures 9-3 to 9-5 of the Appendix. Using these data, the CPs were located at the hydrophilic side of the phase diagrams. Looking at Figure 9-3 presenting the correlations in the ChCl+Lev ternary systems, the correlations were rather indistinctive with only a little increase around 20 wt% TriA. The correlations of the ChCl+Lac system (cf. Figure 9-4) were more pronounced, implying a CP at around 40 wt% TriA. The ternary system of water/EtOH/TriA (cf. Figure 9-5) was the only one that exhibited pronounced correlation curves and, thus, according to P. Degot *et al.* [47], could be considered a classical SFME. The CP could be determined between 30 and 40 wt% of TriA. The CPs in all systems are marked by the labeled, turquoise points in Figure 4-3. The correlations of the NADES systems were hardly pronounced, implying that the found signals were caused rather by slight fluctuations instead of defined aggregates like micelles. Hence, this suggested that the found CPs are classical ones. Further, even though the ternary mixtures of NADES/EtOH/TriA could not be classified as SFMEs, this had no influence on the solubilization power of curcumin [126].

After analyzing the ternary mixtures, the binary ones NADES/EtOH and EtOH/TriA were examined as well. The belonging correlation functions can be viewed in Figures 9-6 to 9-8 of the Appendix. Since the water and EtOH mixtures had already been examined by T. Buchecker and S. Krickl *et al.* [139], they have not been measured again. No significant correlations in these binary mixtures had been found, although the existence of inhomogeneities between these two molecules is known. Through their high diffusion, the produced fluctuations are too fast to be detectable by DLS. Thus, no RCP in this mixture was determined. Both NADES/EtOH binary mixtures showed an increase in correlation with an increasing NADES content (cf. Figures 9-6 and 9-7). For both systems, the maximum correlation functions were found at a NADES content of 40-50 wt%. Surpassing this NADES content, the ChCl+Lev system demixed and turned two-phasic, while the correlation curves became bimodal in the ChCl+Lac system. This change of phase behavior was chosen to set the RCP. Correlation functions in the binary EtOH/TriA mixtures increased only weakly and reached a maximum at 50 wt% of EtOH [126].

Indeed, determining critical points via DLS is not perfect, especially when the correlation functions change only slightly, like they did in the NADES/EtOH mixtures. However, to support the findings of the scattering experiments, a phase diagram of the binary EtOH/TriA was simulated using COSMO-RS. The goal was to find a critical temperature at which the two liquids were not miscible anymore. Above and at ambient temperatures, EtOH and TriA are fully miscible. Thus, it was hypothesized that an upper critical solution temperature (UCST), as defined by IUPAC, should be found [126,150]. The composition with the highest correlation functions at ambient temperatures was expected to coincide with the composition at which the phase transition at lowered temperatures would occur. This should mark the critical point of the original binary mixture. From this CP, the RCP could be inferred to the binary line of the system at room temperature [126].

The simulation, on the other hand, was difficult due to severe convergence issues during the calculation of the liquid-liquid equilibria (LLE). Hence, the presented results were only rudimentary assessments of the latter. The explanation would exceed the scope of this study, but to illustrate the found LLE, a preliminary phase diagram contextualized within the ternary ChCl+Lev/EtOH/TriA at 25 °C is given in Figure 9-9 of the Appendix [126].

Nonetheless, two LLEs at ratios of 65:35 and 80:20 EtOH/TriA were found at a temperature of -30 °C, which served as an indication of a biphasic system. The simulation at -20 °C, on the other hand, did not show any LLE. Thus, most probably, a UCST between -20 °C and -30 °C was encountered, suggesting that above -30 °C EtOH and TriA are fully miscible at any proportion. This led to the description of RCPs, which are basically shadows of the critical point at the UCST below -20 °C that can still be detected at room temperature via DLS through slight fluctuations. Yet, the experimental data and the simulation, due to calculation difficulties and temperature effects, differ. Nevertheless, some sort of solving anomaly, like fluctuations in the binary EtOH/TriA, was found [126].

Critical fluctuations in the solvent can be imagined as nano-fissures, which might act as starting points for changes, like phase separation, in the liquid. It is possible that favorable interactions between the solvent and introduced compounds will emerge, caused by the formation and deformation of these fissures. In the case presented here, these interactions might appear as preferential solubility of curcumin inside the solvent. This is what P. Degot *et al.* partly described when examining the solubility synergy between EtOH and TriA, which was at its maximum close to the RCP of this mixture. When looking at the presented solubility maps Figure 4-3, the maximum solubility of curcumin was close to the CPs and RCPs of the mixtures. This gave an indication that the high solubility close to the RCPs of the underlying binary systems had an influence on the high solubility in the ternary mixtures around the CPs. This is analogous to the reports of P. Bauduin *et al.* [151] who added short propylene glycol alkyl ethers to microemulsions. The demixing temperatures of the examined microemulsions were tuned according to the characteristics of propylene glycol alkyl esters. This means, the formulation induced the temperature dependence, while in the presented case the temperature sensibility was intrinsic [126].

When only taking a look at the solubility, the maximum solubility of curcumin was largely higher in the NADES systems as compared to the water system. The solubility could be improved by employing a hydrophilic phase, which was also capable of solving curcumin. The improvement followed the trend found in Figure 4-2, which could be described as ChCl+Lev > ChCl+Lac > water. Water only decreased the solubility in the ternary systems while the addition of NADES shifted the maximum solubility from the 40:60 EtOH/TriA binary mixture to the ternary, from the RCPs towards the CP of the ternary mixture. By basing the ternary systems on the ChCl+Lev NADES, a 2- to 7-fold increase of curcumin solubility, with regard to the best compositions in the ChCl+Lac and water systems respectively, was achieved. Nevertheless, achieving such a strong increase of solubility by exchanging water with highly polar NADES is still remarkable [70,126].

4.3.3 Extraction Ability

In consideration of the region of highest solubility in the ternary system, the optimum mixture of 35:27.5:37.5 ChCl+Lac/EtOH/TriA (cf. Figure 4-3 b) was chosen to determine the optimum powder to solvent ratio for satisfactory extraction results of the curcuminoids from ground rhizomes of *Curcuma longa* L. (cf. Figure 4-4) [70]. Triplicates of all samples were examined for accuracy. The quantification of curcuminoids was done via HPLC using an external calibration, the corresponding calibration curves are presented in Figure 9-10 of the Appendix. Figure 4-4 shows that the quality of extraction only weakly depended on the powder to solvent ratio. A ratio of 1:8 (*w/w*) rhizome powder to extraction solvent was necessary to ensure a reasonable extraction yield. Below this ratio (cf. 1:6 (*w/w*)), the extraction yield was not satisfactory, yielding ~ 20% less curcuminoids in total compared to the higher ratios. On the other hand, surpassing a powder to solvent ratio of 1:8 (*w/w*) did not significantly improve the extraction yield while also disagreeing with the principles of green chemistry and extraction according to P. Anastas [6] and F. Chemat [7]. Thus, higher ratios for experiments would only be a waste of solvent. Therefore, the optimum ratio of 1:8 (*w/w*) was chosen to be used in the following extraction experiments of the NADES systems [70,126].

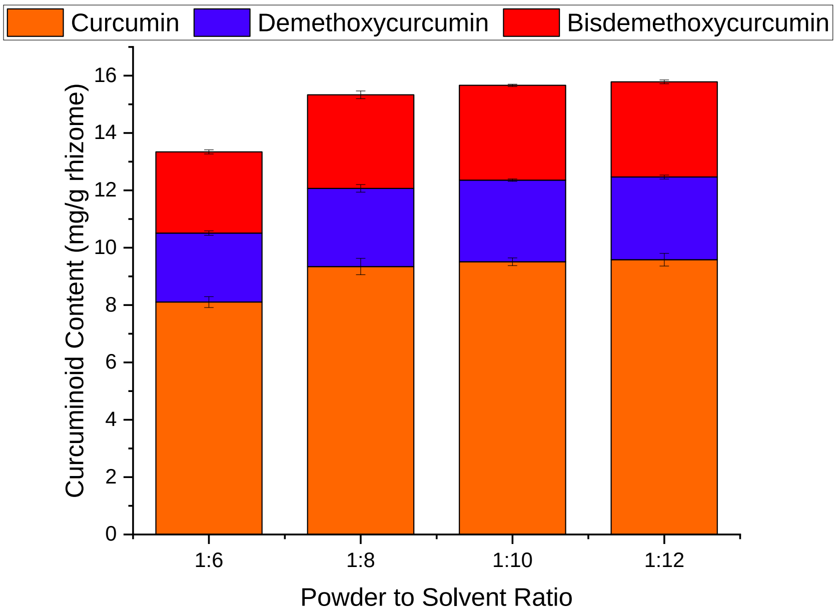

Figure 4-4: Determination of the optimum powder to solvent ratio (w/w) in view of the extraction yield using the optimum composition of ChCl+Lac/EtOH/TriA 35:27.5:37.5 [70].

The optimum powder to solvent ratio was not revalued for the ChCl+Lev system as its constituents were very similar to the examined ChCl+Lac system. Thus, it was assumed that it should also behave similarly to the ChCl+Lac system in matters of extraction [70,126].

During the quantitative examination of the extracts (cf. Figure 4-5), the standard Soxhlet extraction, as described above (cf. Section 2.2.1Soxhlet Extraction) and performed by P. Degot *et al.* [47], was used as a reference. Noting again, heating is necessary to have the solvent evaporate before extracting and returning to the solvent reservoir loaded with the extractant in the classical setup. However, heat impact on the extractants, in this case the curcuminoids, is problematic as they thermally degrade. Therefore, the total curcuminoid content was undervalued. To improve the precision of the determination of the total curcuminoid content, the classical setup was ameliorated by introducing an oil pump and valve for pressure control. According to the Clausius-Clapeyron relation, as given above (cf. Equation (3-4)), lowering the pressure will also reduce the boiling temperature of the solvent. Thus, this provided a gentler way to extract the thermolabile curcuminoids at a temperature of only 30 °C. The improvement of the extraction yield from the classical Soxhlet to the pressure-controlled one can be seen in Figure 4-5 and the quantitative results in detail can be viewed in Table 9-8 of the Appendix [70,126].

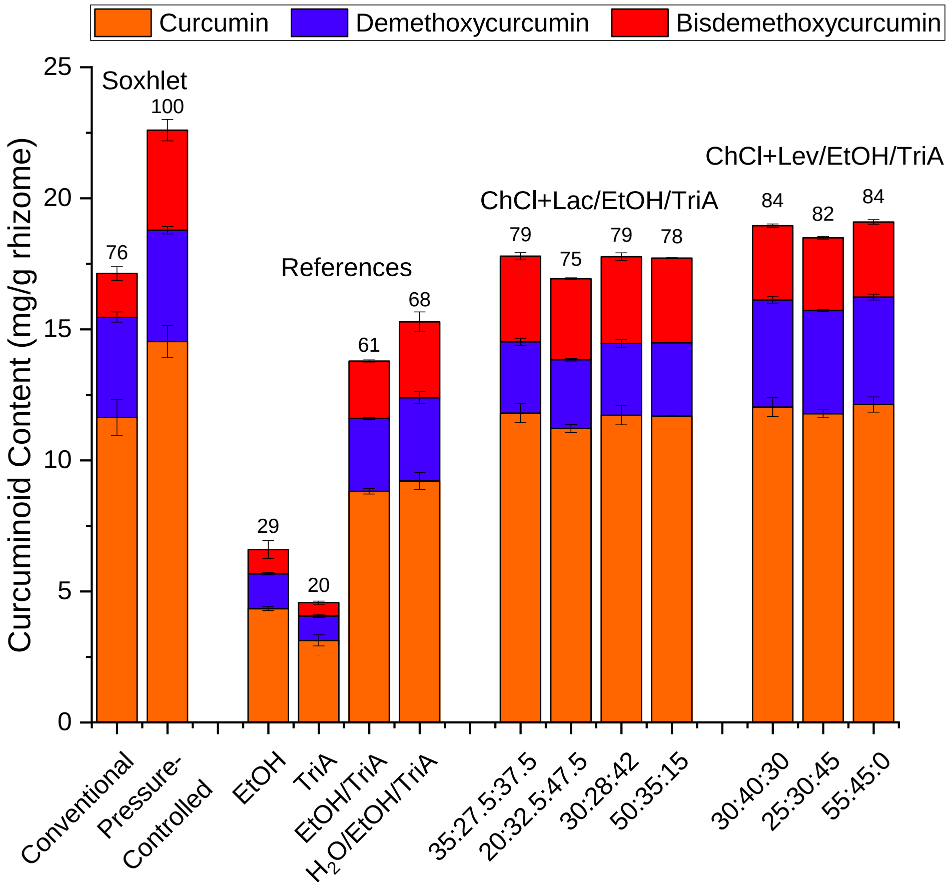

Figure 4-5: Overview of the yield of all extraction experiments. Curcumin is presented in orange, demethoxycurcumin in blue, and bisdemethoxycurcumin in red. The results are separated into four blocks for clarity. The first block represents the conventional [47] *and pressure-controlled* [126] *Soxhlet extractions, the second block the references of pure EtOH and TriA, their optimum binary mixture of 40:60, and the best ternary mixture of 40:24:36, which were provided by P. Degot et al.* [47], *the third the extraction results of the ternary ChCl+Lac/EtOH/TriA mixtures* [70], *and the fourth the extraction results of the ternary mixtures of ChCl+Lev/EtOH/TriA* [126]. *The numbers above the columns give the extraction yield in percent in comparison to the reference, which was the yield obtained via pressure controlled Soxhlet extraction.*

By using the pressure controlled Soxhlet device, a total of 5.3 mg more curcuminoids per gram rhizomes could be extracted. In detail this improves the extraction of curcumin by 20%, of demethoxycurcumin by 10%, and of bisdemethoxycurcumin by 56%. This confirms that bisdemethoxycurcumin is most sensitive to temperature. Even though the results could be improved with the amended Soxhlet method, there is still no guarantee that the total of curcuminoids was extracted or that no thermos-degradation occurred. Yet, the strong improvement of the total curcuminoid content at lower temperatures (30 °C instead of > 56 °C, which is the boiling point of acetone) suggests that a more accurate value of the total curcuminoid content could be reached. Therefore, the yields of the pressure controlled Soxhlet represent the 100% reference and the numbers given in Figure 4-5 and Table 4-3 denote the relative extraction yield with regard to the reference [70,126].

Several compositions in the NADES systems were tested and the data of the water/EtOH/TriA system, as provided by P. Degot *et al.* [47], served as reference. Generally, all systems containing NADES yielded the best results with extraction yields between 75-84%, while the unary solvents, pure EtOH and TriA, performed worst with yields of 29% and 20% respectively. The system based on the ChCl+Lev NADES (~ 84%) performed better than the ChCl+Lac NADES systems (~ 79%) and water system (~ 68%). It can be argued that the NADES, similarly to the water, might be able to swell and burst the plant cells for better solvent penetration and mass transport. Though, other mechanisms of cell membrane opening are conceivable, especially since ChCl and Lac already exist in cells [70,126].

To identify the mechanism and to evaluate the plausibility of the cell swelling theory, the extraction power of the optimum composition of the ChCl+Lac/etOH/TriA 35:27.5:37.5 (*w/w/w*) with the addition of water was checked (cf. Table 9-8). Upon the addition of water to the optimum system ternary system, the extraction yields plummeted with an increasing water content, even though the yield of dimethoxy- and bisdemethoxycurcumin could be increased. This is possible as these two curcuminoids are more polar and in turn better soluble in aqueous systems. Thus, the mechanism of extraction was not solely governed by the ability of the solvent to destroy and penetrate the plant matrix. This raised the question about the driving force of the extraction. Thus, as a next step, the extraction of the curcuminoids from the ground rhizomes by using a binary mixture of 55:45 (*w/w*) ChCl+Lev/EtOH was examined. Viewing Figure 4-3 a, the solubility of the binary mixture was approximately 25% lower than in the optimum ternary composition of ChCl+Lev/EtOH/TriA 30:40:30 (*w/w/w*). However, when comparing their extraction power, both compositions achieve a similar extraction yield with a difference of 0.13 ± 0.07 mg per g rhizome. Seemingly, the solubility as well was not the only factor influencing the quality of extraction. It was concluded that a combination of both factors, the solubility and solvent penetration, could be the responsible driving force for the extraction. Other additional effects, like preferred interactions of solvent and solute, in this case cation-π interactions, could affect the quality of extraction. Unfortunately, no final conclusion about all underlying factors could be drawn as this would have exceeded the scope of this study [70,126].

By replacing water in the ternary systems by different NADES, the solubility of curcumin was improved. To exploit the full potential of this high solving capability, cycle extractions were performed as described by P. Degot *et al.* [48]. The results can be seen in Figure 4-6. While keeping the amount of solvent to a minimum, a higher amount of fresh rhizomes should be extracted. The repeated use of the solvent comes with benefits in terms of waste prevention or in this case reduction and solvent economics. To assess the greenness and sustainability of the developed solvents, the process mass intensity (PMI) was consulted (cf. Equation (4-4)). In this case, the PMI was divided by the factor 1000 to obtain smaller numbers:

$$PMI = \frac{\left(\frac{m_{Rhizome} + m_{Solvent}}{m_{Extracted}}\right)}{1000} \tag{4-4}$$

The PMI is a measure of the total mass of materials necessary to produce a product. It can make a statement about the quality of an extraction, evaluating the greenness and/or waste of solvent [152–155]. While the relative extraction yield can give information about one cycle of extraction, the PMI can give insight into the improvement during a number of extraction cycles. The comparison of the PMI and extraction yield are given in Table 4-3.

The smaller the PMI, the better and more powerful is the examined extraction. Like already evaluated above, the PMI also rates the pressure controlled Soxhlet extraction better than it does the classical one. However, the 100% reference, the pressure controlled Soxhlet extraction, scored a worse PMI than the single extraction cycles of the ternary extraction cycles. This could be expected since the Soxhlet process needs more solvent to extract the same mass of rhizomes, concluding that the easy room temperature extraction in the ternary systems is more effective in terms of solvent use. Of course, when only looking at one extraction cycle, a high extraction yield and a low PMI coincide, confirming the optimum compositions in both NADES/EtOH/TriA systems. However, through the repeated use of the extraction solvents, the PMI could be improved further, while the extraction yield ceased to be analyzable.

Table 4-3: Comparison of extraction yield and PMI.

Extraction System	Yield	PMI
Pressure-controlled Soxhlet[d]	100%	2.39
Soxhlet[b]	76%	3.15
EtOH[b]	29%	3.03
TriA[b]	20%	4.37
H_2O/EtOH/TriA 40:24:36[b]	68%	1.31

ChCl+Lac/EtOH/TriA 35:27.5:37.5 Optimum Composition[c]	79%	1.01
ChCl+Lac/EtOH/TriA 20:32.5:47.5[c]	75%	1.06
ChCl+Lac/EtOH/TriA 30:28.1:41.9[c]	79%	1.01
ChCl+Lac/EtOH/TriA 50/35/15[c]	75%	1.06
ChCl+Lev/EtOH/TriA 30:40:30 Optimum Composition[d]	84%	0.95
ChCl+Lev/EtOH/TriA 25:30:45[d]	82%	0.97
ChCl+Lev/EtOH 55/45[d]	84%	0.94
H_2O/EtOH/TriA 40:24:36 Cycle 4[e]	127%	0.35
ChCl+Lac/EtOH/TriA 35:27.5:37.5 Cycle 7[c]	117%	0.25
ChCl+Lev/EtOH/TriA 30:40:30 Cycle 7 [d]	117%	0.25
ChCl+Lev/EtOH/TriA 30:40:30 Cycle 12 [d]	62%	0.33

[b] Data taken from P. Degot *et al.* [47].

[c] Published in V. Huber *et al.* [70].

[d] Published in V. Huber *et al.* [126].

[e] Published in P. Degot et al [48].

Coming back to the cycle extractions themselves, which are presented in Figure 4-6, all experiments were conducted using a 1:16 (*w/w*) powder to solvent ratio to be able to neglect the solvent loss. Performing the extraction cycles, one can see that the total amount of extracted curcuminoids increased for every system. P. Degot *et al.* described a linear increase of curcuminoids with every extraction cycle until saturation [48], which occurred already after 3 cycles. The results are indicated by the black squares. The linear increase was also found true for all curcuminoids in both NADES systems (cf. Figures 9-12 and 9-13). For the ChCl+Lac system (red dots), a saturation was reached after 7 cycles of extraction as the amount of extracted curcuminoids did not increase significantly and leveled off at ~ 170 mg. This was expected since the solubility in the ChCl+Lac system was roughly twice as high as in the water system and could, therefore, be used for twice as many extraction cycles. Comparing the ChCl+Lac system with the ChCl+Lev one, it was expected to be able to complete roughly double the amount of cycles as well, due to the twofold solubility increase. Indeed, the extraction mixture could be enriched in curcuminoids up to cycle 7 leveling off at ~ 180 mg curcuminoids in total. Referring to the PMI calculations additionally, it was confirmed that the NADES systems outperformed the water system. However, no significant further increase in curcuminoid content was possible in the ChCl+Lev system. Considering the fact that after 10 cycles of extraction still a small increase of curcuminoids in comparison to the 7th cycle was observed, it could be concluded that a slow saturation occurred. However, an increase that small could not justify the experimental effort of adding three cycles. Hence, cycle 7 was considered the final one [70,126].

The curcuminoid content in the ChCl+Lev system decreased again after 12 cycles of extraction. While in Figure 4-6 and 9-13 only the total curcuminoid content is presented, the concentration reached after 12 cycles is shown in Figure 9-14. The concentrations of every cycle still increased but not the total amount of extracted curcuminoids, showing that the increase was a relative concept. This phenomenon of first increasing the curcuminoid mass and successively losing curcuminoids also arose during the study of P. Degot *et al.* [48]. This was counterintuitive and was investigated in the following.

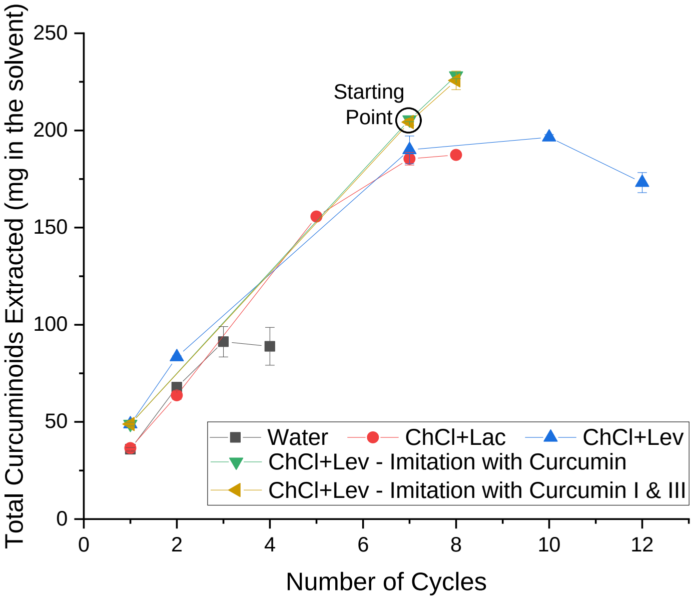

Figure 4-6: Total curcuminoid content of the ternary cycle extraction systems of water/EtOH/TriA 40:24:36 (black squares) [48], *ChCl+Lac/EtOH/TriA 35:27.5:37.5 (red dots)* [70], *and ChCl+Lev/EtOH/TriA 30:40:30 (triangles). The blue triangles represent the repeated extraction of fresh, ground rhizomes without additives. The green down-facing triangles show the extraction samples prepared with synthetic curcumin, the yellow left-facing triangles with a blend of synthetic curcumin and bisdemethoxycurcumin. Both systems were prepared to imitate a starting point at cycle 7 before performing one cycle of extraction* [126].

To evaluate whether a premature saturation was reached, two samples containing synthetic curcuminoids were prepared to imitate the curcuminoid content at cycle 7. One sample, represented by the green triangles, was prepared by adding synthetic curcumin only and the other sample, indicated by the yellow triangles, with a mixture of curcumin and bisdemethoxycurcumin. Twice the amount of bisdemethoxycurcumin that was extracted in the natural 7th cycle was added to imitate the content of demethoxy- and bisdemethoxycurcumin in total as demethoxycurcumin was too expensive. According to Figure 4-6, the composition of the curcuminoids hardly influenced the successive extraction of the rhizomes. The increase of curcuminoids in the artificially prepared systems after performing an extraction indeed showed that it was still possible to enrich the solvent. No premature saturation was reached, apparently. Thus, the question of why the extraction solvent could not be enriched further by simply reusing the solvent arose [126].

Considering that one extraction cycle takes roughly 1 h, multiple cycles demand a lot of time (> 12 h for 12 cycles). Therefore, there is a likely possibility that the solvent was altered over time. Especially the combination of TriA, a molecule with three ester bonds (cf. Table 9-2), with the NADES, which was made of an acid, may react by hydrolyzing TriA. To verify this assumption, ^{13}C-NMR samples were examined over three days. The spectra are given in Figures 9-15 to 9-17. Supposing that hydrolysis had taken place, two new peaks at around 20 and 175 ppm as an indication of acetic acid should have appeared. Yet, the NMR spectra did not change over the course of three days, ruling out the possibility of acidic hydrolysis. Additionally, the peaks representing EtOH did not change in terms of intensity, eliminating the possibility of evaporation as solvent alteration as well [126].

Since neither TriA nor EtOH seemed to be the reason for the premature saturation, the NADES content was examined via conductivity measurements as ChCl is an electrolyte. A calibration curve of the conductivity of the solvent with different NADES contents was recorded (cf. Figure 4-7 a). By diluting the optimum composition ChCl+Lev/EtOH/TriA 30:40:30 (*w/w/w*) with a binary mixture of 40:60 EtOH/TriA (*w/w*), the conductivity could be examined. The starting point of the optimum mixture was found at ~ 4.3 mS/cm. As expected, with fewer charge carriers in the systems with lower NADES contents, the conductivity sank [126].

Successively, the optimum composition was used for extraction experiments and the conductivity after every extraction cycle was measured and can be seen in Figure 4-7 b. With every cycle, the conductivity decreased strongly, down to ~ 3.7 mS/cm after seven extractions. Assuming that the measurable conductivity originates only from ChCl in the NADES, the comparison of Figure 4-7 a and b yields a ~ 25 wt% decrease of NADES. Most likely, during every cycle of extraction, ChCl was lost to the plant material, altering the solvent composition and simultaneously the conductivity. Literature reported that ChCl can share strong ionic interactions with the negatively charged cellulose residues inside the plant matrix [156,157]. *Curcuma longa* L., just like any other plant, contains dietary fibers like starch or cellulose [135]. As a result of these interactions, ChCl could be trapped inside the plant matrix after the extraction. When replacing the old rhizomes by fresh ones for the successive extraction steps, the composition of the solvent will be altered. After several extraction cycles, the solvent's composition will be changed to such an extent that the curcumin solubility is way lower than at the beginning (cf. Figure 4-3 a). This gives reason to a slow saturation between the 7th and 10th cycle. The decrease of curcuminoids by cycle 12 can be explained as well: The previously extracted curcuminoids might have saturated the solvent already and could not be kept in solution when altering the solvent composition even more. Hence, they stayed behind and the amount of curcuminoids in total decreased [126].

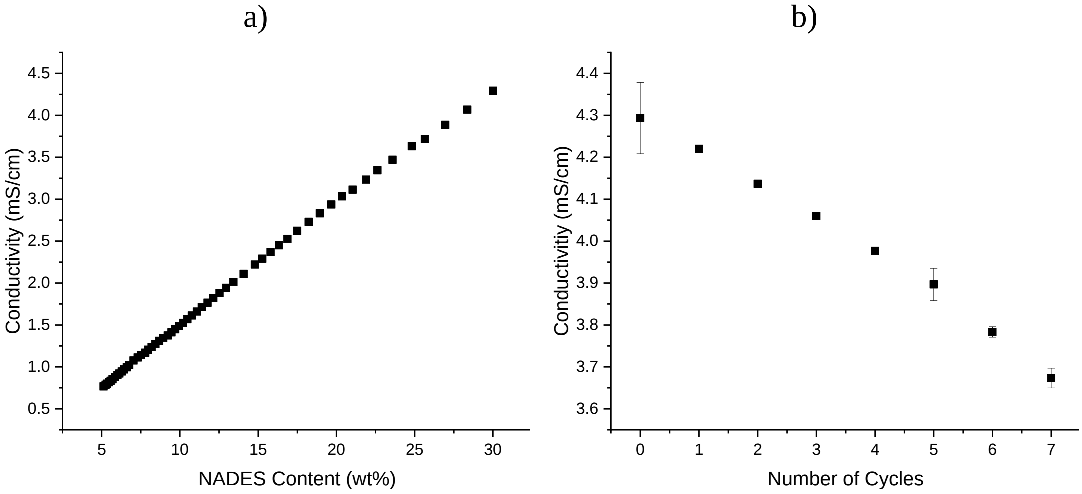

Figure 4-7: Conductivity measurements in the ChCl+Lev/EtOH/TriA system at the optimum composition (30:40:30) a) diluted with a binary EtOH/TriA 40:60 mixture and b) after multiple cycles of extraction [126].

4.4 Conclusion

The focus of this study was placed on the extraction of curcuminoids from *Curcuma longa* L. Inspired by P. Degot *et al.* [47], ternary solvent systems made from EtOH, TriA, and natural deep eutectic solvents were examined. Qualitative UV/Vis examinations were performed to find the best NADES and the domains of highest solubility in the ternary systems. Successively, extraction experiments were conducted and evaluated via HPLC elution. The reusability and change of the NADES-based solvents were assessed after multiple cycles of extraction by UV/Vis, NMR, and conductivity experiments.

During the NADES screening, eleven 1:1 (*n/n*) eutectics based on AcCl, ChCl, and Pro in combination with Cit, Lac, Lev, and Mal, mixed with EtOH and TriA, were saturated with curcumin. The NADES most capable of solving curcumin was determined via UV/Vis analysis. Both, the HBAs and the acids had an influence on the solubilization power of the system. Especially the HBAs with a positively charged nitrogen atom, AcCh and ChCl, seemed very promising, while Lev and Lac were the best HBDs. The best mixtures reached even higher solubilities of curcumin than acetone or EtOH/Tria 40:60 (*w/w*). Follow-up experiments to assess the reasons for the solubility enhancement are still necessary. It is important to find out why exactly the quaternary ammonium ions performed so well and if there is a trend concerning their additional functionalities. Furthermore, it would be interesting to see how the HBAs and HBDs interact when solving curcumin and how the solvent affects their abilities.

Ternary phase diagrams of ChCl+Lac/EtOH/TriA anc ChCl+Lev/EtOH/TriA were recorded and mapped out concerning the solubility of curcumin. In comparison to the ternary system containing water, the maximum solubility in the NADES mixtures was shifted from the binary EtOH/TriA system to the center. Light scattering experiments suggested that there could be a connection between the critical points of the ternary and binary mixtures. However, this could have easily been a coincidence and, thus, was not followed up in more detail.

The NADES mixtures' quality of extraction was compared to a reference of a pressure controlled Soxhlet extraction. With regard to the results presented by P. Degot *et al.* [47], the extraction could be improved with yields up to 79% and 84% for the ChCl+Lac and ChCl+Lev mixtures respectively. The difference between the systems based on Lac and Lev were justified by the higher solubility of curcumin in the ChCl+Lev system. Cycle extractions were performed at the optimum compositions of both ternary NADES systems. According to PMI calculations, the true value of extracting with these solvents emerged through their reusability.

Even though the solubility in the ChCl+Lev system was approximately two times higher than in the ChCl+Lac systems, only seven cycles of extraction were achieved.

It was hypothesized that the extraction solvent must change over time, leaving the optimum composition and leading to a lower solubility of the solutes. NMR measurements, however, suggested that neither the hydrolysis of TriA through the addition of acidic NADES nor the evaporation of EtOH were the reason. Conductivity measurements followed the fate of the NADES. By monitoring the dilution of charge carriers (ChCl), it was found that after every cycle of extraction, conductivity and, therefore, ChCl was lost. This served as an explanation why fewer extractions than expected could be performed successfully. By keeping the NADES and, therefore, the ChCl constant after each cycle of extraction, it should be possible to exploit the full potential of the solvent.

Even if the attempt of mixing NADES with solvents such as EtOH and TriA may seem exotic, a step towards green extractions was made. Like stated above, it cannot be expected that a newly proposed method or extraction solvent will replace the conventional methods. However, with further research and equipment, the process might become refined enough to actually compete with the status quo.

CHAPTER 5

UNCOVERING THE CURCUMIN SOLUBILIZATION ABILITY OF NADES

CONTENTS

The influence of quaternary ammonium compounds (QAs) and organic acids on the solubility of curcumin and possible solving mechanisms will be examined in the following chapter.

5 Uncovering the Curcumin Solubilization Ability of NADES

The results of this section have been published in the article *Uncovering the Curcumin Solubilization Ability of Selected Natural Deep Eutectic Solvents Based on Quaternary Ammonium Compounds* by V. Huber *et al.* [158]. No licensing was required. The creation of this chapter was aided by the contributions of **Lukas Moser** and **Katharina Funkner**, assisting the solubility measurements, **Vanessa Rudolph** and **Lea Sammet** for arbitrary data collection, and **Dr. Johnny Hioe**, curating the COSMO-RS data.

5.1 Introduction

Curcumin is a natural pigment found in *Curcuma longa* L., also known as turmeric. The structure of the phytochemical can be viewed in Figure 4-1 and Table 9-2. A thorough introduction to turmeric and its active ingredients was given above (cf. 4.1), thus, it will be foregone in this chapter.

The topic discussed in the following deals with the underlying mechanism with which the phytochemical is solved in ethanol mixed with different additives. In the preceding studies, summarized in Chapter 4 [70,126], through a screening of water-free, ternary solvent mixtures, it was found that varying NADES are differently capable of solving curcumin. Especially levulinic acid and QAs showed a positive effect on curcumin's solubility. Specific intermolecular interactions like hydrogen bonding or π-cation interactions between the NADES and the solute could be the reason behind the favorable solubility. To the knowledge of the authors, this was the first study to investigate the specific interactions and the reason for the improved curcumin solubility. Through a combination of COSMO-RS and NOESY NMR measurements, an attempt was made to break down the interactions between curcumin and nine different NADES in ethanolic solutions and to figure out the reason for the solubility enhancement.

5.2 Experimental

5.2.1 Chemicals

All chemicals with their abbreviations, purities, and vendors which were used in this section can be found in the following Table 5-1.

Table 5-1: Chemicals used in Section 5.

Chemical	Abbreviation	Purity	Vendor
Curcumin	Cur	> 97%	TCI (Eschborn, Germany)
Betaine	Bet	> 97%	
Carnitine	Car	> 98%	
Choline Chloride	ChCl	> 99%	Sigma Aldrich (Darmstadt, Germany)
Lactic Acid	Lac	> 85%, FCC	
Levulinic Acid	Lev	> 98%	
Pyruvic Acid	Pyr	> 97%, FG	
2-Oxabutyric Acid	Oxa	> 95%, FG	
2-Oxavaleric Acid	Ova	> 98%	
4-Acetylbutyric Acid	Aba	> 97%	
Hexadeuterodimethylsulfoxid	DMSO-*d6*	> 99%	
Tetradeuteromethanol	MeOD	> 99%	
Mandelic Acid	Man	> 99%	Alfa Aesar (Kandel, Germany)
Hexanoic Acid	Hex	> 98%	Merck (Darmstadt, Germany)
Ethanol	EtOH	> 99%	

All chemicals were used without further purification. Information about the chemical structures can be found in Section 9.1 of the Appendix.

5.2.2 Methods and Techniques

5.2.2.1 Sample Preparation

Samples were prepared by mixing different weight ratios (up to 70 wt%) of the QAs, acids, and NADES with ethanol and stirring them until they turned homogeneous. Successively, the samples were saturated with synthetic curcumin and left to stir at room temperature for 1 h. To remove the excess curcumin, the solutions were filtered through 0.45 µm PTFE filters. All samples were prepared in triplicate [158].

5.2.2.2 Solubility Examination via Optical Density Measurements

A qualitative analysis of the curcumin solubility was carried out by optical density measurements via UV/Vis spectroscopy. The samples were adequately diluted in ethanol before measurement and analyzed in the visible spectral region of 350-700 nm while the absorbance at the wavelength of maximum absorbance λ_{max} = 425 nm was used to compare all samples. A Lambda 18 UV/Vis spectrometer by Perkin Elmer (Waltham, USA) was employed to perform the measurements.

5.2.2.3 NMR Analysis

Intermolecular interactions between curcumin and the QAs and acids were characterized via ^{1}H-NMR and NOESY-NMR spectra. Deuterated dimethyl sulfoxide (DMSO-*d6*) and methanol (MeOD) were used as solvents, in which the pure compounds were saturated. For the analysis of two compounds at the same time, 1:1 (*n/n*) mixtures were prepared in the same solvents. Before transferring the solutions into Boro400-5-8 NMR tubes by Deutero (Kastellaun, Germany), they were filtered using 0.45 µm PTFE filters. ^{1}H and NOESY experiments were performed on a Bruker Avance III HD 400 MHz spectrometer equipped with a 5 mm BBO 400S1 BBF-H-D sample head with Z-gradient according to the pre-programmed methods. Processing, evaluation, and plotting of the data was carried out using the TopSpin 3.2 software and the spectra were characterized according to the NMR guidelines by ACS [159].

5.2.2.4 COSMO-RS Calculations

The chemical potential of curcumin in binary mixtures of various hydrogen bond donors or acids with ethanol was predicted using the 19.0.4 version by COSMO*logic*, based on the COSMO-RS theory. The program “mixture” was employed to calculate the chemical potential at infinite dilution at a TZVPD-FINE level. The necessary molecules were provided in the COSMO*base* TZVPD-FINE 19.0 database [160,161].

5.2.2.5 NADES Preparation

A variety of 9 different NADES based on choline chloride, betaine, carnitine, lactic acid, levulinic acid, and pyruvic acid was investigated. The preparation was carried out as described in the previous chapter 4.2.2.1. In this study, 1:1 and 1:2 (n/n) mixtures were examined.

5.2.2.6 Karl-Fischer Measurements

The water content of the NADES was examined using a Karl Fischer titrator (870 KF Titrino plus) by Metrohm (Filderstadt, Germany). The titer was determined by titrating 20-50 mg samples of Millipore water in conditioned, water-free methanol with the 8-

component Karl Fischer reagent via the Titer Ipol program. The NADES samples were titrated five times each using the KF Ipol program.

5.3 Results and Discussion

5.3.1 Influence of Quaternary Ammonium Compounds

The starting point of this investigation were the articles published by V. Huber *et al.* [70,126], in which the influence of different NADES on the solubilization and extraction power of curcumin was investigated. It was presumed that a positively charged nitrogen atom had positive effects on the solubility. In order to verify this guess, four QAs were examined: choline chloride (ChCl), betaine (Bet), carnitine (Car), and tetrapropylammonium bromide ($N_{3333}Br$). Their curcumin solving ability was compared via UV/Vis, and the results are presented in Figure 5-1 [158].

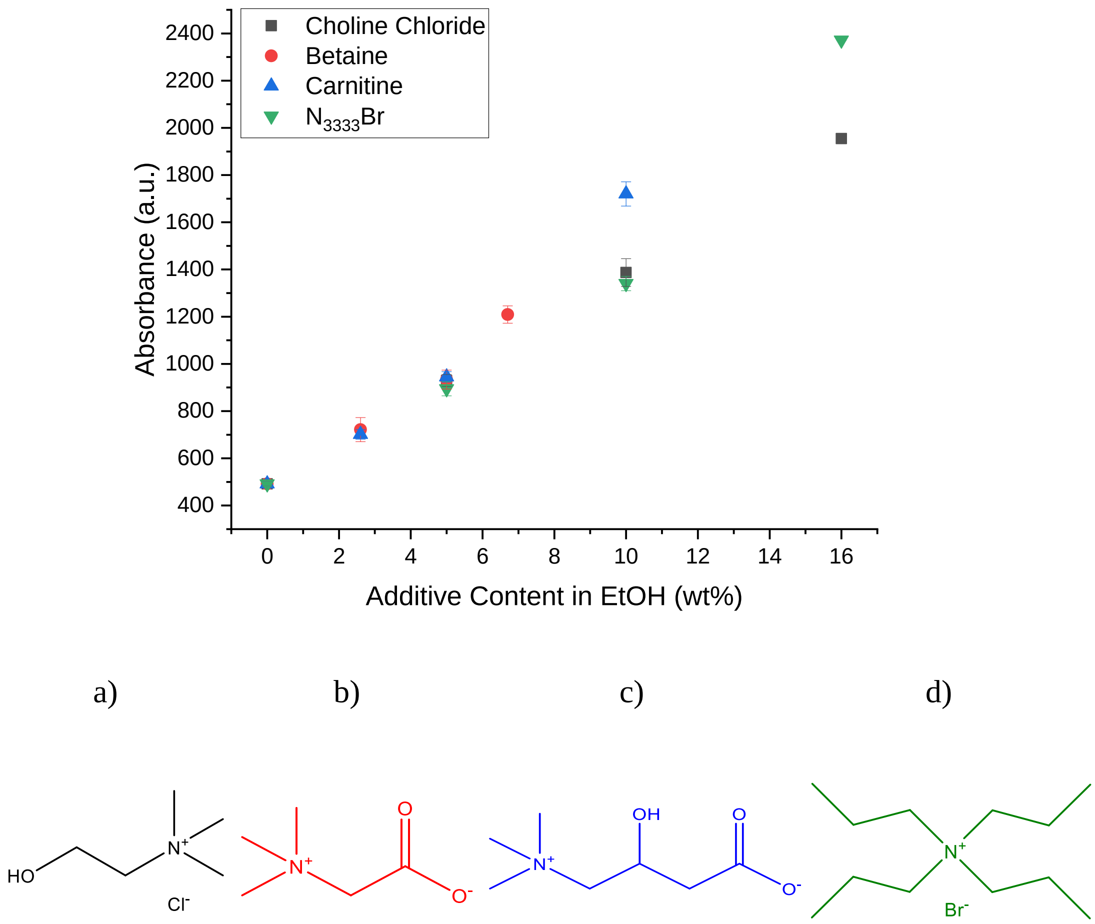

Figure 5-1: Assessment of the curcumin solubility in ethanolic solutions of a) choline chloride (black), b) betaine (red), c) carnitine (blue), and d) tetrapropylammonium bromide (green) [158].

ChCl, Bet, and Car were specifically selected since they are part of the human body and are sold as dietary supplements, which makes them also food-approved. The influence of their different functional groups, hydroxy and carboxy groups, and mixtures thereof respectively, on their ability to solve curcumin could be investigated. Even though N_{3333}Br is toxic towards water- and microorganisms and poses a potential hazard to humans [68,162], it was used as a reference with no additional functionalities to the quaternary ammonium group. With these four QA representatives, the influence of the presence and absence of different functionalities was covered. The molecular structures along with the solubility data are presented in Figure 5-1. Figure 9-18 of the Appendix shows the solubility data in mol% [158].

The QAs were examined in ethanolic solution either to their saturation or until 16 wt%, which was the maximum of solubility of ChCl (black squares) in EtOH. Bet was the least soluble molecule with a maximum solubility of 7 wt%. The solubility of curcumin could be enhanced by all QAs similarly in a linear manner. Only after 10 wt%, a small deviation of this linear behavior could be detected that was even less pronounced in the depiction in mol%. However, a 3-fold solubility increase of curcumin could be reached after 10 wt% of QA additive. The low solubility of the QAs in EtOH, on the other hand, limited an even higher curcumin solubility in ethanolic solutions [158].

Since all QAs showed an almost identical trend when solving curcumin, the presence or absence of hydroxy or carboxy groups had hardly any influence on it. Therefore, only the group all the additives shared, the quaternary ammonium, must be responsible. Like in the previous articles, it was assumed that cation-π interactions could be the mainspring driving the solubility enhancement. As reported in literature, these interactions should cause significant peak shifts in NMR spectra [163]. Thus, 1D and 2D NMR measurements in DMSO-*d6* were made. The peak coming from the solvent stayed at the same position of 2.55 ppm throughout all measurements and did not superimpose any signals emanating from the molecules of interest. In addition, no significant cross-peaks were caused by the solvent in the 2D spectra. To evaluate the influence of the solvent on the spectra, supplementary measurements of curcumin and curcumin + ChCl were recorded in deuterated methanol (MeOD). The choice fell on this deuterated solvent due to similarities with EtOH, the solvent used throughout all the experiments. All spectra can be regarded in Figures 9-19 to 9-41 of the Appendix. The peaks were noted according to the NMR guidelines by ACS [159]. The chemical shifts only differed slightly in the different solvent environments. However, the analysis of the interactions was rendered impossible in MeOD as the signals of the hydroxy groups and C^2 vanished (cf. Figure 9-20). However, it was possible to determine the ratio between the keto and enol tautomers of curcumin (cf. Figures 9-33 to 9-36 and Table 9-9). In both solvents the equilibrium was strongly shifted to the enol side, to 99% in DMSO-*d6* and to ~ 94% in MeOD. This proved that the conformation of curcumin, of course, was dependent on the solvent, while the preferred form was the enol form. Problematically, the shift to 99% of the enol form in DMSO-*d6* may mask interactions that could occur between the additives and the keto form. To assess this, ^{1}H NMR spectra of mixtures of curcumin with ChCl were evaluated as well. It was found that the addition of ChCl hardly influenced the keto-enol-ratio in both solvents (cf. Table 9-9). Therefore, DMSO-*d6* was used to evaluate the interactions between curcumin and the QAs. In future analyses, the solvent effects should be examined more in depth. This, however, exceeds the scope of this study [158].

When taking a look at the overlaid NOESY spectra of curcumin, QA, and their mixtures (cf. Figures 9-37 to 9-41), no extraordinary cross-peaks could be detected upon mixture of curcumin with the QAs. Thus, the existence of strong hydrogen bonding or cation-π interactions could be ruled out [164]. In particular, according to literature, the detection of cation-π interactions should have been possible via 2D NMR trials [68]. Even though the 2D data were not conclusive about any interactions, the 1D spectra showed that especially the peaks indicating curcumin’s hydroxy groups shifted significantly upon QA addition. The shifts with their corresponding assignment to the molecular structure are shown in Table 5-2 [158].

While the shifts of the hydroxy groups were strongly noticeable, the conjugated protons only experienced a negligible shift. Hence, it was concluded that no cation-π interactions came to be between the positively charged nitrogen atoms of the QAs and curcumin’s aromatic rings. If the aromatic hydrogen atoms had shifted, it would have been an indication for cation-π interactions [163,165]. The lack of this specific interaction could be caused by the geometry of curcumin in solution. Instead of being present in a planar fashion, curcumin is strongly bent, sterically prohibiting the usually preferred *en face* binding of the relatively bulky cations [166]. Typically, only interactions between QAs and small planar benzene derivatives including amino acids or interactions of small metal cations with relatively large molecules like crown ethers are the main topic when dealing with cation-π interactions [158,165].

Table 5-2: Change of the chemical shift of curcumin depending on the additives. The shift changes of the outer hydroxy groups are marked in red and the shift changes of the enol hydroxy group are in blue [158].

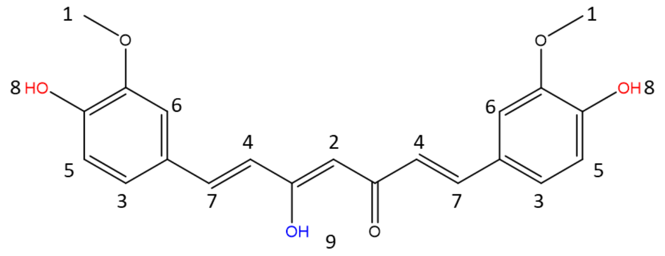

	1	2	3	4	5	6	7	8	9
Cur δ_{ppm}	3.84	6.02	6.71	6.85	7.14	7.30	7.58	9.66	16.51
+ ChCl	0.02	-0.03	-0.02	0.01	0.01	-0.00	0.07	-0.11	0.13
+ Bet	0.02	-0.02	-0.01	0.04	0.01	-0.00	0.06	-0.18	0.11
+ Car	0.02	-0.02	-0.00	0.04	0.02	0.00	0.07	0.07	0.15
+N_{3333}Br	0.02	-0.03	-0.02	0.05	0.01	-0.01	0.07	0.02	0.12

ChCl and Bet caused an upfield shift of the hydroxy groups marked in red, indicating a higher electron density around the hydrogen atom, possibly instigated by hydrogen bond donation of the QAs. However, this is only senseful in the case of ChCl as Bet is not capable of donating protons. Consequently, this shift could not be used for the identification of any trend or cause of preferential solvation. The shift of the enolic hydrogen, on the other hand, was more eminent. As determined before, the enol form, independent of the presence of any additive, was almost fully present (cf. Table 9-9). A downfield shift of the enolic hydrogen atom indicated a deshielding effect, which comes along with a depletion of electron density, suggesting hydrogen bond donation from curcumin. Unfortunately, these results were not enough to find a satisfactory conclusion about the interactions in the solvent. Yet, by combining the knowledge obtained via NMR with predictions of the σ-potentials and -profiles by COSMO-RS the preferential interactions could be revised [158].

Figure 5-2 shows the σ-potentials and -profiles. The orange curve, depicting curcumin's σ-potential, was quite symmetric, pointing in the negative direction with both ends. This was an indication for a favored interaction with both HBDs and HBAs, due to the presence of both hydroxy and methoxy groups in curcumin. Through steeper or more leveled slopes, ChCl (black) showed a similar curve progression as curcumin, with a weaker affinity for HBDs and a higher one for HBAs [158].

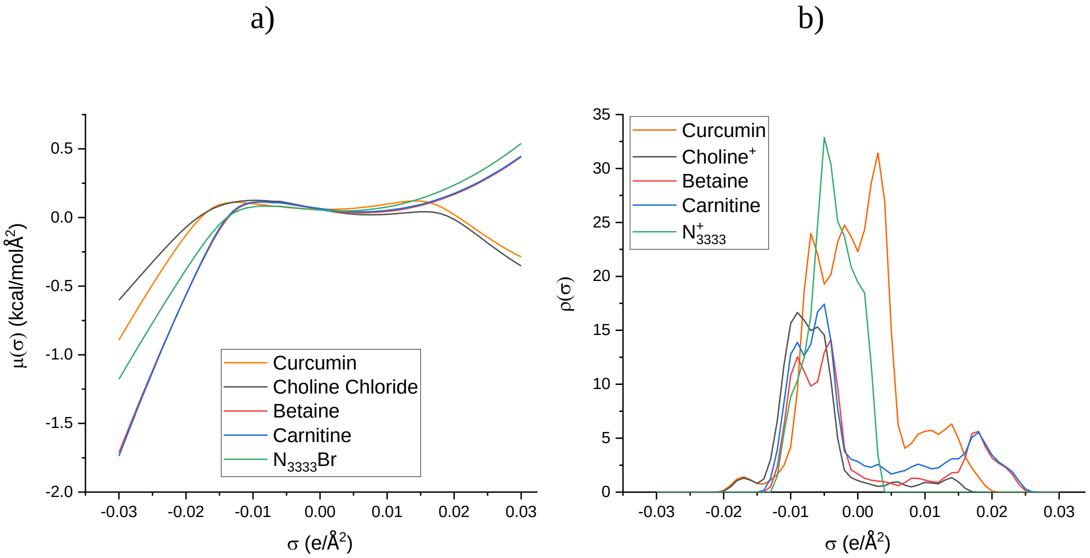

Figure 5-2: Conformationally averaged COSMO-RS predictions of a) σ-potentials and b) σ-profiles of curcumin (orange), and the QAs ChCl (black), Bet (red), Car (blue), and N$_{3333}$*Br and its corresponding cation* [99,100,103,158,160,161].

The remaining three QAs' curves, on the other hand, were very similar to each other but asymmetric. According to these curves, an affinity to interactions with HDSs but not with HBAs was predicted [98]. This behavior was caused by the negatively charged carboxy groups of Bet and Car, which can only accept but not donate hydrogen bonds, resulting in an aversion towards other accepting groups. The reason for N$_{3333}$Br was different since it does not possess any hydrogen bonding functionality. The bromide counterion was solely responsible for the accepting properties. The σ-profiles, given in Figure 5-2 b, were in good accordance with the expectations. A strong peak at the hydrogen bond accepting side at ~ -0.01 e/Å was visible for all QAs, counterbalancing the misfit of the broad donation peak of the target. Combining these finds, knowing that curcumin can donate hydrogen atoms through its phenylic hydroxy groups and the enol group, with the results obtained via NMR, the hydrogen bonding interactions between the QAs and curcumin were clear. These unspecific interactions seemed to be the driving force for the solubility enhancement [158].

5.3.2 Influence of Acids

After the assessment of the QAs, the influence of the acids on the solubility of curcumin in ethanolic solutions was regarded. The selection of acids was based on the articles by V. Huber *et al* . [70,126], in which the NADES based on lactic acid (Lac) and levulinic acid (Lev) have been the most promising ones. Additionally, pyruvic acid (Pyr) as a compromise between chain length and functionalities of both previously mentioned acids was examined as well since it consists of a backbone of three carbon units like Lac but with a keto group like Lev. To investigate the influences of the chain length and functionalities on the solubility of curcumin, the chain length of α-keto acids was varied to 4 and 5 (Obu and Ova), while also the position of the keto group from α to γ to δ (Aba). TriA from the previous studies summarized in Chapter 4 [47] and hexanoic acids with no additional functionalities were used as references. The curcumin solubility in ethanolic solutions with the acids as additives are given in Figure 5-3. For a depiction in mol, see Figure 9-42. The examination of the additives was performed up to a content of 70 wt% as this was enough for a visible trend. The acids of interest, Lac, Lev, and Pyr, were examined in their pure states as well for an idea about possible solubility synergies with EtOH [158].

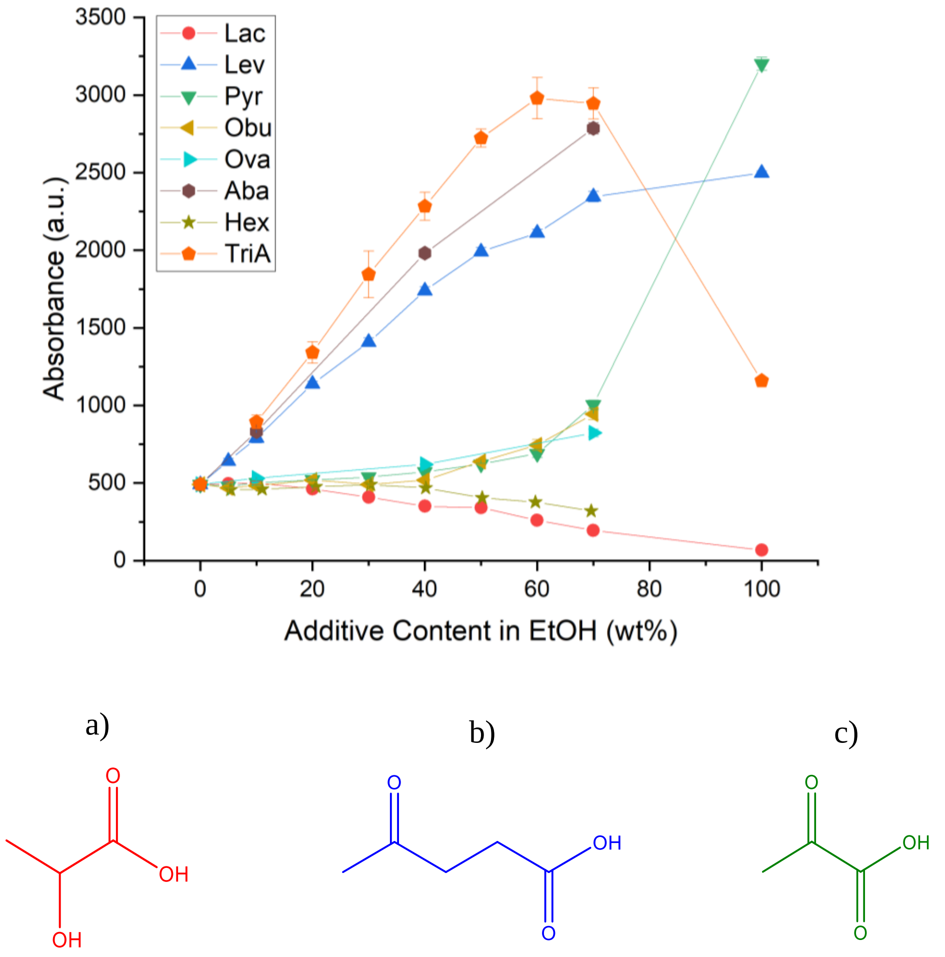

Figure 5-3: Curcumin solubility in ethanolic solutions of a) lactic acid (red circles), b) levulinic acid (blue triangles), and c) pyruvic acid (green down-facing triangles). The solubility of curcumin in solutions with 2-oxobutyric acid (yellow left-facing triangles), 2-oxovaleric acid (turquoise right-facing triangles), 4-acetylbutyric acid (brown hexagons), were examined as well as the references hexanoic acid (beige stars) and triacetin

(orange pentagons) [158]. *The solubility data of TriA was provided by P. Degot et al.* [47]. *The rest of the structures can be viewed in Table 9-2 of the Appendix.*

The solubility of curcumin in pure EtOH was the starting point of all measurements, while TriA and Hex framed the rest. Three trends concerning the solubility could be fleshed out from the bottom to the top [158]:

- Worsening the solubility compared to pure EtOH
- Remaining in the region of pure ethanol, hardly changing the solubility
- Significantly improving the solubility

Lac and Hex acid were the candidates to yield the worst results, while Lac was even worse than the reference. In comparison to pure EtOH, Lac and Hex decreased the curcumin solubility with increasing additive content (up to 70 wt%) to ~ 40% and 65% respectively. No solubility synergy between the additives and EtOH was found comparably to the EtOH/TriA mixture as both were gradually worse in terms of solving. This served as an indication that no functionalities were bad for the solubilization of curcumin, but HBD groups were even more fatal [158].

With regard to the second case, the solubility of curcumin could be roughly double with an additive content of 70 wt% of α-keto acids. Even though the solubility could not be increased remarkably in comparison to pure EtOH, it was a strong improvement as opposed to the two acids before. Pyr, as an integral part of human metabolism, was also investigated in its pure form, yielding the highest solubility with a 6.5-fold increase in front of pure EtOH while also surpassing the binary mixture of EtOH/TriA. No solubility synergy was found in the EtOH/Pyr system either as the solubility could only be increased towards the pure acid. The result obtained with pure Pyr even surpassed mixtures of Lev and Aba, the acids of case three, yielding 5- to 6-fold increases in solubility respectively. The third group only yielded superior results in comparison to mixtures of low Pyr content. Different theoretical approaches were followed to explain this phenomenon [158].

The Hansen space with the distances of all acids to curcumin are presented in Figure 9-43 and Table 9-10 of the Appendix. The assessment via HSPs, however, delivered no satisfactory clues about the suitability of the acids in terms of solving curcumin. Consulting the theory, small distances between molecules signify a good solubility [95]. Especially the predictions about Hex (beige sphere) and Pyr (green sphere) in this case were incorrect. As well, TriA and Lev had different distances while yielding similar results in the experiments. The only correct prediction was the one about Lac, which performed badly in the experiments and exhibited the greatest distance. With these results in mind, HSPs were not suitable to predict the solubility as the systems might have been too complex [158].

Alternatively, COSMO-RS calculations were consulted for more precise results. The most interesting acids Lac, Lev, and Pyr were selected for the prediction of the chemical potential in binary blends with EtOH. The reference TriA was provided by P. Degot *et al.* [47]. The calculated results are presented in Figure 5-4 [158].

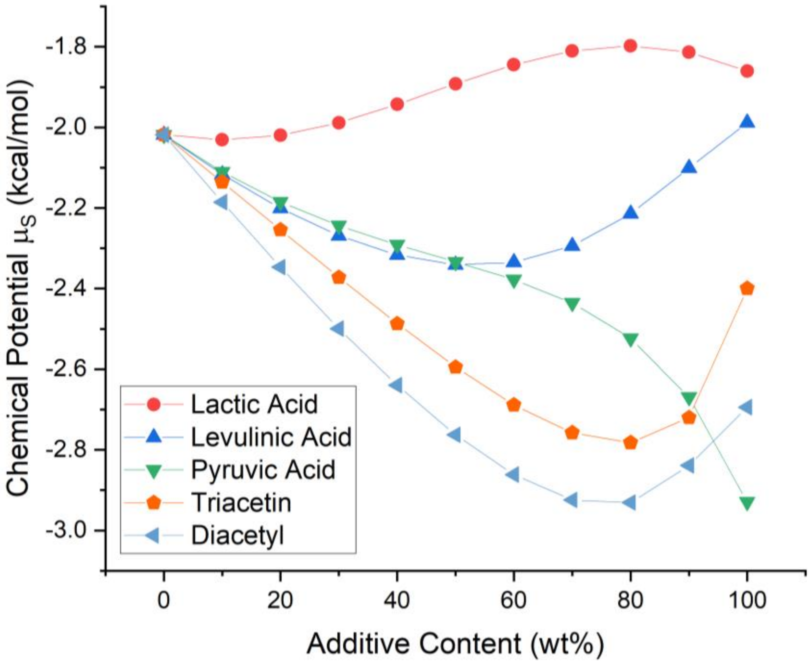

Figure 5-4: Prediction of the chemical potential concerning the solubility of curcumin in mixtures of ethanol with lactic acid (red circles), levulinic acid (blue triangles), pyruvic acid (green down-facing triangles), triacetin (orange pentagons), and diacetyl (bright blue left-facing triangles) [158].

Comparing Figure 5-4 with Figure 5-3, the predictions matched the trends found during the experiments: Lac < Pyr < Lev < TriA. This, in turn, meant that COSMO-RS was a more reliable tool for the theoretic approximation of the curcumin solubility in mixed, complex systems [158].

Including diacetyl in the predictions came to be as especially the solubility results of ketones (cf. Figure 5-3) seemed to have a positive influence on the solubility. Due to health risks related to diacetyl, no experiments were performed in the lab, but it was included theoretically as a proof of concept of the beneficial influences of ketones. These were confirmed since diacetyl/ethanol blends were calculated to have the lowest chemical potential, arguing for the positive effects of ketones. The bad results obtained by Lac in the solubility experiments could be explained by this find as Lac does not possess a keto group but a hydroxy one. Through the calculations, even a negative solving synergy could be found in the mixture of EtOH/Lac. However, TriA and the keto acids, especially Lev, Aba, and Pyr, performed well during the experiments, affirming the assumption about the positive effect of ketones. The reason for the subpar performances of the a-keto acids at lower concentrations could not be explained so far via COSMO-RS predictions. To elucidate this problem, the chemical potential of curcumin in solutions of Lev and Pyr mixed with EtOH was calculated regarding their conformations as well. The results are presented in Figure 5-5 [158].

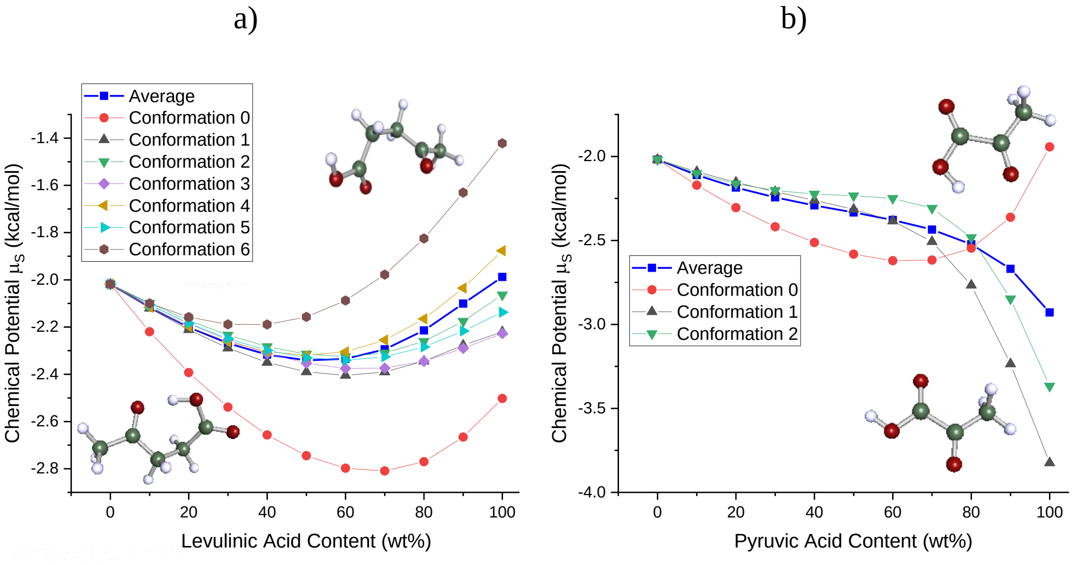

Figure 5-5: Predicted chemical potential of curcumin in ethanolic solutions of a) levulinic acid and b) pyruvic acid depending on the molecules' conformations. The worst and best conformations according to COSMO-RS are represented by the given structures. The weighted average of all conformations in solution is signified by the bright blue curves [158].

The weighted average of all conformations of Lev and Pyr, shown by the blue squares in Figure 5-5 a and b, were taken from Figure 5-4. The different conformations indeed showed different curve progressions of the chemical potentials. This was an indication that the molecular shape of the molecules in solution had considerable influence on the solubility of curcumin. Conformation 0, represented by the red dots along with their corresponding molecular structures, in both cases characterized the cyclic form of Lev and Pyr. In these conformations, the keto functions acted as an acceptor of the acidic hydrogen atom. Their curve progressions deviated significantly from the remaining conformers showing a solubility synergy, indicated by negative local extrema at ~ -2.8 kcal/mol. The curve progressions of both cyclic forms were very similar, hinting at analogous solving mechanisms. Supposedly, the differences in solubility could have been a product of different ring sizes. Figure 9-44 shows the direct comparison of the chemical potentials predicted for both cyclic conformations of Lev and Pyr [158].

The predicted chemical potential of Pyr, though, was far different from the results obtained experimentally. Thus, the cyclic conformation could hardly be present in the real live samples. This could be the explanation of why only a strong curcumin solubility increase could be reached at higher Pyr contents (~ 70 wt%) instead of following a gradual increase. It was suspected that due to steric hinderance, the five-membered cyclic form of Pyr, as induced by intramolecular hydrogen bonding, was not stable. An easier integration into the hydrogen bonding web of EtOH could also have promoted the presence of the open-chain conformations. Thus, the solubility increased only at high Pyr contents, where the cyclic form was more comfortable [158].

When regarding Lev, the opposite was the case as the cyclic form had a strong effect during the extraction experiments because the prediction of conformation 0 concurred more with the actual results obtained in the lab. In Figure 5-4, the average curve was influenced more by the open chain form (cf. Figure 5-5 a, upper molecular structure), forecasting a strong solubility decrease at higher Lev contest. In comparison to the prediction of TriA, Lev should strongly underperform as an additive. However, by regarding the conformations Lev can adapt, the similar solving capability could be explained. A seven-membered geometry is less rigid and can indeed allow the presence of the cyclic conformation in solution leading to a higher solubility of curcumin. To prove the hypothesis about the involvement of the cyclic form of Lev in enhancing the curcumin solubility, NOESY NMR spectra were recorded. An overlay of the spectra of curcumin (pink), Lev (purple/bright green), and their 1:1 (*n/n*) mixture (blue/dark green) is shown in Figure 5-6. The belonging ^{1}H NMR spectra of the single components and the mixture are given in Figures 9-19, 9-29, and 9-30 of the Appendix [158].

The signals next to the diagonal, the so-called cross peaks, served to evaluate the interactions of the molecules. Diffuse interactions of all hydrogen atoms of curcumin were no surprise due to the conjugated system. However, when regarding Lev, signals found at 2.49 ppm and 2.76 ppm distinctly interacted with the signal at 12.17 ppm. Consulting the ^{1}H NMR spectrum of Lev (cf. Figure 9-29), the peaks at 2.49-2.76 ppm could be assigned to the two methylene groups, while the peak at 12.17 ppm represented the acidic hydrogen atom. The interaction between these hydrogen atoms confirmed the suspicion that the cyclic conformation of Lev as shown in Figure 5-5 a was indeed present [158].

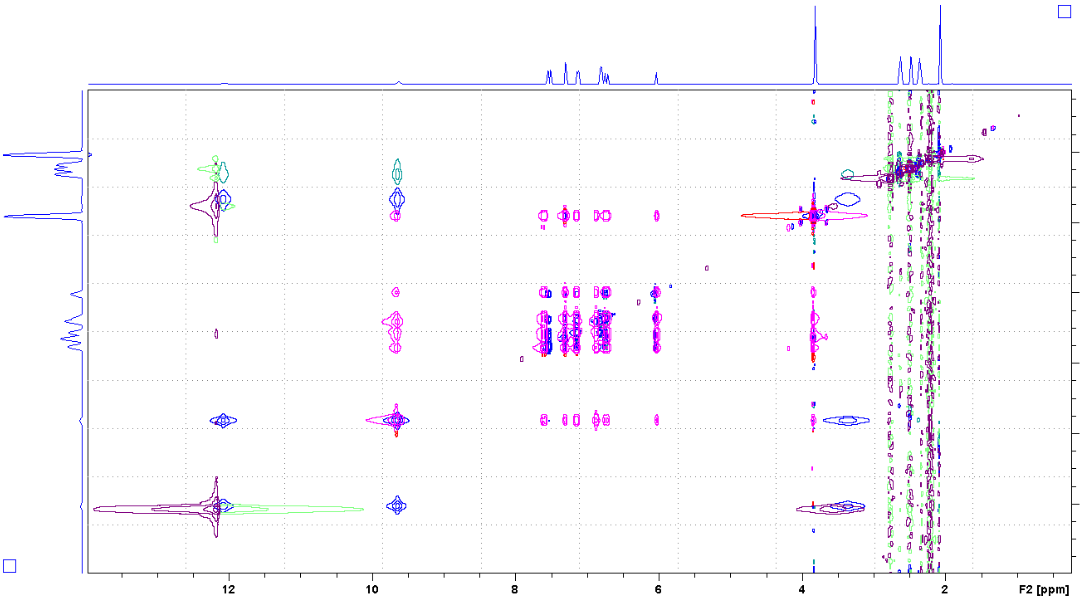

Figure 5-6: Overlaid NOESY spectra of curcumin/Lev 1:1 (n/n) (blue/green), curcumin (pink), and Lev (purple) in DMSO-d_6 [158].

New cross peaks at 2.49-2.76 ppm and 9.66 ppm appeared upon mixing curcumin and Lev. This peak can be ascribed to a nuclear Overhauser relaxation effect between Lev's methylene groups and the phenylic hydroxy groups of curcumin. These relaxation effects can only be observed over small distances below ~ 5 Å [78,165]. Coming back to the calculations by COSMO-RS, curcumin is a slightly curved molecule enabling the two aromatic rings to face each other. In terms of conformation in solution, curcumin may fold around the cyclic Lev like a clamp. There is also a possibility that Lev is forced into the cyclic conformation in the presence of curcumin, elevating its solubility even more. Stating as an educated guess, the cyclization or conformation change of additives in EtOH combined with their hydrogen bonding abilities could be the incentive behind the enhancement of curcumin solubility. This might apply to Aba and TriA, too [158].

5.3.3 Influence of NADES

After the influences of the single components on the curcumin solubility were evaluated, nine corresponding NADES were synthesized and reviewed. QA-based NADES are common topics of research in the literature, thus only the typical molar ratios [68,72] of 2:1, 1:1, and 1:2 were tested. Whether the formation of NADEs was successful, was assessed visually by determining if a homogeneous liquid was obtained after heating to 80 °C for 90 min with successive cooling of the samples. The adequate molar ratios are given in Table 5-3 [158].

Table 5-3: Examined NADES with their molar ratio and water content in weight percent [158].

QAs	HBD	Composition (*n/n*)	Water Content
ChCl	Lac	1:1	5.8 ± 0.1%
	Lev	1:1	0.86 ± 0.05%
	Pyr	1:2	1.6 ± 0.1%
Bet	Lac	1:2	8.80 ± 0.05%
	Lev	1:2	1.15 ± 0.09%
	Pyr	1:2	2.99 ± 0.03%
Car	Lac	1:1	7.6 ± 0.2%
	Lev	1:2	1.08 ± 0.8%
	Pyr	1:2	1.7 ± 0.1%

The water content of all examined NADES was assessed via Karl-Fischer titrations as well and can also be viewed in Table 5-3. When working with deep eutectic solvents, the water content is an arbitrary quantity and is often used to facilitate the formation of the eutectics while also being able to tune the viscosity. As an integral constituent of deep eutectic solvents, it also affects their polarity and aids in the formation and disruption of the hydrogen bonding network [72,167]. Regarding Table 5-3, independently of the QAs, Lac contained the highest water contents. Therefore, the water could only come from Lac itself. This allowed the review of the solubility results of the pure acids discussed above: Apparently, the solubility in Lac was even worse than in EtOH because of an elevated water content of the acid. On the contrary, the water content in the remaining six NADES was relatively low (< 3 %). Thus, the NADES were not dried further to assess their impact on the curcumin solubility. A break-down of the total water content of the most concentrated Lac-NADES solutions in EtOH yielded a maximum water content of ~ 6% in the most hydrated Bet+Lac/EtOH mixtures. This negligible content did not justify the additional effort of removing water with only a perspective of obtaining better results [158].

Successively, the ability of the nine NADES to enhance the solubility of curcumin in ethanolic solutions was evaluated via UV/Vis spectroscopy. The results are presented in Figure 5-7. The solubility results were plotted depending solely on the QA content in wt% of the NADES/EtOH mixtures. This allowed a direct comparison of the effect of the NADES and the QAs. To see the comparison of the effect of the acids in wt% in combination with the QAs, confer to Figure 9-45 [158].

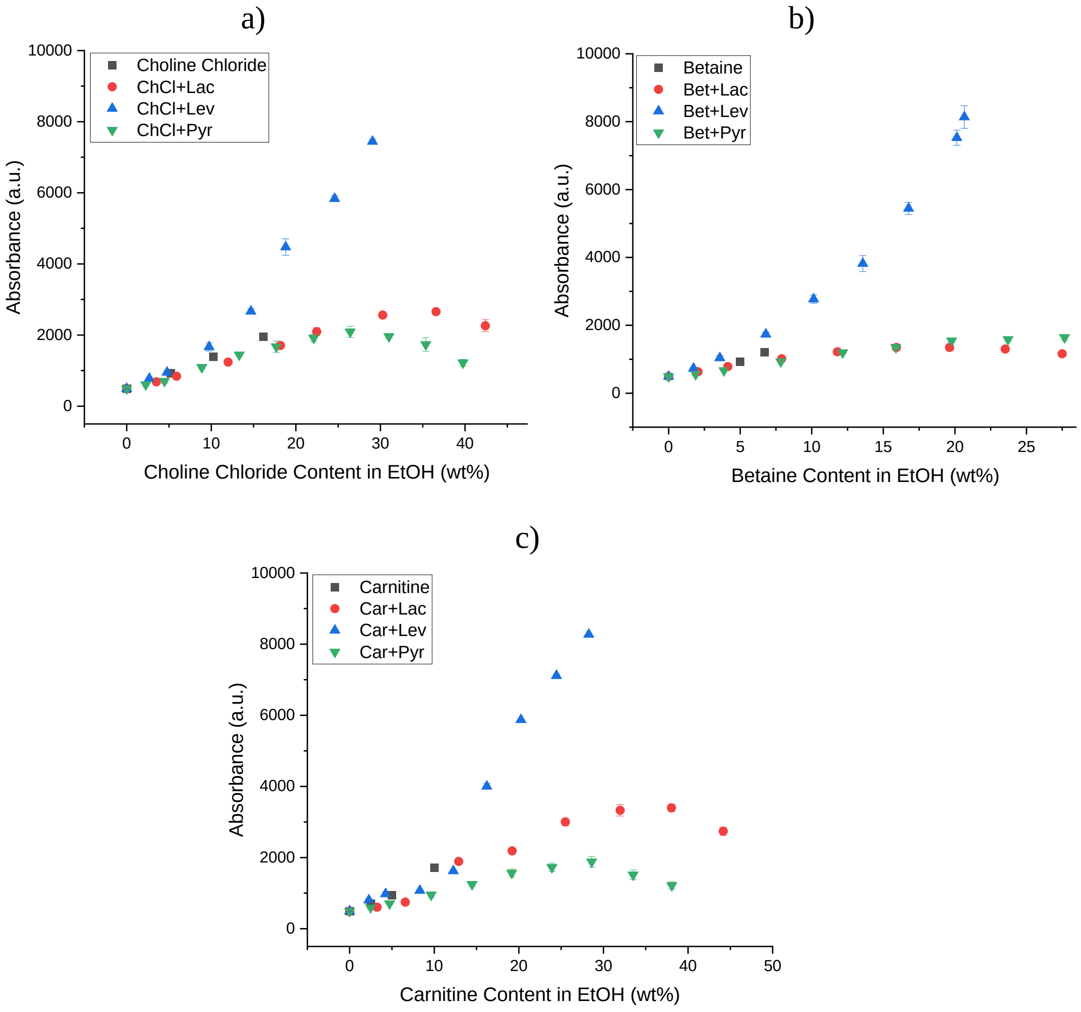

Figure 5-7: Curcumin solubility in mixtures of a) choline chloride-, b) betaine-, and c) carnitine-based NADES in dependence of the quaternary ammonium compound content in wt%. The red circles indicate the NADES containing lactic acid, the blue triangles levulinic acid, and the green down-facing triangles pyruvic acid [158]. *The black squares represent the pure QAs as shown in Figure 5-1.*

Figure 5-7 shows that all examined NADES had a positive influence on the solubility of curcumin in ethanolic solutions. When comparing the NADES to the pure QAs, the solubility increased to an almost equal extent. This suggests that the solubility enhancement at low QA contents was uniquely driven by the QAs themselves. Thus, the improvement of solubility in low QA ranges (< 16 wt%) must be a result of diffuse, non-directed hydrogen bonding interactions as assessed in Section 5.3.1 [158].

By incorporating the QAs in a NADES, the solubility limit of the pure QAs in EtOH (8-16 wt%) could be beat. This was another confirmation of the formation of NADES, considering the two compounds formed a sort of entity, allowing the solubilization of QAs in EtOH without separating from their complementing acid. After surpassing the solubility limit of the QAs, two trends in the solubility of curcumin were identified upon NADES addition [158]:

- A stagnating or moderately increasing curcumin solubility
- A strong solubility improvement

Bet, Pyr, and Lac played an important role in the first case. Even with an almost quadrupled Bet solubility in EtOH (~ 30 wt%), no significant solubility increase was reached in comparison to the enhancement achieved with only Bet. This led to the conclusion that the maximum solubilization power of Bet was already reached in EtOH, while a further Bet increase would not improve the curcumin solubility. The similar slopes of the NADES and pure Bet points also supported this assumption [158].

Ensuing, the acids in the mixtures could, of course, not have a positive influence either, as hardly any was observed before in their pure state (cf. Figure 5-3). With regard to Figure 9-45 c, in the Pyr mixtures, the solubility enhancement was only caused by the diffuse hydrogen bonding interactions coming from the QAs. A linear solubility increase could be observed that resembled the curve progression of the pure QAs. Thus, the NADES compound Pyr only acted as a solubilizer for the interacting QA species. Figure 5-7 confirms this, as all Pyr-based NADES performed worse in comparison to the others, even though the Lac-based ones were only slightly better in increasing the solubility. Looking at Lac's molecular structure, its hydroxy group may interact with the hydrogen bonding web formed by the QAs in ethanolic solutions. Only the mixture of Bet+Lac delivered truly bad results, implying that Bet's carbonyl group captured the hydrogen atom donated by Lac, depleting the system of interacting hydrogen atoms. Thus, interaction only occurred between Bet and Lac, leaving out the solvent. This hypothesis also leads to believe that the diffuse hydrogen bonding of the QAs and acids alike, without directed interactions between themselves, could be somewhat additive [158].

A strong solubility increase, on the other hand, was achieved with all QAs combined with Lev. In retrospect of Section 5.3.2, in which the driving force for the rise of curcumin solubility was characterized to be the directed hydrogen bonding interactions by Lev, it can be expected that these interactions also play a role when using Lev-based NADES [168]. Two different slopes could be noticed when regarding the experiments using Lev-based NADES. They can be seen even better in Figure 9-45. At low QA contents, the slope was leveled and reminiscent of the curve obtained with pure QAs in EtOH. This again confirmed that the mainspring behind the solubility increase at low NADES contents came from the QAs' interactions. Yet, the solubility advanced at a steeper slope after passing the solubility limit of pure QAs in EtOH. By consulting the results obtained with the Lac-based NADES, an additive behavior of intermolecular interactions could be expected. However, when comparing the single influences to the solubility achieved with the QA+Lev NADES entities, the solubility exceeded the added amounts of both. This was evidence for a synergistic effect between diffuse hydrogen bonding caused by the QAs and the specific intermolecular interactions created by Lev. The interplay interactions resulted in an even higher solubility, driven by both, the QAs and Lev [158].

5.4 Conclusion

In this study the underlying mechanism of the curcumin solubility increase upon addition of QAs, acids, and NADES was investigated. To common knowledge, this was the first study dealing with the root cause of the high solubility of a hydrophobic phytochemical in hydrophilic NADES. The methods used for the assessment included a qualitative UV/Vis analysis of the curcumin content, the prediction of the chemical potential of curcumin in ethanolic solutions with different additives, and 1D and 2D NMR spectroscopy.

The influence of the single compounds was examined first. All QAs showed a linear, positive effect on the curcumin solubility without regard for further functionalities of their molecular structure. COSMO-RS predictions and NMR measurements showed that diffuse, nonpoint hydrogen bonding caused the increase in curcumin solubility. However, no direct conclusions could be drawn about the effects of the QAs [158].

For the examined small organic acids, on the other hand, a clear trend concerning the functionalities was found. While hydroxy groups or the absence of any functionalities rather decreased the solubility of curcumin, the presence of keto groups was definitely advantageous. The position of the keto groups mattered as well, showing better solubilities with larger distances to the carboxy group: $\alpha < \gamma < \delta$. Through COSMO-

RS calculations combined with NMR analysis, a targeted hydrogen bonding interaction between curcumin and the cyclic conformation of Lev was found. This interaction was most probably the source of the strong amelioration of the curcumin solubility [158].

Successively, the effects of NADES made from the investigated single constituents were examined in their ability to solve curcumin. The interplay of intermolecular interactions of the QAs and acids yielded even higher solubilities than the single compounds could achieve. Especially, combining the nonpoint hydrogen bonding interactions of the QAs and the specific interactions of Lev did not lead to an additive, but a synergistic effect, accounting for the highest observed solubility of curcumin in NADES/EtOH blends. Thus, combinations of different intermolecular interactions of NADES constituents with the solute can explain the advantage of using these kinds of solvents [158].

This investigation only focused on the phytochemical curcumin and a limited set of nine NADES. However, a foundation was built to continue figuring out the mechanism. In further studies, it would be highly interesting to investigate more keto acids to find which other factors influence the solubility as well. The position of the keto group and the length of the carbon backbone should be inspected closer. Additionally, comparisons to already cyclic molecules should be done, too, with regard to ring size and hydrophobic moieties. Apart from looking at ketoacids, other functionalities, like aromatic rings and aldehydes have to be investigated as well. In this case, nature may give inspiration as natural aromas fulfil these interesting criteria. Eventually, other phytochemicals should be regarded as well, to see if the trends of this study can be applied to other compounds, too.

Chapter 6

Cinnamomum Cassia Essential Oil as Green Solvent

Contents

Natural aromas, especially the essential oil of *Cinnamomum cassia*, were investigated concerning their ability to improve the solubility of curcumin in ethanol.

6 *Cinnamomum Cassia* Essential Oil as Green Solvent

In 2022, the results of this section will be published in the article *Towards a Sustainable and Green Extraction of Curcuminoids Using the Essential Oil of Cinnamomum Cassia* by V. Huber and M. Schmidt *et al.* [169]. The realization of this work was aided by **Michael Schmidt**, in charge of the solubility investigation and characterization of the phase diagrams, and **Antoine Fourriere**, **Mira Jahn**, and **Jennifer Schuster** assisting with the solubility experiments. The generation of GC-FID results was assisted by **Marcel Flemming** and **Nadja Ulmann**. Also, the University of Regensburg's **central analysis department** supported this study by performing GC-MS measurements and providing the data.

6.1 Introduction

Due to their big versatility in application, there is a high demand for curcuminoids [138], the yellow pigments found in the rhizomes of *Curcuma longa* L. The curcuminoids' structures are presented in Figure 4-1 and Table 9-2 and additional information about their origin and health promoting features were given in Section 4.1. Thus, no further details will be given in this chapter. However, the extraction of turmeric's active ingredients is of high interest. Therefore, a new solvent system based on the essential oil of cinnamon was examined in the following.

Recalling Section 2.3, advances are continuously made to find new classes of solvents that are greener alternatives to the conventional ones. F. Chemat *et al.* [57] presented a nice overview of naturally derivable solvents. Particularly interesting was their mention of bio-based solvents, which are solvents produced from agricultural biomass, amongst which also are essential oils. Nature provides a plethora of natural compounds that can be used as extraction solvents, like terpenes, alcohols, and many more, to replace the petroleum-based, classical ones. Of course, as they are naturally derived, the quality of the oils depends strongly on environmental factors, which makes them hard to study in their applications. However, in the scarce literature about essential oils as solvent media, it could be proven that they work as an alternative and even contribute beneficial effects, like antioxidative properties [10,54,170,171].

In this study, focus was put on the essential oil of cinnamon. Apart from being one of the most popular spices worldwide, cinnamon is also known for its medicinal applications [172]. Approximately 250 species of the *Cinnamomum* genus have been identified. Two species in particular, namely *Cinnamomum cassia* and *Cinnamomum verum* or *zeylanicum*, were regarded during this study which are, just like turmeric, native to Southeast Asia. They can be characterized as evergreen, tropical trees that can reach a size of 10-20 m [173–176].

The plants are rich in phytochemicals and almost all parts of the plants are of medicinal or culinary interest. Particularly the oil found in the bark, which is rich in cinnamaldehyde (up to 80%), is of grave importance [172,173,176–178]. Besides cinnamaldehyde, derivatives of the latter like cinnamyl acetate and cinnamic acid are common in the oil. The structures can be seen in Figure 6-1 and Table 9-3.

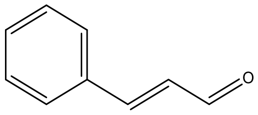

Figure 6-1: Molecular structure of cinnamaldehyde.

It is important to note, however, that *Cinnamomum cassia* contains relatively high amounts of coumarin, while *Cinnamomum verum* possesses only negligible amounts [174,175]. Coumarin can be the cause of liver and kidney damage and is thus regulated to a tolerably daily intake of 0.1 mg/kg body weight. Due to lacking regulations, though, the essential oil of *Cinnamomum cassia* as a coumarin source can still be used as flavoring agent [177,179].

However, the two species *Cinnamomum cassia* and *verum* can be distinguished from one another by the appearance of their quills, the pipes of rolled bark. *Cinnamomum verum* is soft, light, and rolled in layers, whereas *Cinnamomum cassia* is hard, dark, and rolled only in one layer [177]. The bark oil is known for its various health benefitting properties, like antioxidant, anti-inflammatory, antidiabetic, and anti-microbial effects amongst others [172,177].

The oil in combination with ethanol was investigated for the purpose of solving curcumin with the goal of successively extracting it. This study is one of the first ones to examine the essential oil of cinnamon as an extraction solvent. Making use of the close geographical location of both plants, cinnamon and turmeric [127,128,172,177], being able to extract the curcuminoids with the oil would also be ecologically beneficial as transportation of one raw material to the other can be skimped. By sustainable production of all raw materials, the essential oil [180], and ethanol [57,181] also an effort to be environmentally conscious was made.

6.2 Experimental

6.2.1 Chemicals

All chemicals with their abbreviations, purities, and vendors which were used in this section can be found in the following Table 6-1.

Table 6-1: Chemicals used in Section 6.

Chemical	Abbreviation	Purity	Vendor
Rhizome Powder of *Curcuma longa L.*	-	-	Kwizda (Linz, Austria)
Curcumin	Cur	> 97%	TCI (Eschborn, Germany)
***Cinnamomum Zeylanicum* Oil**	Zeylanicum	-	Jean Pütz Produkte GmbH (Gelsenkirchen, Germany)
***Cinnamomum Cassia* Essential Oil**	Cassia	-	Parfum Cosmetic World (PCW, Grasse, France)
***Cinnamomum Verum* Essential Oil**	Verum	-	
Cinnamaldehyde	Cin	> 98%	Merck (Darmstadt, Germany)
Benzaldehyde	Bza	99%	
Cinnamyl Acetate	-	> 97%	TCI (Eschborn, Germany)
Benzyl benzoate	-	> 99%	
3-Phenylpropyl Acetate	-	> 98%	
α-Hexyl cinnamaldehyde	-	> 90%	
3-Phenylpropoinal – Hydrocinnamaldehyde	HCi	95%	Fisher Scientific GmbH (Schwerte, Germany)
Citral	-	N/A	All Organic Treasures GmbH (Wiggensbach, Germany)
trans-Anethole	-	> 99%	Merck (Darmstadt, Germany)
Limonene	-	> 93%	
Ethanol	EtOH	> 99%	
Tetradeuteromethanol	MeOD	> 99%	

All chemicals were used without further purification.

6.2.2 Methods and Techniques

6.2.2.1 *Sample Preparation*

The samples were prepared as described before (cf. 5.2.2.1) by mixing ethanol and the natural flavors or cinnamon oils at different weight ratios until homogenization. For the solubility map, ternary mixtures of ethanol, water, and cinnamon oil were prepared analogously. Successively, the solutions were saturated with synthetic curcumin and left to stir for an hour at room temperature and then filtered with 0.45 µm PTFE filters to remove the excess. All samples were prepared in triplicates.

6.2.2.2 *Optical Density Measurements*

As described above (cf. 5.2.2.2), the solubility of curcumin in the aroma mixtures was assessed qualitatively by optical density measurements via UV/Vis. The adequately diluted samples were analyzed using a Lambda 18 UV/Vis spectrometer by Perkin Elmer (Waltham, USA), scanning the visible spectral region of 350-700 nm. The samples were compared through their maximum absorbance at the wavelength λ_{max} = 425 nm.

6.2.2.3 *COSMO-RS Calculations*

The chemical potential of curcumin at infinite dilution in ethanolic solutions of different flavor compounds at different molar ratios (*n/n*) was calculated analogously to Section 5.2.2.4 with the 19.0.4 version by COSMO*logic*. The precalculated molecules were taken from the COSMO*base* TZVPD-FINE 19.0 database, while for the missing ones, conformer COSMO files were calculated on TZVPD-FINE level with the COSMO*confX* software (version 4.3) using its respective calculation template. For curcumin's the keto-enol tautomer, only the COSMO files of the four sensible conformations were calculated [160,161].

6.2.2.4 *NMR Analysis*

The interactions of cinnamaldehyde and hydrocinnamaldehyde with curcumin and the NMR solvents was analyzed via ^{1}H and NOESY NMR analysis. The NMR device used in this case was a Bruker Avance III HD 400 MHz spectrometer with a 5 mm BBO 400SB BB-H-D sample head with Z-gradient by Bruker (Billerica, USA). Solvent samples of aroma/methanol-*d4* in a ratio of 30:70 (*n/n*) were prepared and 0.05 mol of curcumin were solved. This amount was used as it is close to curcumin's solubility limit in hydrocinnamaldehyde. The data evaluation and processing of the

NMR data was achieved using MNova, version 14.1.2 by Mestrelab Research (Santiago de Compostela, Spain).

6.2.2.5 GC-FID Analysis

To identify the ratio of cinnamaldehyde inside the oil samples, GC-FID analysis was performed. Samples of a cinnamaldehyde or cinnamon oil concentration of 1 mg/mL were prepared in MeOH and filtered into GC vials before measurement.

Then, 1 µL of the sample was injected with a 1:20 split ratio and eluted with a helium gas flow of 1 mL/min. The elution was carried out on a GC-FID 7890A system by Agilent (Santa Clara, USA) with a VF-5ms column (30 m × 250 µm × 0.25 µm) and detection was performed through flame ionization at 275 °C. To ensure adequate separation, a gradient temperature program was used based on results presented by A. Chakraborty *et al.* [173], starting with an oven temperature of 60 °C, which was kept for 5 min. Then, the temperature was ramped up to 250 °C with a heating velocity of 20 °C/min. A second ramp to 300 °C followed at a speed of 50 °C/min to bake out the column. The peak areas were used to determine the ratio of the respective compounds in the cinnamon oils. Cinnamaldehyde in the real live samples was characterized by comparing the retention times to the chromatogram of pure cinnamaldehyde by Merck.

6.2.2.6 GC-MS Analysis

The various volatile compounds contained in the natural cinnamon oils were separated and analyzed via GC-MS. To this purpose, samples were eluted using a 7890B GC system by Agilent (Santa Clara, USA) equipped with a ZB-5MSplus column (30 m × 250 µm × 0.25 µm) by Phenomenex Inc. (Aschaffenburg, Germany). The samples were injected at a volume of 1 µL with a 1:200 split ratio and eluted with a helium gas flow of 1.2 mL/min. A temperature gradient was applied, starting at 60 °C ramping up to 300 °C with a heating rate of 20 °C/min. The end temperature was held for 0.5 min to bake out the column. The characterization of the separated compounds was performed via MS detection with an AccuTOF GCX apparatus by Jeoul GmbH (Freising, Germany), using a positive electron impact ionization at a voltage of 70 V. The NIST database was used to assign the mass spectra to their compounds.

6.2.2.7 Determination of Ternary Phase Diagrams

A ternary phase diagram of water, EtOH, and *Cinnamomum Cassia* oil by PCW as the hydrophobic phase was recorded. To establish the domain of the miscibility gap, binary samples of water/EtOH and oil/EtOH were prepared and the third component, cassia oil or water respectively, was added dropwise until a visible change in the phase behavior was observed, which signaled a phase separation. This indication was determined by the bare eye. The exact amounts of all compounds were recorded to identify the two-phasic region.

6.2.2.8 Determination of the Critical Point

The critical point of the water/EtOH/oil cassia system was determined via dynamic light scattering combined with an optical assessment. The DLS experiments were conducted analogously to the experiments presented in Section 4.2.2.4, looking for the most pronounced correlation functions. As a verification of the CP found via DLS, the samples exhibiting the highest correlation functions were evaluated optically as well. To this intent, three samples in the monophasic domain were prepared and diluted step by step with 20 µL of water until phase separation. The sample separating into two phases of identical volume was determined as the critical point.

6.2.2.9 Cyclic Solvent Extraction of Curcuma Longa L.

Based on the solvent economization method introduced by P. Degot *et al.* [47], the repeated use solvent to extract the curcuminoids from their matrix was examined. The process was executed analogously to the cycle extraction presented in Section 4.2.2.6.4 [70,126]. 2 g of fresh rhizomes were extracted using 32 g of the optimum solvent mixture. Unlike presented above, the extracts were not analyzed via HPLC elution but via UV/Vis as a proof of concept of the method.

6.3 Results and Discussion

6.3.1 Screening of Natural Aromas

According to the study by V. Huber *et al.* [158], the solubility of curcumin in ethanolic solutions can be increased depending on the additives. Thus, a screening of the curcumin solubility in mixtures of six natural aromas, namely cinnamaldehyde (Cin, brown squares), benzaldehyde (Bza, purple circles), citral (orange triangles), anethole (red down-facing triangles), benzyl benzoate (green diamonds), and limonene (blue left-facing triangles), with EtOH was made. The solubility results along with the COSMO-RS prediction of curcumin’s chemical potential are presented in Figure 6-2. A depiction of the results in wt% are shown in Figure 9-46 of the Appendix [169].

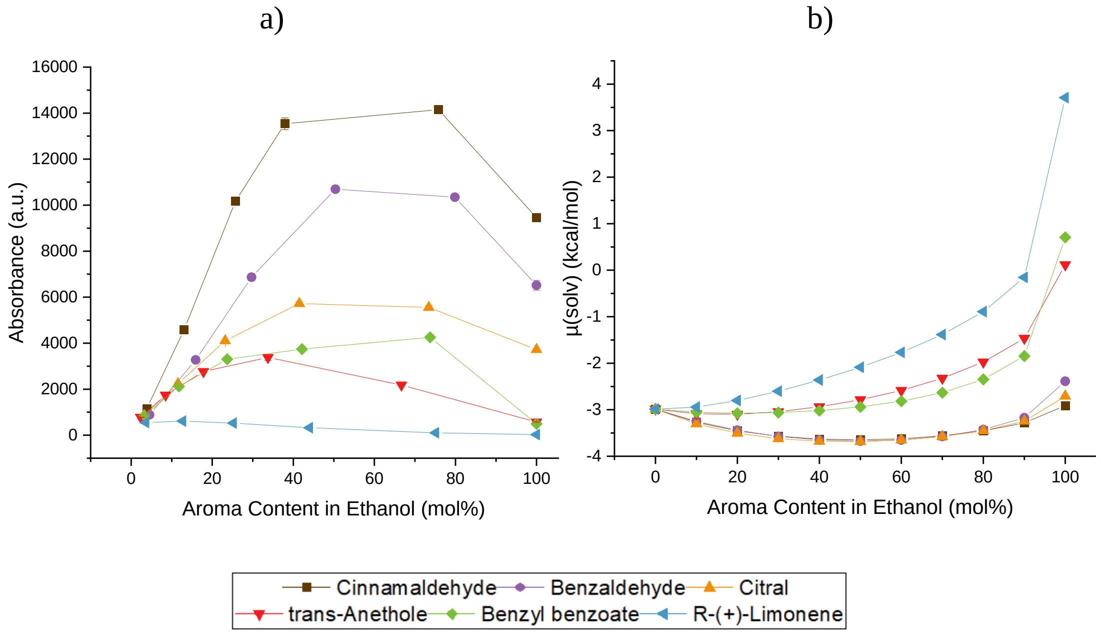

Figure 6-2: UV/Vis (a) and COSMO-RS (b) examination of the solubility and chemical potential of curcumin in ethanolic solutions of natural flavors (n/n) respectively. Cinnamaldehyde is presented by brown squares, benzaldehyde by purple circles, citral by orange triangles, trans-anethole by red down-facing triangles, benzyl benzoate by green diamonds, and limonene by blue left-facing triangles [169].

These natural aromas were chosen due to their different structural elements. Cin and Bza are aromatic aldehydes with differently sized conjugated systems, benzyl benzoate is an aromatic ester and anethole an aromatic ether, while limonene is a non-functionalized terpene and citral is a terpenoid aldehyde [169]. The molecules' respective structures can be viewed in Table 9-3 of the Appendix.

Looking at Figure 6-2 b, three solubility trends in the EtOH/aroma mixtures were predicted when regarding the chemical potential of the phytochemical:

- Strongly decreasing the curcumin solubility
- Hardly any effect of the mixtures on the solubility
- Improving the curcumin solubility

Starting with the first case, limonene was responsible for the bad solubility. In comparison to all the other tested molecules, limonene showed no positive solubility synergy with EtOH. The other mixtures managed to have a solving synergy with a maximum curcumin content between 70-90 wt% of the aroma additive, whereas limonene had a quasi-linear curve progression, worsening the curcumin solubility with increasing contents. The experiment could be validated using COSMO-RS calculations, which also predicted a continuously worse solubility. This indicated, like proven by V. Huber *et al.*, when looking at hexanoic acid [158], that the absence of functionalities affects the solubility of curcumin in a negative way [169].

Anethole and benzyl benzoate make up the second case. At low contents, they managed to enhance the curcumin solubility in the mixture approximately by a factor of 5 in comparison to EtOH. They also show a similar curve progression in the predictions with a positive trend of the chemical potential, which is an indication for a bad solubility. However, especially the solubility in the pure aromas was not as bad during the experiments as it was predicted. Overall, both the ester and the ether group seemed to have a decent effect when solving curcumin [169].

The third group is comprised of all aldehydes. Cin, Bza, and citral have an almost identical curve progression concerning the prediction of the chemical potential. A positive solubility synergy is predicted as the mixtures of the aromas with EtOH should have a lower chemical potential. The experiments, on the other hand, do not deliver such similar results. Citral mixtures already yielded a 10-fold solubility improvement in comparison to pure ethanol, while mixtures of Bza and Cin with EtOH almost doubled and tripled citral’s effects respectively. Thus, Bza and Cin must interact with the solute in a way which COSMO-RS could or would not consider. π-π interactions or stacking come to mind. Looking at the two molecules’ structures, both are planar, aromatic molecules with Cin having a bigger conjugated system and looking roughly like half the structure of curcumin. It is possible to imagine that both aromas may stack with curcumin, forming a complex which is preferentially soluble in EtOH [169].

To summarize, the improved solubility of curcumin in EtOH upon addition of natural flavors was found to be dictated by two effects. The lesser one was the solubility of curcumin in the flavors themselves, depending on their functionalization, which could be ranked as follows: Aromatic system in conjugation with an aldehyde > aldehyde in simple conjugation > ester > ether > non-functionalized molecules. Secondly, and more importantly, preferential interactions between the additives and the solute lead to very high solubilities of curcumin [169].

Cinnamaldehyde fulfilled both necessary prerequisites and yielded the highest solubility of curcumin. A natural product rich Cin was found in cinnamon bark oil, which can achieve Cin contents of up to 80% [174,175]. However, before considering natural products, derivatives of Cin were examined in order to be able to predict their effect on the curcumin solubility as well. The corresponding UV/Vis and COSMO-RS results in ethanolic solutions are presented in Figure 6-3, while solubility data depending on the weight content can be seen in Figure 9-52 of the Appendix. The examined derivatives, which could most likely also occur in natural cinnamon oils [178], included cinnamyl acetate (marron circles), 3-phenylpropyl acetate (orange triangles), α-hexyl cinnamaldehyde (golden down-facing triangles), and hydrocinnamaldehyde (HCi, yellow diamonds) [169]. To see the molecular structures, regard Table 9-3 of the Appendix.

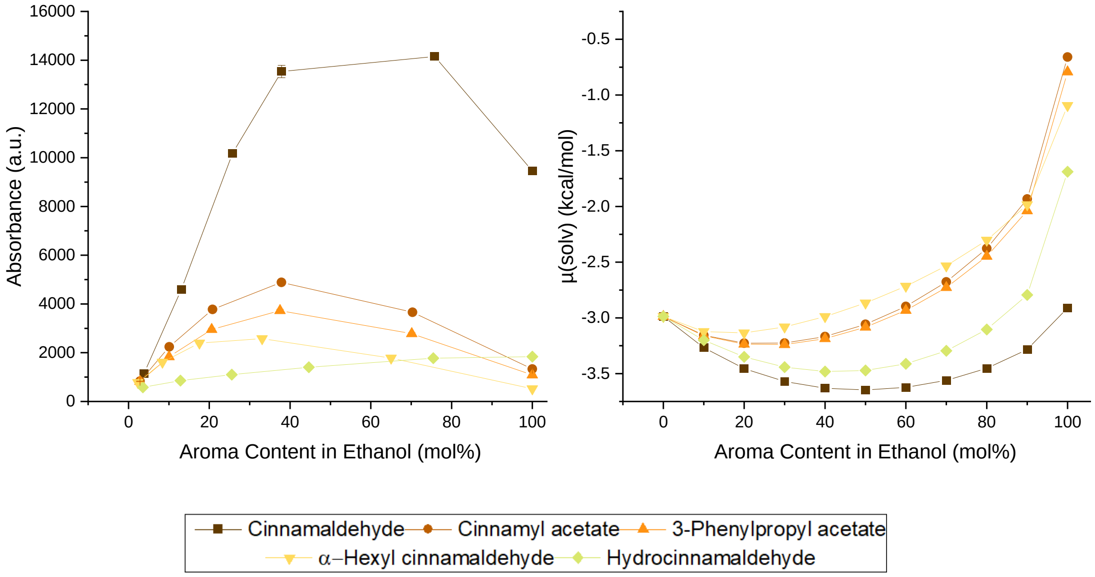

Figure 6-3: UV/Vis (a) and COSMO-RS (b) examination of the solubility and chemical potential of curcumin in ethanolic solutions of natural flavors (n/n) respectively. Cinnamaldehyde is presented by brown squares, cinnamyl acetate by marron circles, 3-phenylpropyl acetate by orange triangles, α-hexyl cinnamaldehyde by golden down-facing triangles, and hydrocinnamaldehyde by yellow diamonds [169].

Just like in the screening above, cinnamaldehyde held the highest position regarding the solubility of curcumin, while its derivatives showed rather mediocre improvements. This was also validated by the COSMO-RS predictions. However, particularly interesting was the effect of hydrocinnamaldehyde. While COSMO-RS predicted its solving effect to be similar to the effect of Cin, no positive solubility synergy between EtOH and hydrocinnamaldehyde was observed. ^{1}H NMR measurements in MeOD were made to find an explanation for this unexpected behavior. A spectrum of solely curcumin in MeOD was recorded as a reference (cf. Figure 9-47) [169].

It was assumed that a reaction between the aldehyde and the alcohol took place and would lead to the formation of a hemiacetal. By consulting the ^{1}H NMR spectra (cf.

Figures 9-48 and 9-49), indeed peaks appeared, indicating the presence of hemiacetals in both cases. In total, a hemiacetal content of 16% and 89% were found in the Cin and HCi samples respectively. These reactions also served as an explanation for the incorrect COSMO-RS predictions of the curcumin solubility in the binary HCi/EtOH mixtures. As only small amounts of HCi were present in the solution eventually, the solubilization was rather driven by the high abundance of hemiacetal instead of HCi itself. In the Cin samples, hardly the hemiacetal but mostly the aldehyde was present. Through the conjugated system and resonance stabilization of Cin, the aldehyde group was protected, and the equilibrium of the hemiacetal formation stayed strongly on the aldehyde side [182]. Since hydrocinnamaldehyde does not have a conjugated π-system that extended to reach its aldehyde group, the equilibrium must have been shifted to the hemiacetal side. Due to this side reaction, ensuing a drastic solvent change, the diverging trend in curcumin solubility could be explained [169].

However, this was not the only information the NMR spectra presented. Successively, the chemical shifts of curcumin's signals in the binary mixtures of Cin or HCi with MeOD, which are presented in Table 6-2, were investigated.

Table 6-2: Chemical shift of curcumin's hydrogen atoms (the assignment of the protons can be seen in Figures 9-47 to 9-49 of the Appendix)in methanol-d4 mixed with the aroma, either Cin or HCi, in a ratio of 70:30 (n/n). An upfield shift of the signals is marked in blue, while a downfield shift is signified in red [169].

# H	**1, 4**	**27**	**21, 24**	**10, 13**	**11, 12**	**7, 16**	**19, 20**	**3, 6**	**22**
Methanol-*d4*	3.91	-	6.63	6.82	7.11	7.22	7.57	-	-
Cin	3.76	-	6.88	-	7.02	-	7.60	-	-
HCi	3.73	5.97	6.66	6.96	-	-	7.74	-	-

No changes of the chemical shift of the signals given by the aroma compounds were observed. However, shifted signals were found for curcumin. The shift of signals, downfield (marked in red) or upfield (marked in blue) due to a depletion or enrichment of electron density, respectively, are an indication of mesomeric effects of functional groups [183,184]. While the allylic hydrogen atoms of curcumin (21,24 and 19,20) as well as the phenylic protons (10, 13) experienced a slight downfield shift in presence of HCin, the phenylic hydrogen atoms (11, 12) were shifted upfield in the presence of Cin. In both solvent mixtures, curcumin's methoxy groups (1, 4) experienced an upfield shift. The combination of these results with the cross-peaks found in the respective NOESY spectra (cf. Figures 9-50 and 9-51 of the Appendix) also gives an indication about the difference of solubility in both cases [169].

Cross-peaks between all protons of cinnamaldehyde and the methoxy groups of curcumin could be found in the respective NOESY spectrum (cf. Figure 9-50). Through their positive mesomeric (+ M) effect, the electron density of the aromatic ring was amplified, while the electron density at the methoxy groups was decreased. Thus, interactions of the electron-depleted methoxy protons and all rather electron-rich hydrogen atoms of the aromatic, allylic, and aldehyde groups of cinnamaldehyde were possible. This was also in accordance with the changes of the chemical shifts. Through the high electron density surrounding the methoxy protons, the + M effect could be intensified leading to even higher electron densities in the aromatic ring of curcumin, resulting in a downfield shift of the aromatic protons (11 and 12). This effect, however, could not be seen for the hydrogen nuclei (10, 13 and 7, 16) as they overlapped with the cinnamaldehyde signals. The protons conjugated to the carbonyl group, which has a negative mesomeric effect, were shifted downfield. While only a slight shift was experienced by the hydrogen nuclei (19, 20), the signal of the protons (21, 24) was shifted by + 0.25 ppm. The remaining cross-peaks found in the NOESY spectrum show only interactions between the cinnamaldehyde and curcumin species themselves [169].

Looking at the effects of HCi, curcumin’s methoxy groups (1, 4) in the presence of HCi were shifted upfield as well. When regarding the NOESY spectrum (cf. Figure 9-51), however, no cross-peaks between curcumin and HCi were found. This was unexpected, as it was assumed that at least hydrocinnamaldehyde’s aromatic ring should still be able to interact with the electron-poor methoxy groups. The only weak cross-peaks that indicate an interaction of these two groups could easily be mistaken as the background. This find is in accordance with the observed solubility of curcumin in ethanolic solutions of HCi (cf. Figure 6-3), as a slight increase of solubility was indeed visible. Additionally, no interactions between the aldehyde proton and the methoxy groups were found, as mostly the hemiacetal was present. Yet, no cross-peaks between the hemiacetal and the methoxy groups were found either. The newly formed methoxy and hydroxy groups of the hemiacetal both exhibit a + M effect, which would increase the electron density at the hemiacetal itself. In theory, these effects should lead to favorable interactions with curcumin’s methoxy groups. However, as determined by V. Huber *et al.* [158], hydroxy groups affect the solubility of curcumin in solution in a negative way and it can be suspected that they also prevent further interactions. A further evaluation of this, however, would exceed the scope of this study [169].

Following these insights, adding up to cinnamaldehyde being the most promising of the investigated aromas, three natural cinnamon bark oils were examined with regard to their quality of enhancing the solubility of curcumin: *Cinnamomum cassia* oil by PCW (cassia), and two *Cinnamomum verum* oils, one by PCW (verum) and one by Jean Pütz (zeylanicum). Before the solubility tests, the oils were characterized concerning their overall Cin content via GC-FID, and the side ingredients apart from Cin were identified via GC-MS. The chromatograms and mass spectra can be viewed in Figures 9-53 to 9-87 [169].

The cassia oil was richest in cinnamaldehyde with 79%, followed closely by the zeylanicum oil with 74%, and verum oil containing 62% Cin. The pure Cin reference, with which the curcumin solubility curve in EtOH was recorded had a content of 97 %. Thus, it was expected that none of the oils could meet its high curcumin solubility. However, when regarding Figure 6-4, the cassia oil matched the curve progression of pure Cin almost perfectly and enhanced the solubility of curcumin in ethanolic solutions approximately in the same way [169].

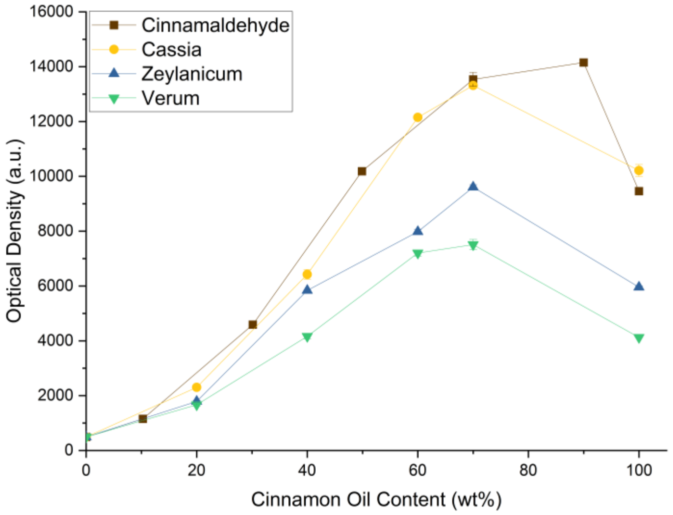

Figure 6-4: Comparison of the curcumin solubility in ethanolic solutions of the cinnamon oils, Cinnamomum cassia oil by PCW (yellow circles), Cinnamomum zeylanicum by Jean Pütz (blue triangles), and Cinnamomum verum (green down-facing triangles), with cinnamaldehyde (brown squares) as a reference [169].

Even though the zeylanicum oil contained only 5% less Cin than the cassia oil, it performed worse in solubilizing curcumin, and only managed to solubilize ~ 65% of the amount that was possible to achieve with cassia oil. The difference in solubilizing quality between the zeylanicum and verum oil, however, was less pronounced, even though their Cin content differed by 12%. This could be explained easily when looking at the GC-MS data (cf. Figures 9-57 to 9-87). In contrast to the cassia oil, which mostly contained Cin derivatives, the other two oils exhibited high contents of terpenoids. Coming back to Figure 6-2, it was shown that limonene, as a representative of terpenes, worsened the solubility of curcumin. Thus, since the terpene/terpenoid content in both *Cinnamomum verum* oils was high, the curcumin solving ability of the solvent mixture was diminished and the quantity of Cin was not enough to balance their effects. On the other hand, the *Cinnamomum cassia* oil did not contain any terpenes, but aromatic esters and aldehydes. As determined before, functionalized aromatic compounds were able to improve the curcumin solubility in solution, which is the reason why a good solubility could be achieved. Since the cassia oil with a Cin content of 79% showed an almost equal power to solve curcumin like the pure Cin reference, the Cin content alone could not be solely responsible for the enhancement of the curcumin solubility in ethanolic solutions. It could be assumed that the combination of all ingredients inside the oil were able to create their own solubility synergy, providing a suitable solvent environment for curcumin. Thus, for the purpose of this study, the following experiments were conducted using the *Cinnamomum cassia* oil by PCW [169].

This, however, should be taken with a grain of salt. Regarding the mass spectrum shown in Figure 9-63, the cassia oil also contained coumarin. Coumarins are known to cause liver disease in rats and dogs. Even though the metabolomic pathway in the human body is different, coumarins and their metabolites can still cause harm. Therefore, the United States Food and Drug Administration banned coumarins as a food flavoring agent. In Europe, on the other hand, the Food Safety Authority approved a tolerable daily intake of 0.1 mg/kg body weight. Nevertheless, the regulations about coumarins already occurring in foodstuffs, like the oil of cinnamon bark, are ambiguous. As such, there is still no problem when using *Cinnamomum cassia* oil in any application [176,179,185]. If coumarins are undesirable in any process, the problem could be bypassed by processing the oils in question. Either by removing the coumarin from the *Cinnamomum cassia* oil or by rectifying *Cinnamomum verum* oils in order to remove the terpenoid contents, oils of high curcumin solving power without coumarins should be obtained [169].

6.3.2 Preparation for Extraction Experiments – A Proof of Concept

After determining the oil of *Cinnamomum cassia* to be the most capable of solving curcumin, while also being food approved, a ternary phase diagram was recorded. It is presented in Figure 6-5. Although the cassia oil is a mixture of multiple components, it will be seen as one entity, allowing the denomination as ternary. Reminiscent of C. Benkert *et al.*, who used spear mint essential oil [9], the cinnamon bark oil served as the oil phase, which was mixed with water by aid of EtOH as a solubilizer. A large two-phasic domain was found between the hydrophobic and hydrophilic compounds. Neither water nor the cinnamon oil were soluble in each other at any proportion. Although it cannot be seen in the diagram, water and EtOH are fully miscible. But only one small drop of the cinnamon oil was enough to turn the binary water/EtOH mixtures containing less than 40 wt% EtOH turbid. Eventually, a content of ~ 40 wt% of EtOH was necessary to achieve full miscibility of all compounds at all proportions. Via DLS measurements (cf. Figure 9-88), the critical point located on the oil side of the system could be determined [169].

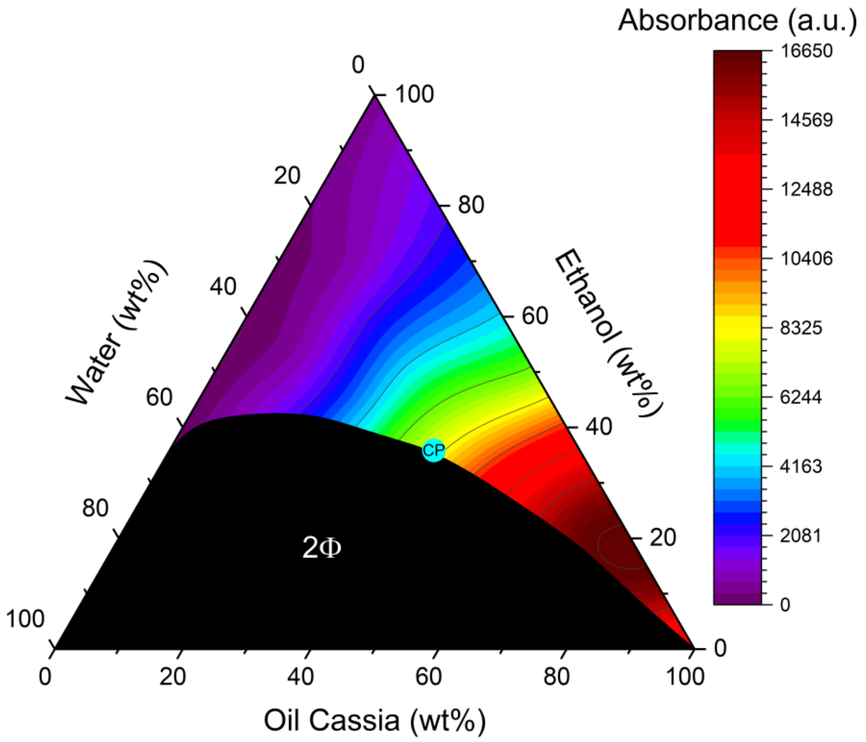

Figure 6-5: Ternary phase diagram of water, ethanol, and Cinnamomum Cassia oil (PCW). The heat map of the monophasic domain shows the solubility of curcumin with red indicating a high solubility, while purple shows a low one. The black area labelled 2Φ identifies the miscibility gap and the critical point of the mixture is signified by the turquoise circle labeled CP [169].

The contour map of the monophasic domain characterizes the curcumin solubility in different ternary mixtures, where red identifies a high solubility and purple a low one.

The highest solubility was found in the lower right corner, the cinnamon oil apex while the binary water/EtOH edge exhibited the lowest curcumin solubility. However, the highest solubility did not correlate with the critical point of the mixture but rather depended on the cinnamon oil content. The higher the amount of oil was in the mixtures, the higher was the solubility. Additionally, according to the direction in which the solubility decreased (from high oil contents to low ones), it seemed as if the solubility was predominantly dictated by the amount of cassia oil. This again supported the finds of the NMR analysis that curcumin and Cin (and potentially its derivatives) share special interactions which are responsible for the preferential solubility. While an optimum oil content of ~ 80 wt% has been found before in binary mixtures during the aroma screening (cf. Figure 9-46), this find was confirmed as well in the ternary ones. Even though water was the limiting factor of curcumin solubility in the previous studies [47,70,126], it seemed to have a positive influence in this case. Just like P. Degot *et al.* reported in the ternary mixture of water/sodium salicylate/ethyl acetate [186], an addition of a small amount of water, in this case 5 wt%, achieved an even higher solubility of curcumin, yielding an optimum composition of water/EtOH/cassia of 5:22:73 (*w/w/w*). This marked, as well, the solvent composition which was used for the extraction experiments [169].

Cycle extractions were performed to prove that an enrichment of curcuminoids in a ternary system of water/EtOH/cassia oil was indeed possible. The problem with the cycle extractions in the previous studies by P. Degot and V. Huber *et al.* [48,126] was that either the solubility in the systems was too low, saturating the solvent only after a few cycles, or that the solvent was changed by interacting with the plant material. In lights of this, cycle extractions were trialed using the ternary cinnamon oil solvent. The analysis of the extracts was performed via optical density measurements using UV/Vis according to P. Degot *et al.* [48]. No distinction between the single curcuminoids was possible, of course, as they all have a similar wavelength of highest absorption. The results are presented in Figure 6-6 [169].

A fairly linear increase of absorbance was detected, signifying that the concentration of curcuminoids could be increased after every cycle of extraction in the water/EtOH/cinnamon oil system. The divergence from the perfect linear behavior could be attributed to environmental conditions as the extractions were performed at room temperature over the course of two days. The negative deviations may have been a product of temperature variations, which could not be controlled. These deviations are not visible when looking at the reference systems of water/EtOH/TriA as saturation was reached earlier. Since less cycles were necessary to achieve saturation, the extractions did not take such a long time, which means effects during the day did not affect them as strongly. In any case, the curcuminoids could be concentrated in all three systems similarly, which proved the concept of cycle extraction [169].

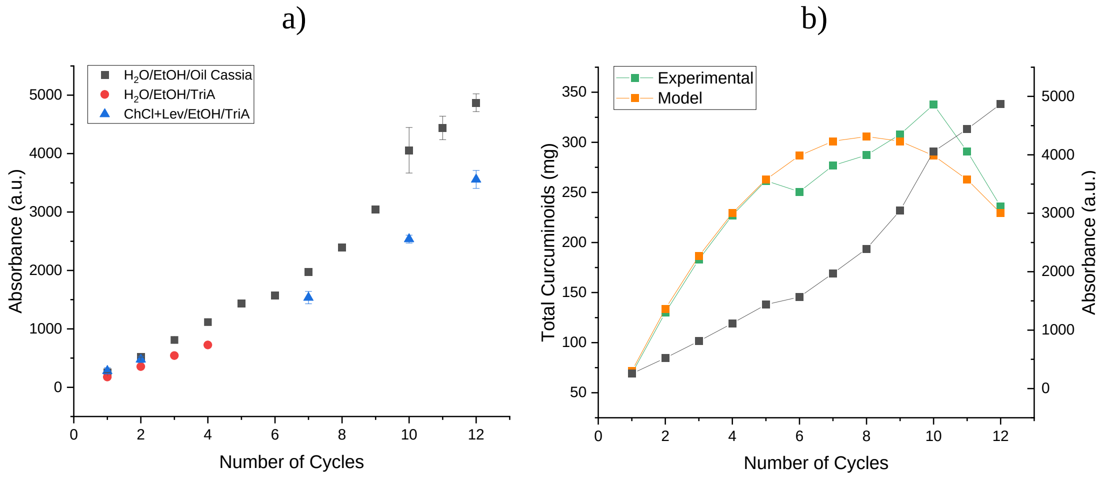

Figure 6-6: Absorbance of curcuminoid extracts in water/EtOH/oil cassia (black squares), water/EtOH/TriA (red circles) [48], *and ChCl+Lev/EtOH/TriA (blue triangles)* [126] *after several cycles of extraction [169]. The references in red and blue given by P. Degot and V. Huber et al. were determined according to the calibration curve given in Figure 9-89 of the Appendix.*

When looking at the total curcuminoid content (cf. Figure 6-6 b), it was found that, just as in the experiments with natural deep eutectic solvent [126], a saturation occurred after ten cycles, even though the limit of solubility should not have been reached. In the previous study, this premature saturation was attributed to the change in solvent due to a loss of choline chloride in the plant matrix. This may very well still be true, as the slope of the absorbance in Figure 6-6 a is lower in the NADES samples than it is for the ternary cassia oil system. In the present case, however, such a loss should not ensue. The explanation for the fast saturation came from looking at the solvent loss during the cycle experiments. When extracting 2 g of rhizomes in each cycle, a volume of ~ 2 g of solvent was lost. Since the amount of solvent to solid ratio has a significant impact on the quality of extraction [2], this may certainly play a role when conducting these experiments. In the following Equation (6-1) a theoretical model was proposed to determine the maximum mass of curcuminoids before saturation, depending on the number of cycles [169].

$$m(n) = \frac{nA}{\varepsilon l}(V - nV_2) \tag{6-1}$$

With m(n) = curcuminoid mass after n cycles, n = number of cycles, A = absorbance, in this case the mean increase of absorbance per extraction cycle, ε = extinction coefficient, l = illuminated layer thickness, V = initial solvent volume, and V_2 = volume loss of solvent after one cycle of extraction.

Regarding this model, the extracted mass of curcumin is effectively limited by V_2, the solvent loss after every cycle of extraction. V_2 is the only variable which can be influenced during the process. By decreasing the lost volume, the number of cycles should be enhanced, and as such, the effectivity of the solvent could be taken advantage of. Reviewing the extraction process, replacing the centrifugation with a more effective method, or changing the batch process to a continuous one could be ideas to reduce the lost amount of solvent. Proving this theory and ameliorating the process, however, could be the topic of a follow-up study [169].

6.4 Conclusion

The focus of this study was to find alternative natural solvents for the solubilization and extraction of curcuminoids from their plant matrix. This study is one of the few ones considering essential oils as solvents. UV/Vis examinations along with COSMO-RS predictions, NMR measurements, and GC analysis were employed to find natural aromas suitable of solving curcuminoids. Two breakthroughs could be presented during these examinations.

By screening six natural flavors found in large amounts in natural sources, a trend in the functionalization of natural molecules was found to determine their ability to solubilize curcumin. Molecules, like terpenes, without functionalization worsened the curcumin solubility, while the presence of an aromatic, conjugated system combined with an aldehyde function yielded the highest solubility results. An up to 30-fold solubility enhancement in binary aroma/EtOH mixtures compared to pure EtOH could be achieved using cinnamaldehyde as the aroma. NMR measurements also confirmed that interactions between the conjugated systems of cinnamaldehyde and curcumin might be the reason for the high solubility. Following these results, cinnamon bark oil, a natural source of cinnamaldehyde, was examined as a natural solvent.

Three different cinnamon oils were investigated. Via GC-FID and GC-MS analysis, it was found that a content of 79% cinnamaldehyde in *Cinnamomum cassia* oil was enough to achieve solubilities as good as the reference. This could be justified as the side ingredients of this oil were only structural analogues of cinnamaldehyde, which had similar positive effects on the solubility of curcumin. The *Cinnamomum verum* oils, on the other hand, possessed higher terpene contents, which, as determined above, were responsible for limiting the curcumin solubility. Their presence was the reason for the worse performance of the *Cinnamomum verum* oils. These finds mark the first innovation, as essential oils could indeed be used for the solubilization of curcumin while their composition was responsible for modulating their solving capacity [169].

Successively, extraction experiments with focus on taking advantage of the full solving capacity were performed. To this purpose, the maximum curcumin solubility was searched in ternary mixtures and found at a composition of 5:22:73 water/EtOH/oil cassia. While the concentration of curcuminoids could be increased continuously in a linear way, their maximum mass was extracted only after ten cycles before losing some amount of curcuminoids to the plant matrix again. To explain this behavior, a theoretical model was proposed that relates the premature saturation of the solvent to the loss of solvent after each cycle. In future studies, this model should be verified while also proposing ideas to amend the process [169].

In the following, the extraction of phytochemicals using essential oils of natural sources should as well be examined in more detail. The influence of water on the extraction of the single curcuminoids should be regarded before trying to apply the system for extractions of other phytochemicals as well. However, a basis for the assessment of novel extraction processes of various phytochemicals, which rely solely on sustainable and renewable sources, could be made [169].

CHAPTER 7

COLLECTIVE CONCLUSION

7 Collective Conclusion

The preceding Chapters 3-6 each gave an insight into the possibilities of green chemistry in extraction. From the presented results above, one can see that there is a broad field, in which sustainability and greenness play a role and should be taken into account.

This study focused especially on the examination of alternative solvents. Interestingly, nature provides a plethora of compounds, which can be employed as solvents. Chapter 3 showed that it is possible to extract fragrances by using a fatty acid, which was already part of the plant matrix from which the target compounds should be extracted. Natural deep eutectic solvents, which are mixtures of small, naturally occurring molecules with high abundance throughout nature, were investigated in Chapters 4 and 5. Understanding the mechanism with which the natural deep eutectics interacted with the solute curcumin was an important step. These studies opened the door to investigate extractions of even more phytochemicals by employing these solvents. Lastly, essential oils were examined in terms of their effectivity of solving and successively extracting curcumin in Chapter 6. Essential oils are easily overlooked when searching for alternative solvents. However, they showed to be very promising in terms of solving and extracting.

These experiments laid some foundation stones that will hopefully drive future innovations and applications using green alternative solvents.

CHAPTER 8

BIBLIOGRAPHY

8 Bibliography

1. Tram, B. *Handbook of Plant Food Phytochemicals*; Tiwari, B.K., Brunton, N.P., Brennan, C.S., Eds.; Wiley-Blackwell, 2013; ISBN 9781444338102.
2. Zhang, Q.W.; Lin, L.G.; Ye, W.C. Techniques for extraction and isolation of natural products: A comprehensive review. *Chinese Med. (United Kingdom)* **2018**, *13*, 20–46, doi:10.1186/s13020-018-0177-x.
3. Abubakar, A.R.; Haque, M. Preparation of Medicinal Plants: Basic Extraction and Fractionation Procedures for Experimental Purposes. *J. Pharm. Bioallied Sci.* **2020**, *12*, 1–10, doi:10.4103/jpbs.JPBS.
4. Palma, M.; Barbero, G.F.; Piñeiro, Z.; Liazid, A.; Barroso, C.G.; Rostagno, M.A.; Prado, J.M.; Meireles, M.A.A. Extraction of Natural Products: Principles and fundamental Aspects. In *Natural Product Extraction: Principles and Applications*; RSC Green Chemistry, 2013; pp. 58–88 ISBN 9781849736060.
5. Natural Extracts Market Size, Share & Trends Analysis Report By Product (Essential Oils, Oleoresins, Herbal Extracts, Natural Colors, Dried Crops), By Application, By Region, And Segment Forecasts, 2021 - 2028 Available online: https://www.grandviewresearch.com/industry-analysis/natural-extracts-market (accessed on Aug 16, 2022).
6. Anastas, P.; Eghbali, N. Green chemistry: Principles and practice. *Chem. Soc. Rev.* **2010**, *39*, 301–312, doi:10.1039/b918763b.
7. Chemat, F.; Vian, M.A.; Cravotto, G. Green extraction of natural products: Concept and principles. *Int. J. Mol. Sci.* **2012**, *13*, 8615–8627, doi:10.3390/ijms13078615.
8. Choi, Y.H.; van Spronsen, J.; Dai, Y.; Verberne, M.; Hollmann, F.; Arends, I.W.C.E.; Witkamp, G.J.; Verpoorte, R. Are natural deep eutectic solvents the missing link in understanding cellular metabolism and physiology? *Plant Physiol.* **2011**, *156*, 1701–1705, doi:10.1104/pp.111.178426.
9. Benkert, C.; Freyburger, A.; Huber, V.; Touraud, D.; Kunz, W. Development of a fully water-dilutable mint concentrate based on a food-approved microemulsion. *Food Chem.* **2022**, *372*, 131230–131238, doi:10.1016/j.foodchem.2021.131230.
10. Marturano, V.; Bizzarro, V.; De Luise, A.; Calarco, A.; Ambrogi, V.; Giamberini, M.; Tylkowski, B.; Cerruti, P. Essential oils as solvents and core

materials for the preparation of photo-responsive polymer nanocapsules. *Nano Res.* **2018**, *11*, 2783–2795, doi:10.1007/s12274-017-1908-5.

11. Anulika, N.P.; Ignatius, E.O.; Raymond, E.S.; Osasere, O.-I.; Abiola, A.H. The chemistry of natural product: Plant secondary metabolites. *Inernational J. Technol. Enhanc. Emerg. Eng. Res.* **2016**, *4*, 1–8.
12. Eljounaidi, K.; Lichman, B.R. Nature’s Chemists: The Discovery and Engineering of Phytochemical Biosynthesis. *Front. Chem.* **2020**, *8*, 596479–596489, doi:10.3389/fchem.2020.596479.
13. Whitehead, S.R.; Schneider, G.F.; Dybzinski, R.; Nelson, A.S.; Gelammbi, M.; Jos, E.; Beckman, N.G. Fruits, frugivores, and the evolution of phytochemical diversity. *Oikos* **2021**, *2022*, n/a, doi:10.1111/oik.05876.
14. Mera, I.F.G.; Falconí, D.E.G.; Córdova, V.M. Secondary metabolites in plants: Main classes, phytochemical analysis and pharmacological activities. *Bionatura* **2019**, *4*, 1000–1009, doi:10.21931/RB/2019.04.04.11.
15. Nahar, L.; Xiao, J.; Sarker, S.D. Introduction of Phytonutrients. In *Handbook of Dietary Phytochemicals*; 2020; pp. 1–17 ISBN 9789811317453.
16. Koche, D.; Shirsat, R.; Kawale, M. An Overerview of Major Classes of Phytochemicals: Their Types and Role in Disease Prevention. *Hislopia J.* **2016**, *9*, 1–11.
17. Kennedy, D.O.; Wightman, E.L. Herbal extracts and phytochemicals: Plant secondary metabolites and the enhancement of human brain function. *Adv. Nutr.* **2011**, *2*, 32–50, doi:10.3945/an.110.000117.
18. *Phytochemicals: Dietary Sources, Innovative Extraction and Health Benefits*; Aguilera Guitérrez, Y., Benítez García, V., Eds.; Foods, 2021; ISBN 9783036530000.
19. Erb, M.; Kliebenstein, D.J. Plant Secondary Metabolites as Defenses, Regulators, and Primary Metabolites: The Blurred Functional Trichotomy. *Plant Physiol.* **2020**, *184*, 39–52, doi:10.1104/PP.20.00433.
20. Zullaikah, S.; Rachmaniah, O.; Utomo, A.T.; Niawanti, H.; Ju, Y.H. Green Separation of Bioactive Natural Products Using Liquefied Mixture of Solids. In *Green Chemistry*; Saleh, H.M., Koller, M., Eds.; IntechOpen Limited: London, 2018; pp. 17–39.
21. Mendoza, N.; Escamilla Silca, E.M. Introduction to Phytochemicals: Secondary Metabolites from Plants with Active Principles for Pharmacological

Importance. In *Phytochemicals - Source of Antioxidants and Role in Disease Prevention*; Asao, T., Asaduzzaman, M., Eds.; IntechOpen Limited, 2018; pp. 25–47.

22. Castro-Moretti, F.R.; Gentzel, I.N.; Mackey, D.; Alonso, A.P. Metabolomics as an emerging tool for the study of plant–pathogen interactions. *Metabolites* **2020**, *10*, 52–74, doi:10.3390/metabo10020052.
23. Wang, S.; Alseekh, S.; Fernie, A.R.; Luo, J. The Structure and Function of Major Plant Metabolite Modifications. *Mol. Plant* **2019**, *12*, 899–919, doi:10.1016/j.molp.2019.06.001.
24. Behl, T.; Kumar, K.; Brisc, C.; Rus, M.; Nistor-Cseppento, D.C.; Bustea, C.; Aron, R.A.C.; Pantis, C.; Zengin, G.; Sehgal, A.; et al. Exploring the multifocal role of phytochemicals as immunomodulators. *Biomed. Pharmacother.* **2021**, *133*, 110959–110977, doi:10.1016/j.biopha.2020.110959.
25. Gonzáles Mera, I.F.; Gonzáles Falconí, D.E.; Morera Córdova, V. Secondary metabolites in plants: Main classes, phytochemical analysis and pharmacological activities. *Bionatura* **2019**, *4*, 1000–1009, doi:10.21931/RB/2019.04.04.11.
26. Dillard, C.J.; German, J.B. Phytochemicals: Nutraceuticals and human health. *J. Sci. Food Agric.* **2000**, *80*, 1744–1756, doi:10.1002/1097-0010(20000915)80:12<1744::AID-JSFA725>3.0.CO;2-W.
27. Govindarajan, M.; Sivakumar, R.; Rajeswari, M.; Yogalakshmi, K. Chemical composition and larvicidal activity of essential oil from Mentha spicata (Linn.) against three mosquito species. *Parasitol. Res.* **2012**, *110*, 2023–2032, doi:10.1007/s00436-011-2731-7.
28. Şarer, E.; Toprak, S.Y.; Otlu, B.; Durmaz, R. Composition and antimicrobial activity of the essential oil from mentha spicata l. subsp. spicata. *J. Essent. Oil Res.* **2011**, *23*, 105–108, doi:10.1080/10412905.2011.9700435.
29. Alara, O.R.; Abdurahman, N.H.; Ukaegbu, C.I. Extraction of phenolic compounds: A review. *Curr. Res. Food Sci.* **2021**, *4*, 200–214, doi:10.1016/j.crfs.2021.03.011.
30. Pott, D.M.; Osorio, S.; Vallarino, J.G. From central to specialized metabolism: An overview of some secondary compounds derived from the primary metabolism for their role in conferring nutritional and organoleptic characteristics to fruit. *Front. Plant Sci.* **2019**, *10*, 835–854,

doi:10.3389/fpls.2019.00835.

31. Benvenutti, L.; Zielinski, A.A.F.; Ferreira, S.R.S. Which is the best food emerging solvent: IL, DES or NADES? *Trends Food Sci. Technol.* **2019**, *90*, 133–146, doi:10.1016/j.tifs.2019.06.003.

32. Kale, R.; Kadam, A.; Deshmukh, R. Food Colors Market Size, Share & Growth | Industry Report 2027 Available online: https://www.alliedmarketresearch.com/food-color-market (accessed on Aug 8, 2022).

33. Downham, A.; Collins, P. Colouring our foods in the last and next millennium. *Int. J. Food Sci. Technol.* **2000**, *35*, 5–22, doi:10.1046/j.1365-2621.2000.00373.x.

34. Polyphenols Market Size & Share Report, 2022-2030 Available online: https://www.grandviewresearch.com/industry-analysis/polyphenols-market-analysis# (accessed on Aug 8, 2022).

35. Gey, M.H. *Instrumentelle Analytik und Bioanalytik*; 2021; ISBN 9783662639511.

36. Chemat, F.; Abert Vian, M.; Fabiano-Tixier, A.S.; Nutrizio, M.; Režek Jambrak, A.; Munekata, P.E.S.; Lorenzo, J.M.; Barba, F.J.; Binello, A.; Cravotto, G. A review of sustainable and intensified techniques for extraction of food and natural products. *Green Chem.* **2020**, *22*, 2325–2353, doi:10.1039/c9gc03878g.

37. Ferhat, M.A.; Meklati, B.Y.; Chemat, F. Comparison of different isolation methods of essential oil from Citrus fruits: cold pressing, hydrodistillation and microwave “dry” distillation. *Flavour Fragr. J.* **2007**, *22*, 494–504, doi:10.1002/ffj.1829.

38. Cravotto, G.; Binello, A.; Orio, L. Green extraction techniques for high-quality natural products. *Agro Food Ind. Hi Tech* **2011**, *22*, 57–59.

39. Savoire, R.; Lanoisellé, J.L.; Vorobiev, E. Mechanical Continuous Oil Expression from Oilseeds: A Review. *Food Bioprocess Technol.* **2013**, *6*, 1–16, doi:10.1007/s11947-012-0947-x.

40. Letcher, T.M.; Battino, R. An Introduction to the Understanding of Solubility. *J. Chem. Educ.* **2001**, *78*, 103–111, doi:10.1021/ed078p103.

41. Gupta, A.; Naraniwal, M.; Kothari, V. Modern Extraction Methods for Preparation of Bioactive Plant Extracts. *Int. J. Appl. Nat. Sci.* **2012**, *1*, 8–26.

42. Chaves, J.O.; de Souza, M.C.; da Silva, L.C.; Lachos-Perez, D.; Torres-Mayanga, P.C.; Machado, A.P. da F.; Forster-Carneiro, T.; Vázquez-Espinosa, M.; González-de-Peredo, A.V.; Barbero, G.F.; et al. Extraction of Flavonoids From Natural Sources Using Modern Techniques. *Front. Chem.* **2020**, *8*, 507887–507912, doi:10.3389/fchem.2020.507887.

43. Handa, S.S.; Singh Khanuja, S.P.; Longo, G.; Rakesh, D.D. *Extraction Technologies for Medicinal and Aromatic Plants*; 2008;

44. Tambun, R.; Alexander, V.; Ginting, Y. Performance comparison of maceration method, soxhletation method, and microwave-assisted extraction in extracting active compounds from soursop leaves (Annona muricata): A review. *IOP Conf. Ser. Mater. Sci. Eng.* **2021**, *1122*, 12095–12103, doi:10.1088/1757-899x/1122/1/012095.

45. Jones, W.P.; Kinghorn, A.D. Extraction of Plant Secondary Metabolites. In *Natrural Products Isolation*; Sarker, S.D., Latif, Z., Gray, A.I., Eds.; Humana Press, 2006; Vol. 20, pp. 323–351 ISBN 9781617796234.

46. Both, S.; Chemat, F.; Strube, J. Extraction of polyphenols from black tea - Conventional and ultrasound assisted extraction. *Ultrason. Sonochem.* **2014**, *21*, 1030–1034, doi:10.1016/j.ultsonch.2013.11.005.

47. Degot, P.; Huber, V.; Hofmann, E.; Hahn, M.; Touraud, D.; Kunz, W. Solubilization and extraction of curcumin from Curcuma Longa using green, sustainable, and food-approved surfactant-free microemulsions. *Food Chem.* **2021**, *336*, 127660–127668, doi:10.1016/j.foodchem.2020.127660.

48. Degot, P.; Huber, V.; Touraud, D.; Kunz, W. Curcumin extracts from Curcuma Longa – Improvement of concentration, purity, and stability in food-approved and water-soluble surfactant-free microemulsions. *Food Chem.* **2021**, *339*, 128140–128148, doi:10.1016/j.foodchem.2020.128140.

49. Carson, R. *Silent Spring*; First Mari.; Houghton Mifflin Company: New York, 1962; ISBN 0-618-24906-0.

50. Anelli, C.M.; Krupke, C.H.; Prasad, R.P. Professional Entomology and the 44 Noisy Years since Silent Spring. Part 1. *Am. Entomol.* **2006**, *52*, 224–233, doi:10.1093/ae/52.4.224.

51. Anastas, P.T.; Warner, J.C. *Green Chemistry: Theory and Practice*; Reprint Ed.; Oxford University Press Inc, 2000; ISBN 0198502346.

52. Kurt, S.; Osueke, K.K. The Effects of Color on the Moods of College Students.

SAGE Open **2014**, *4*, 215824401452542, doi:10.1177/2158244014525423.

53. Anastas, P.T.; Beach, E.S. Green chemistry: The emergence of a transformative framework. *Green Chem. Lett. Rev.* **2007**, *1*, 9–24, doi:10.1080/17518250701882441.
54. Clarke, C.J.; Tu, W.C.; Levers, O.; Bröhl, A.; Hallett, J.P. Green and Sustainable Solvents in Chemical Processes. *Chem. Rev.* **2018**, *118*, 747–800, doi:10.1021/acs.chemrev.7b00571.
55. Alonso, D.A.; Baeza, A.; Chinchilla, R.; Guillena, G.; Pastor, I.M.; Ramón, D.J. Deep Eutectic Solvents: The Organic Reaction Medium of the Century. *European J. Org. Chem.* **2016**, *2016*, 612–632, doi:10.1002/ejoc.201501197.
56. Capello, C.; Fischer, U.; Hungerbühler, K. What is a green solvent? A comprehensive framework for the environmental assessment of solvents. *Green Chem.* **2007**, *9*, 927–93, doi:10.1039/b617536h.
57. Chemat, F.; Vian, M.A.; Ravi, H.K.; Khadhraoui, B.; Hilali, S.; Perino, S.; Tixier, A.S.F. Review of alternative solvents for green extraction of food and natural products: Panorama, principles, applications and prospects. *Molecules* **2019**, *24*, 3007–3034, doi:10.3390/molecules24163007.
58. Prat, D.; Wells, A.; Hayler, J.; Sneddon, H.; McElroy, C.R.; Abou-Shehada, S.; Dunn, P.J. CHEM21 selection guide of classical- and less classical-solvents. *Green Chem.* **2015**, *18*, 288–296, doi:10.1039/c5gc01008j.
59. Byrne, F.P.; Jin, S.; Paggiola, G.; Petchey, T.H.M.; Clark, J.H.; Farmer, T.J.; Hunt, A.J.; Robert McElroy, C.; Sherwood, J. Tools and techniques for solvent selection: green solvent selection guides. *Sustain. Chem. Process.* **2016**, *4*, doi:10.1186/s40508-016-0051-z.
60. Huber, V.; Häckl, K.; Touraud, D.; Kunz, W. Natural deep eutectic solvents: From simple systems to complex colloidal mixtures. *Adv. Bot. Res.* **2021**, *97*, 17–40, doi:10.1016/bs.abr.2020.09.001.
61. Schuur, B.; Brouwer, T.; Smink, D.; Sprakel, L.M.J. Green solvents for sustainable separation processes. *Curr. Opin. Green Sustain. Chem.* **2019**, *18*, 57–65, doi:10.1016/j.cogsc.2018.12.009.
62. Sánchez-Camargo, A. del P.; Bueno, M.; Parada-Alfonso, F.; Cifuentes, A.; Ibáñez, E. Hansen solubility parameters for selection of green extraction solvents. *TrAC - Trends Anal. Chem.* **2019**, *118*, 227–237, doi:10.1016/j.trac.2019.05.046.

63. Abbott, A.P.; Capper, G.; Davies, D.L.; Munro, H.L.; Rasheed, R.K.; Tambyrajah, V. Preparation of novel, moisture-stable, lewis-acidic ionic liquids containing quaternary ammonium salts with functional side chains. *Chem. Commun.* **2001**, 2010–2011, doi:10.1039/b106357j.
64. de los Ángeles Fernández, M.; Boiteux, J.; Espino, M.; Gomez, F.J.V.; Silva, M.F. Natural deep eutectic solvents-mediated extractions: The way forward for sustainable analytical developments. *Anal. Chim. Acta* **2018**, *1038*, 1–10, doi:10.1016/j.aca.2018.07.059.
65. El Achkar, T.; Greige-Gerges, H.; Fourmentin, S. Basics and properties of deep eutectic solvents: a review. *Environ. Chem. Lett.* **2021**, *19*, 3397–3408, doi:10.1007/s10311-021-01225-8.
66. Smith, E.L.; Abbott, A.P.; Ryder, K.S. Deep Eutectic Solvents (DESs) and Their Applications. *Chem. Rev.* **2014**, *114*, 11060–11082, doi:10.1021/cr300162p.
67. Zainal-Abidin, M.H.; Hayyan, M.; Hayyan, A.; Jayakumar, N.S. New horizons in the extraction of bioactive compounds using deep eutectic solvents: A review. *Anal. Chim. Acta* **2017**, *979*, 1–23, doi:10.1016/j.aca.2017.05.012.
68. Dai, Y.; van Spronsen, J.; Witkamp, G.J.; Verpoorte, R.; Choi, Y.H. Natural deep eutectic solvents as new potential media for green technology. *Anal. Chim. Acta* **2013**, *766*, 61–68, doi:10.1016/j.aca.2012.12.019.
69. Plechkova, N. V.; Seddon, K.R. Applications of ionic liquids in the chemical industry. *Chem. Soc. Rev.* **2008**, *37*, 123–150, doi:10.1039/b006677j.
70. Huber, V.; Muller, L.; Degot, P.; Touraud, D.; Kunz, W. NADES-based surfactant-free microemulsions for solubilization and extraction of curcumin from Curcuma Longa. *Food Chem.* **2021**, *355*, 129624–129631, doi:10.1016/j.foodchem.2021.129624.
71. Mišan, A.; Nađpal, J.; Stupar, A.; Pojić, M.; Mandić, A.; Verpoorte, R.; Choi, Y.H. The perspectives of natural deep eutectic solvents in agri-food sector. *Crit. Rev. Food Sci. Nutr.* **2020**, *60*, 2564–2592, doi:10.1080/10408398.2019.1650717.
72. Liu, Y.; Friesen, J.B.; McAlpine, J.B.; Lankin, D.C.; Chen, S.N.; Pauli, G.F. Natural Deep Eutectic Solvents: Properties, Applications, and Perspectives. *J. Nat. Prod.* **2018**, *81*, 679–690, doi:10.1021/acs.jnatprod.7b00945.
73. Perna, F.M.; Vitale, P.; Capriati, V. Deep eutectic solvents and their

applications as green solvents. *Curr. Opin. Green Sustain. Chem.* **2020**, *21*, 27–33, doi:10.1016/j.cogsc.2019.09.004.

74. Yang, Z. Natural Deep Eutectic Solvents and Their Applications in Biotechnology. *Adv. Biochem. Eng. Biotechnol.* **2019**, *168*, 31–59, doi:10.1007/10_2018_67.
75. Giusti, M.M.; Wrolstad, R.E. Characterization and Measurement of Anthocyanins by UV-Visible Spectroscopy. *Curr. Protoc. Food Anal. Chem.* **2001**, *1*, 1–13, doi:https://doi.org/10.1002/0471142913.faf0102s00.
76. Agilent UV-Vis Spectroscopy & Spectrophotometer FAQs Available online: https://www.agilent.com/en/support/molecular-spectroscopy/uv-vis-uv-vis-nir-spectroscopy/uv-vis-spectroscopy-spectrophotometer-basics (accessed on Aug 8, 2022).
77. Hage, D.S. Chromatography. In *Principles and Applications of Clinical Mass Spectrometry: Small Molecules, Peptides, and Pathogens*; 2018; pp. 1–32 ISBN 9780128160633.
78. Hesse, M.; Meier, H.; Zeeh, B.; Bienz, S.; Bigler, L.; Fox, T. *Spektroskopische Methoden in der Chemie*; 8th ed.; Georg Thieme Verlag, 2012; Vol. 8; ISBN 978-3-13-576108-4.
79. Hinderer, F. *Prinzip der UV/Vis-Absorptions- und Fluoreszenz-Spektroskopie*; Springer Spektrum, 2020; ISBN 9783658254407.
80. Matissek, R.; Fischer, M. *Lebensmittelanalytik*; 7th ed.; Springer Spektrum: Berlin, 2021; ISBN ISBN 978-3-662-63409-7.
81. Matissek, R. *Lebensmittelchemie*; 9th ed.; Springer-Verlag GmbH Deutschland: Berlin, 2019; ISBN 9783662596685.
82. Rahman, A.; Iqbal Choudhary, M.; Wahab, A. *Solving Problems with NMR Spectroscopy*; 2nd ed.; Elsevier Inc.: London, 2016; ISBN 978-0-12-411589-7.
83. Friebolin, H. *Ein- und zweidimensionale NMR-Spektroskopie*; 4th ed.; Wiley-VCH Verlag: Weinheim, 2006; ISBN 978-3-527-31571-0.
84. Lambert, J.B.; Gronert, S.; Shurvell, H.F.; Lightner, D.A. *Spektroskopie. Strukturaufklärung in der Organischen Chemie*; Mönch, K., Kachnij, A., Marsmann, H.C., Kuck, D., Eds.; 2nd ed.; Pearson, 2012; ISBN 978-3-86894-146-3.
85. Kumar, A.; Wagner, G.; Wüthrich, K.; Kumar, A.; Ernst, R.R. Buildup Rates of the Nuclear Overhauser Effect Measured by Two-Dimensional Proton

Magnetic Resonance Spectroscopy: Implications for Studies of Protein Conformation. *J. Am. Chem. Soc.* **1981**, *103*, 3654–3658, doi:10.1021/ja00403a008.

86. Neuhaus, D. Nuclear Overhauser Effect. *Encycl. Magn. Reson.* **2011**, 1–16, doi:10.1002/9780470034590.emrstm0350.pub2.
87. Jeener, J.; Meier, B.H.; Bach Investigation of exchange processes by two-dimensional NMR spectroscopy. *J. Chem. Phys.* **1979**, *71*, 4546–4553, doi:https://doi.org/10.1063/1.438208.
88. Ettre, L.S. Chromatography: The separation technique of the 20th Century. *Chromatographia* **2000**, *51*, 7–17, doi:10.1007/BF02490689.
89. Dong, M.W. *HPLC and UHPLC for Practicing Scientists*; Dong, M.W., Ed.; 2nd ed.; Wiley, 2019; ISBN 9781119313786.
90. Van Deemter, J.J.; Klinkenberg, A.; Zuiderweg, F.J. Longitudinal diffusion and resistance to mass transfer as causes of nonideality in chromatography. *Chem. Eng. Sci.* **1956**, *5*, 271–289, doi:10.1016/0009-2509(56)80003-1.
91. Edge, T. Turbulent flow chromatography in bioanalysis. In *Handbook of Analytical Separations*; Elsevier B.V., 2003; Vol. 4, pp. 91–128 ISBN 9780444506580.
92. Meyer, V.R. CHROMATOGRAPHY | Principles. In *Encyclopedia of Analytical Science*; Elsevier Inc., 2019; pp. 105–112 ISBN 9780081019832.
93. Töppner, K.; Hansen, D.; Herbig, E. Reinstwasser für die HPLC-Analyse Available online: https://www.bionity.com/de/whitepaper/1126683/reinstwasser-fuer-die-hplc-analyse.html (accessed on Aug 8, 2022).
94. Hansen, C.M. The Universality of the Solubility Parameter. *I&EC Prod. Res. Dev.* **1969**, *8*, 2–11, doi:https://doi.org/10.1021/i360029a002.
95. Hansen, C.M. *Hansen Solubility Parameters - A User's Handbook*; 2nd ed.; CRC Press, 2007; ISBN 9781420006834.
96. Zeng, W.; Du, Y.; Xue, Y.; Frisch, H.L. Solubility Parameters. In *Physical Properties of Polymers Handbook*; Mark, J.E., Ed.; SpringerMaterials, 2007; pp. 289–303.
97. Hansen, C.M.; Abbot, S.; Yamamoto, H. Hansen Solubilit Parameters Available online: https://www.hansen-solubility.com/ (accessed on Aug 9, 2022).
98. Klamt, A. Conductor-like Screening Model for Real Solvents: A New Approach

to the Quantitative Calculation of Solvation Phenomena. *J. Phys. Chem.* **1995**, *99*, 2224–2235.

99. Klamt, A.; Volker, J.; Bürger, T.; Lohrenz, J.C.W. Refinement and Parametrization of COSMO-RS. *J. Phys. Chem. A* **1998**, *102*, 5074–5085, doi:10.1021/jp980017s.

100. Klamt, A. *COSMO-RS: From Quantum Chemistry to Fluid Phase Thermodynamics*; Elsevier Science, 2005; ISBN 978-0444519948.

101. Klamt, A.; Krooshof, G.J.P.; Taylor, R. COSMOSPACE : Alternative to Conventional Activity-Coefficient Models. *AIChE J.* **2002**, *48*, 2332–2349, doi:10.1002/aic.690481023.

102. Eckert, F.; Klamt, A. Fast solvent screening via quantum chemistry: COSMO-RS approach. *AIChE J.* **2002**, *48*, 369–385, doi:10.1002/aic.690480220.

103. Klamt, A.; Schüürmann, G. COSMO: A New Approach to Dielectric Screening in Solvents with Explicit Expressions for the Screening Energy and its Gradient. *J. Chem. Soc. Perkin Trans. 2* **1993**, 799–805, doi:10.1039/P29930000799.

104. Amin, H.I.M.; Hussain, F.H.S.; Najmaldin, S.K.; Thu, Z.M.; Ibrahim, M.F.; Gilardoni, G.; Vidari, G. Phytochemistry and biological activities of iris species growing in iraqi kurdistan and phenolic constituents of the traditional plant iris postii. *Molecules* **2021**, *26*, 264–285, doi:10.3390/molecules26020264.

105. Cantor, M. New perspectives on medicinal properties and uses of Iris sp. In *Hop and Medicinal Plants*; Muntean, L.S., Ed.; AcademicPres, 2016; pp. 24–37.

106. Yousefsani, B.S.; Boozari, M.; Shirani, K.; Jamshidi, A.; Dadmehr, M. A review on phytochemical and therapeutic potential of Iris germanica. *J. Pharm. Pharmacol.* **2021**, *73*, 611–625, doi:10.1093/jpp/rgab008.

107. Kukula-Koch, W.; Sieniawska, E.; Widelski, J.; Urjin, O.; Głowniak, P.; Skalicka-Woźniak, K. Major secondary metabolites of Iris spp. *Phytochem. Rev.* **2015**, *14*, 51–80, doi:10.1007/s11101-013-9333-1.

108. Akbar, S. Iris germanica L. In *Handbook of 200 Medicinal Plants: A Comprehensive Review of Their Traditional Medical Uses and Scientific Justifications*; Springer Nature Switzerland AG, 2020; pp. 1043–1047 ISBN 9783030168070.

109. Bauer, R.; Blaschek, W.; Buff, W.; Classen, B.; Heise, E.M.; Hensel, A.; Krenn, L.; Lichius, J.J.; Lindequist, U.; Loew, D.; et al. Veilchenwurzel. Iridis rhizoma. In *Wichtl - Teedrogen und Phytopharmaka: Ein Handbuch für die Praxis*;

Blaschek, W., Ed.; Wissenschaftliche Verlagsgesellschaft, 2015; pp. 351–353.

110. Yuan, Y.; Sun, Y.; Zhao, Y.; Liu, C.; Chen, X.; Li, F.; Bao, J. Identification of floral scent profiles in bearded irises. *Molecules* **2019**, *24*, 1–17, doi:10.3390/molecules24091773.

111. Jaenicke, L.; Marner, F.J. The irones and their origin. *Pure Appl. Chem.* **1990**, *62*, 1365–1368, doi:10.1351/pac199062071365.

112. *Chemical Dictionary of Economic Plants*; Harborne, J.B., Baxter, H., Eds.; John Wiley & Sons: New York, 2001; ISBN 978-0-471-49226-9.

113. Hickman, K.C.D. High-Vacuum Short-Path Distillation - A Review. *Chem. Rev.* **1944**, *34*, 51–106, doi:https://doi.org/10.1021/cr60107a002.

114. Motschmann, H.; Hofmann, M. *Physikalische Chemie*; De Gruyter: Berlin, 2014; ISBN 9783486587258.

115. Sattler, K.; Feindt, H.J. Distillation and Partial Condensation. In *Thermal Separation Processes: Principles and Design*; VCH, 1995; pp. 101–237 ISBN 9783527615476.

116. Ketenoglu, O.; Tekin, A. Applications of molecular distillation technique in food products. *Ital. J. Food Sci.* **2015**, *27*, 277–281.

117. Hickman, K.C.D.; Mees, G.C. Molecular Distillation. *Ind. Eng. Chem. Res.* **1946**, *38*, 28–29, doi:https://doi.org/10.1021/ie50433a023.

118. Lutišan, J.; Cvengroš, J. Mean free path of molecules on molecular distillation. *Chem. Eng. J. Biochem. Eng. J.* **1995**, *56*, 39–50, doi:10.1016/0923-0467(94)02857-7.

119. Lei, Z.; Chen, B.; Ding, Z. *Special Distillation Processes*; Elsevier B.V, 2005; ISBN 0-444-51648-4.

120. PubChem Myristic acid Available online: https://pubchem.ncbi.nlm.nih.gov/compound/Myristic-acid (accessed on Aug 10, 2022).

121. MacDougal, D.T.; Spoehr, H.A. THE SOLUTION AND FIXATION ACCOMPANYING SWELLING AND DRYING OF BIOCOLLOIDS AND PLANT TISSUES. *The Plant World* **1919**, *22*, 129–137.

122. Hess, F.D.; Foy, C.L. Interaction of Surfactants with Plant Cuticles. *Weed Technol.* **2000**, *14*, 807–813.

123. Bedienungsanleitung zur Labor-Kurzweg-Destillationsanlage KDL5 2012.

124. Céondo Chemical Properties of «alpha»-Ionone (CAS 30685-95-1) Available

online: https://www.chemeo.com/cid/70-050-8/«alpha»-Ionone (accessed on Aug 10, 2022).

125. Cheng, Y.; Huang, Y.; Alexander, K.; Dollimore, D. A thermal analysis study of methyl salicylate. *Thermochim. Acta* **2001**, *367–368,* 69–74, doi:10.1016/S0040-6031(00)00689-4.

126. Huber, V.; Muller, L.; Hioe, J.; Degot, P.; Touraud, D.; Kunz, W. Improvement of the Solubilization and Extraction of Curcumin in an Edible Ternary Solvent Mixture. **2021**, *26*, 7702–7722, doi:10.3390/molecules26247702.

127. Scartezzini, P.; Speroni, E. Review on some plants of Indian traditional medicine with antioxidant activity. *J. Ethnopharmacol.* **2000**, *71*, 23–43, doi:10.1016/S0378-8741(00)00213-0.

128. Nair, K.P. *Turmeric (Curcuma longa L.) and Ginger (Zingiber officinale Rosc.) - World's Invaluable Medicinal Spices*; Springer, 2019; ISBN 9783030291884.

129. Akbar, S. Curcuma longa L (Zingiberaceae). In *Handbook of 200 Medicinal Plants: A Comprehensive Review of Their Traditional Medical Uses and Scientific Justifications*; Springer Nature Switzerland AG, 2020; pp. 781–807 ISBN 978-3-030-16807-0.

130. Prasad, S.; Aggarwal, B.B. Turmeric, the Golden Spice. In *Herbal Medicine: Biomolecular and Clinical Aspects*; Benzie, I.F.F., Wachtel-Galor, S., Eds.; CRC Press/Taylor&Francis, 2011; pp. 263–289.

131. Priyadarsini, K. The Chemistry of Curcumin: From Extraction to Therapeutic Agent. *Molecules* **2014**, *19*, 20091–20112, doi:10.3390/molecules191220091.

132. Geethanjali, A.; Lalitha, P.; Firdhouse, M.J. Analysis of Curcumin Content of Turmeric Samples from Various States of India. *Int. J. Pharma Chem. Res.* **2016**, *2*, 55–62.

133. Tayyem, R.F.; Heath, D.D.; Al-Delaimy, W.K.; Rock, C.L. Curcumin Content of Turmeric and Curry Powders Curcumin Content of Turmeric and Curry Powders. *Nutr. Cancer* **2006**, *55*, 126–131, doi:10.1207/s15327914nc5502_2.

134. Schrott, E.; Ammon, H.P.T. *Heilpflanzen der ayurvedischen und der westlichen Medizin*; Springer, 2012; ISBN 9783642131240.

135. Bauer, R.; Blaschek, W.; Buff, W.; Classen, B.; Heise, E.M.; Hensel, A.; Krenn, L.; Lichius, J.J.; Lindequist, U.; Loew, D.; et al. Curcumawurzelstock. Curcumae longae rhizoma. In *Wichtl - Teedrogen und Phytopharmaka: Ein Handbuch für die Praxis*; Blaschek, W., Ed.; Wissenschaftliche

Verlagsgesellschaft, 2015; pp. 210–212.

136. Bagchi, A. Extraction of Curcumin. *IOSR J. Environ. Sci. Toxicol. Food Technol.* **2012**, *1*, 1–16, doi:10.9790/2402-0130116.

137. Raduly, F.M.; Raditoiu, V.; Raditoiu, A.; Purcar, V. Curcumin: Modern applications for a versatile additive. *Coatings* **2021**, *11*, 519–541, doi:10.3390/coatings11050519.

138. Curcumin Market Size, Share & Trends Analysis Report By Application (Pharmaceutical, Food, Cosmetics), By Region (North America, Europe, Asia Pacific, CSA, MEA), And Segment Forecasts, 2020 - 2028 Available online: https://www.grandviewresearch.com/industry-analysis/turmeric-extract-curcumin-market (accessed on Aug 23, 2022).

139. Buchecker, T.; Krickl, S.; Winkler, R.; Grillo, I.; Bauduin, P.; Touraud, D.; Pfitzner, A.; Kunz, W. The impact of the structuring of hydrotropes in water on the mesoscale solubilisation of a third hydrophobic component. *Phys. Chem. Chem. Phys.* **2017**, *19*, 1806–1816, doi:10.1039/c6cp06696h.

140. Rente, D.; Paiva, A.; Duarte, A.R. The role of hydrogen bond donor on the extraction of phenolic compounds from natural matrices using deep eutectic systems. *Molecules* **2021**, *26*, doi:10.3390/molecules26082336.

141. Sánchez, P.B.; González, B.; Salgado, J.; José Parajó, J.; Domínguez, Á. Physical properties of seven deep eutectic solvents based on L-proline or betaine. *J. Chem. Thermodyn.* **2019**, *131*, 517–523, doi:10.1016/j.jct.2018.12.017.

142. Bajkacz, S.; Rusin, K.; Wolny, A.; Adamek, J.; Erfurt, K.; Chrobok, A. Highly efficient extraction procedures based on natural deep eutectic solvents or ionic liquids for determination of 20-hydroxyecdysone in spinach. *Molecules* **2020**, *25*, 1–14, doi:10.3390/molecules25204736.

143. Li, S.; Yuan, W.; Deng, G.; Wang, P.; Yang, P.; Aggarwal, B. Chemical composition and product quality control of turmeric Chemical composition and product quality control of turmeric (Curcuma longa L.). *Pharm. Crop.* **2011**, *2*, 28–54.

144. Rapp, C.; Goldberger, E.; Tishbi, N.; Kirshenbaum, R. Cation-π interactions of methylated ammonium ions: A quantum mechanical study. *Proteins Struct. Funct. Bioinforma.* **2014**, *82*, 1494–1502, doi:10.1002/prot.24519.

145. Dougherty, D.A. The Cation-π Interaction. *Acc Chem Res* **2013**, *46*, 885–893,

doi:10.1021/ar300265y.

146. Khan, H.M.; MacKerell, A.D.; Reuter, N. Cation-π Interactions between Methylated Ammonium Groups and Tryptophan in the CHARMM36 Additive Force Field. *J. Chem. Theory Comput.* **2019**, *15*, 7–12, doi:10.1021/acs.jctc.8b00839.

147. Mecozzi, S.; West, A.P.; Dougherty, D.A. Cation-π interactions in aromatics of biological and medicinal interest: Electrostatic potential surfaces as a useful qualitative guide. *Proc. Natl. Acad. Sci. U. S. A.* **1996**, *93*, 10566–10571, doi:10.1073/pnas.93.20.10566.

148. Honorat, P.; Roux, D.; Bellocq, A.M. Light Scattering Study of the Critical Behaviour in a Ternary Microemulsion System. *J. Phys. Lettres* **1984**, *45*, 961–968, doi:10.1051/jphyslet:019840045019096100.

149. Sorensen, C.M. Dynamic light-scattering study of tetrahydrofuran and water solutions. *J. Phys. Chem.* **1988**, *92*, 2367–2370, doi:10.1021/j100319a052.

150. Upper Critical Solution Temperature. *IUPAC Compend. Chem. Terminol.* **2008**, *1985*, 7280, doi:10.1351/goldbook.ut07280.

151. Bauduin, P.; Touraud, D.; Kunz, W. Design of low-toxic and temperature-sensitive anionic microemulsions using short propyleneglycol alkyl ethers as cosurfactants. *Langmuir* **2005**, *21*, 8138–8145, doi:10.1021/la0509652.

152. Huber, V.; Degot, P.; Touraud, D.; Kunz, W. Comment on “Impact of Conventional and Sustainable Solvents on the Yield, Selectivity, and Recovery of Curcuminoids from Turmeric.” *ACS Sustain. Chem. Eng.* **2022**, *10*, 2271–2272, doi:10.1021/acssuschemeng.1c08125.

153. Kisanthia, R.; Hunt, A.J.; Sherwood, J.; Somsakeesit, L.; Phaosiri, C. Impact of Conventional and Sustainable Solvents on the Yield, Selectivity, and Recovery of Curcuminoids from Turmeric. *ACS Sustain. Chem. Eng.* **2021**, doi:10.1021/acssuschemeng.1c04882.

154. Jimenez-Gonzalez, C.; Ponder, C.S.; Broxterman, Q.B.; Manley, J.B. Using the right green yardstick: Why process mass intensity is used in the pharmaceutical industry to drive more sustainable processes. *Org. Process Res. Dev.* **2011**, *15*, 912–917, doi:10.1021/op200097d.

155. Monteith, E.R.; Mampuys, P.; Summerton, L.; Clark, J.H.; Maes, B.U.W.; McElroy, C.R. Why we might be misusing process mass intensity (PMI) and a methodology to apply it effectively as a discovery level metric. *Green Chem.*

2020, *22*, 123–135, doi:10.1039/c9gc01537j.

156. Tenhunen, T.M.; Lewandowska, A.E.; Orelma, H.; Johansson, L.S.; Virtanen, T.; Harlin, A.; Österberg, M.; Eichhorn, S.J.; Tammelin, T. Understanding the interactions of cellulose fibres and deep eutectic solvent of choline chloride and urea. *Cellulose* **2018**, *25*, 137–150, doi:10.1007/s10570-017-1587-0.
157. Häkkinen, R.; Abbott, A. Solvation of carbohydrates in five choline chloride-based deep eutectic solvents and the implication for cellulose solubility. *Green Chem.* **2019**, *21*, 4673–4682, doi:10.1039/c9gc00559e.
158. Huber, V.; Hioe, J.; Touraud, D.; Kunz, W. Uncovering the curcumin solubilization ability of selected natural deep eutectic solvents based on quaternary ammonium compounds. *J. Mol. Liq.* **2022**, *361*, 119661–119672, doi:10.1016/j.molliq.2022.119661.
159. NMR Guidelines for ACS Journals. **2013**.
160. COSMOlogic GmbH & Co. KG - a Dassault Systèmes company COSMOtherm, Release 19 © 2019.
161. COSMOlogic GmbH & Co. KG *COSMOthermX User Guide Version 19.0*; 2019;
162. Hrubec, T.C.; Seguin, R.P.; Xu, L.; Cortopassi, G.A.; Datta, S.; Hanlon, A.L.; Lozano, A.J.; McDonald, V.A.; Healy, C.A.; Anderson, T.C.; et al. Altered toxicological endpoints in humans from common quaternary ammonium compound disinfectant exposure. *Toxicol. Reports* **2021**, *8*, 646–656, doi:10.1016/j.toxrep.2021.03.006.
163. Bartoli, S.; Roelens, S. Electrostatic attraction of counterion dominates the cation-π interaction of acetylcholine and tetramethylammonium with aromatics in chloroform [8]. *J. Am. Chem. Soc.* **1999**, *121*, 11908–11909, doi:10.1021/ja992415u.
164. Pletneva, E. V.; Laederach, A.T.; Fulton, D.B.; Kostić, N.M. The role of cation-π interactions in biomolecular association. Design of peptides favoring interactions between cationic and aromatic amino acid side chains. *J. Am. Chem. Soc.* **2001**, *123*, 6232–6245, doi:10.1021/ja010401u.
165. Meadows, E.S.; De Wall, S.L.; Barbour, L.J.; Gokel, G.W. Alkali metal cation - π Interactions observed by using a lariat ether model system. *J. Am. Chem. Soc.* **2001**, *123*, 3092–3107, doi:10.1021/ja003059e.
166. Orabi, E.A.; Lamoureux, G. Cation-π Interactions between Quaternary

Ammonium Ions and Amino Acid Aromatic Groups in Aqueous Solution. *J. Phys. Chem. B* **2018**, *122*, 2251–2260, doi:10.1021/acs.jpcb.7b11983.

167. Farias, F.O.; Passos, H.; Lima, Á.S.; Mafra, M.R.; Coutinho, J.A.P. Is It Possible to Create Ternary-like Aqueous Biphasic Systems with Deep Eutectic Solvents? *ACS Sustain. Chem. Eng.* **2017**, *5*, 9402–9411, doi:10.1021/acssuschemeng.7b02514.
168. Kumar, K.; Umapathi, R.; Bisht, M.; Ghoreishian, S.M.; Huh, Y.S.; Venkatesu, P. Tweaking Behavior of Hydrogen Bond Donor in Choline Chloride-Based Deep Eutectic Solvents for Regulating the Phase Transition of Poly(N-vinylcaprolactam): A Sustainable Medium for an Early Hydrophobic Collapse. *ACS Sustain. Chem. Eng.* **2021**, *9*, 14335–14344, doi:10.1021/acssuschemeng.1c05753.
169. Huber, V.; Schmidt, M.; Touraud, D.; Kunz, W. Towards a Sustainable and Green Extraction of Curcuminoids Using the Essential Oil of Cinnamomum Cassia. *Submitt. to Stustainable Food Technol.*
170. Li, Y.; Fabiano-Tixier, A.-S.; Chemat, F. Essential Oils as Green Solvents. In *Essential Oils as Reagents in Green Chemistry*; SpringerBriefs, 2014; pp. 55–61 ISBN 9783319084497.
171. Tanzi, C.D.; Vian, M.A.; Ginies, C.; Elmaataoui, M.; Chemat, F. Terpenes as green solvents for extraction of oil from microalgae. *Molecules* **2012**, *17*, 8196–8205, doi:10.3390/molecules17078196.
172. Rao, P.V.; Gan, S.H. Cinnamon: A multifaceted medicinal plant. *Evidence-based Complement. Altern. Med.* **2014**, *2014*, 642942–642964, doi:10.1155/2014/642942.
173. Chakraborty, A.; Sankaran, V.; Ramar, M.; Chellappan, D.R. Chemical analysis of leaf essential oil of Cinnamomum verum from Palni hills, Tamil Nadu. *J. Chem. Pharm. Sci.* **2015**, *8*, 476–479.
174. Akbar, S. Cinnamomum cassia (L.) J. Presl. In *Handbook of 200 Medicinal Plants: A Comprehensive Review of Their Traditional Medical Uses and Scientific Justifications*; Springer Nature Switzerland AG, 2020; pp. 629–643 ISBN 9783030168070.
175. Akbar, S. Cinnamomum verum J. Presl. In *Handbook of 200 Medicinal Plants: A Comprehensive Review of Their Traditional Medical Uses and Scientific Justifications*; Springer Nature Switzerland AG, 2020; pp. 645–661 ISBN

9783030168070.

176. Lončar, M.; Jakovljević, M.; Šubarić, D.; Pavlić, M.; Služek, V.B.; Cindrić, I.; Molnar, M. *Coumarins in food and methods of their determination*; 2020; Vol. 9; ISBN 3853122434.

177. Kawatra, P.; Rajagopalan, R. Cinnamon: Mystic powers of a minute ingredient. *Pharmacognosy Res.* **2015**, *7*, 1–6, doi:10.4103/0974-8490.157990.

178. Bauer, R.; Blaschek, W.; Buff, W.; Classen, B.; Heise, E.M.; Hensel, A.; Krenn, L.; Lichius, J.J.; Lindequist, U.; Loew, D.; et al. Cinnamomi cortex. In *Wichtl - Teedrogen und Phytopharmaka: Ein Handbuch für die Praxis*; Wichtl, M., Ed.; Wissenschaftliche Verlagsgesellschaft, 2015; Vol. 6, pp. 180–182.

179. Wang, Y.H.; Avula, B.; Nanayakkara, N.P.D.; Zhao, J.; Khan, I.A. Cassia cinnamon as a source of coumarin in cinnamon-flavored food and food supplements in the United States. *J. Agric. Food Chem.* **2013**, *61*, 4470–4476, doi:10.1021/jf4005862.

180. Al-Hilphy, A.R.; Ahmed, A.H.K.; Gavahian, M.; Chen, H.H.; Chemat, F.; Al-Behadli, T.K.M.; Mohd Nor, M.Z.; Ahmad, S. Solar energy-based extraction of essential oils from cloves, cinnamon, orange, lemon, eucalyptus, and cardamom: A clean energy technology for green extraction. *J. Food Process Eng.* **2022**, *45*, n/a, doi:10.1111/jfpe.14038.

181. Bušić, A.; Mardetko, N.; Kundas, S.; Morzak, G.; Belskaya, H.; Šantek, M.I.; Komes, D.; Novak, S.; Šantek, B. Bioethanol production from renewable raw materials and its separation and purification: A review. *Food Technol. Biotechnol.* **2018**, *56*, 289–311, doi:10.17113/ftb.56.03.18.5546.

182. Philipps, A.P.; Murphy, J.G. The correlation of structure and reactivity of aromatic aldehydes. III. The condensation of aromatic Aldehydes with Hydantoin. *J. Org. Chem.* **1951**, *16*, 954–962, doi:https://doi.org/10.1021/jo01146a020.

183. Ingold, C.K. Principles of an Electronic Theory of Organic Reactions. *Chem. Rev.* **1934**, *15*, 225–274.

184. Shimizu, H.; Katayama, M.; Fujiwara, S. Chemical Shifts of Proton Resonance and Mesomeric Effects in Substituted Benzene. *Bull. Chem. Soc. Jpn.* **1959**, *32*, 419–420.

185. Heghes, S.C.; Vostinaru, O.; Mogosan, C.; Miere, D.; Iuga, C.A.; Filip, L. Safety Profile of Nutraceuticals Rich in Coumarins: An Update. *Front.*

Pharmacol. **2022**, *13*, 803338–803347, doi:10.3389/fphar.2022.803338.

186. Degot, P.; Huber, V.; El Maangar, A.; Gramüller, J.; Rohr, L.; Touraud, D.; Zemb, T.; Gschwind, R.M.; Kunz, W. Triple role of sodium salicylate in solubilization, extraction, and stabilization of curcumin from Curcuma Longa. *Mol. Liq.* **2021**, 115538–115549, doi:https://doi.org/10.1016/j.molliq.2021.115538.

CHAPTER 9

APPENDIX

9 Appendix

9.1 Important Chemicals and their Structures

Table 9-1: Chemicals of Section 3 with their corresponding abbreviations and structures.

Name	Abbreviation	Structure
cis-γ-Irone	-	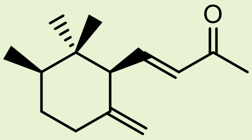
α-Ionone	-	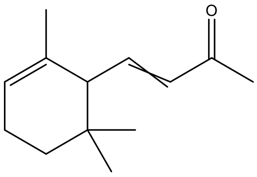
cis- & trans-α-Irone	-	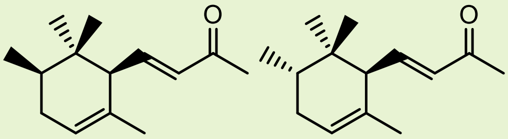
Myristic Acid	HMyr	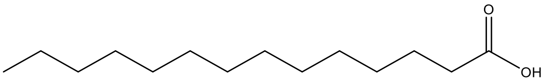

Table 9-2: Chemicals of Sections 4 and 5 with their corresponding abbreviations and structures.

Name	Abbreviation	Structure
Curcumin	Cur	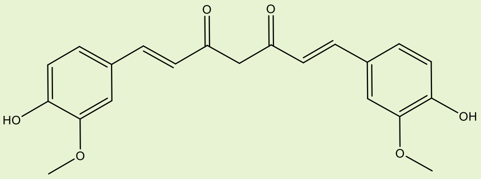 The curcuminoids can be distinguished from one another by the number of methoxy groups
Demethoxy-curcumin	DC	
Bisdemetoxy-curcumin	BDC	
Triacetin	TriA	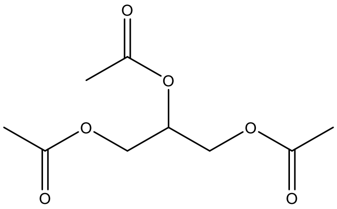
Acetylcholine	AcCh	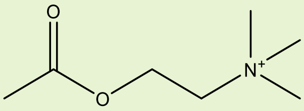

Choline Chloride	ChCl	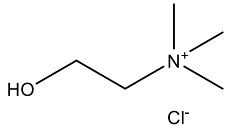
Proline	Pro	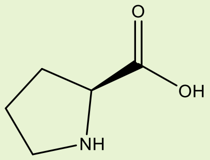
Citric Acid	Cit	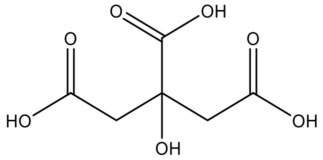
Lactic Acid	Lac	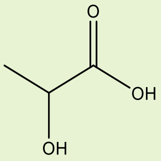
Levulinic Acid	Lev	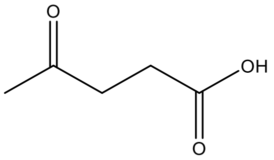
Malic Acid	Mal	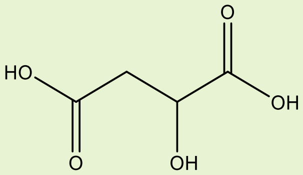
Betaine	Bet	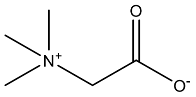
Carnitine	Car	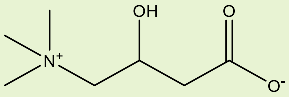
Pyruvic Acid	Pyr	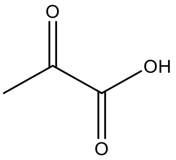
Mandelic Acid	Man	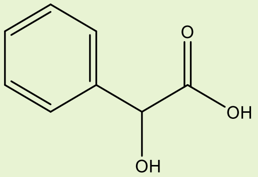
2-Oxobutanoic Acid	Obu	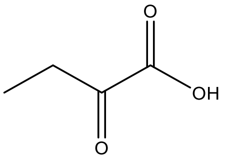

2-Oxovaleric Acid	Ova	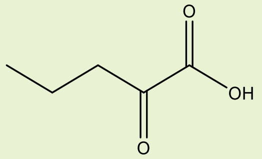
Acetylbutyric Acid	Aba	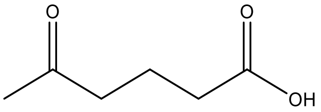
Diacetyl	-	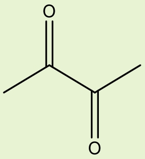

Table 9-3: Chemicals of Section 6 with their corresponding abbreviations and structures.

Name	Abbreviation	Structure
3-Phenylpropyl Acetate	-	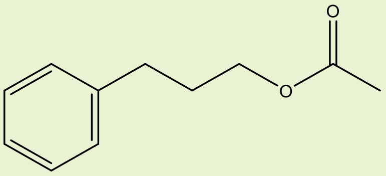
3-Phenylpropoinal Hydro-cinnamaldehyde	HCi	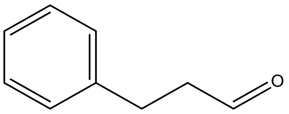
Anethole	-	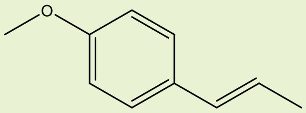
Benzaldehyde	Bza	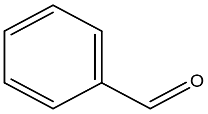
Benzyl Benzoate	-	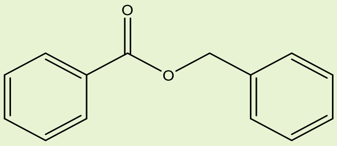
Cinnamaldehyde	Cin	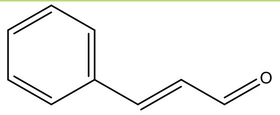
Cinnamic Acid	-	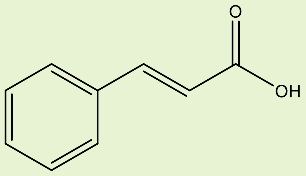

Cinnamyl Acetate	-	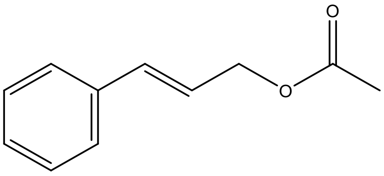
Citral	-	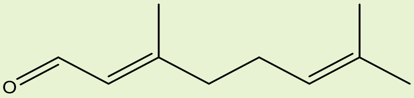
Limonene	-	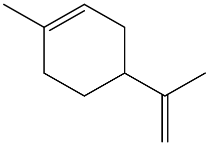
α-Hexyl cinnamaldehyde	-	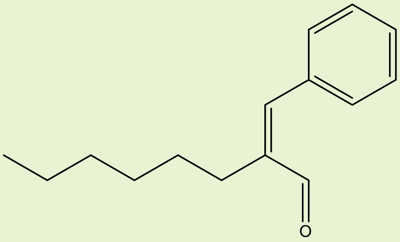

9.2 Supplementary Information of Chapter 2

9.2.1 The 12 Principles of Green Chemistry [6]

- **Waste Prevention:** The prevention of generating waste is preferred over cleaning it up afterward.
- **Atom Economy:** Reactions should be improved by reducing waste at a molecular level. The number of atoms from all reagents should be found in the final product
- **Less Hazardous Chemical Synthesis:** The hazard level in terms of toxicity towards the environment or human health of synthetic pathways, solvents, and products should be reduced.
- **Designing Safer Chemicals:** While keeping the efficacy, safer and healthier alternatives to the commonly used chemicals should be found.
- **Safer Solvents and Auxiliaries:** The number of solvents and auxiliaries should be minimized. If any are necessary, the least hazardous alternative should be chosen.
- **Design for Energy Efficiency:** Processes should be reevaluated concerning their consumption of energy. In the optimum case, heating, cooling, and pressurizing should be avoided.
- **Use of Renewable Feedstocks:** Chemicals with natural and renewable origins are preferred over petrochemical resources.
- **Reduce Derivatives:** Derivatization in terms of temporal protection groups should be avoided as those additional reaction steps consume energy.
- **Catalysis:** Selectivity and turnover rate of reactions should be enhanced using the right catalysts.
- **Design for Degradation:** Chemicals and their reaction products should be designed in a way that they are easily biodegradable. Neither them nor their degradation products should be harmful to the environment, toxic or accumulative, and persistent in any way.
- **Real-Time Pollution Prevention:** Reactions should be monitored constantly to prevent the release or formation of any harmful products.
- **Safer Chemistry for Accident Prevention:** Procedures and reactions should be chosen thoughtfully regarding their safety and low risk of accidents.

9.2.2 Comparison of Ionic Liquids and Deep Eutectic Solvents

Table 9-4: Characterizing differences and similarities of ionic liquids and deep eutectic solvents. Inspired by Y. Liu et al. [72,73].

	Ionic Liquids	**Deep Eutectic Solvents**
Differences		
Constituents	Salts	Salts, sugars, organic acids, amino acids, quaternary ammonium compounds
Composition	Single salt	Mixture
Intermolecular Force	Ionic bonding	Hydrogen bonding
Molecular Force	Strong	Weak
Intermolecular Distance	< 1.2 Å	2-5 Å
Cytotoxicity	Often	Hard to detect
Similarities		
Vapor Pressure	Negligible	
Thermal Stability	High	
Conductivity	Moderate to poor, depending on the constituents	

9.3 Supplementary Information of Chapter 3

9.3.1 GC Chromatogram of the Technical Mixture of Irone Isomers

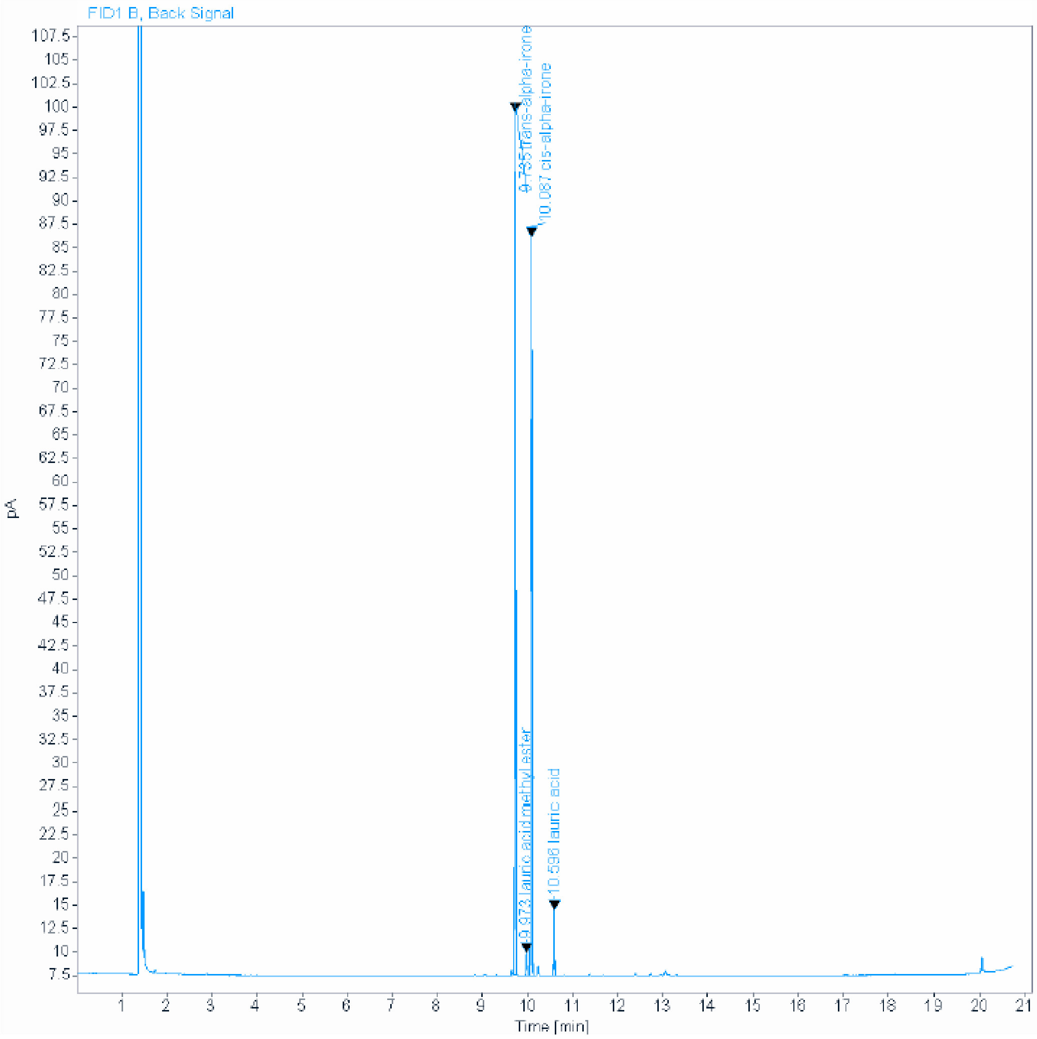

Figure 9-1: GC-FID chromatogram of the technical irone mixture by Sigma Aldrich (Darmstadt, Germany).

Table 9-5: Assignment of the peaks, found in the chromatogram depicted in Figure 9-1.

Retention time (min)	**Area**	**Area%**	**Name**
9.735	149.3785	50.4147	**trans-alpha-irone**
9.973	4.0133	1.3545	lauric acid methyl ester
10.087	131.6931	44.4460	**cis-alpha-irone**
10.596	11.2144	3.7848	lauric acid

9.3.2 Clausius-Clapeyron Calculations

The values presented in Table 9-6 were calculated according to the Clausius-Clapeyron equation (3-6) presented in Section 3.3.2.

Table 9-6: Clausius-Clapeyron Calculations of α-ionone, α-irone, and γ-irone at 120 °C, 123 °C, and 126 °C. The bold values corresponding to α-ionone were used as the starting point of the screening and the ones corresponding to γ-irone were used to distillate the real sample in Section 3.3.2.

Compound	$\Delta_{vap}H^f$ (kJ/mol)	Temperature (°C)	Pressure (mbar)
α-Ionone	51.16	**120**	**0.97**
		123	1.09
		126	1.23
α-Irone	53.05	120	1.25
		123	1.41
		126	1.59
γ-Irone	52.28	120	1.13
		123	**1.27**
		126	1.43

[f] *$\Delta_{vap}H$ values were taken from* Cheméo [124].

9.3.3 Distillation Results

Table 9-7: Relative distilled amount of γ-irone after different distillation steps compared to the respective extraction yield.

	Extraction	**Distillation 1**	**Distillation 2**
γ-Irone content	0.018 ± 0.003%	0.054 ± 0.002%	0.32 ± 0.02%
Distilled amount	-	51 ± 7%	78 ± 12%
Yield regarding the total γ-irone content of 1 mg/g in the rhizomes	88 ± 16%	44 ± 3%	34 ± 4%

9.4 Supplementary Information of Chapter 4

All figures and tables presented in this chapter were reprinted from the supplementary material of the studies by P. Degot and V. Huber *et al.* [126,186]. For convenience reasons, the reference is stated in this paragraph as a disclaimer.

9.4.1 Curcumin Solubility in Binary Mixtures of Water with ChCl and NADES

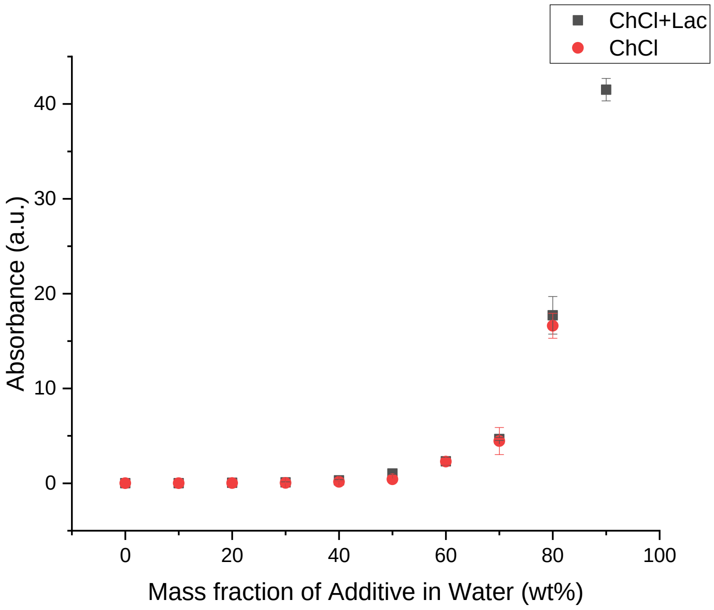

Figure 9-2: Curcumin solubility in a binary mixture of ChCl and ChCl+Lac with water. The scaling on the y-axis does not correspond to the scaling in the main text. The values were calculated as if the samples had not been diluted instead of applying the 1:5000 dilution factor which would make the results unreadable [70].

9.4.2 Dynamic Light Scattering Examination

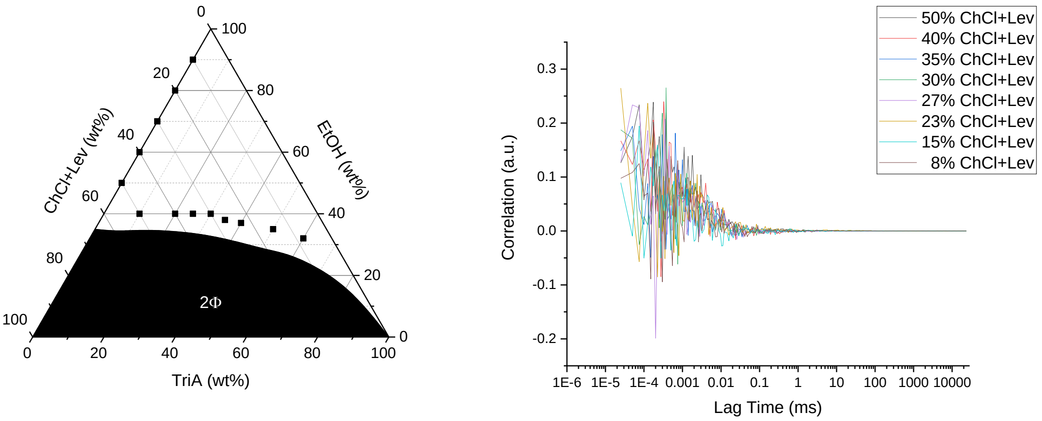
a) b)

Figure 9-3: a) Ternary phase diagram of ChCl+Lev/EtOH/TriA with the ternary and binary points examined via DLS and b) correlation curves in the ternary system ChCl+Lev/EtOH/TriA close above the two-phasic region [126].

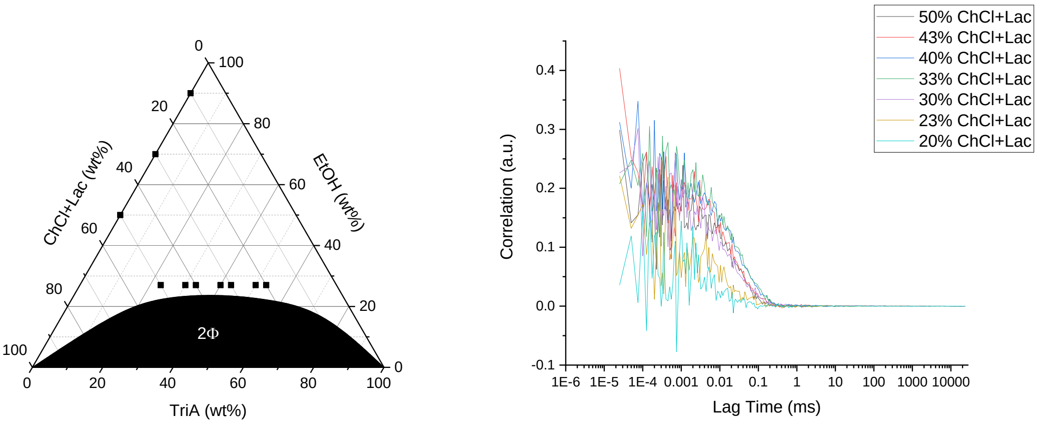
a) b)

Figure 9-4: a) Ternary phase diagram of ChCl+Lac/EtOH/TriA with the ternary and binary points examined via DLS and b) correlation curves in the ternary system ChCl+Lac/EtOH/TriA close above the two-phasic region [126].

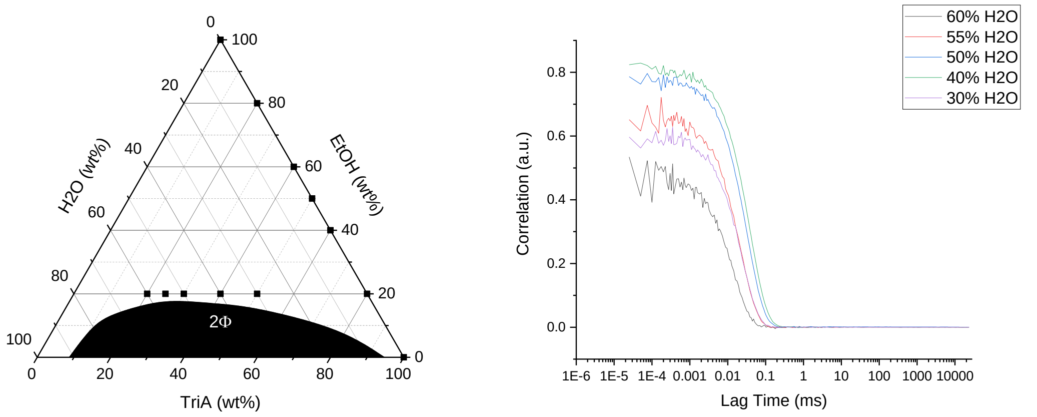
a) b)

Figure 9-5: a) Ternary phase diagram of H_2O/EtOH/TriA with the ternary and binary points examined via DLS and b) correlation curves in the ternary system H_2O/EtOH/TriA close above the two-phasic region [126].

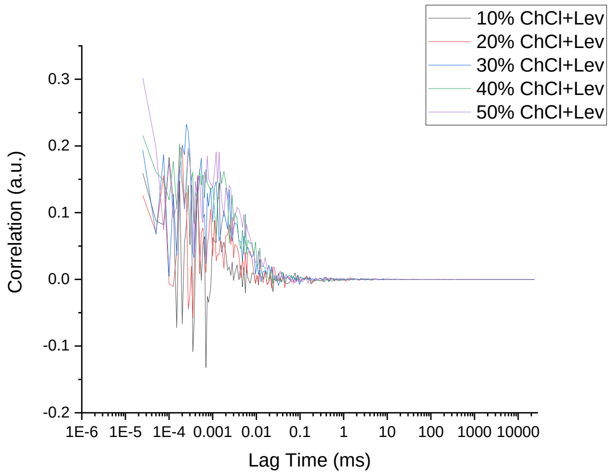

Figure 9-6: Correlation curves in the binary system ChCl+Lev/EtOH. The respective points can be viewed in Figure 9-3 [126].

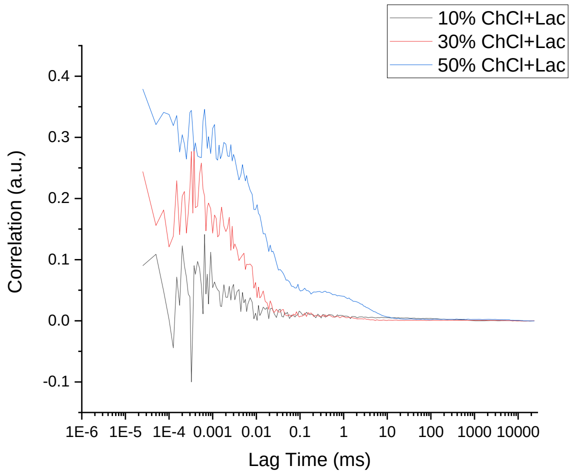

Figure 9-7: Correlation curves in the binary system ChCl+Lac/EtOH. The respective points can be viewed in Figure 9-4 [126].

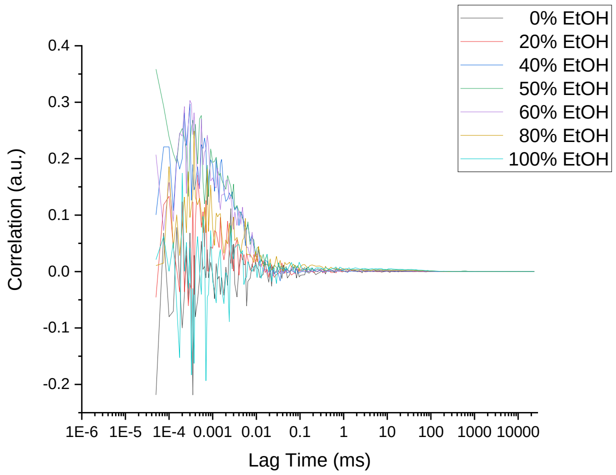

Figure 9-8: Correlation curves in the binary system EtOH/TriA. The respective points can be viewed in Figure 9-5. The data were provided by P. Degot et al.[47].

9.4.3 Prediction of the Ethanol/Triacetin Phase Diagram

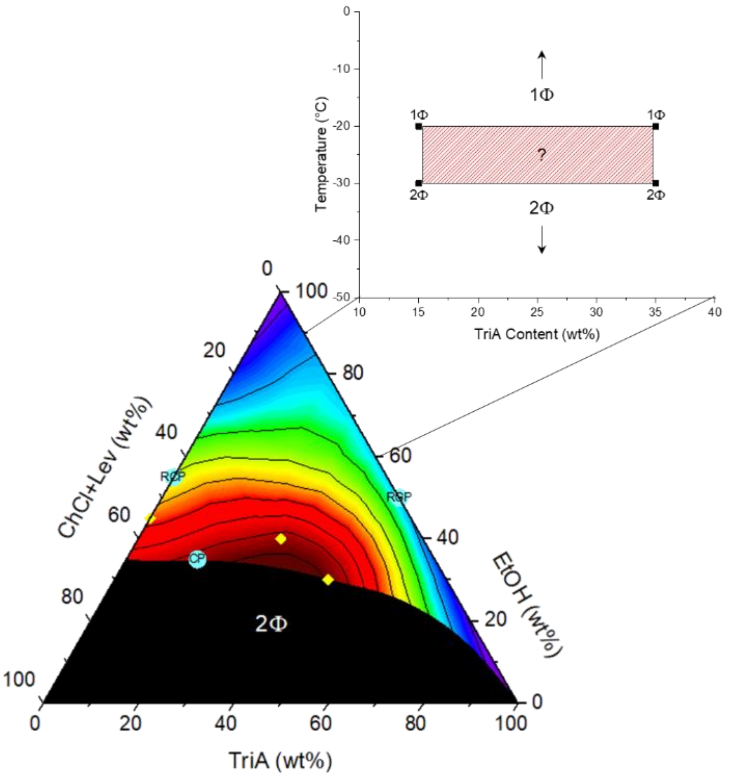

Figure 9-9: Temperature-dependent phase diagram of the binary mixture of EtOH/TriA with LLE points at -20 °C and -30 °C, contextualized within the ternary phase diagram at 25 °C. No LLE points were found at -20 °C but at -30 °C there were. The hatched area in the binary phase diagram is a representation of the uncertain area in which the phase transition should occur [126].

9.4.4 HPLC Calibration Curves

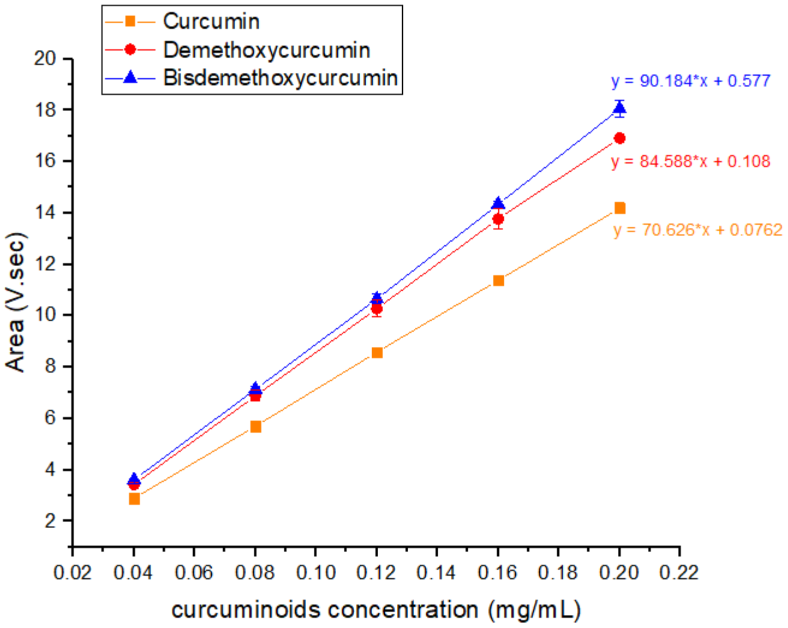

Figure 9-10: Calibration curve in acetonitrile of curcumin (orange square), demethoxycurcumin (red dot), and bisdemethoxycurcumin (blue triangle) obtained by HPLC using an ACE Equivalent 3 C18-Column (300 Å, 150 × 2.1 mm), plotting the concentration in mg per mL against the peak area [186].

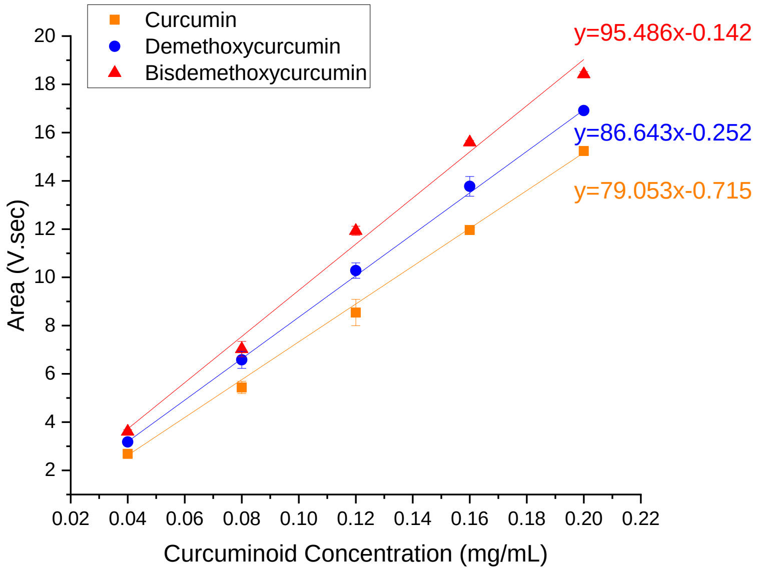

Figure 9-11: Calibration curves of curcumin (orange square), demethoxycurcumin (blue circle), and bisdemethoxycurcumin (red triangle) obtained by elution via HPLC using a Knauer Eurospher 5 C18-Column (100 Å, 250 × 4.6 mm) [126]. *The concentration in mg per mL is plotted against the peak area.*

9.4.5 Extraction Yields in Numbers

Table 9-8: Extraction yields of the curcuminoids in mg/g.

Extraction System		**Curcumin (mg/g)**	**Demethoxy-curcumin (mg/g)**	**Bisdemethoxy-curcumin (mg/g)**
Soxhlet[b]		11.64 ± 0.70	3.82 ± 0.21	1.67 ± 0.26
EtOH[b]		4.34 ± 0.08	1.34 ± 0.05	0.92 ± 0.04
TriA[b]		3.13 ± 0.21	0.94 ± 0.06	0.51 ± 0.06
H_2O/EtOH/TriA 40:24:36[b]		9.21 ± 0.32	3.18 ± 0.23	2.89 ± 0.38
Pressure-controlled Soxhlet [d]		14.53 ± 0.62	4.25 ± 0.14	3.82 ±0.41
ChCl+Lac/EtOH/TriA 35:27.5:37.5 Optimum Composition[c]		11.80 ± 0.29	2.73 ± 0.13	3.26 ± 0.14
	+ 5% H_2O[c]	11.28 ± 0.08	2.73 ± 0.13	3.12 ± 0.04
	+ 10% H_2O[c]	10.90 ± 0.26	3.01 ± 0.06	3.15 ± 0.07
	+ 15% H_2O[c]	9.87 ± 0.67	3.02 ± 0.20	3.96 ± 0.19
ChCl+Lac/EtOH/TriA 20:32.5:47.5[c]		11.21 ± 0.05	2.63 ± 0.05	3.09 ± 0.03
ChCl+Lac/EtOH/TriA 30:28:42[c]		11.72 ± 0.37	2.74 ± 0.15	3.31 ± 0.15
ChCl+Lac/EtOH/TriA 50 :35 :15[c]		11.69 ± 0.04	2.081 ± 0.004	3.23 ± 0.02
ChCl+Lev/EtOH/TriA 30:40:30		12.04 ± 0.36	4.09 ± 0.13	2.83 ± 0.07

Optimum Composition[d]			
ChCl+Lev/EtOH/TriA 25:30:45[d]	11.78 ± 0.15	3.94 ± 0.04	2.78 ± 0.05
ChCl+Lev/EtOH 55:45[d]	12.13 ± 0.29	4.10 ± 0.11	2.86 ± 0.09
ChCl+Lac/EtOH/TriA 35:27.5:37.5 Cycle 7[c]	119.0 ± 2.0	31.4 ± 0.7	35.0 ± 0.8
ChCl+Lev/EtOH/TriA 30:40:30 Cycle 7[d]	116.8 ± 1.9	39.1 ± 2.4	29.7 ± 2.8
ChCl+Lev/EtOH/TriA 30:40:30 Cycle 12[d]	103.9 ± 2.6	36.3 ± 1.1	29.0 ± 1.3

[b] Data taken from P. Degot *et al.* [47].

[c] Published in V. Huber *et al.* [70].

[d] Published in V. Huber *et al.* [126].

9.4.6 Curcuminoid Content after Every Cycle of Extraction

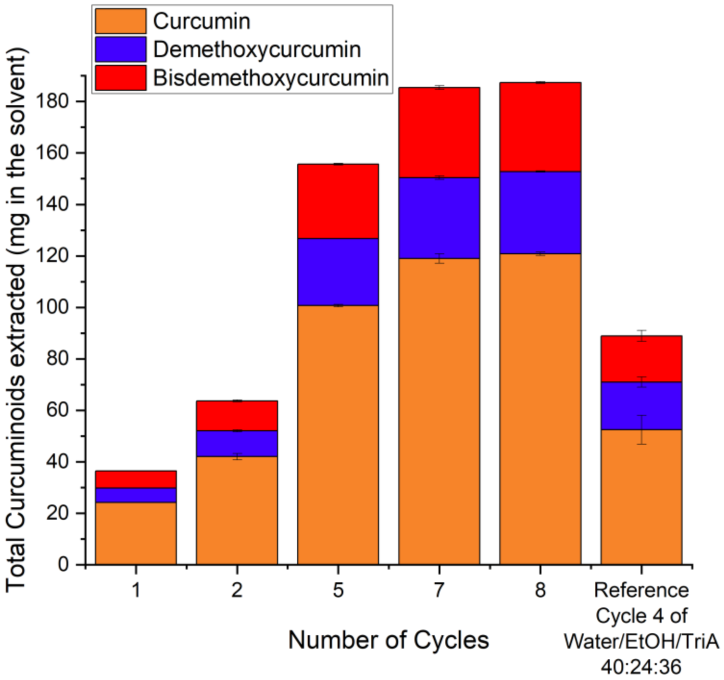

Figure 9-12: Curcuminoid cycle extraction in the system ChCl+Lac/EtOH/TriA 35:27.5:37.5 with the reference being cycle 4 of the water/EtOH/TriA 40:24:26 system as provided by P. Degot et al. [48,70].

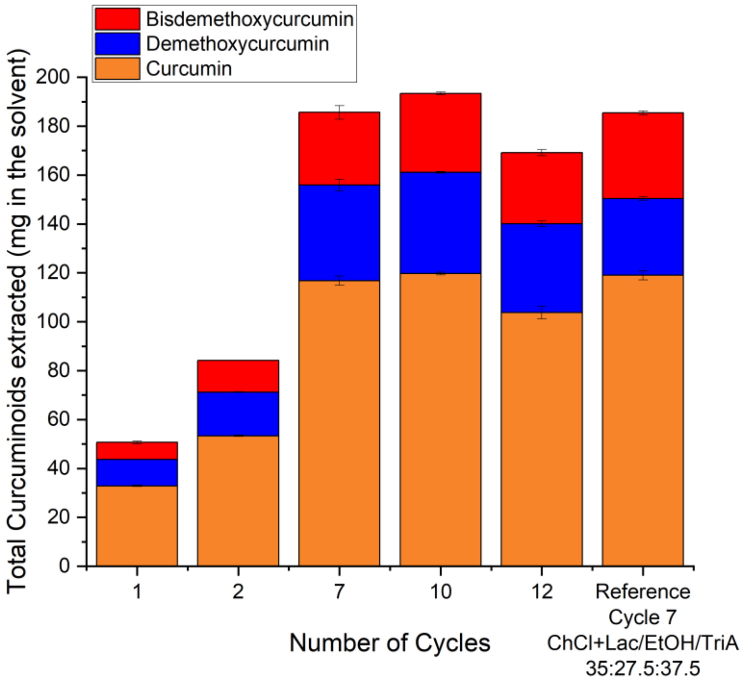

Figure 9-13: Curcuminoid cycle extraction of the ChCl+Lev/EtOH/TriA 30:40:30 system with the reference being cycle 7 of the system ChCl+Lac/EtOH/TriA 35:27.5:37.5 as provided by V. Huber et al. [70,126].

9.4.7 Curcuminoid Concentration after Different Extraction Cycles

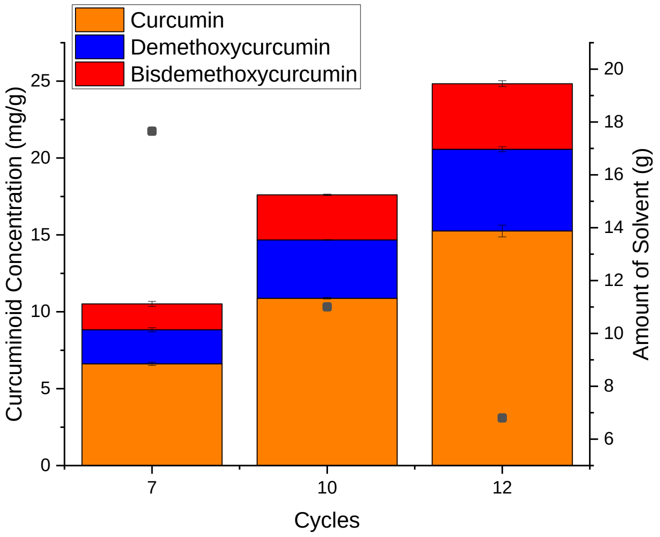

Figure 9-14: Curcuminoid concentration in mg/g solvent after 7, 10, and 12 extraction cycles. The grey squares represent the amount of solvent remaining after every cycle [126].

9.4.8 NMR Spectra of the Extraction Solvent over Time

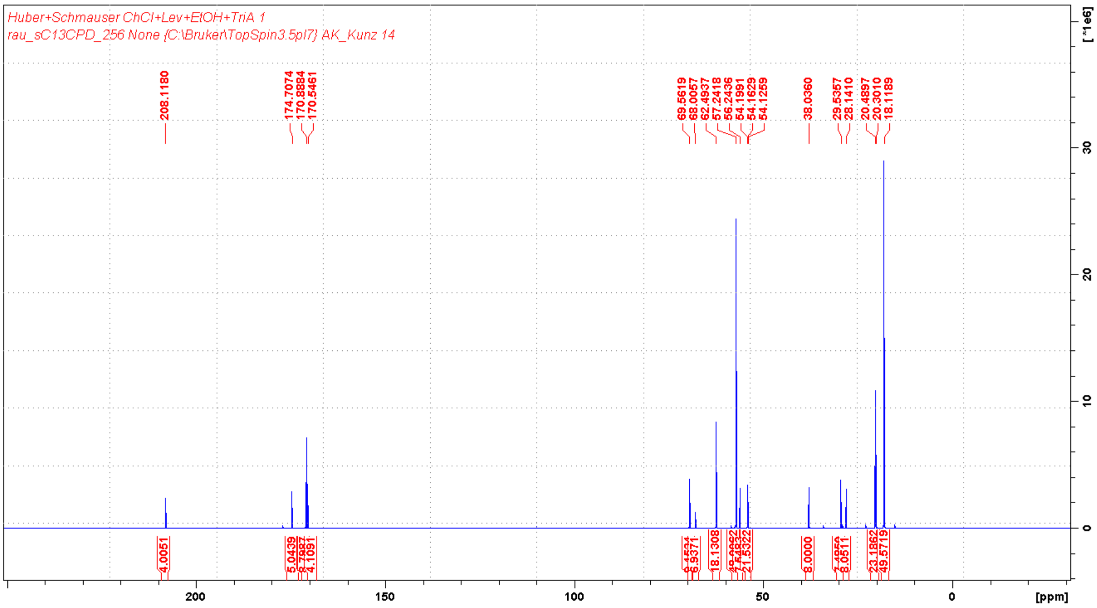

Figure 9-15: ^{13}C-NMR spectrum of the ternary extraction solvent of ChCl+Lev/EtOH/TriA (30:40:30) in weight fresh after preparation [126].

ChCl+Lev/EtOH/TriA (30:40:30): ^{13}C-NMR (400 MHz): δ_{ppm} 18.12, 20.30, 20.49, 28.14, 29.54, 38.04, 54.13, 54.16, 54.20, 56.24, 57.24, 62.49, 68.01, 69.56, 170.55, 170.89, 174.71, 208.12.

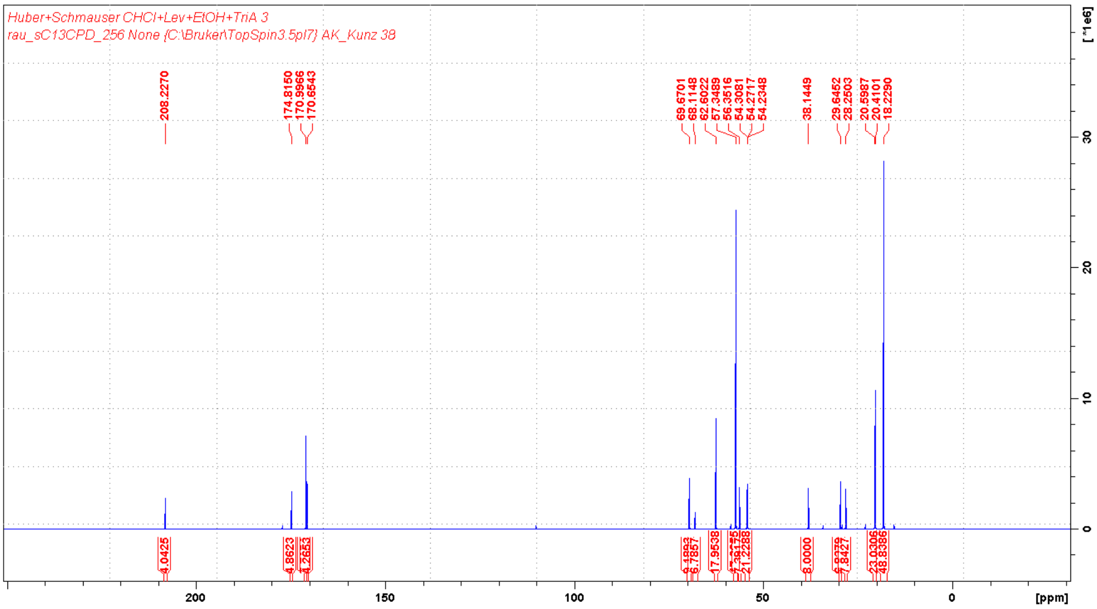

Figure 9-16: ^{13}C-NMR spectrum of the ternary extraction solvent of ChCl+Lev/EtOH/TriA (30:40:30) in weight one day after preparation [126].

ChCl+Lev/EtOH/TriA (30:40:30): ^{13}C-NMR (400 MHz): δ_{ppm} 18.23, 20.41, 20.60, 28.25, 29.65, 38.15, 54.24, 54.27, 54.31, 56.35, 57.35, 62.60, 68.12, 69.67, 170.65, 171.00, 174.82, 208.23.

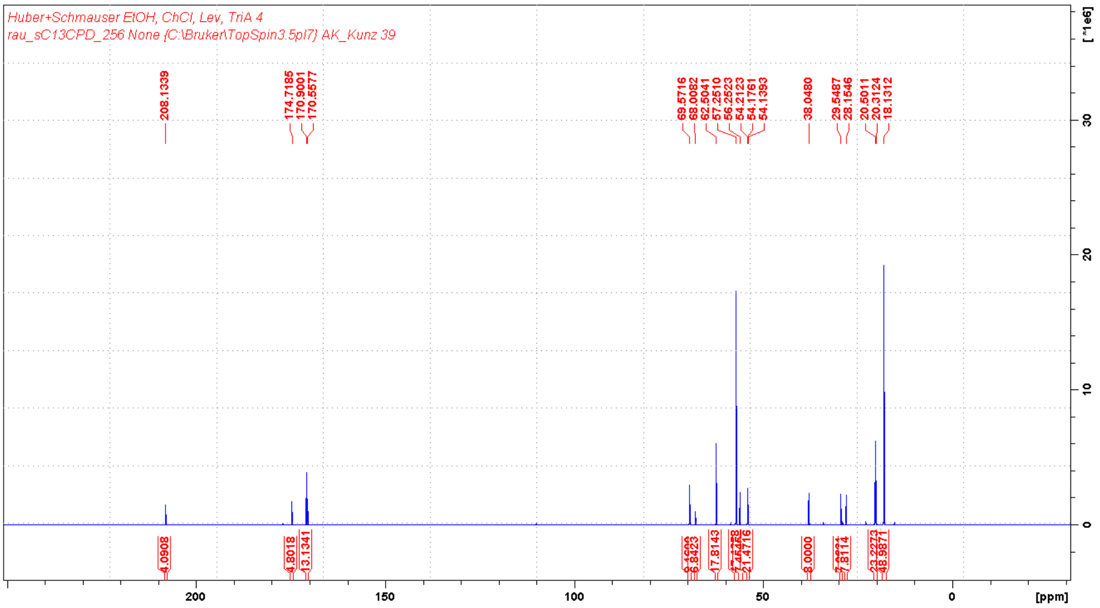

Figure 9-17: ^{13}C-NMR spectrum of the ternary extraction solvent of ChCl+Lev/EtOH/TriA (30:40:30) in weight three days after preparation [126].

ChCl+Lev/EtOH/TriA (30:40:30): ^{13}C-NMR (400 MHz): δ_{ppm} 18.13, 20.31, 20.50, 28.16, 29.56, 38.05, 54.14, 54.18, 54.21, 56.25, 57.25, 62.50, 68.01, 69.57, 170.56, 170.90, 174.72, 208.13.

9.5 Supplementary Information of Chapter 5

All figures and tables were reprinted from the supplementary material belonging to the study by V. Huber *et al.* [158]. For the sake of convenience, the reference is stated in this paragraph as a disclaimer.

9.5.1 Curcumin Solubility in EtOH Depending on Additive Content in mol%

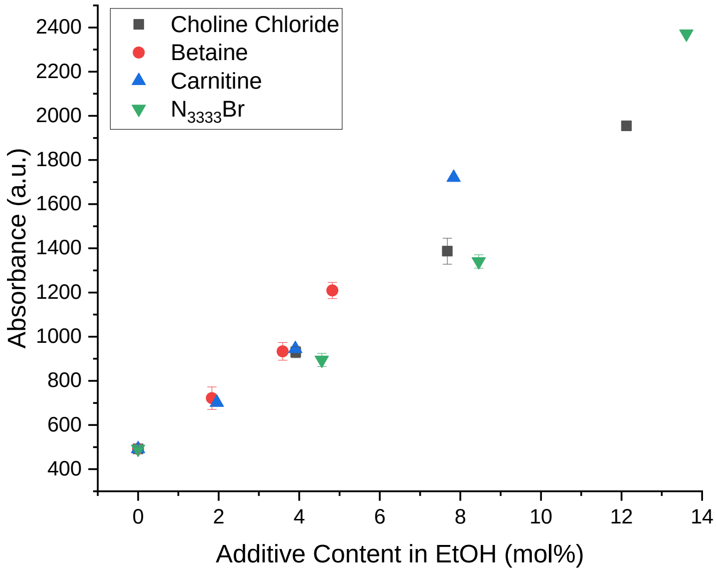

Figure 9-18: Solubility of curcumin in ethanolic solutions in mol% of choline chloride (grey), betaine (red), carnitine (blue), and tetrapropylammonium bromide (green) [158].

9.5.2 ^{1}H-NMR spectra of Curcumin and the QAs

The peaks were characterized as singlet (s), doublet (d), doublet of doublets (dd), triplet (t), quartet (q), quintet (quint), and multiplet (m).

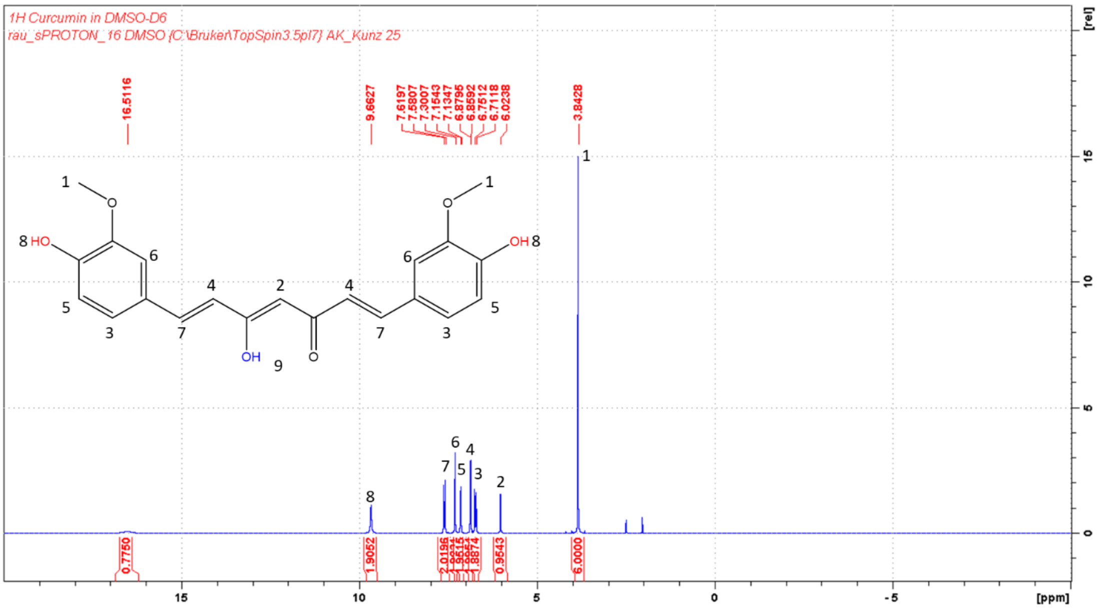

Figure 9-19: ^{1}H-NMR of curcumin in DMSO-d_6 [158].

Curcumin: ^{1}H-NMR (DMSO-d_6, 400 MHz): δ_{ppm} 3.84 (s, 3H), 6.02 (s, 1H), 6.71 (dd, 1H), 6.86 (dd, 1H), 7.14 (d, 1H), 7.30 (d, 1H), 7.58 (dd, 1H), 9.66 (s, 1H), 16.51 (s, 1H).

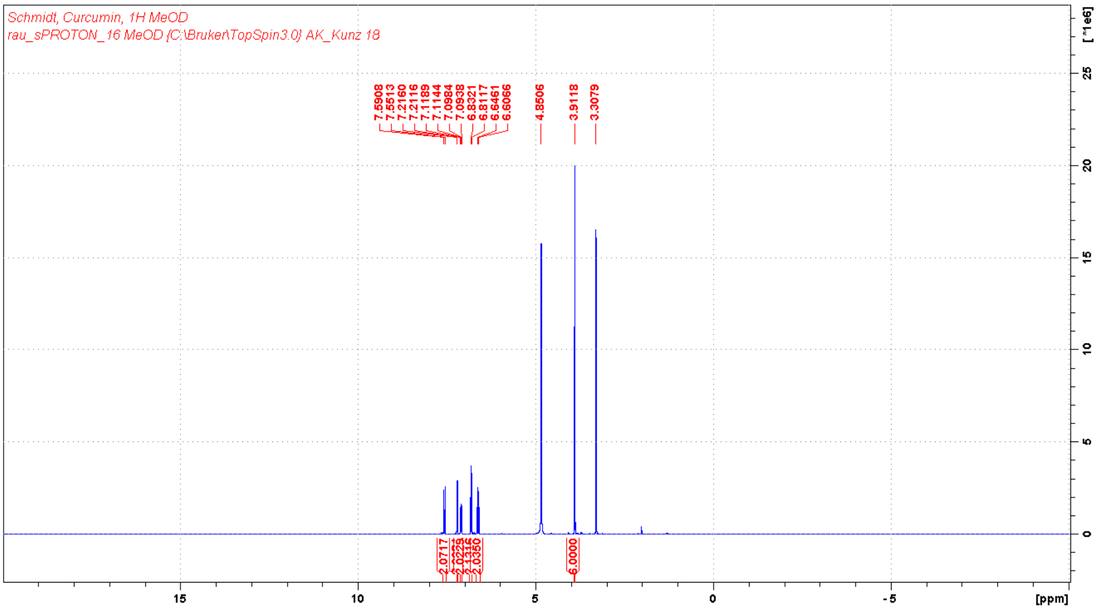

Figure 9-20: ^{1}H-NMR of curcumin in methanol-d_4 [158].

Curcumin: ^{1}H-NMR (Methanol-d_4, 400 MHz): δ_{ppm} 3.91 (s, 3H), 6.61 (d, 1H), 6.81 (d, 1H), 7.09 (dd, 1H), 7.21 (d, 1H), 7.55 (d, 1H).

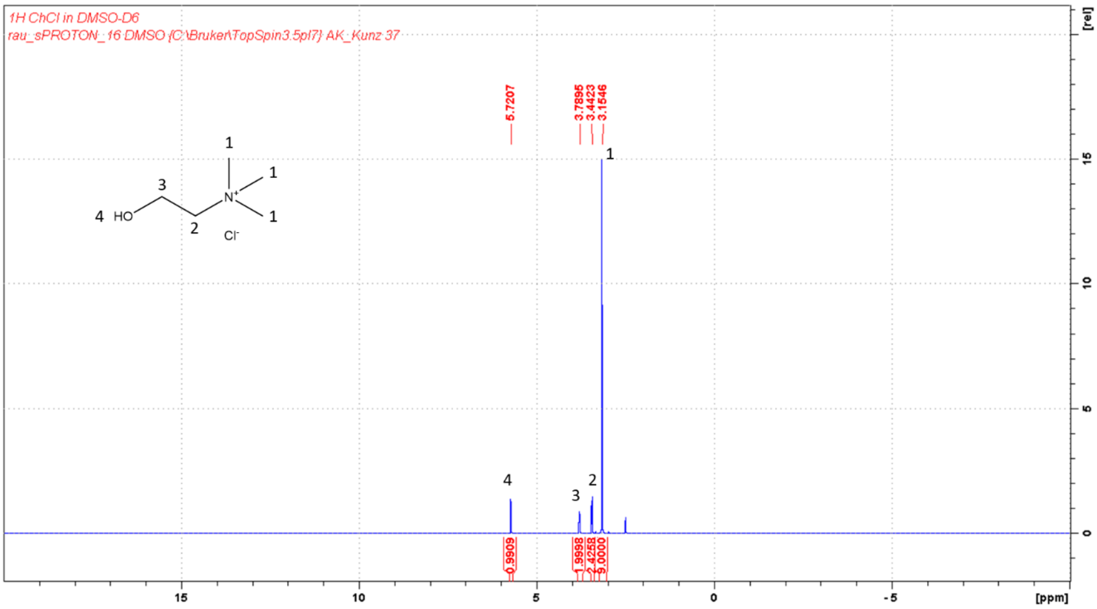

Figure S 1: ^{1}H-NMR of choline chloride in DMSO-d$_6$ [158].

Choline chloride: ^{1}H-NMR (DMSO-d_6, 400 MHz): δ_{ppm} 3.16 (s, 3H), 3.44 (d, 2H), 3.9 (s, 2H), 5.72 (s, 1H).

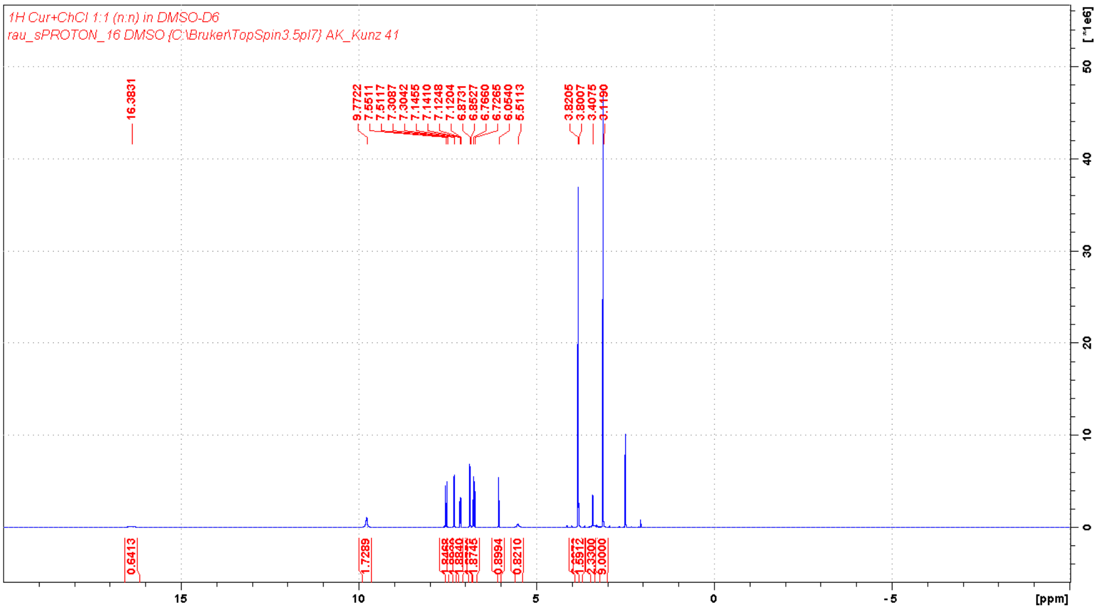

Figure 9-21: ^{1}H-NMR of curcumin and choline chloride (1:1 n/n) in DMSO-d$_6$ [158].

Curcumin + choline chloride: ^{1}H-NMR (DMSO-d_6, 400 MHz): δ_{ppm} 3.12 (s, 3H), 3.41 (quint, 2H), 3.80 (s, 2H), 3.82 (s, 3H) 5.51 (s, 1H), 6.05 (s, 1H), 6.73 (d, 1H), 6.85 (d, 1H), 7.12 (dd, 1H), 7.30 (d, 1H), 7.51 (d, 1H), 9.77 (s, 1H), 16.38 (s, 1H).

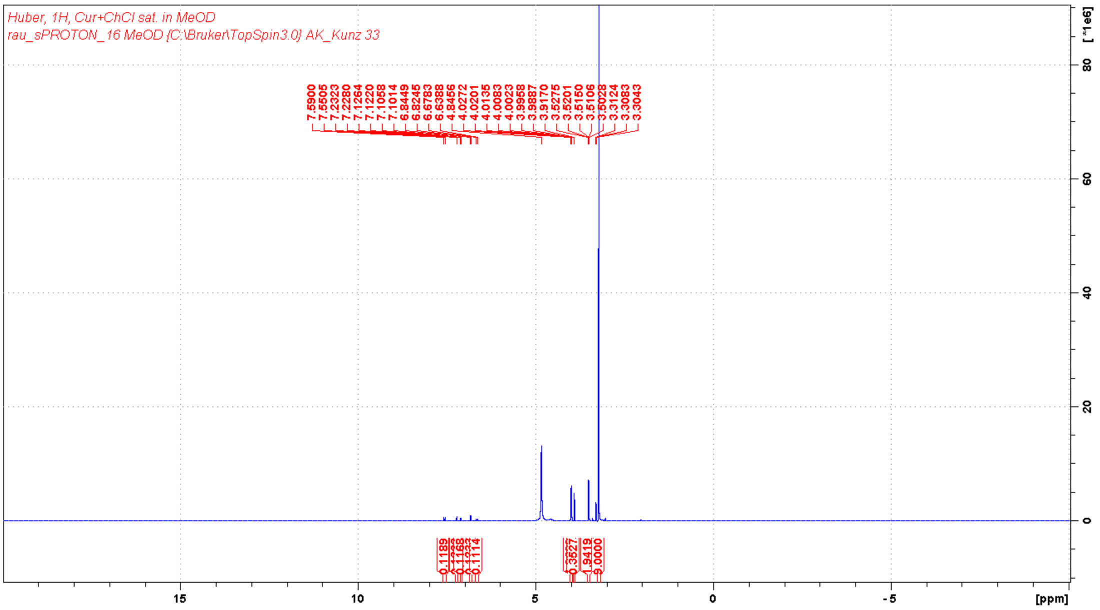

Figure 9-22: ^{1}H-NMR of curcumin and choline chloride saturated in methanol-d$_4$ [158].

Curcumin + choline chloride: ^{1}H-NMR (methanol-*d$_6$*, 400 MHz): δ_{ppm} 3.23 (s, 3H), 3.50 (quint, 2H), 3.91 (s, 3H), 3.99 (m, 2H) 5.51 (s, 1H), 6.64 (d, 1H), 6.83 (d, 1H), 7.10 (dd, 1H), 7.23 (d, 1H), 7.55 (d, 1H).

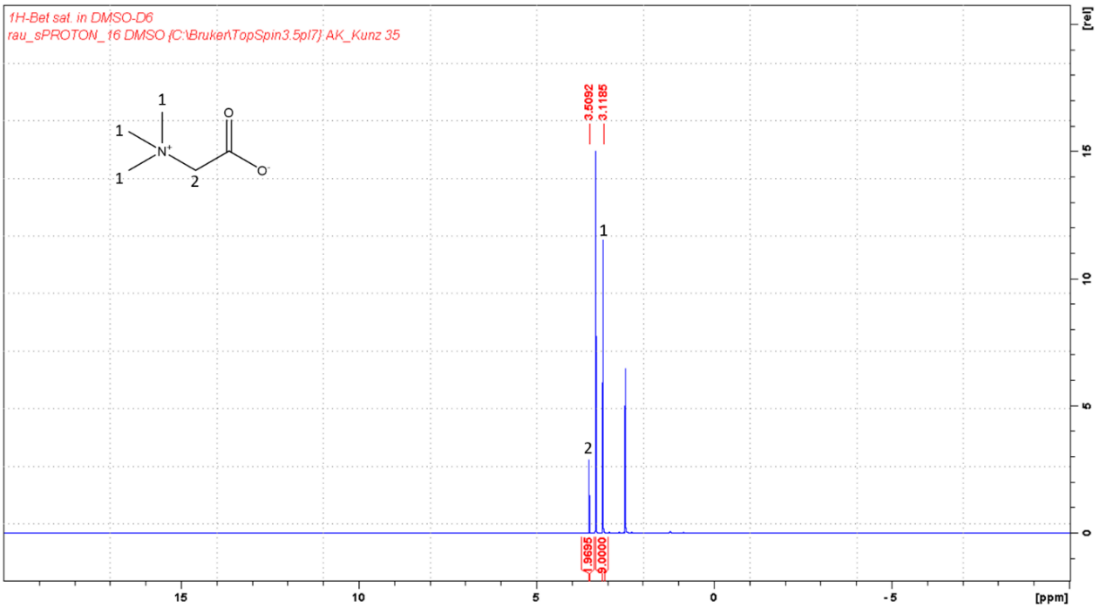

Figure 9-23: ^{1}H-NMR of betaine in DMSO-d_6 [158].

Betaine: ^{1}H-NMR (DMSO-d_6, 400 MHz): δ_{ppm} 3.12 (s, 3H), 3.51 (s, 1H).

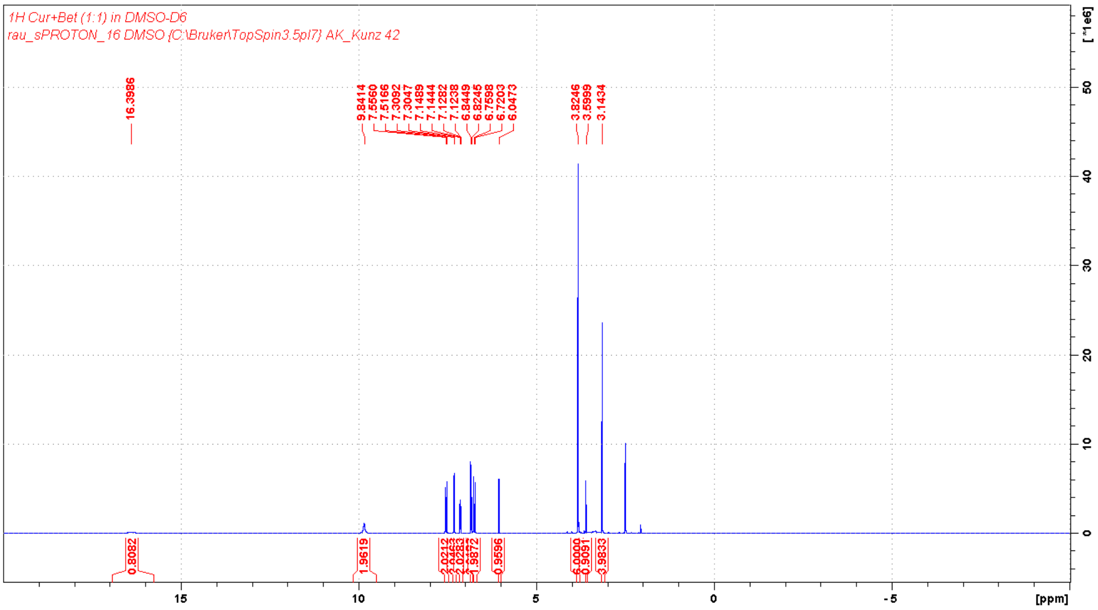

Figure 9-24: ^{1}H-NMR of curcumin and betaine (1:1 n/n) in DMSO-d_6 [158].

Curcumin + betaine: ^{1}H-NMR (DMSO-d_6, 400 MHz): δ_{ppm} 3.14 (s, 3H), 3.59 (s, 1H), 3.82 (s, 3H), 6.05 (s, 1H), 6.72 (d, 1H), 6.83 (d, 1H), 7.12 (dd, 1H), 7.31 (d, 1H), 7.52 (d, 1H), 9.84 (s, 1H), 16.40 (s 1H).

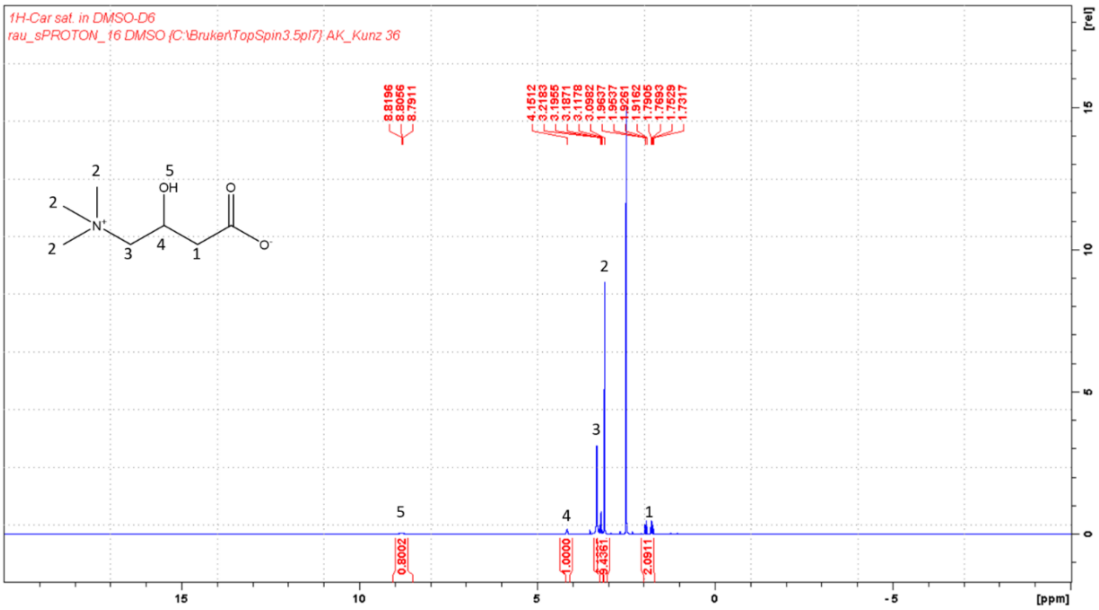

Figure 9-25: ^{1}H-NMR of carnitine in DMSO-d_6 [158].

Carnitine: ^{1}H-NMR (DMSO-d_6, 400 MHz): δ_{ppm} 1.73 (m, 2H), 3.10 (s, 3H), 3.20 (m, 2H), 4.15 (quint, 1H), 8.81 (s, 1H).

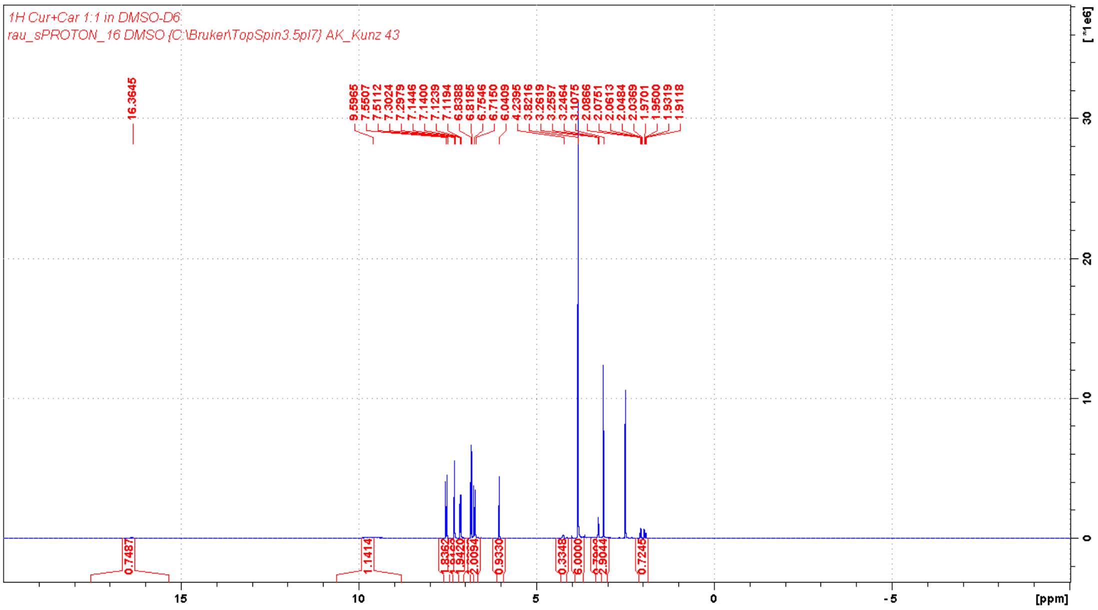

Figure 9-26: ^{1}H-NMR of curcumin and carnitine (1:1 n/n) in DMSO-d_6 [158].

Curcumin + carnitine: ^{1}H-NMR (DMSO-d_6, 400 MHz): δ_{ppm} 1.91 (m, 2H), 3.11 (s, 3H), 3.25 (m, 2H), 3.82 (s, 3H), 4.24 (quint, 1H), 6.04 (s, 1H), 6.72 (d, 1H), 6.82 (d, 1H), 7.12 (dd, 1H), 7.30 (d, 1H), 7.51 (d, 1H), 9.60 (s, 1H), 16,37 (s, 1H).

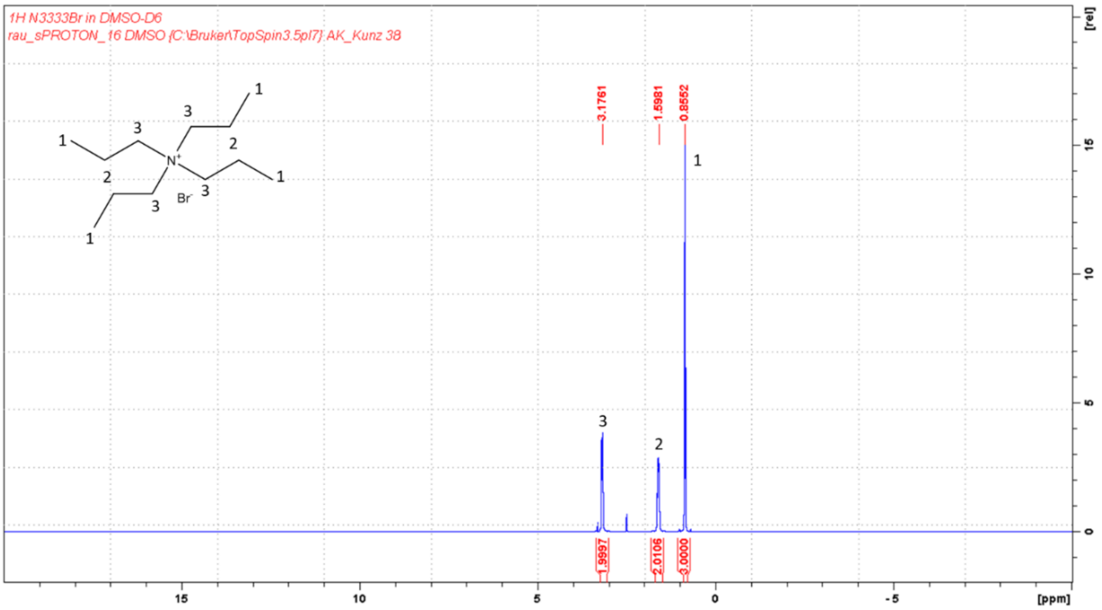

Figure 9-27: ^{1}H-NMR of N$_{3333}$Br in DMSO-d$_6$ [158].

Tetrapropylammonium bromide: ^{1}H-NMR (DMSO-d_6, 400 MHz): δ_{ppm} 0.86 (t, 3H), 1.60 (m, 2H), 3.18 (quint, 2H).

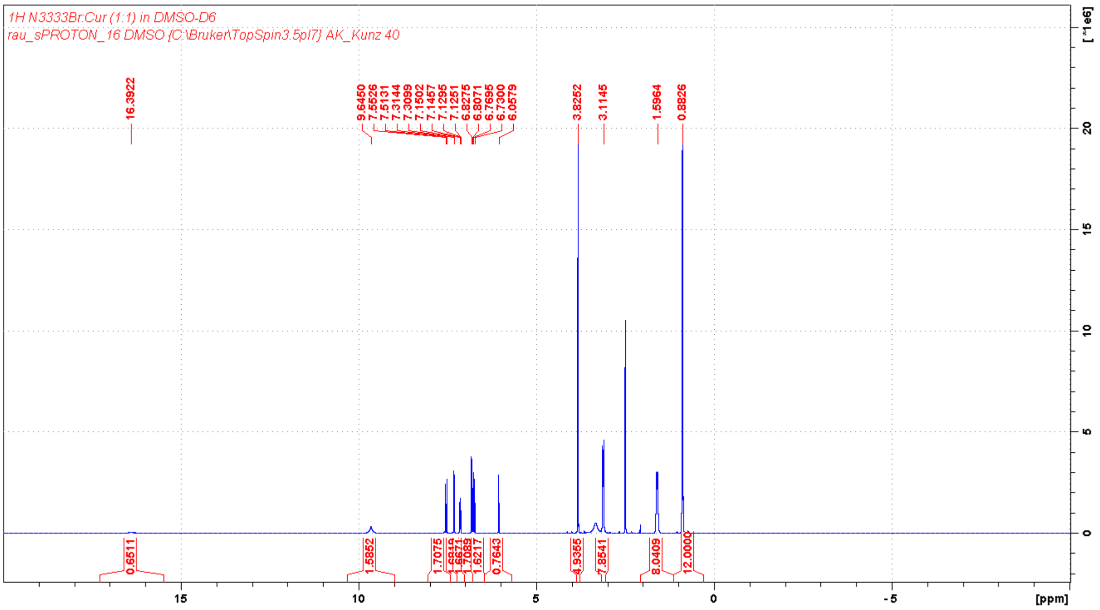

Figure 9-28: ^{1}H-NMR of curcumin and tetrapropylammonium bromine (1:1 n/n) in DMSO-d$_6$ [158].

Curcumin + tetrapropylammonium bromide: ^{1}H-NMR (DMSO-d_6, 400 MHz): δ_{ppm} 0.88 (t, 3H), 1.60 (m, 2H), 3.11 (quint, 2H), 3.83 (s, 3H), 6.06 (s, 1H), 6.73 (d, 1H), 6.81 (d, 1H), 7.13 (dd, 1H), 7.31 (d, 1H), 7.51 (d, 1H), 9.65 (s, 1H), 16.39 (s, 1H).

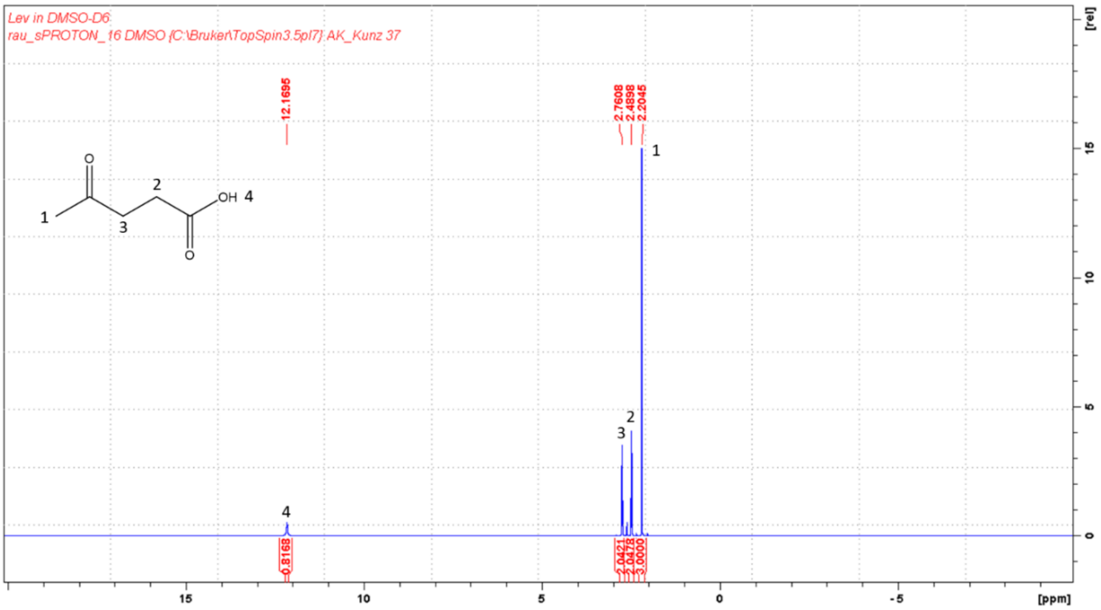

Figure 9-29: ^{1}H-NMR of levulinic acid in DMSO-d$_6$ [158].

Levulinic acid: ^{1}H-NMR (DMSO-d_6, 400 MHz): δ_{ppm} 2.21 (s, 3H), 2.49 (t, 2H), 2.76 (t, 2H), 12.17 (s, 1H).

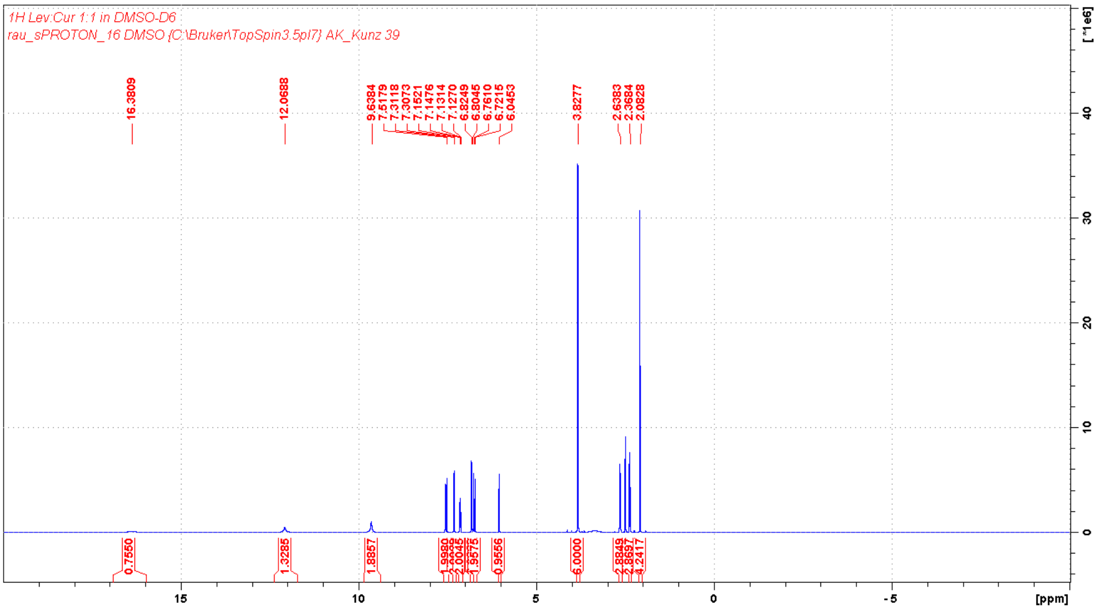

Figure 9-30: ^{1}H-NMR of curcumin and levulinic acid (1:1 n/n) in DMSO-d$_6$ [158].

Curcumin + levulinic acid: ^{1}H-NMR (DMSO-d_6, 400 MHz): δ_{ppm} 2.08 (s, 3H), 2.37 (t, 2H), 2.64 (t, 2H), 3.83 (s, 3H), 6.05 (s, 1H), 6.72 (d, 1H), 6.81 (d, 1H), 7.13 (dd, 1H), 7.31 (d, 1H), 7.52 (d, 1H), 9.64 (s, 1H), 12.07 (s, 1H), 16.38 (s, 1H).

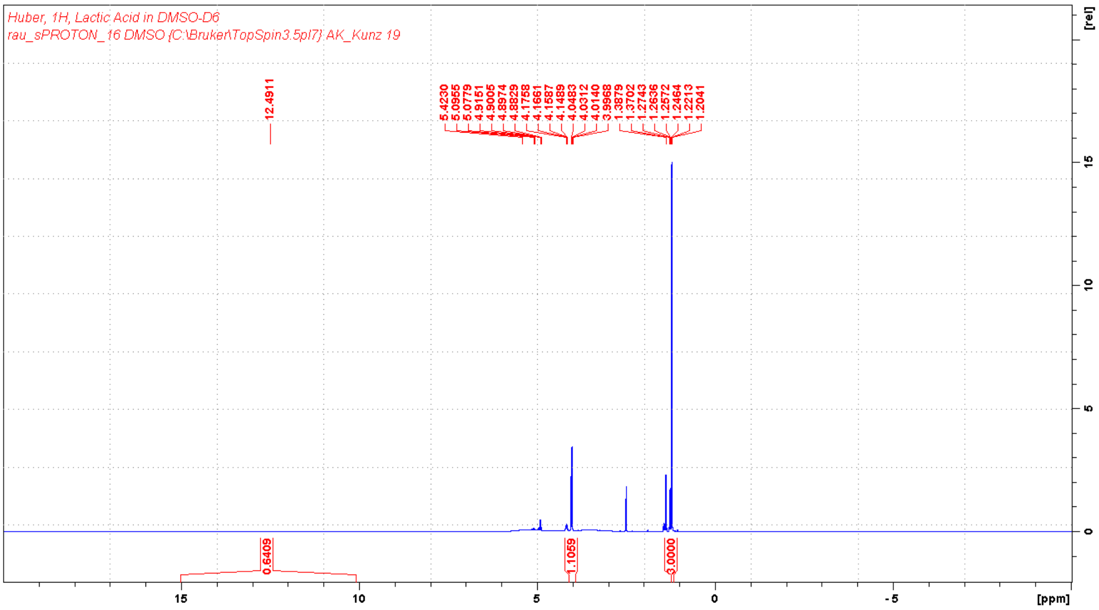

Figure 9-31: ^{1}H-NMR of lactic acid in DMSO-d_6 [158].

Lactic acid: ^{1}H-NMR (DMSO-d_6, 400 MHz): δ_{ppm} 1.20 (s, 3H), 4.0 (q, 1H), 12.49 (s, 1H).

The uncharacterized peaks stem from isomers, oligomers, and degradation products.

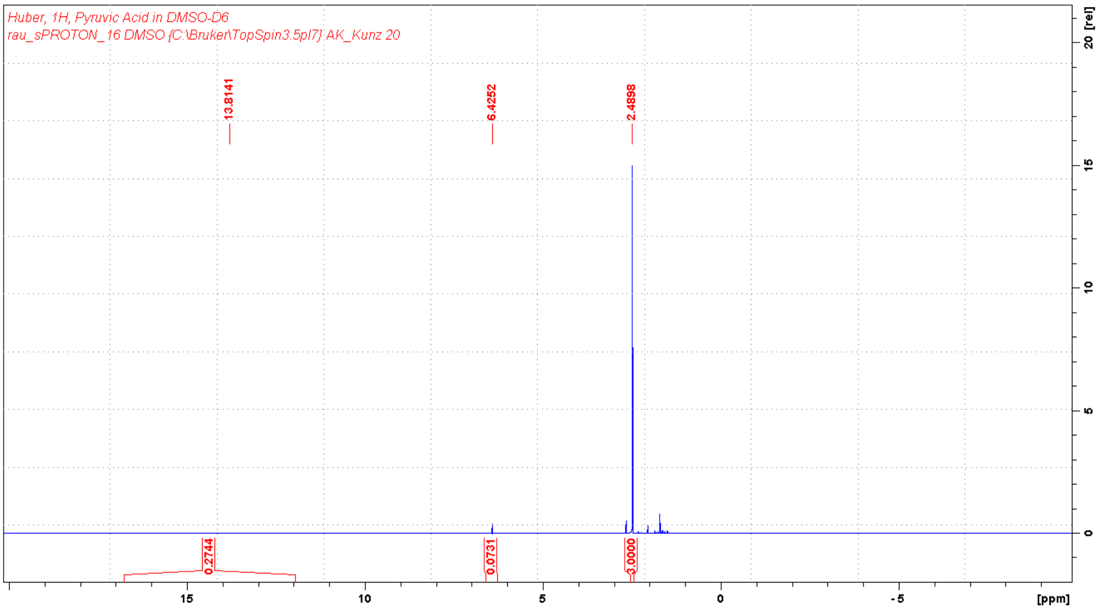

Figure 9-32: ^{1}H-NMR of pyruvic acid in DMSO-d_6 [158].

Pyruvic acid: ^{1}H-NMR (DMSO-d_6, 400 MHz): δ_{ppm} 2.49 (s, 3H), 13.81 (s, 1H).

The uncharacterized peaks stem from isomers and degradation products.

9.5.3 Determination of the Keto-Enol-Ratio

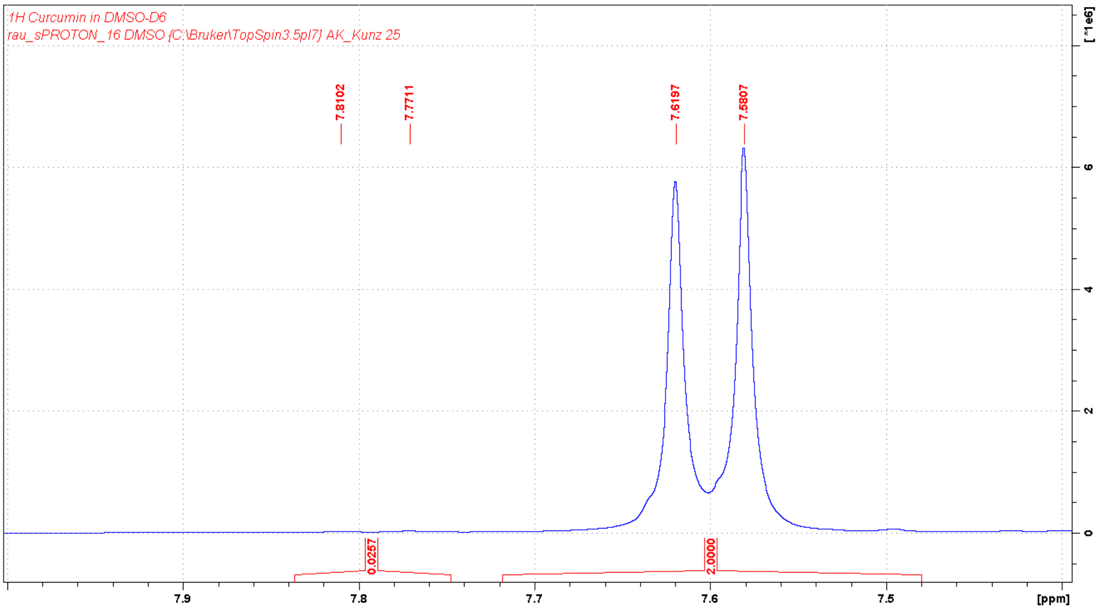

Figure 9-33: Determination of the keto-enol-ratio of curcumin in DMSO-d_6 [158].

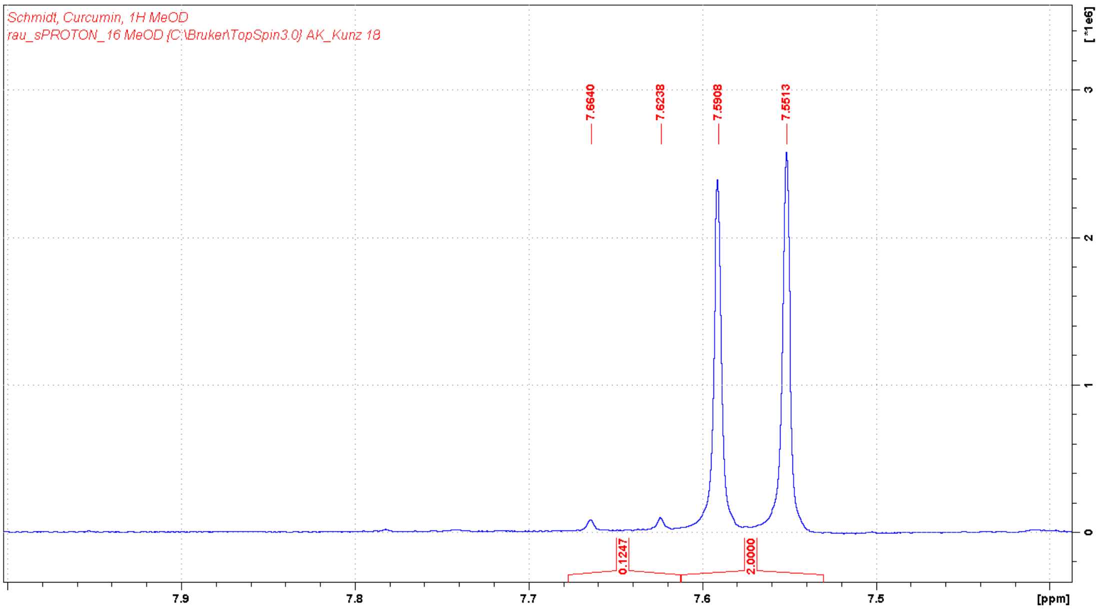

Figure 9-34: Determination of the keto-enol-ratio of curcumin in methanol-d_4 [158].

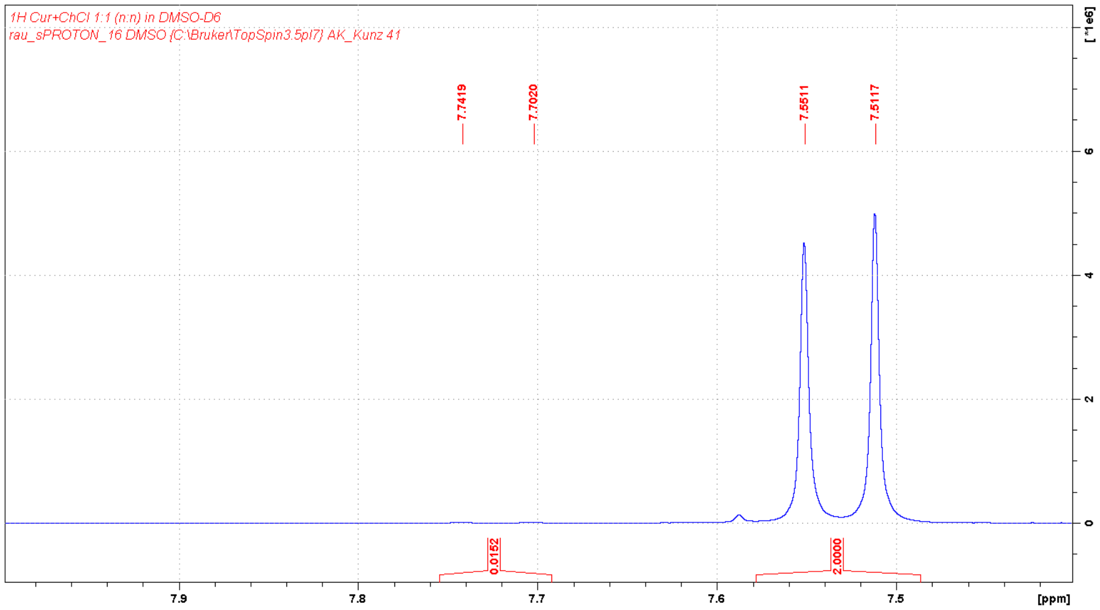

Figure 9-35: Determination of the keto-enol-ratio of curcumin with choline chloride as an additive in DMSO-d$_6$ [158].

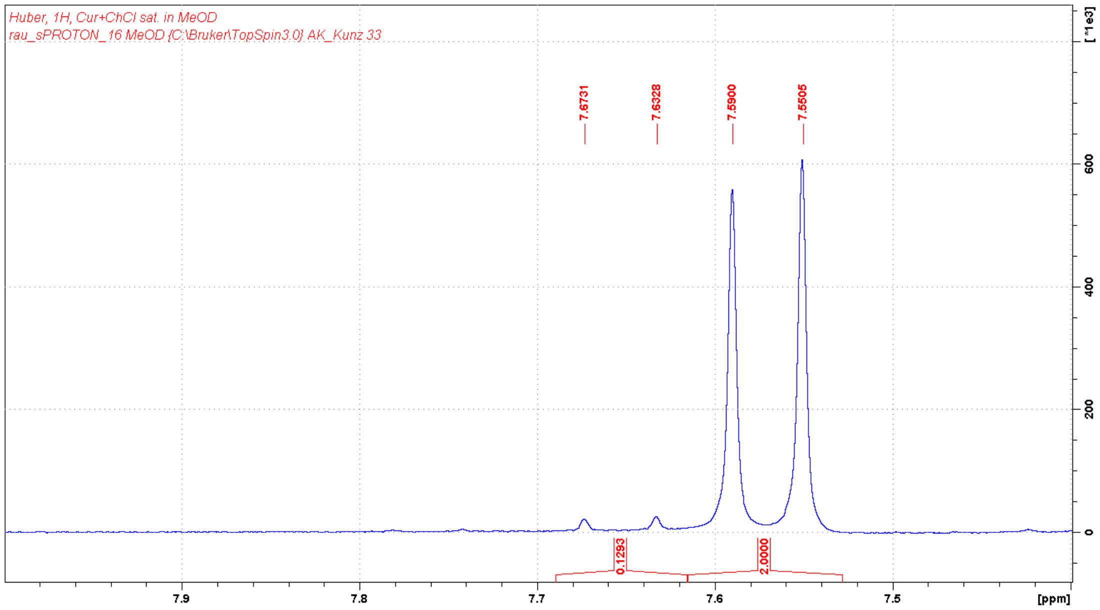

Figure 9-36: Determination of the keto-enol-ratio of curcumin with choline chloride as an additive in methanol-d$_4$ [158].

Table 9-9: Ratio of the enol conformation of curcumin [158].

	DMSO-*d*$_6$	**Methanol-*d*$_4$**
Curcumin	99%	94%
+ ChCl	99%	93%

9.5.4 NOESY Spectra of Curcumin and the QAs

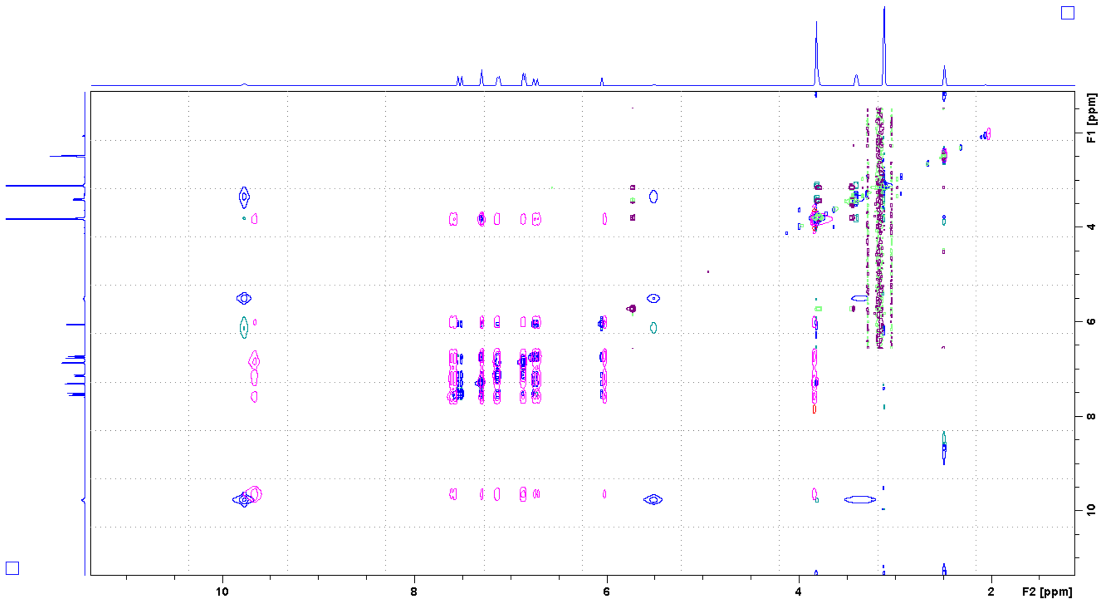

Figure 9-37: NOESY spectrum of curcumin and ChCl 1:1 (n/n) (blue/green), curcumin (pink), and ChCl (purple) in DMSO-d_6 [158].

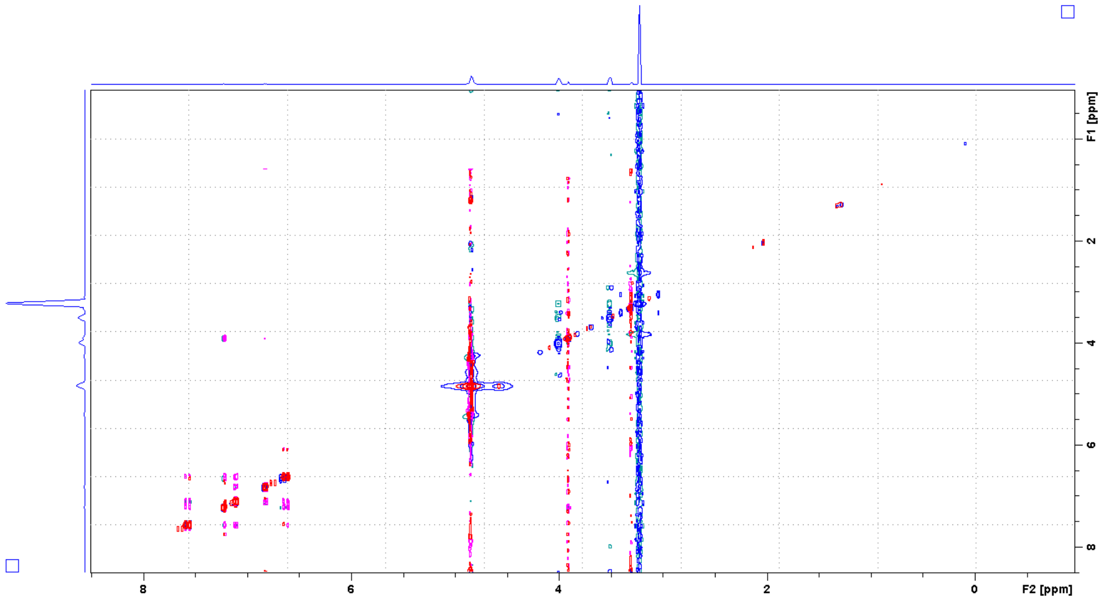

Figure 9-38: NOESY spectrum of curcumin and ChCl 1:1 (n/n) (blue/green) and curcumin (pink/red) in methanol-d_4 [158].

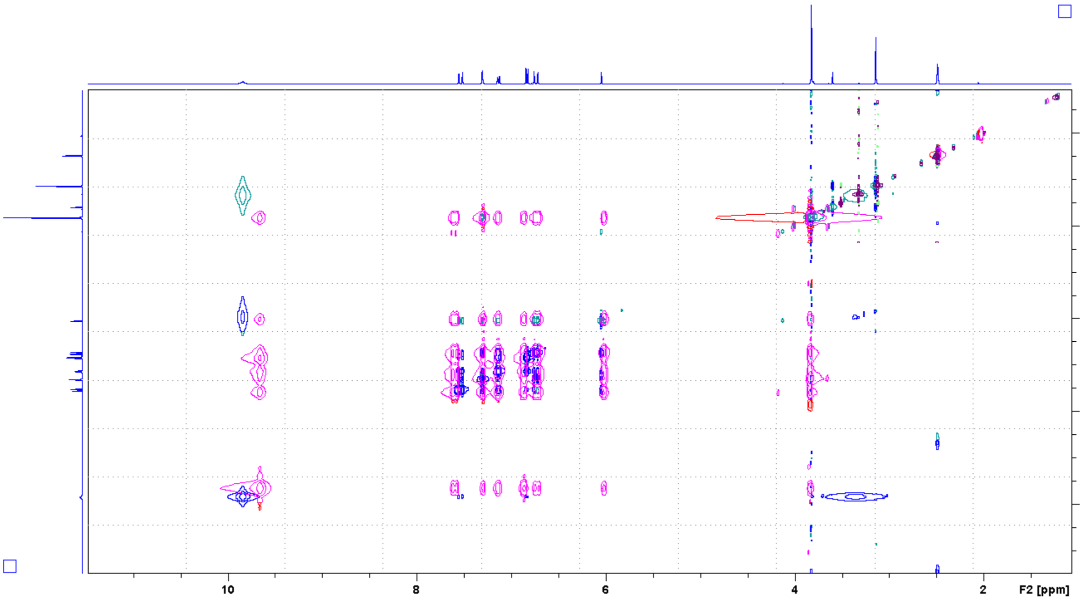

Figure 9-39: NOESY spectrum of curcumin and Bet 1:1 (n/n) (blue/green), curcumin (pink), and Bet (purple) DMSO-d_6 [158].

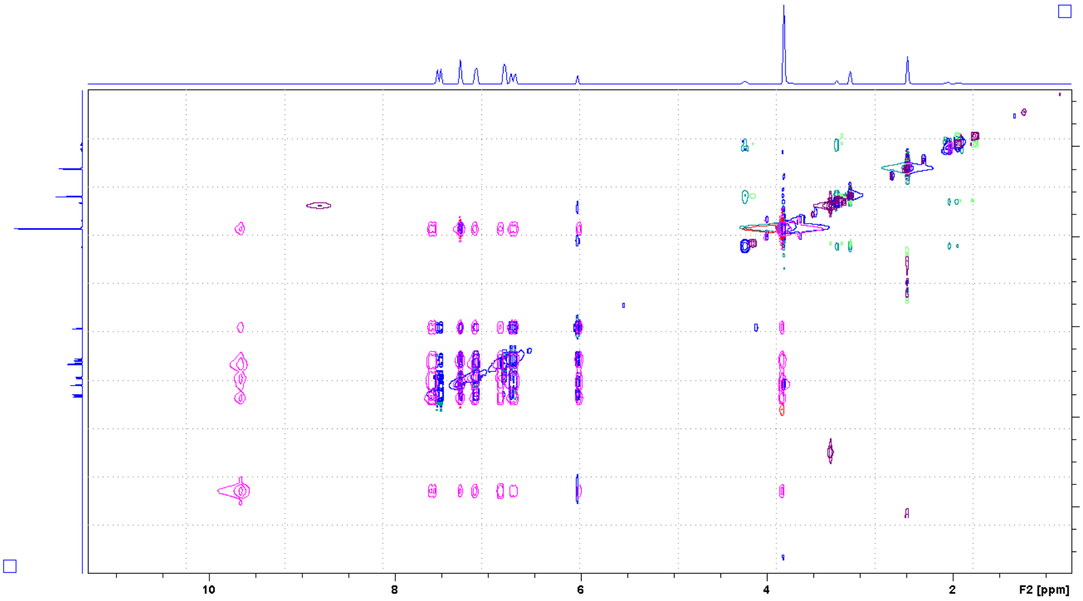

Figure 9-40: NOESY spectrum of curcumin and Car 1:1 (n/n) (blue/green), curcumin (pink), and Car (purple) DMSO-d_6 [158].

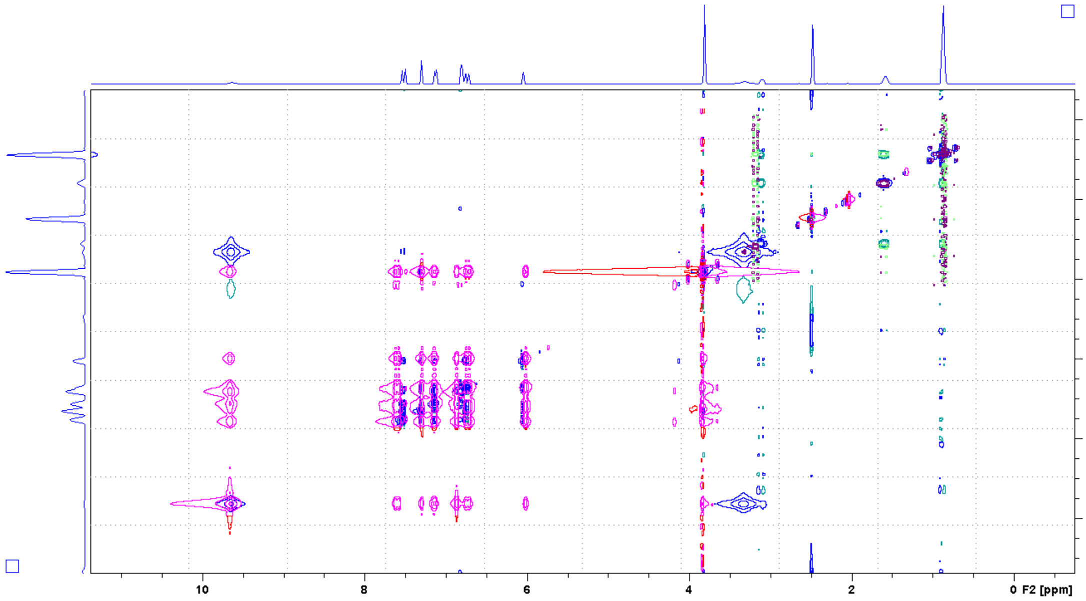

Figure 9-41: NOESY spectrum of curcumin and $N_{3333}Br$ 1:1 (n/n) (blue/green), curcumin (pink), and $N_{3333}Br$ (purple) DMSO-d_6 [158].

9.5.5 Curcumin Solubility in EtOH Depending on the Acid Content in mol%

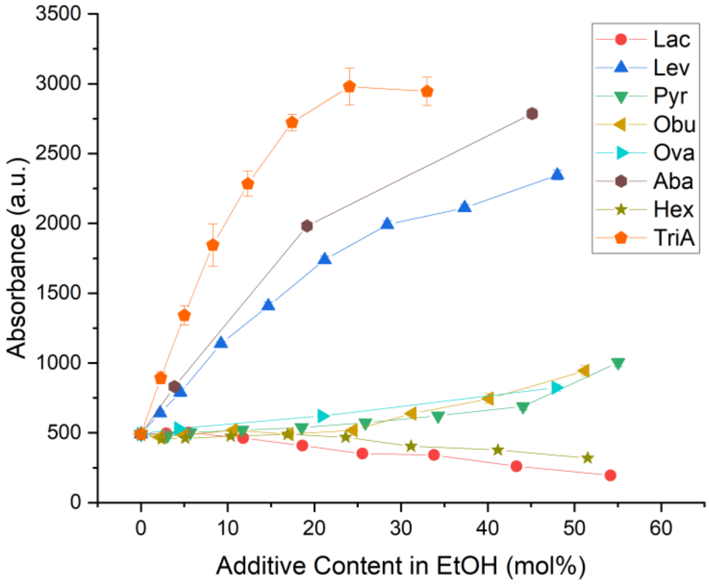

Figure 9-42: Solubility of curcumin in ethanolic solutions in mol% of lactic acid (red squares), levulinic acid (blue circles), pyruvic acid (green up-facing triangles), 2-oxobutyric acid (yellow diamonds), 2-oxovaleric acid (turquoise left-facing triangles), and 4-acetylbutyric acid (brown right-facing triangles), with references hexanoic acid (beige hexagons) and triacetin (orange stars). The solubilities in pure TriA, Lac, Lev, and Pyr are depicted as well [158].

9.5.6 Hansen Space

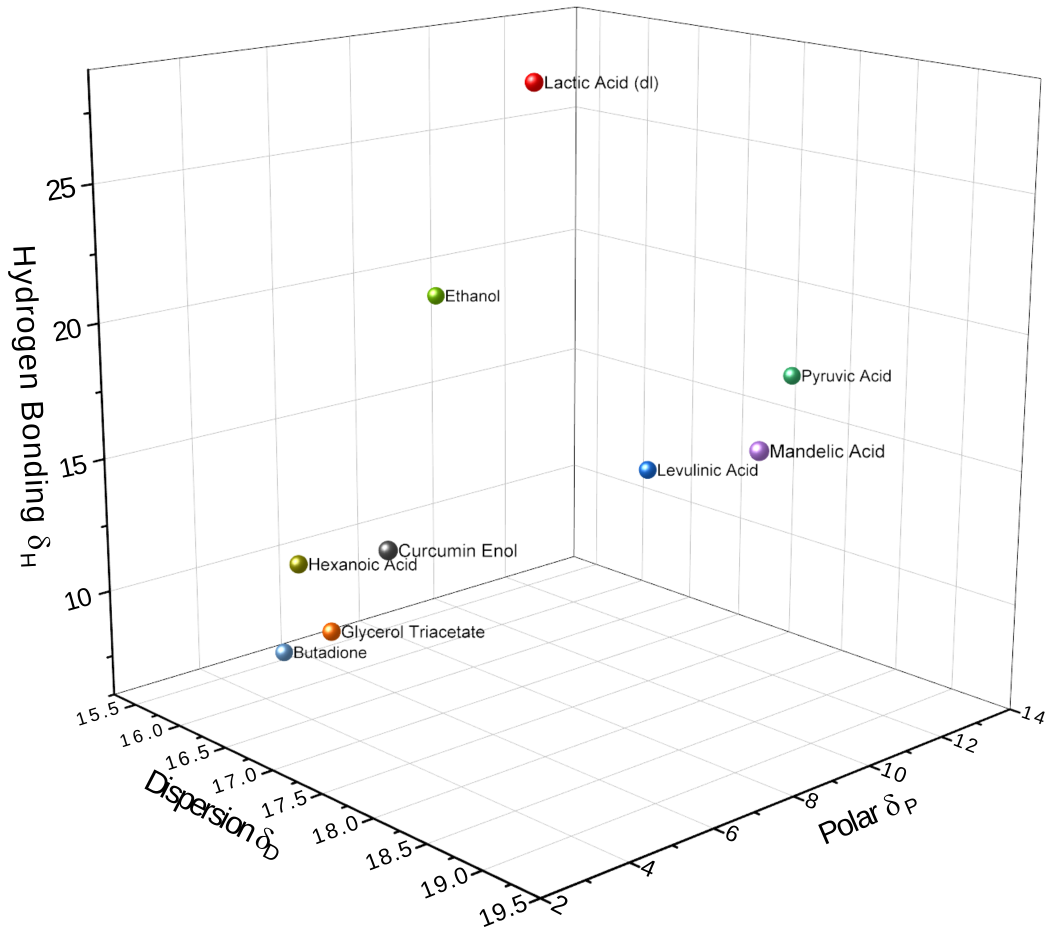

Figure 9-43: Hansen space surrounding curcumin in the enol form [158].

Table 9-10: Hansen Solubility Parameters and corresponding distance to curcumin in the 3D Hansen Space [158].

Solvent	δ_D	δ_P	δ_H	Distance
Curcumin Enol	17.46	3.66	13.84	
Hexanoic Acid	16.3	4.2	11.5	3.34
Lactic Acid (dl)	17	8.3	28.4	15.31
Levulinic Acid	17.34	10.37	13.84	6.71
Pyruvic Acid	17.77	13.05	16.95	9.91
Mandelic Acid	19.19	7.86	17.79	6.72
Triacetin	16.5	4.5	9.1	5.18
Butadione	15.7	5.1	6.8	8.00
Ethanol	15.8	8.8	19.4	7.75

The parameters were acquired via the *Hansen Solubility Parameters in Practice* software. The distance was calculated according to Equation (2-13).

9.5.7 Chemical Potential of Curcumin Solubility via COSMO-RS

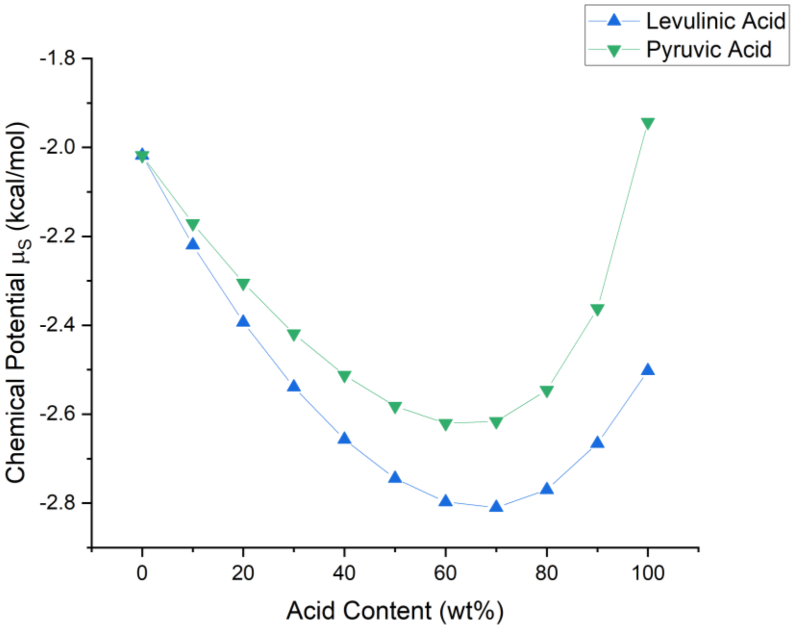

Figure 9-44: Chemical potential of the cyclic conformations of levulinic acid (blue triangles) and pyruvic acid (green down-facing triangles) as predicted via COSMO-RS calculations [158].

9.5.8 Curcumin Solubility in EtOH Depending on the Acid Content in wt%

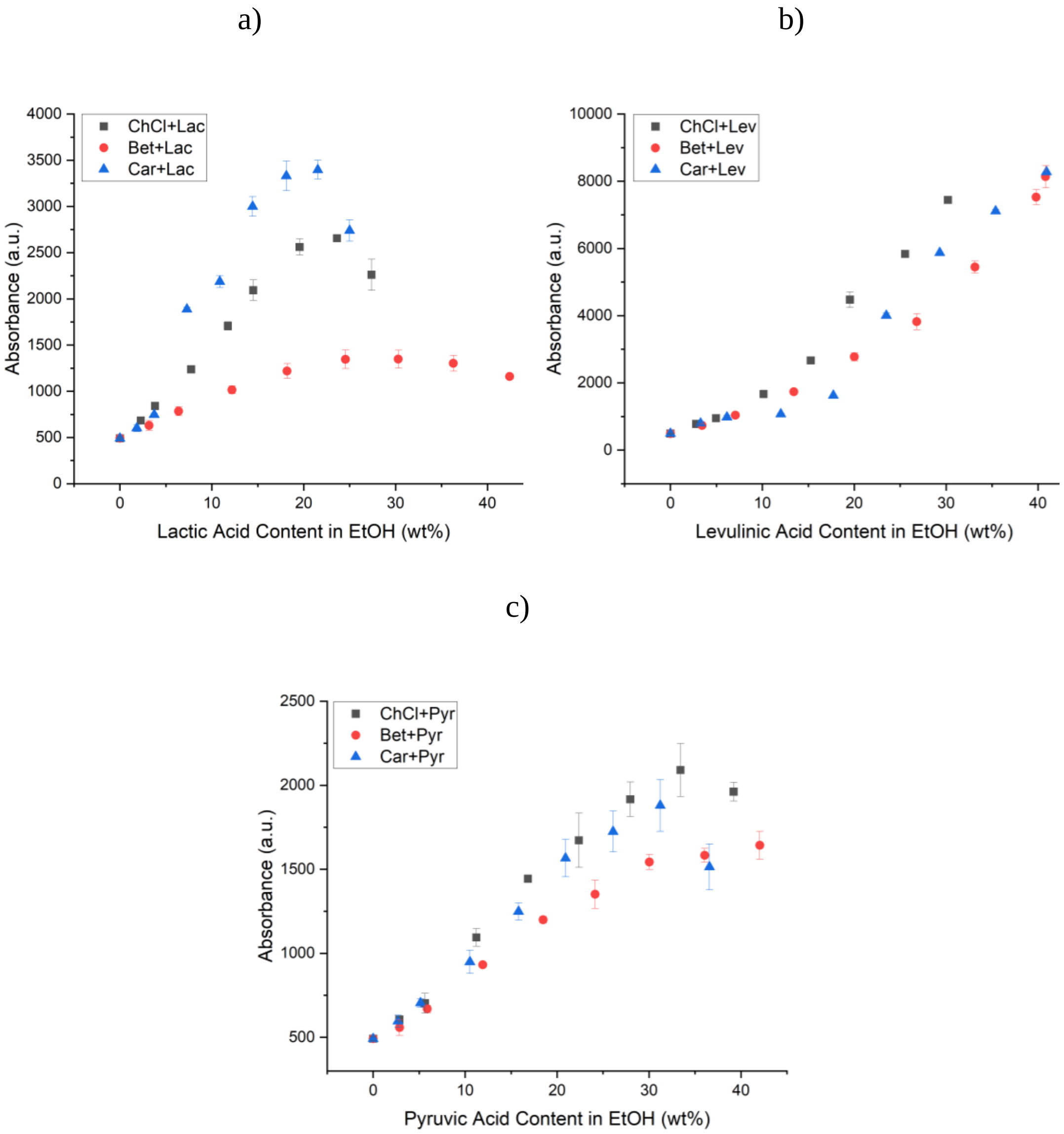

Figure 9-45: Curcumin solubility in mixtures of a) lactic acid, b) levulinic acid, and c) pyruvic acid-based NADES depending on the acid content in wt% where the grey squares represent the choline chloride NADES, the red dots betaine NADES, and the blue triangles the carnitine NADES [158].

9.6 Supplementary Information of Chapter 6

All figures and tables of this chapter will be released in the supplementary material of the publication titled *Towards a Sustainable and Green Extraction of Curcuminoids Using the Essential Oil of Cinnamomum Cassia* by V. Huber and M. Schmidt *et al.* [169], planned in Sust Food Tech. For convenience reasons, the reference is stated as a disclaimer in this paragraph.

9.6.1 Screening of Natural Aromas in wt%

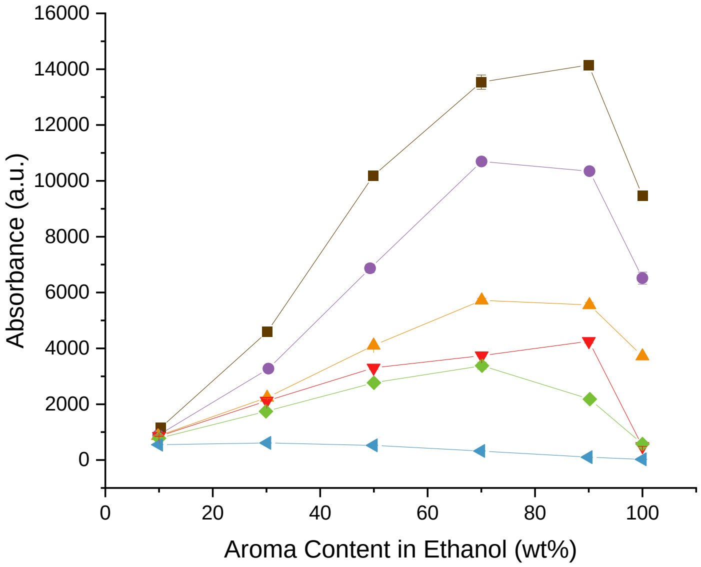

Figure 9-46: UV/Vis examination of the solubility of curcumin in ethanolic solutions of natural flavors (w/w). Cinnamaldehyde is presented by brown squares, benzaldehyde by purple circles, citral by orange triangles, trans-anethole by red down-facing triangles, benzyl benzoate by green diamonds, and limonene by blue left-facing triangles [169].

9.6.2 ^{1}H and NOESY NMR spectra of Curcumin with Cin and HCi

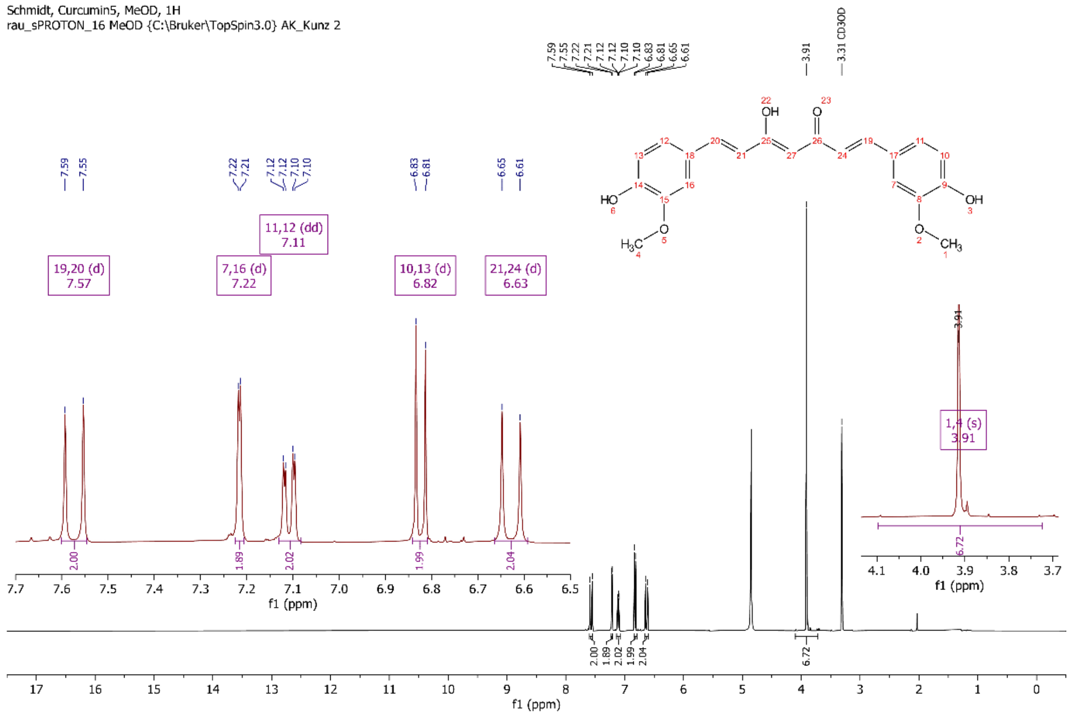

Figure 9-47: ^{1}H NMR spectrum of curcumin in MeOD [169].

Curcumin: ^{1}H-NMR (Methanol-d_4, 400 MHz): δ_{ppm} 3.91 (s, 6H), 6.63 (d, 2H), 6.82 (d, 2H), 7.11 (dd, 2H), 7.16 (d, 2H), 7.57 (d, 2H).

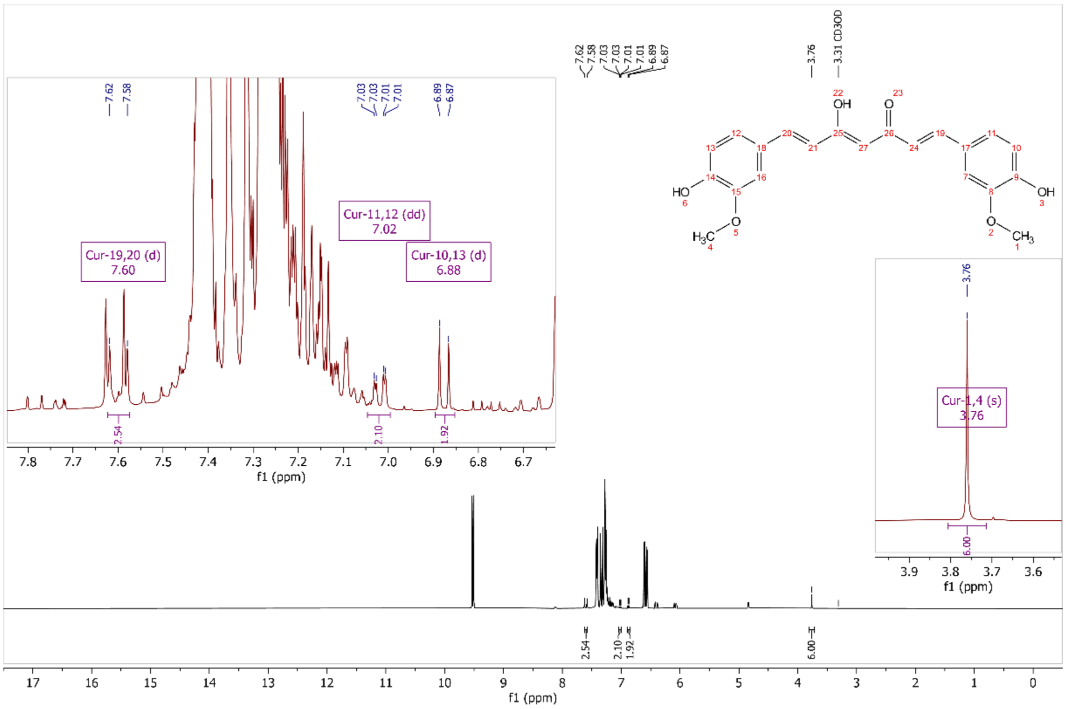

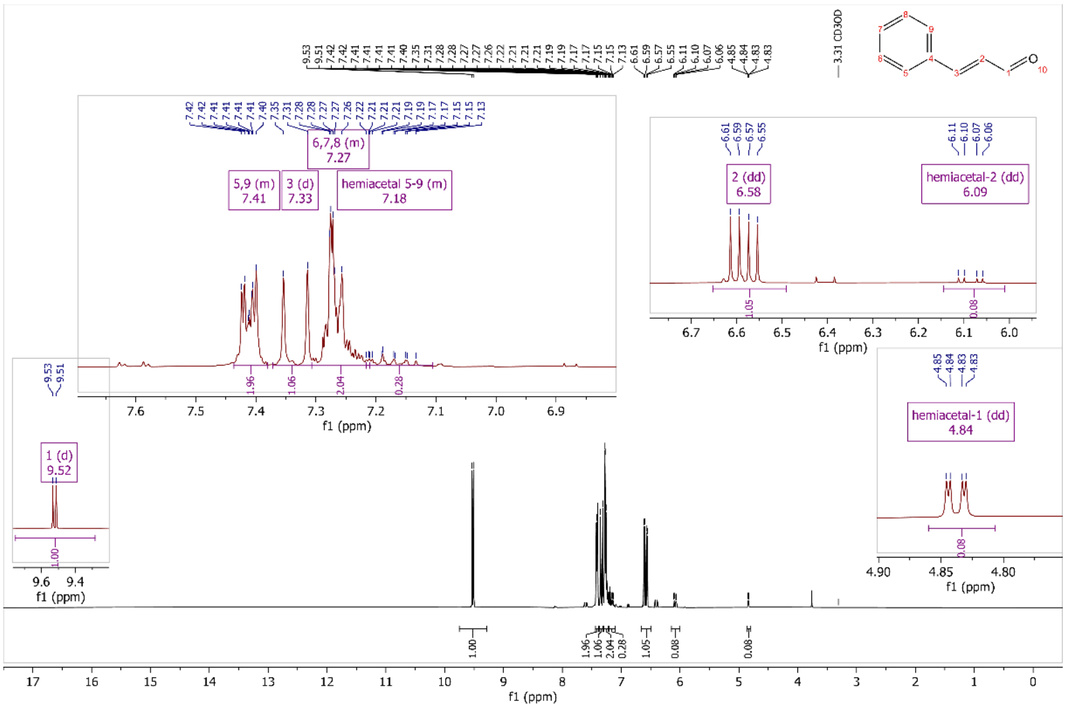

Figure 9-48: ^{1}H NMR of curcumin in cinnamaldehyde and MeOD at a ratio of 30:70 (n/n). The protons of curcumin are assigned at the top and the ones of Cin on the bottom [169].

Curcumin: ^{1}H-NMR (Methanol-*d*$_4$, 400 MHz): δ$_{ppm}$ 3.76 (d, 6H), 6.88 (d, 2H), 7.02 (dd, 2H), 7.60 (d, 3H).

Cinnamaldehyde: ^{1}H-NMR (Methanol-*d*$_4$, 400 MHz): δ$_{ppm}$ 4.84 (dd, 0H), 6.09 (dd, 0H), 6.58 (dd, 1H), 7.11 (m, 0H), 7.21 (m, 2H), 7.33 (d, 1H), 7.38 (m, 2H), 9.52 (d, 1H).

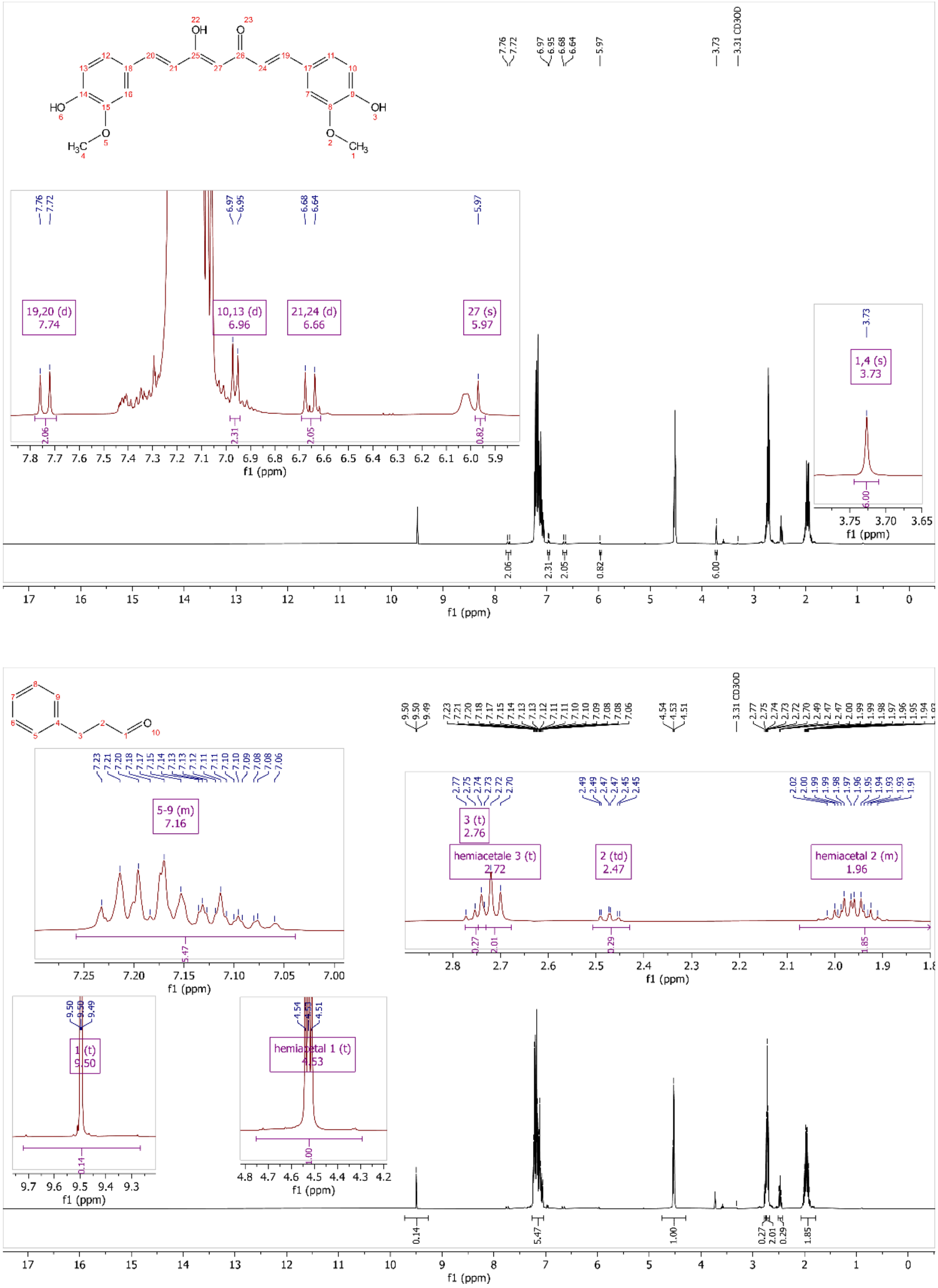

Figure 9-49: ^{1}H NMR spectrum of curcumin in hydrocinnamaldehyde and MeOD at a ratio of 30:70 (n/n). The protons of curcumin are assigned at the top and the ones of HCi on the bottom [169].

Curcumin: ^{1}H-NMR (Methanol-d_4, 400 MHz): δ_{ppm} 3.73 (d, 6H), 5.97 (s, 1H), 6.66 (d, 2H), 6.96 (d, 2H), 7.74 (d, 2H).

Hydrocinnamaldehyde: ^{1}H-NMR (DMSO-d_6, 400 MHz): δ_{ppm} 1.79 (m, 2H), 2.47 (m, 2H), 2.72 (t, 2H), 2.76 (t, 0H), 4.53 (t, 1H), 7.04 (m, 5H).

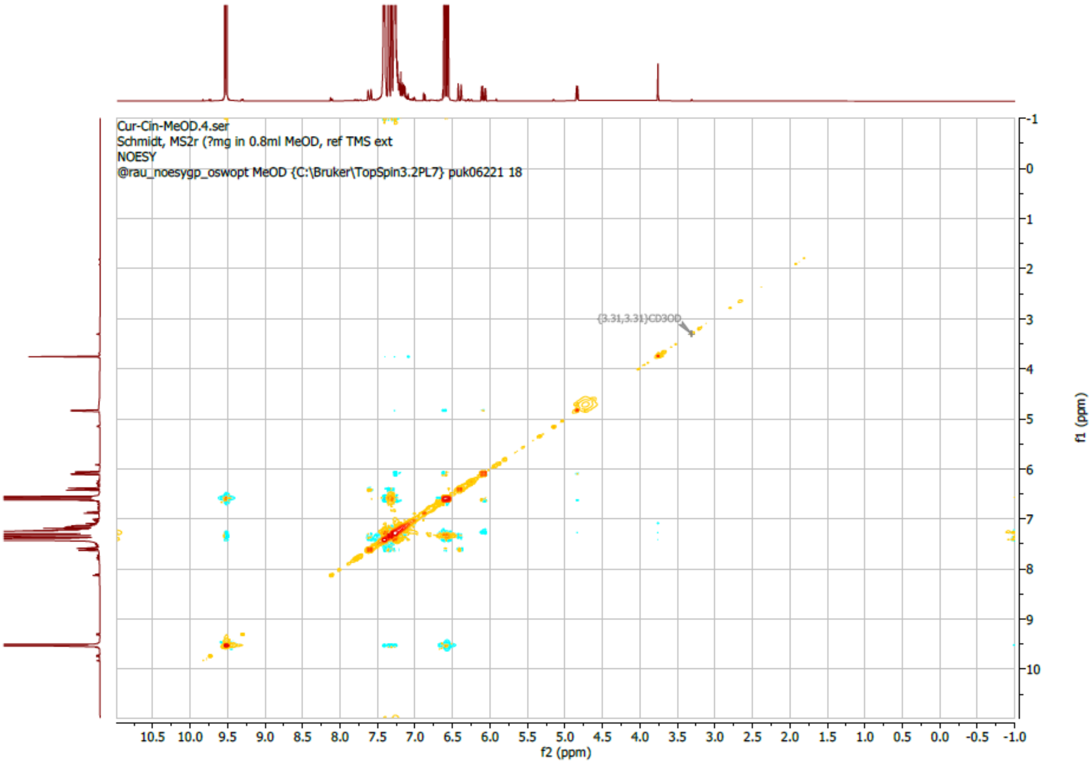

Figure 9-50: NOESY NMR of curcumin in cinnamaldehyde and MeOD at a ratio of 30:70 (n/n) [169].

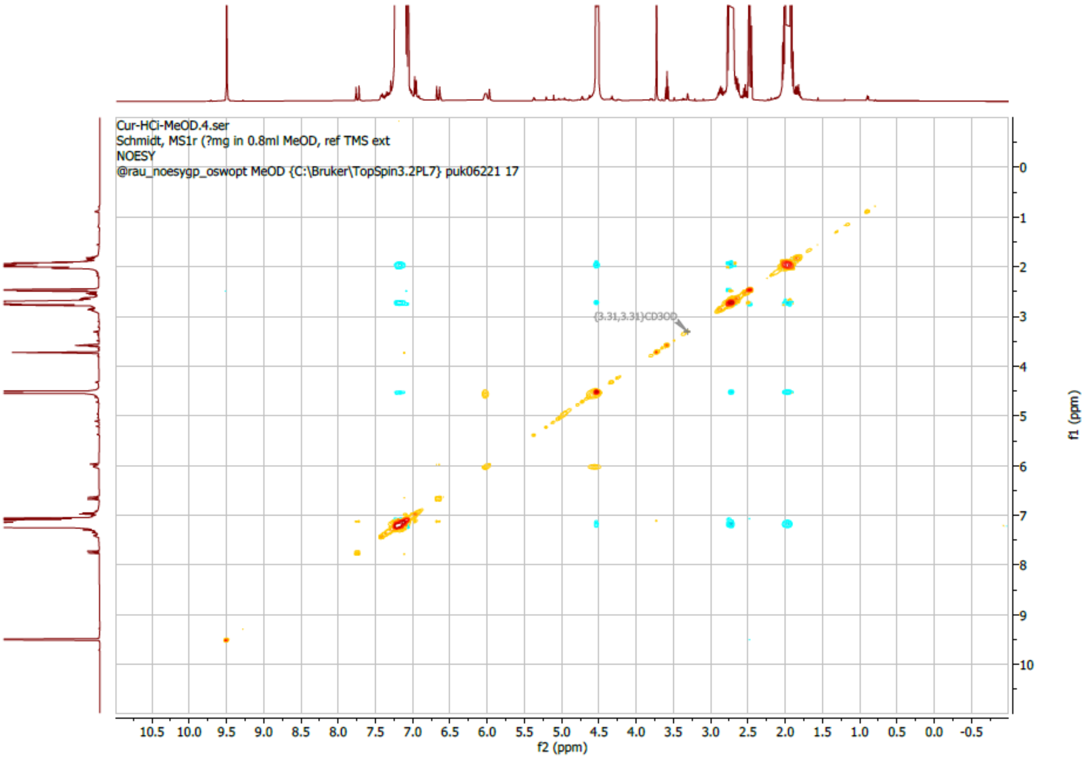

Figure 9-51: NOESY NMR of curcumin in hydrocinnamaldehyde and MeOD at a ratio of 30:70 (n/n) [169].

9.6.3 Screening of Cinnamaldehyde Derivatives

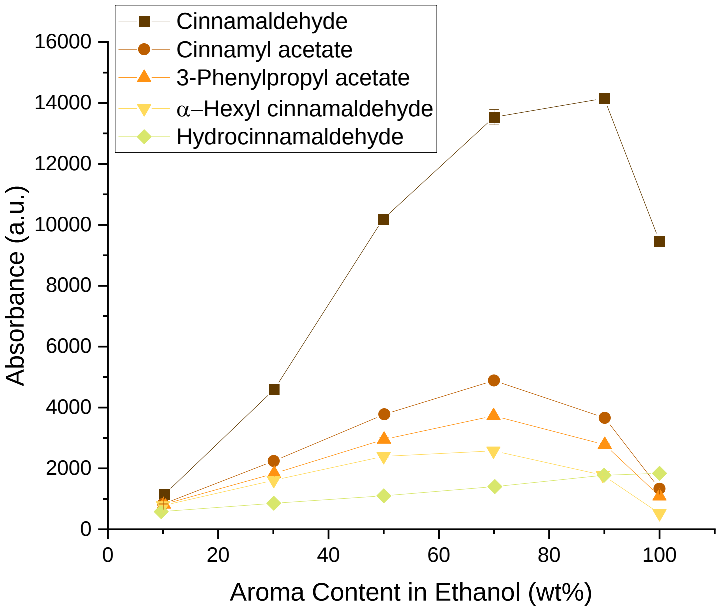

Figure 9-52: UV/Vis examination of curcumin in ethanolic solutions of natural flavors (w/w). Cinnamaldehyde is presented by brown squares, cinnamyl acetate by marron circles, 3-phenylpropyl acetate by orange triangles, α-hexyl cinnamaldehyde by golden down-facing triangles, and hydrocinnamaldehyde by yellow diamonds [169].

9.6.4 GC-FID Chromatograms

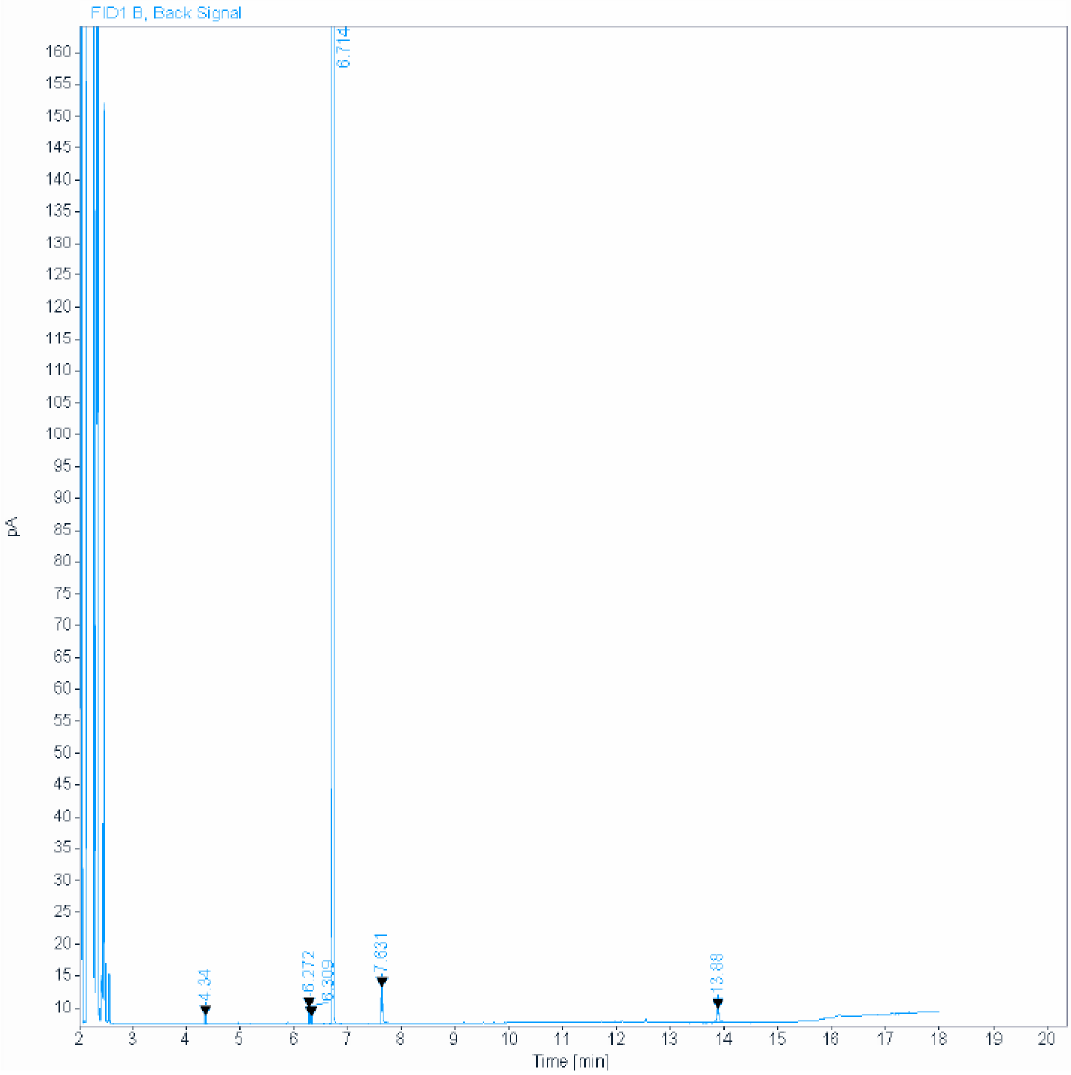

Figure 9-53: Chromatogram of the pure, synthetic cinnamaldehyde as obtained via GC-FID [169].

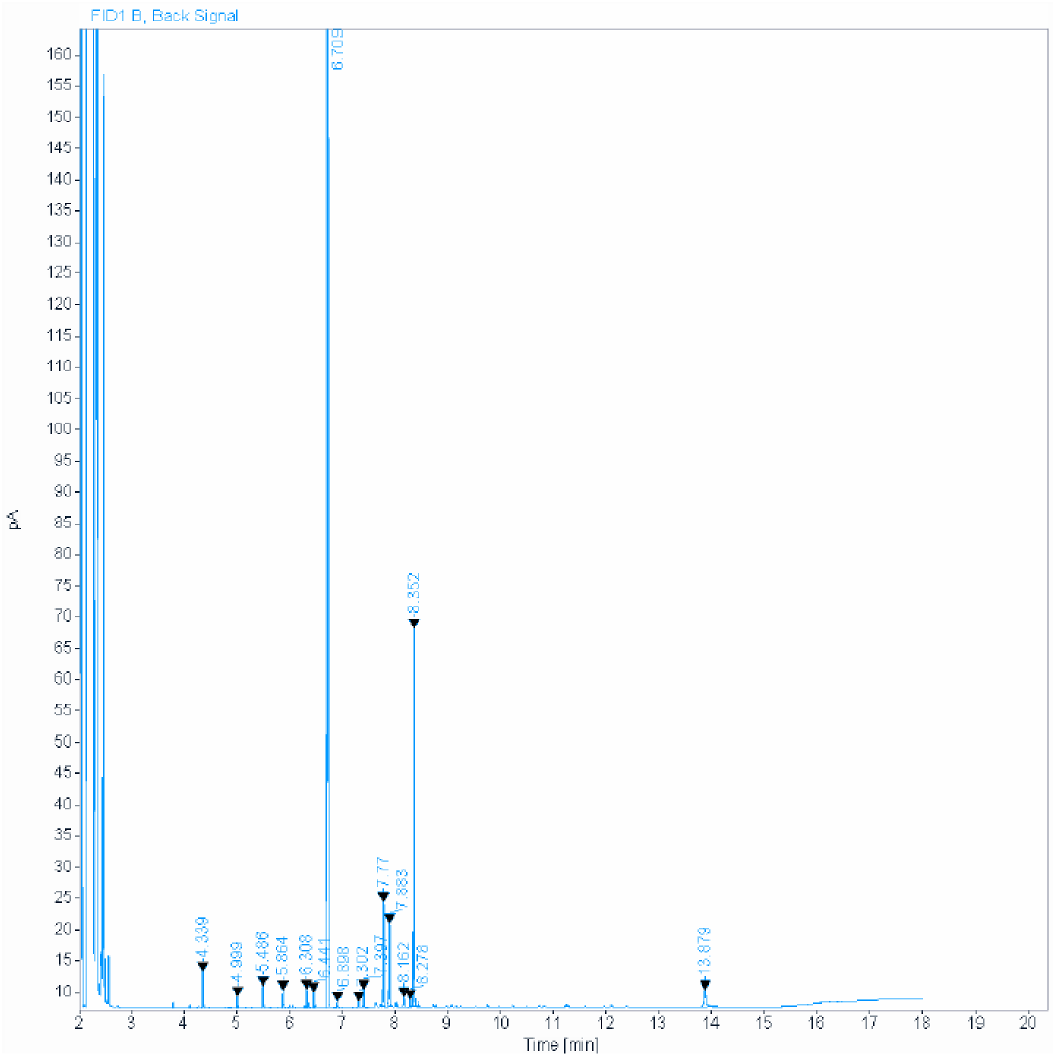

Figure 9-54: Chromatogram of Cinnamomum cassia oil by PCW as obtained via GC-FID [169].

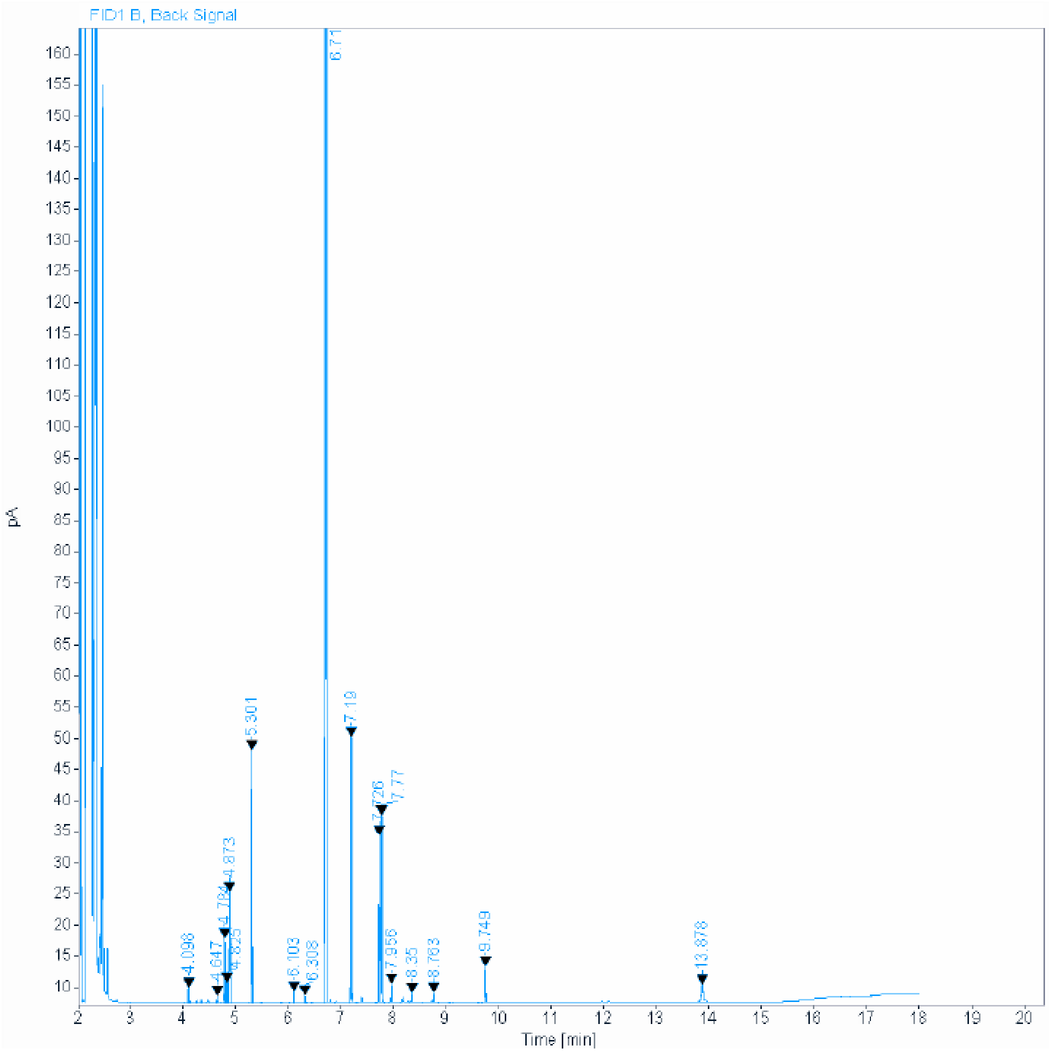

Figure 9-55: Chromatogram of Cinnamomum zeylanicum oil by Jean Pütz as obtained via GC-FID [169].

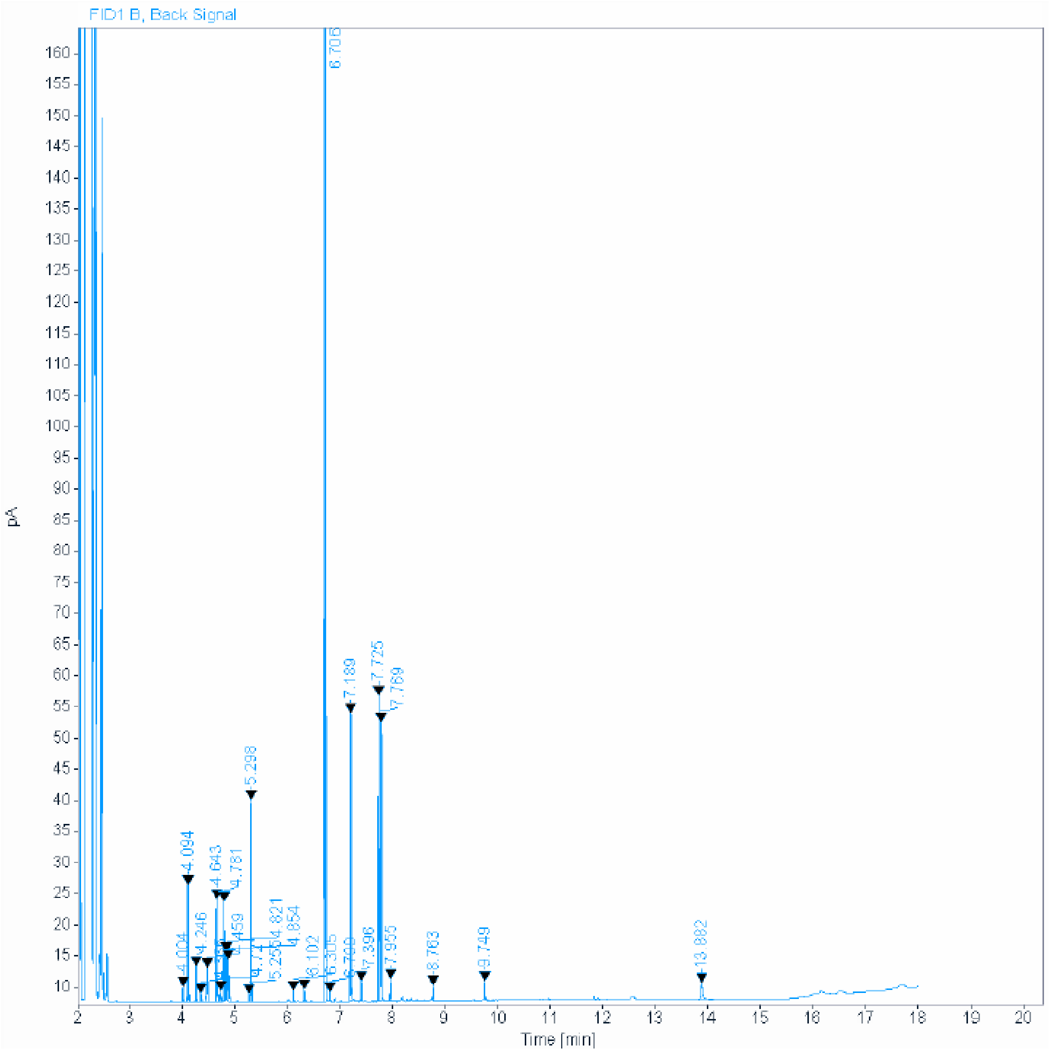

Figure 9-56: Chromatogram of Cinnamomum verum oil by PCW as obtained via GC-FID [169].

Table 9-11: Retention time of Cinnamaldehyde and purity as determined via GC-FID [169].

Retention Time (min)	**Reference Cinnamaldehyde**	**Cassia**	**Zeylanicum**	**Verum**
6.71	97%	79%	74%	62%

9.6.5 GC-MS Data of the *Cinnamomum* Oils

In this section, the GC-MS results of cinnamaldehyde as the reference and the three different cinnamon oils will be presented. The mass spectra were matched to the compounds via the NIST database.

Table 9-12: Retention time of all analyzable ingredients of the different cinnamon oils as assessed via GC-MS [169].

Retention Time (min)	Cassia	Zeylanicum	Verum
3.38	-	-	α-Pinene
3.52	-	-	Camphene
3.59	Benzaldehyde	-	-
3.75	-	-	β-Myrcene
3.94	-	-	α-Phellandrene
4.07	-	o-Cymene	o-Cymene
4.12	-	Limonene	Limonene
4.15	-	-	β-Phellandrene
4.16	-	Eucalyptol	-
4.62	-	Linalool	Linalool
5.98	**Cinnamaldehyde**	**Cinnamaldehyde**	**Cinnamaldehyde**
6.51	-	Eugenol	Eugenol
7.05	-	Caryophyllene	Caryophyllene
7.11	Cinnamyl acetate	Cinnamyl acetate	Cinnamyl acetate
7.15	Coumarin	-	-
7.67	2-Methoxy-cinnamaldehyde	-	-
9.1	-	Benzyl-benzoate	-

9.6.5.1 Cinnamaldehyde Reference

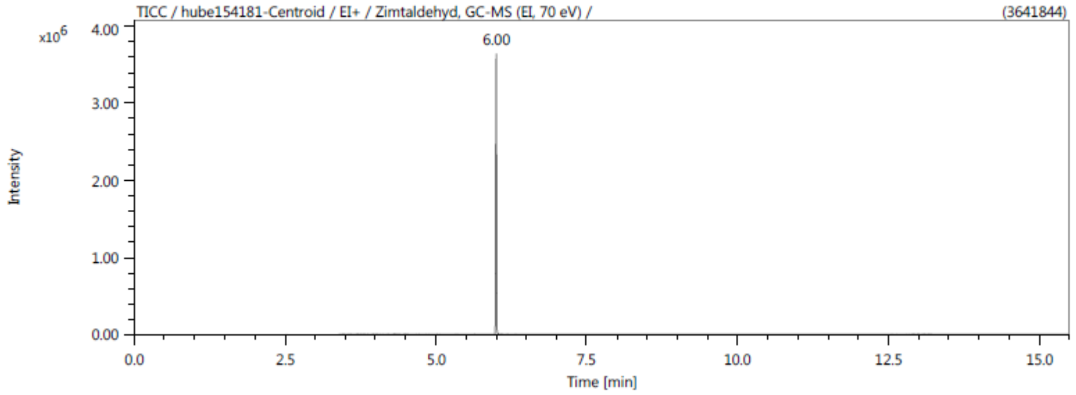

Figure 9-57: Chromatogram of cinnamaldehyde as obtained by GC-MS [169].

Hit 2 : Cinnamaldehyde, (E)-
C9H8O; MF: 958; RMF: 958; Prob 32.3%; CAS: 14371-10-9; Lib: replib; ID: 20946.

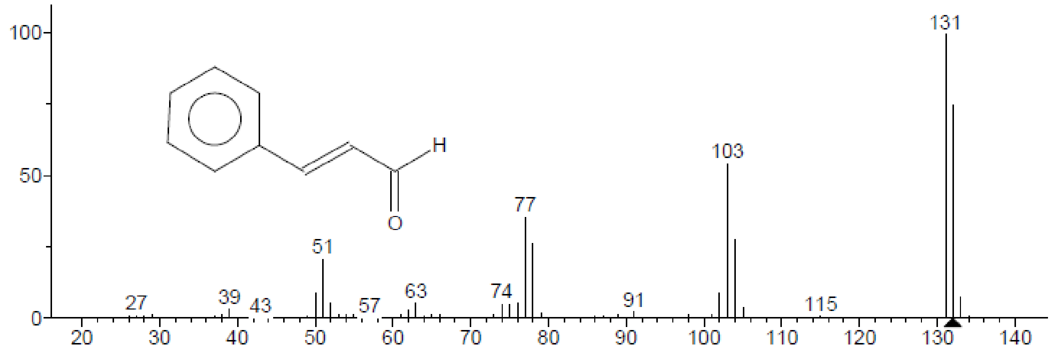

Figure 9-58: Mass spectrum of cinnamaldehyde corresponding to the peak at a retention time of 5.98 min of the chromatogram of pure, synthetic cinnamaldehyde [169].

9.6.5.2 Cinnamomum Cassia Oil by PCW

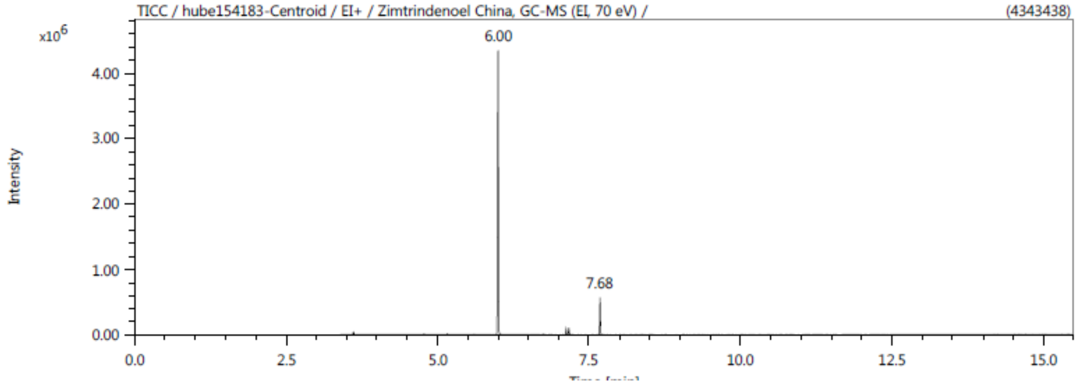

Figure 9-59: Chromatogram of the Cinnamomum cassia oil by PCW as obtained by GC-MS [169].

Hit 1 : Benzaldehyde
C7H6O; MF: 899; RMF: 916; Prob 73.5%; CAS: 100-52-7; Lib: replib; ID: 10911.

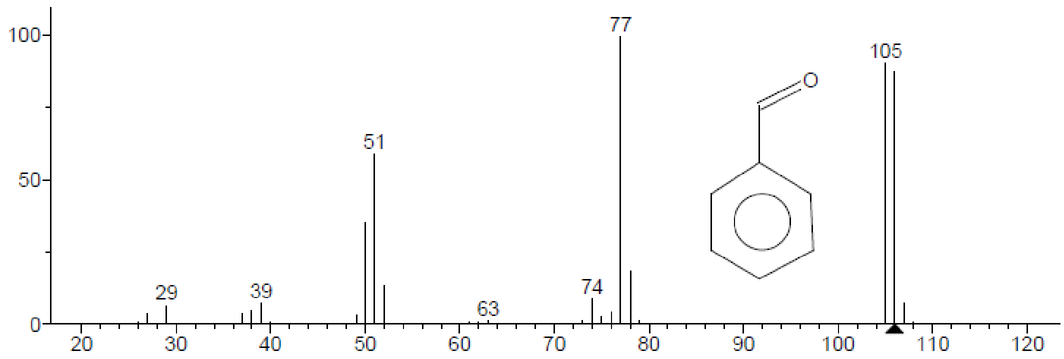

Figure 9-60: Mass spectrum of benzaldehyde corresponding to the peak at a retention time of 3.59 min of the chromatogram of Cinnamomum cassia by PCW [169].

Hit 2 : Cinnamaldehyde, (E)-
C9H8O; MF: 959; RMF: 959; Prob 31.9%; CAS: 14371-10-9; Lib: replib; ID: 20946.

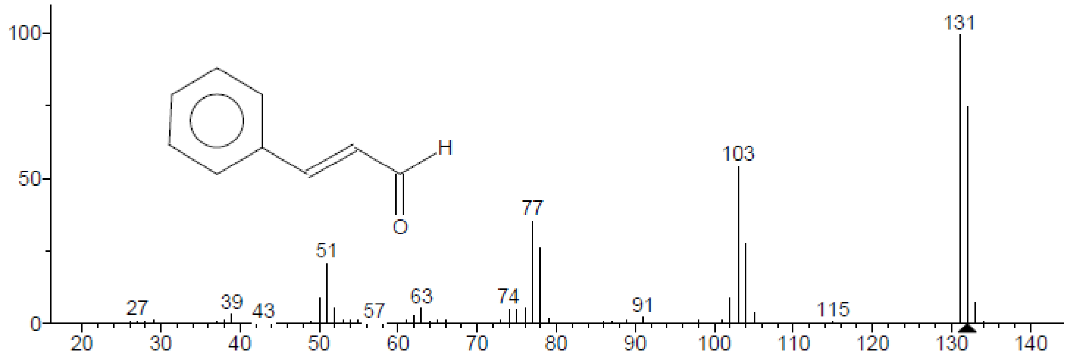

Figure 9-61: Mass spectrum of cinnamaldehyde corresponding to the peak at a retention time of 5.98 min of the chromatogram of Cinnamomum cassia by PCW [169].

Hit 1 : Acetic acid, cinnamyl ester
C11H12O2; MF: 888; RMF: 889; Prob 64.6%; CAS: 103-54-8; Lib: mainlib; ID: 11373.

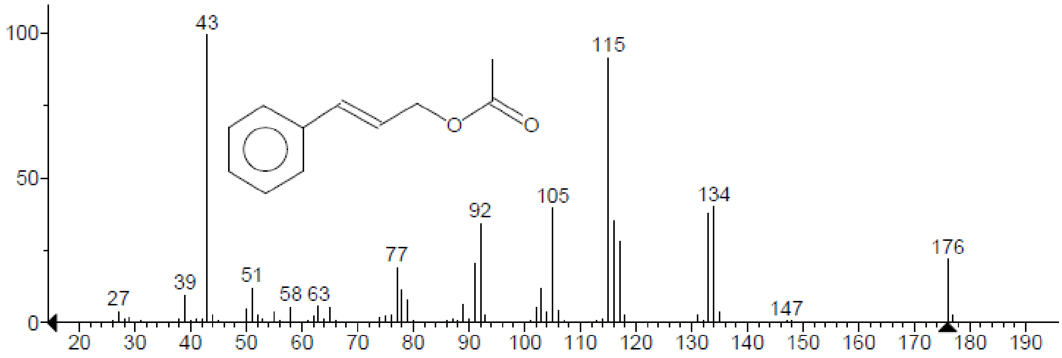

Figure 9-62: Mass spectrum of cinnamyl acetate corresponding to the peak at a retention time of 7.11 min of the chromatogram of Cinnamomum cassia by PCW [169].

Hit 1 : Coumarin
C9H6O2; MF: 937; RMF: 951; Prob 48.7%; CAS: 91-64-5; Lib: replib; ID: 18483.

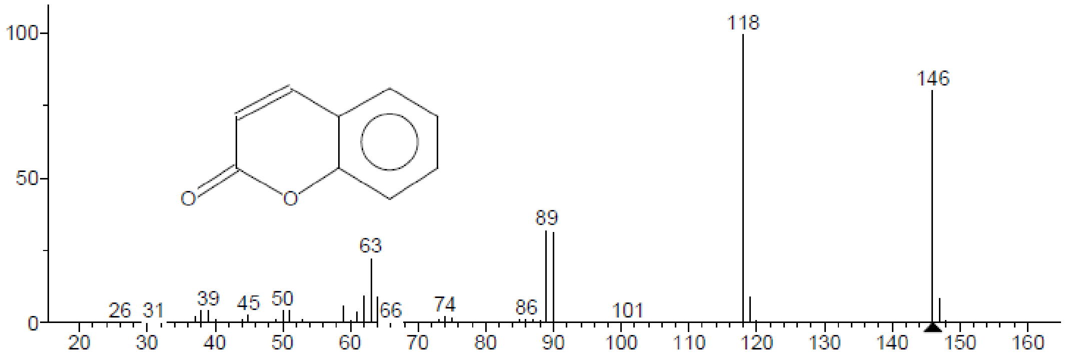

Figure 9-63: Mass spectrum of coumarin corresponding to the peak at a retention time of 7.1 min of the chromatogram of Cinnamomum cassia by PCW [169].

Hit 2 : (Z)-2-Methoxycinnamaldehyde
C10H10O2; MF: 929; RMF: 941; Prob 37.5%; CAS: 76760-43-5; Lib: mainlib; ID: 115636.

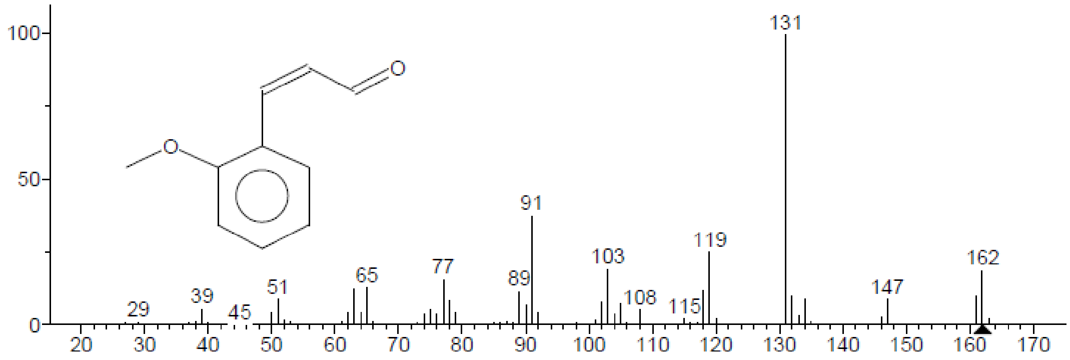

Figure 9-64: Mass spectrum of 2-methoxycinnamaldehyde corresponding to the peak at a retention time of 7.67 min of the chromatogram of Cinnamomum cassia by PCW [169].

9.6.5.3 Cinnamomum Zeylanicum Oil by Jean Pütz

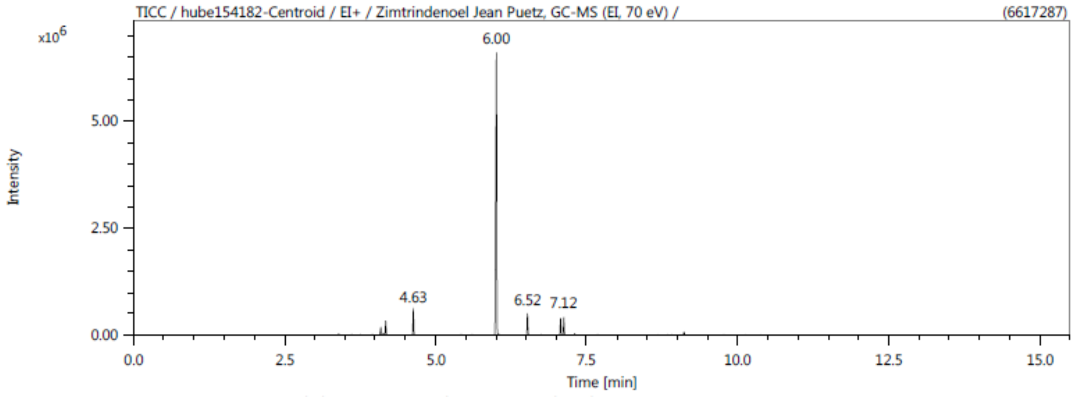

Figure 9-65: Chromatogram of the Cinnamomum verum – zeylanicum oil by Jean Pütz as obtained by GC-MS [169].

Hit 2 : o-Cymene
C10H14; MF: 909; RMF: 910; Prob 21.6%; CAS: 527-84-4; Lib: replib; ID: 18731.

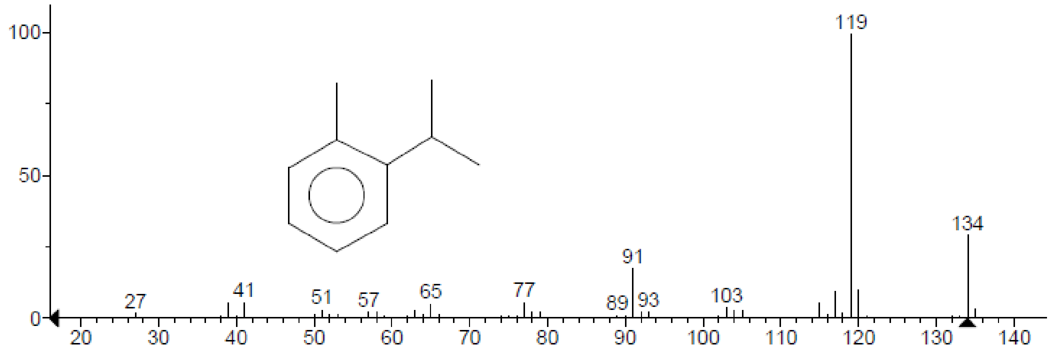

Figure 9-66: Mass spectrum of o-cymene corresponding to the peak at a retention time of 4.0 min of the chromatogram of Cinnamomum zeylanicum by Jean Pütz [169].

Hit 1 : D-Limonene
C10H16; MF: 868; RMF: 868; Prob 61.1%; CAS: 5989-27-5; Lib: replib; ID: 8354.

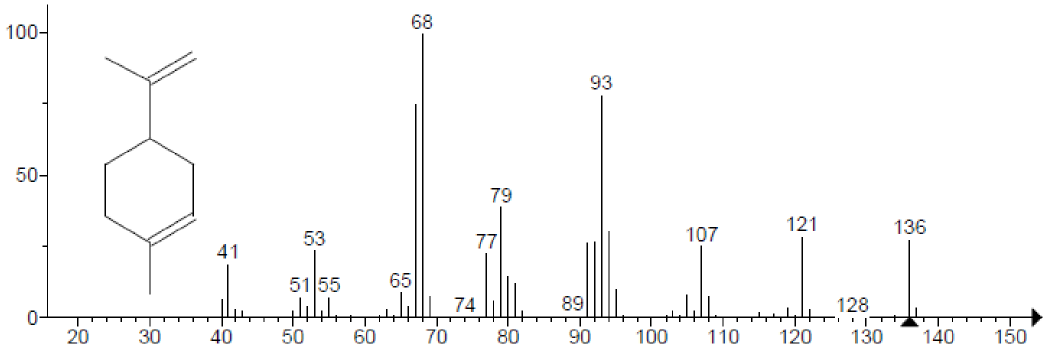

Figure 9-67: Mass spectrum of limonene corresponding to the peak at a retention time of 4.12 min of the chromatogram of Cinnamomum zeylanicum by Jean Pütz [169].

Hit 1 : Eucalyptol
C10H18O; MF: 938; RMF: 941; Prob 91.0%; CAS: 470-82-6; Lib: mainlib; ID: 9537.

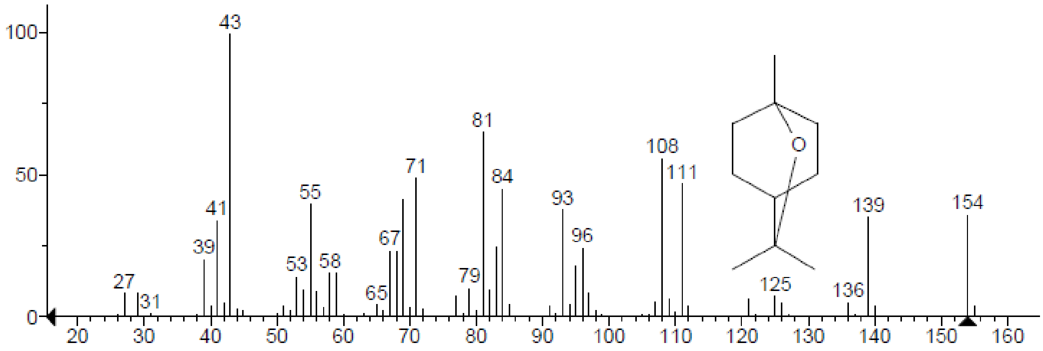

Figure 9-68: Mass spectrum of eucalyptol corresponding to the peak at a retention time of 4.16 min of the chromatogram of Cinnamomum zeylanicum by Jean Pütz [169].

Hit 1 : Linalool
C10H18O; MF: 924; RMF: 925; Prob 72.3%; CAS: 78-70-6; Lib: mainlib; ID: 39161.

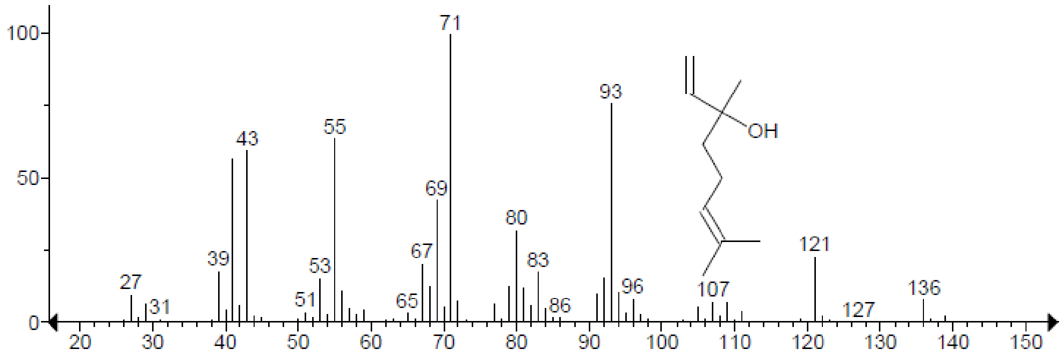

Figure 9-69: Mass spectrum of linalool corresponding to the peak at a retention time of 4.62 min of the chromatogram of Cinnamomum zeylanicum by Jean Pütz [169].

Hit 2 : Cinnamaldehyde, (E)-
C9H8O; MF: 952; RMF: 952; Prob 29.2%; CAS: 14371-10-9; Lib: replib; ID: 20946.

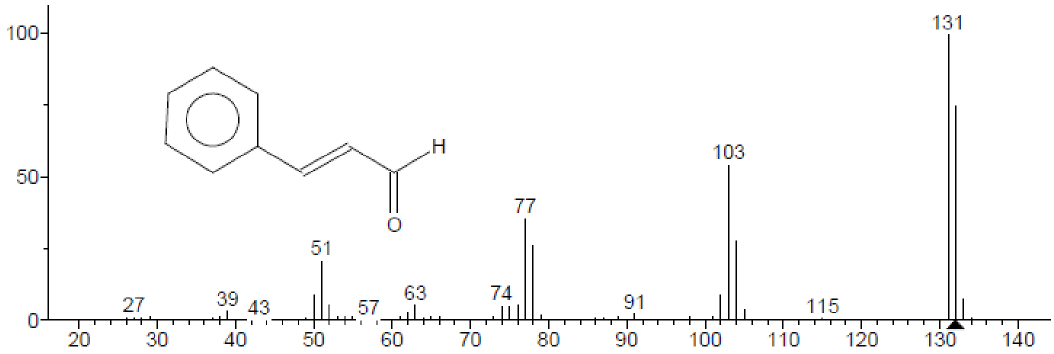

Figure 9-70: Mass spectrum of cinnamaldehyde corresponding to the peak at a retention time of 5.98 min of the chromatogram of Cinnamomum zeylanicum by Jean Pütz [169].

Hit 1 : Eugenol
C10H12O2; MF: 934; RMF: 934; Prob 31.1%; CAS: 97-53-0; Lib: mainlib; ID: 153183.

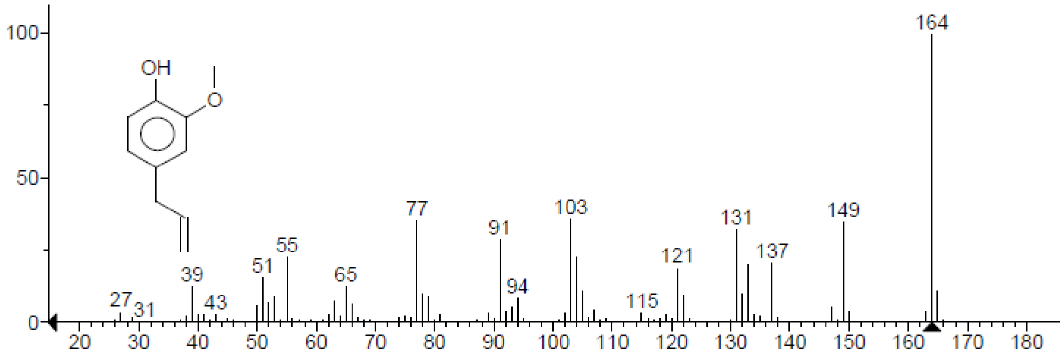

Figure 9-71: Mass spectrum of eugenol corresponding to the peak at a retention time of 6.51 min of the chromatogram of Cinnamomum zeylanicum by Jean Pütz [169].

Hit 1 : Caryophyllene
C15H24; MF: 953; RMF: 954; Prob 36.1%; CAS: 87-44-5; Lib: mainlib; ID: 66572.

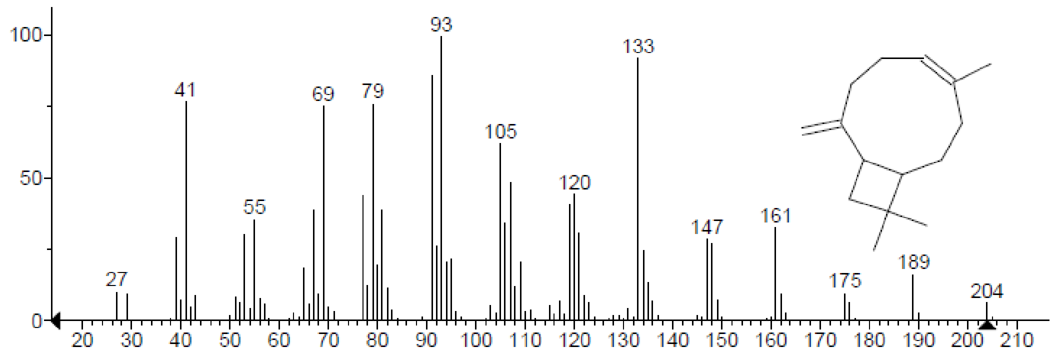

Figure 9-72: Mass spectrum of caryophyllene corresponding to the peak at a retention time of 7.05 min of the chromatogram of Cinnamomum zeylanicum by Jean Pütz [169].

Hit 1 : Acetic acid, cinnamyl ester
C11H12O2; MF: 933; RMF: 933; Prob 67.7%; CAS: 103-54-8; Lib: mainlib; ID: 11373.

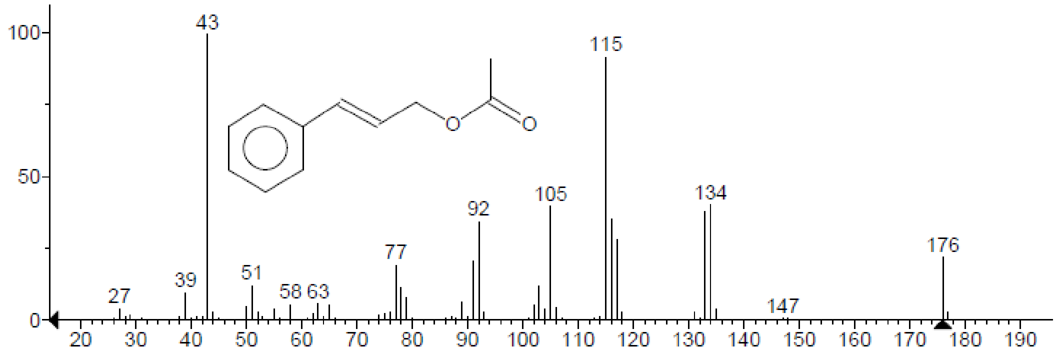

Figure 9-73: Mass spectrum of cinnamyl acetate corresponding to the peak at a retention time of 7.11 min of the chromatogram of Cinnamomum zeylanicum by Jean Pütz [169].

Hit 1 : Benzyl Benzoate
C14H12O2; MF: 929; RMF: 929; Prob 96.2%; CAS: 120-51-4; Lib: replib; ID: 16232.

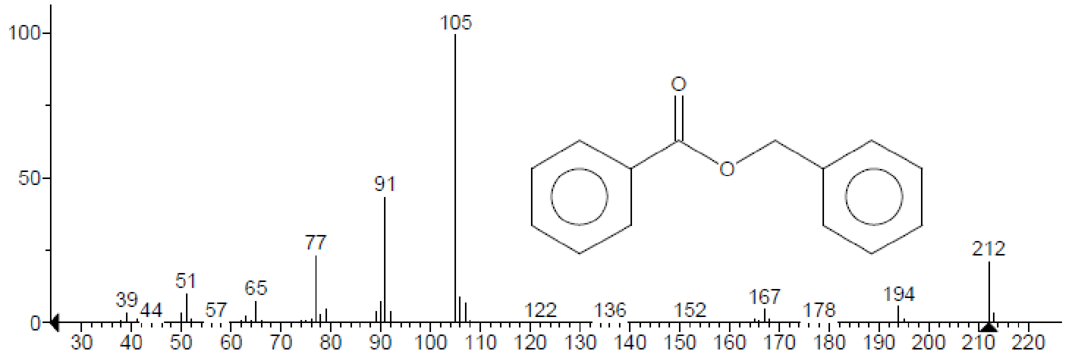

Figure 9-74: Mass spectrum of benzyl benzoate corresponding to the peak at a retention time of 9.10 min of the chromatogram of Cinnamomum zeylanicum by Jean Pütz [169].

9.6.5.4 Cinnamomum Verum Oil by PCW

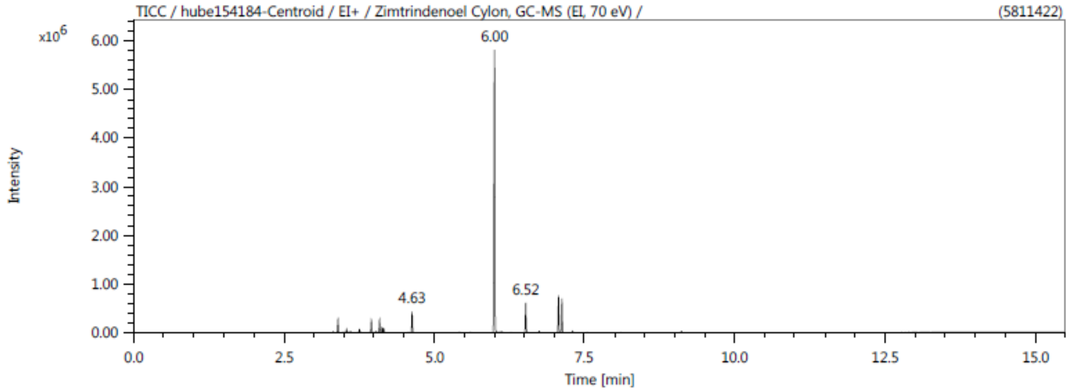

Figure 9-75: Chromatogram of the Cinnamomum verum oil by PCW [169].

Hit 1 : (1R)-2,6,6-Trimethylbicyclo[3.1.1]hept-2-ene
C10H16; MF: 917; RMF: 917; Prob 15.3%; CAS: 7785-70-8; Lib: mainlib; ID: 66241.

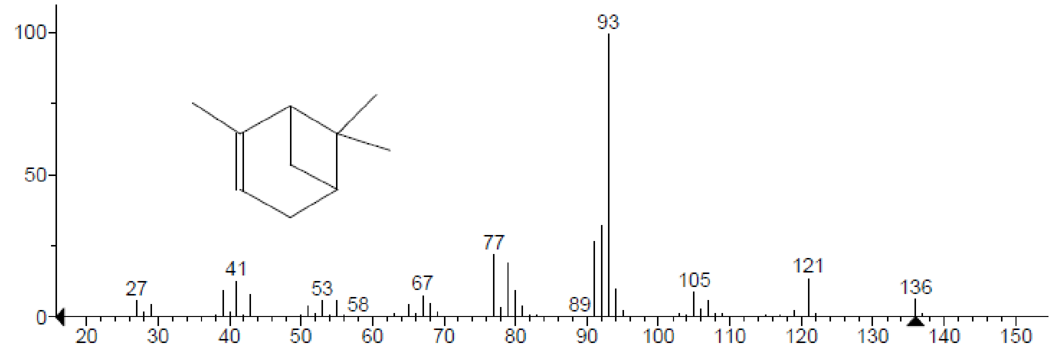

Figure 9-76: Mass spectrum of α-pinene corresponding to the peak at a retention time of 3.38 min of the chromatogram of Cinnamomum verum by PCW [169].

Hit 1 : Camphene
C10H16; MF: 894; RMF: 895; Prob 28.0%; CAS: 79-92-5; Lib: mainlib; ID: 66500.

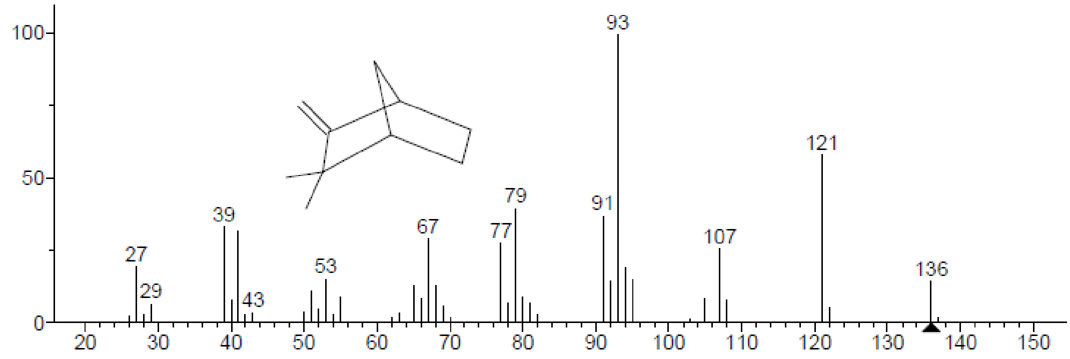

Figure 9-77: Mass spectrum of camphene corresponding to the peak at a retention time of 3.52 min of the chromatogram of Cinnamomum verum by PCW [169].

Hit 1 : β-Myrcene
C10H16; MF: 879; RMF: 886; Prob 28.5%; CAS: 123-35-3; Lib: replib; ID: 14068.

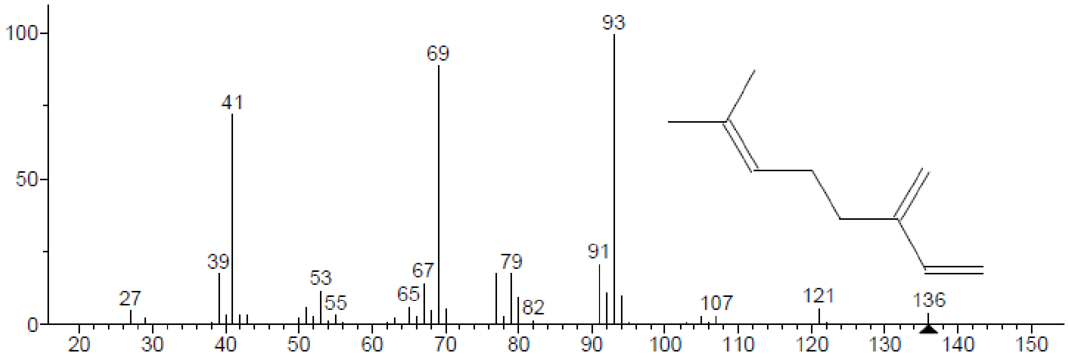

Figure 9-78: Mass spectrum of β-myrcene corresponding to the peak at a retention time of 3.75 min of the chromatogram of Cinnamomum verum by PCW [169].

Hit 1 : α-Phellandrene
C10H16; MF: 911; RMF: 914; Prob 50.2%; CAS: 99-83-2; Lib: replib; ID: 14115.

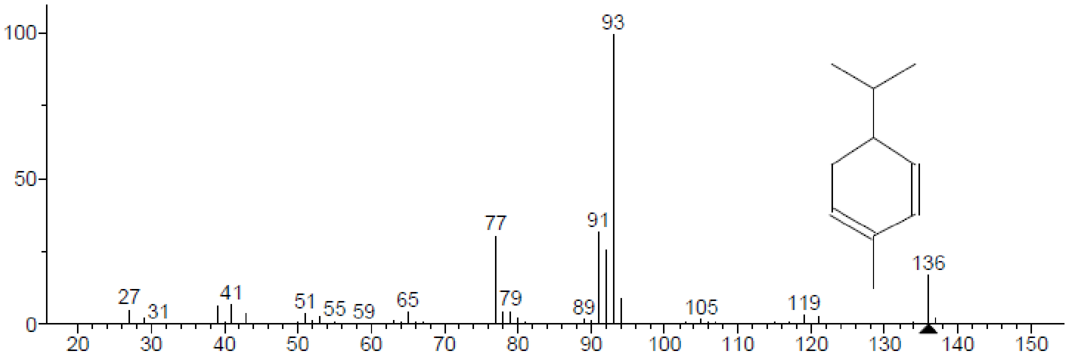

Figure 9-79: Mass spectrum of α-phellandrene corresponding to the peak at a retention time of 3.94 min of the chromatogram of Cinnamomum verum by PCW [169].

Hit 1 : o-Cymene
C10H14; MF: 935; RMF: 935; Prob 27.1%; CAS: 527-84-4; Lib: replib; ID: 18731.

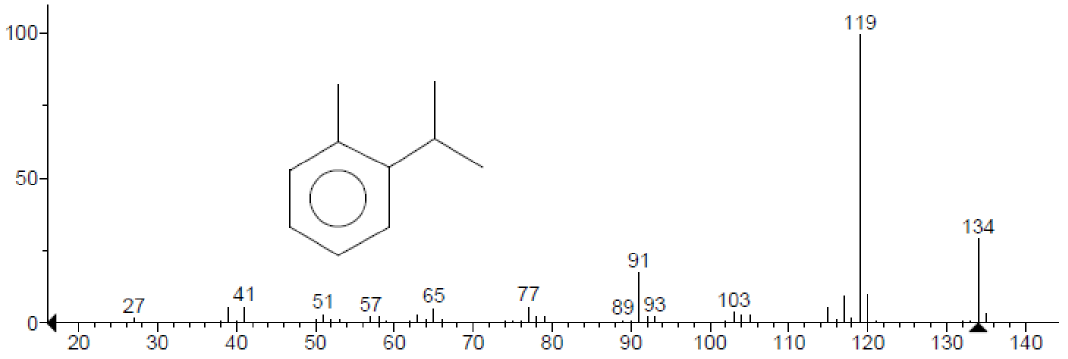

Figure 9-80: Mass spectrum of o-cymene corresponding to the peak at a retention time of 4.07 min of the chromatogram of Cinnamomum verum by PCW [169].

Hit 1 : D-Limonene
C10H16; MF: 923; RMF: 923; Prob 49.8%; CAS: 5989-27-5; Lib: replib; ID: 8354.

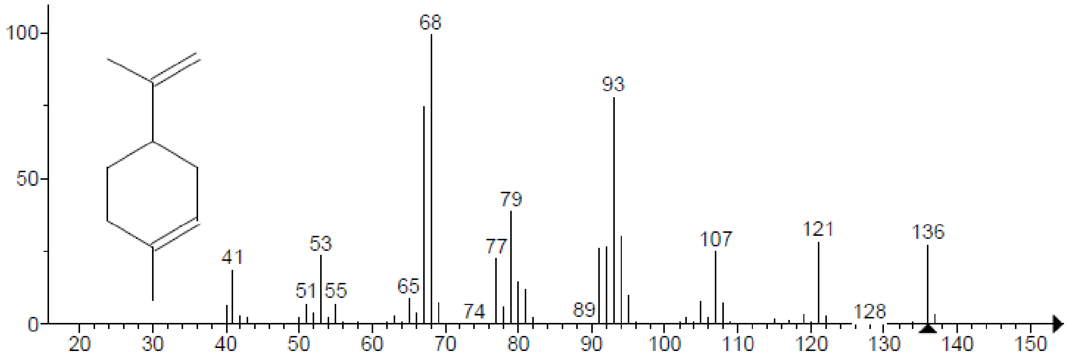

Figure 9-81: Mass spectrum of limonene corresponding to the peak at a retention time of 4.12 min of the chromatogram of Cinnamomum verum by PCW [169].

Hit 2 : β-Phellandrene
C10H16; MF: 925; RMF: 926; Prob 37.3%; CAS: 555-10-2; Lib: mainlib; ID: 66050.

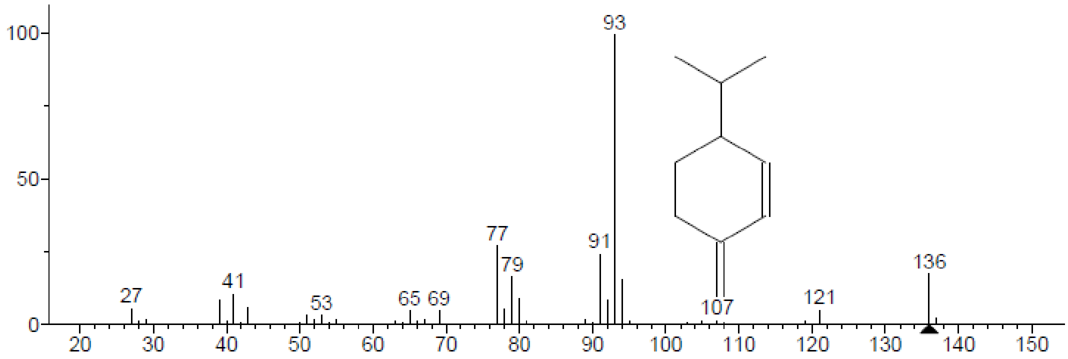

Figure 9-82: Mass spectrum of β-phellandrene corresponding to the peak at a retention time of 4.15 min of the chromatogram of Cinnamomum verum by PCW [169].

Hit 1 : Linalool
C10H18O; MF: 928; RMF: 928; Prob 75.3%; CAS: 78-70-6; Lib: mainlib; ID: 39161.

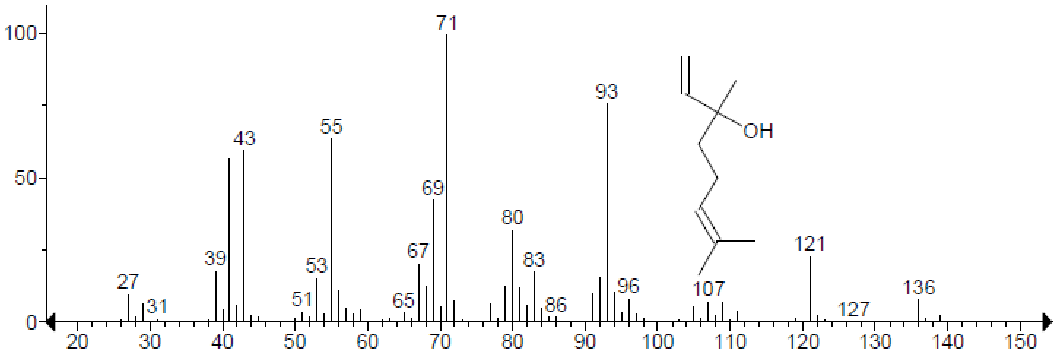

Figure 9-83: Mass spectrum of linalool corresponding to the peak at a retention time of 4.62 min of the chromatogram of Cinnamomum verum by PCW [169].

Hit 1 : 2-Propenal, 3-phenyl-
C9H8O; MF: 960; RMF: 960; Prob 35.8%; CAS: 104-55-2; Lib: mainlib; ID: 115882.

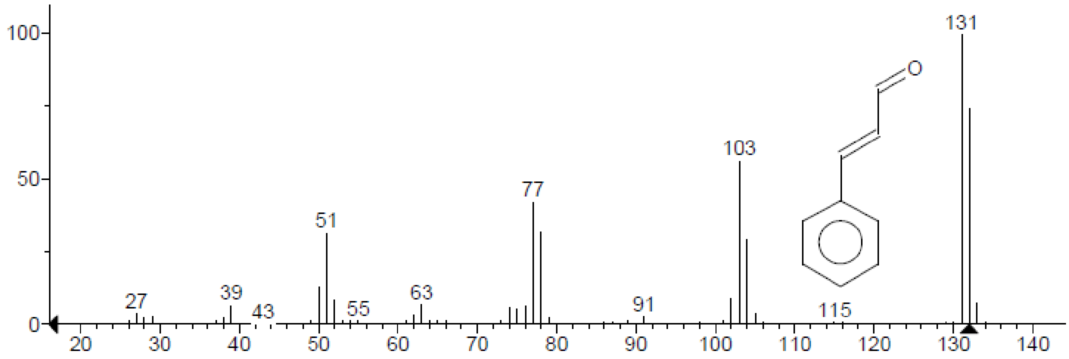

Figure 9-84: Mass spectrum of cinnamaldehyde corresponding to the peak at a retention time of 5.98 min of the chromatogram of Cinnamomum verum by PCW [169].

Hit 1 : Eugenol
C10H12O2; MF: 929; RMF: 929; Prob 26.4%; CAS: 97-53-0; Lib: replib; ID: 25335.

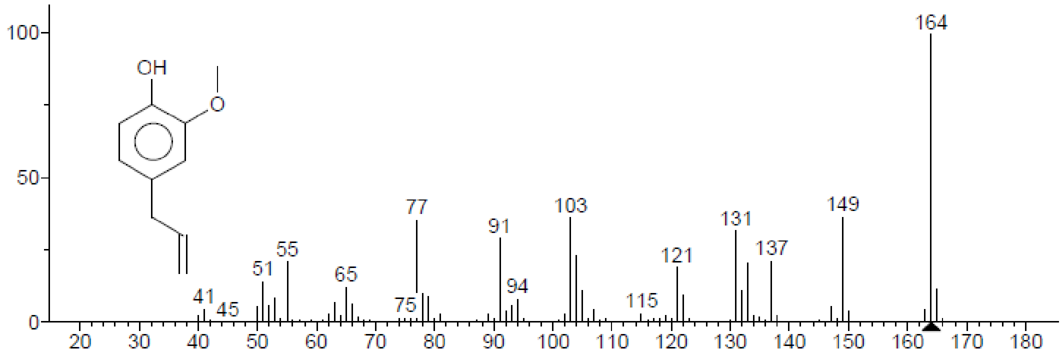

Figure 9-85: Mass spectrum of eugenol corresponding to the peak at a retention time of 6.51 min of the chromatogram of Cinnamomum verum by PCW [169].

Hit 1 : Caryophyllene
C15H24; MF: 963; RMF: 964; Prob 42.2%; CAS: 87-44-5; Lib: mainlib; ID: 66572.

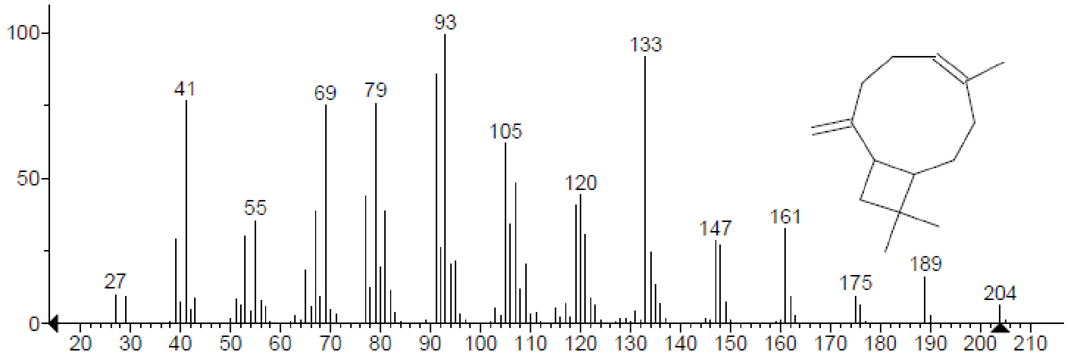

Figure 9-86: Mass spectrum of caryophyllene corresponding to the peak at a retention time of 7.05 min of the chromatogram of Cinnamomum verum by PCW [169].

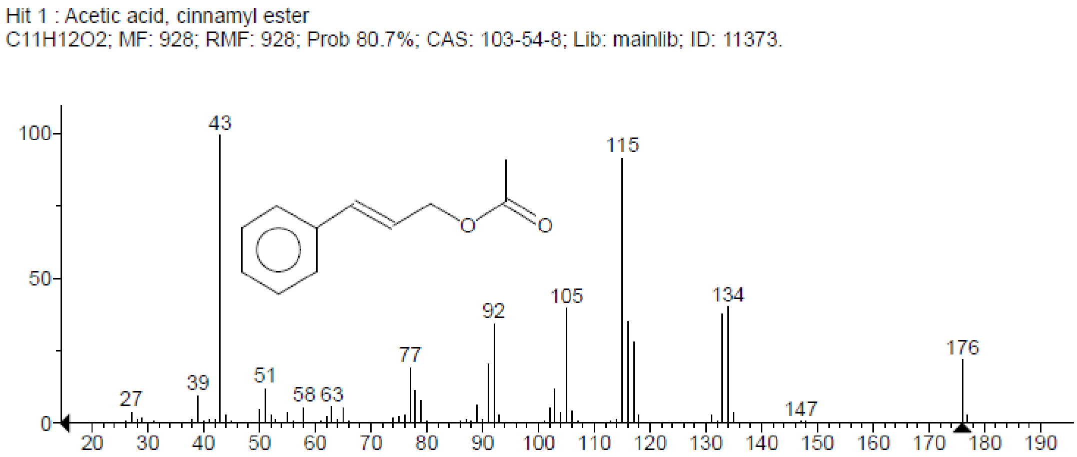

Figure 9-87: Mass spectrum of cinnamyl acetate corresponding to the peak at a retention time of 7.11 min of the chromatogram of Cinnamomum verum by PCW [169].

9.6.6 Characterization of the Ternary Phase Diagram

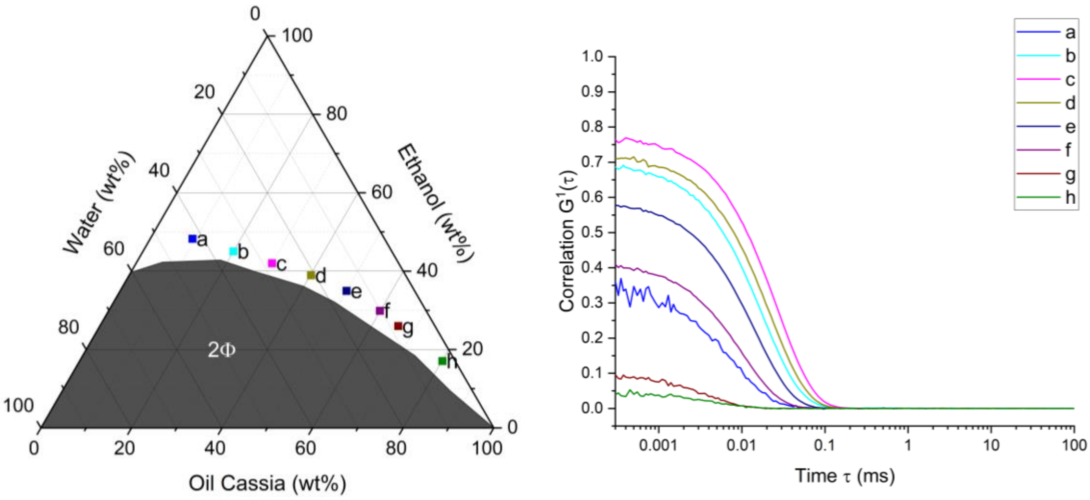

Figure 9-88: Ternary phase diagram of water/ethanol/oil cassia with corresponding correlation curves [169].

9.6.7 Calibration Curves of Curcumin in Ethanol and Acetone

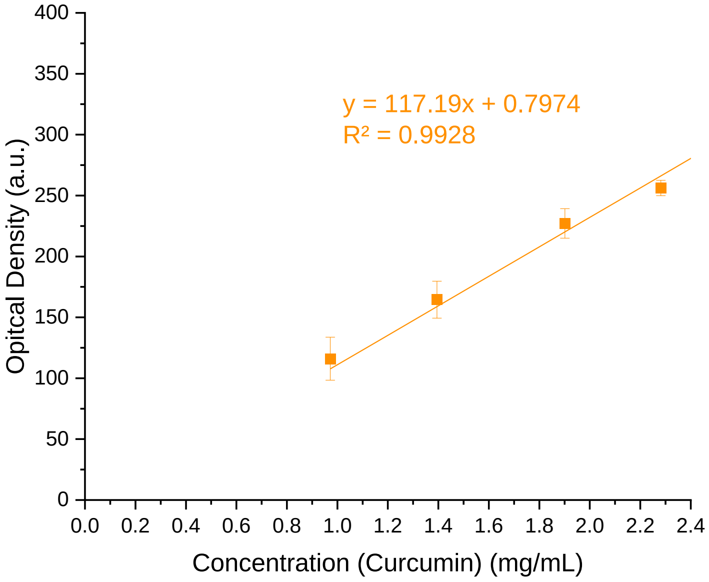

Figure 9-89: Calibration curve of curcumin in EtOH [169].

List of Figures

Figure 2-1: Overview of the two kinds of plant metabolites inspired by [22–24]. The primary metabolites (yellow) in the center are the basic molecules necessary for the functionality of organisms. They are the source materials from which the secondary metabolites (outer ring) can be synthesized. These secondary metabolites are divided into three groups: alkaloids (bright green; represented by caffeine, nicotine, and piperine), terpenes (dark green; represented by limonene, caryophyllene, and pinene), and phenolic compounds (blue; represented by quercetin, cinnamaldehyde, γ-irone, and curcumin. The last three can also be viewed in Section 9.1. 8

Figure 2-2: Laboratory diagram of a Soxhlet apparatus. The templates of the glassware were provided via ChemDraw 18.1 by PerkinElmer. 14

Figure 2-3: Typical phase diagram of a binary eutectic mixture of compounds A and B, with their single melting temperatures T_A and T_B and the eutectic melting temperature T_ε at the eutectic molar ratio [65,66,70]. 19

Figure 2-4: Electromagnetic spectrum with expanded visible (Vis) spectrum of 350-700 nm followed by the ultraviolet (UV) spectrum in a range of 200-350 nm. The picture was taken from Agilent [76]. 22

Figure 2-5: Model of a double beam photometer for optical density measurements. 24

Figure 2-6: Schematic set-up of an HPLC system. The picture was inspired by bionity.com [93]. 30

Figure 2-7: Schematic setup of a GC apparatus. The image was inspired by D. Hage [77]. 32

Figure 3-1: List of irone regioisomers. γ-irone is marked in bold as it is the molecule of interest throughout this study and the only irone present in the used cultivar. 42

Figure 3-2: Extraction yields of γ-irone in mg/g rhizome with different extraction solvents according to the process described in Section 3.2.2.1.1 Laboratory-Scale Pre-Tests. 48

Figure 3-3: Extraction results of the first screening of the molecular distillation. The purple bars indicate the relative mass of α-ionone that was extracted from the original matrix containing 0.2% of α-ionone and the green squares indicate the relative mass of α-ionone in the distillate. The dotted line represents the α-ionone content of 0.2% in the original matrix. 51

Figure 3-4: Extraction results of the molecular distillation screening using the technical mixture of irone isomers. The green and purple bars represent the relative amount of trans- and cis-α-irone extracted from the original matrix and the grey squares indicate the relative mass of the odoriphores in the distillate. The dotted line represents the odoriphore content (~ 0.1% of each, trans-α-irone and cis-α-irone) in the original matrix. 53

Figure 3-5: Comparison of the γ-irone content in the myristic acid matrix after different extraction steps, represented by the purple bars. The grey squares indicate the relative amount of γ-irone that was extracted from the source material, either the rhizomes (Extract) or the extracts (Distillation 1 and 2). 55

Figure 4-1: The three major curcuminoids, curcumin (top), demethoxycurcumin (middle), and bisdemethoxycurcumin (bottom). 62

Figure 4-2: Qualitative screening of the curcumin solubility in eleven different NADES/EtOH/TriA 50:20:30 (w/w/w) mixtures determined via UV/Vis. The references, the ternary mixture of water/EtOH/TriA at the same weight ratio of 50:20:30 as the former mixtures in black on the bottom, the optimum binary mixture of EtOH/TriA 40:60 (w/w) in red, and pure acetone in blue at the top, are represented by the horizontal lines [126]. 71

Figure 4-3: Ternary phase diagrams with curcumin solubility maps consisting of EtOH as the cosolvent, TriA as the oil phase, and the hydrophilic component a) ChCl+Lev, b) ChCl+Lac, and c) water. The black areas labeled 2Φ represent the two phasic regions of immiscibility in the ternary systems. The heat maps in the monophasic parts indicate the curcumin solubility, where red shows a high solubility and purple a low one. The color scale of a) can be applied to all diagrams. The yellow diamonds indicate the points examined in the extraction experiments. The critical and reminiscent critical points are represented by the turquoise points labeled CP and RPC respectively [70,126]. 73

Figure 4-4: Determination of the optimum powder to solvent ratio (w/w) in view of the extraction yield using the optimum composition of ChCl+Lac/EtOH/TriA 35:27.5:37.5 [70]. 78

Figure 4-5: Overview of the yield of all extraction experiments. Curcumin is presented in orange, demethoxycurcumin in blue, and bisdemethoxycurcumin in red. The results are separated into four blocks for clarity. The first block represents the conventional [47] and pressure-controlled [126] Soxhlet extractions, the second block the references of pure EtOH and TriA, their optimum binary mixture of 40:60, and the best ternary mixture of 40:24:36, which were provided by P. Degot et al. [47], the third the extraction results of the ternary ChCl+Lac/EtOH/TriA mixtures [70], and the fourth the extraction results of the ternary mixtures of ChCl+Lev/EtOH/TriA [126]. The numbers above the columns give the extraction yield in percent in comparison to the reference, which was the yield obtained via pressure controlled Soxhlet extraction. 79

Figure 4-6: Total curcuminoid content of the ternary cycle extraction systems of water/EtOH/TriA 40:24:36 (black squares) [48], ChCl+Lac/EtOH/TriA 35:27.5:37.5 (red dots) [70], and ChCl+Lev/EtOH/TriA 30:40:30 (triangles). The blue triangles represent the repeated extraction of fresh, ground rhizomes without additives. The green down-facing triangles show the extraction samples prepared with synthetic curcumin, the yellow left-facing triangles with a blend of synthetic curcumin and bisdemethoxycurcumin. Both systems were prepared to imitate a starting point at cycle 7 before performing one cycle of extraction [126]. 83

Figure 4-7: Conductivity measurements in the ChCl+Lev/EtOH/TriA system at the optimum composition (30:40:30) a) diluted with a binary EtOH/TriA 40:60 mixture and b) after multiple cycles of extraction [126]. 85

Figure 5-1: Assessment of the curcumin solubility in ethanolic solutions of a) choline chloride (black), b) betaine (red), c) carnitine (blue), and d) tetrapropylammonium bromide (green) [158]. 94

Figure 5-2: Conformationally averaged COSMO-RS predictions of a) σ-potentials and b) σ-profiles of curcumin (orange), and the QAs ChCl (black), Bet (red), Car (blue), and N_{3333}Br and its corresponding cation [99,100,103,158,160,161]. 98

Figure 5-3: Curcumin solubility in ethanolic solutions of a) lactic acid (red circles), b) levulinic acid (blue triangles), and c) pyruvic acid (green down-facing triangles). The solubility of curcumin in solutions with 2-oxobutyric acid (yellow left-facing triangles), 2-oxovaleric acid (turquoise right-facing triangles), 4-acetylbutyric acid (brown hexagons), were examined as well as the references hexanoic acid (beige stars) and triacetin (orange pentagons) [158]. The solubility data of TriA was provided by P. Degot et al. [47]. The rest of the structures can be viewed in Table 9-2 of the Appendix. 99

Figure 5-4: Prediction of the chemical potential concerning the solubility of curcumin in mixtures of ethanol with lactic acid (red circles), levulinic acid (blue triangles), pyruvic acid (green down-facing triangles), triacetin (orange pentagons), and diacetyl (bright blue left-facing triangles) [158]. 101

Figure 5-5: Predicted chemical potential of curcumin in ethanolic solutions of a) levulinic acid and b) pyruvic acid depending on the molecules’ conformations. The worst and best conformations according to COSMO-RS are represented by the given structures. The weighted average of all conformations in solution is signified by the bright blue curves [158]. 102

Figure 5-6: Overlaid NOESY spectra of curcumin/Lev 1:1 (n/n) (blue/green), curcumin (pink), and Lev (purple) in DMSO-d_6 [158]................................ 104

Figure 5-7: Curcumin solubility in mixtures of a) choline chloride-, b) betaine-, and c) carnitine-based NADES in dependence of the quaternary ammonium compound content in wt%. The red circles indicate the NADES containing lactic acid, the blue triangles levulinic acid, and the green down-facing triangles pyruvic acid [158]. The black squares represent the pure QAs as shown in Figure 5-1.. 106

Figure 6-1: Molecular structure of cinnamaldehyde. 114

Figure 6-2: UV/Vis (a) and COSMO-RS (b) examination of the solubility and chemical potential of curcumin in ethanolic solutions of natural flavors (n/n) respectively. Cinnamaldehyde is presented by brown squares, benzaldehyde by purple circles, citral by orange triangles, trans-anethole by red down-facing triangles, benzyl benzoate by green diamonds, and limonene by blue left-facing triangles [169]. 119

Figure 6-3: UV/Vis (a) and COSMO-RS (b) examination of the solubility and chemical potential of curcumin in ethanolic solutions of natural flavors (n/n) respectively. Cinnamaldehyde is presented by brown squares, cinnamyl acetate by marron circles, 3-phenylpropyl acetate by orange triangles, α-hexyl cinnamaldehyde by golden down-facing triangles, and hydrocinnamaldehyde by yellow diamonds [169]. 121

Figure 6-4: Comparison of the curcumin solubility in ethanolic solutions of the cinnamon oils, Cinnamomum cassia oil by PCW (yellow circles), Cinnamomum zeylanicum by Jean Pütz (blue triangles), and Cinnamomum verum (green down-facing triangles), with cinnamaldehyde (brown squares) as a reference [169]. 124

Figure 6-5: Ternary phase diagram of water, ethanol, and Cinnamomum Cassia oil (PCW). The heat map of the monophasic domain shows the solubility of curcumin with red indicating a high solubility, while purple shows a low one. The black area labelled 2Φ identifies the miscibility gap and the critical point of the mixture is signified by the turquoise circle labeled CP [169]. 126

Figure 6-6: Absorbance of curcuminoid extracts in water/EtOH/oil cassia (black squares), water/EtOH/TriA (red circles) [48], and ChCl+Lev/EtOH/TriA (blue triangles) [126] after several cycles of extraction [169]. The references in red and blue given by P. Degot and V. Huber et al. were determined according to the calibration curve given in Figure 9-89 of the Appendix. 128

Figure 9-1: GC-FID chromatogram of the technical irone mixture by Sigma Aldrich (Darmstadt, Germany). 163

Figure 9-2: Curcumin solubility in a binary mixture of ChCl and ChCl+Lac with water. The scaling on the y-axis does not correspond to the scaling in the main text. The values were calculated as if the samples had not been diluted instead of applying the 1:5000 dilution factor which would make the results unreadable [70]. 165

Figure 9-3: a) Ternary phase diagram of ChCl+Lev/EtOH/TriA with the ternary and binary points examined via DLS and b) correlation curves in the ternary system ChCl+Lev/EtOH/TriA close above the two-phasic region [126]. 166

Figure 9-4: a) Ternary phase diagram of ChCl+Lac/EtOH/TriA with the ternary and binary points examined via DLS and b) correlation curves in the ternary system ChCl+Lac/EtOH/TriA close above the two-phasic region [126]. 166

Figure 9-5: a) Ternary phase diagram of H_2O/EtOH/TriA with the ternary and binary points examined via DLS and b) correlation curves in the ternary system H_2O/EtOH/TriA close above the two-phasic region [126]. 166

Figure 9-6: Correlation curves in the binary system ChCl+Lev/EtOH. The respective points can be viewed in Figure 9-3 [126]. 167

Figure 9-7: Correlation curves in the binary system ChCl+Lac/EtOH. The respective points can be viewed in Figure 9-4 [126]. 167

Figure 9-8: Correlation curves in the binary system EtOH/TriA. The respective points can be viewed in Figure 9-5. The data were provided by P. Degot et al.[47]. 167

Figure 9-9: Temperature-dependent phase diagram of the binary mixture of EtOH/TriA with LLE points at -20 °C and -30 °C, contextualized within the ternary phase diagram at 25 °C. No LLE points were found at -20 °C but at -30 °C there were. The hatched area in the binary phase diagram is a representation of the uncertain area in which the phase transition should occur [126]. 168

Figure 9-10: Calibration curve in acetonitrile of curcumin (orange square), demethoxycurcumin (red dot), and bisdemethoxycurcumin (blue triangle) obtained by HPLC using an ACE Equivalent 3 C18-Column (300 Å, 150 × 2.1 mm), plotting the concentration in mg per mL against the peak area [186]. 168

Figure 9-11: Calibration curves of curcumin (orange square), demethoxycurcumin (blue circle), and bisdemethoxycurcumin (red triangle) obtained by elution via HPLC using a Knauer Eurospher 5 C18-Column (100 Å, 250 × 4.6 mm) [126]. The concentration in mg per mL is plotted against the peak area. 169

Figure 9-12: Curcuminoid cycle extraction in the system ChCl+Lac/EtOH/TriA 35:27.5:37.5 with the reference being cycle 4 of the water/EtOH/TriA 40:24:26 system as provided by P. Degot et al. [48,70]. 170

Figure 9-13: Curcuminoid cycle extraction of the ChCl+Lev/EtOH/TriA 30:40:30 system with the reference being cycle 7 of the system ChCl+Lac/EtOH/TriA 35:27.5:37.5 as provided by V. Huber et al. [70,126]. 171

Figure 9-14: Curcuminoid concentration in mg/g solvent after 7, 10, and 12 extraction cycles. The grey squares represent the amount of solvent remaining after every cycle [126]. 171

Figure 9-15: ^{13}C-NMR spectrum of the ternary extraction solvent of ChCl+Lev/EtOH/TriA (30:40:30) in weight fresh after preparation [126]. . 172

Figure 9-16: ^{13}C-NMR spectrum of the ternary extraction solvent of ChCl+Lev/EtOH/TriA (30:40:30) in weight one day after preparation [126]. 172

Figure 9-17: ^{13}C-NMR spectrum of the ternary extraction solvent of ChCl+Lev/EtOH/TriA (30:40:30) in weight three days after preparation [126]. 173

Figure 9-18: Solubility of curcumin in ethanolic solutions in mol% of choline chloride (grey), betaine (red), carnitine (blue), and tetrapropylammonium bromide (green) [158]. 174

Figure 9-19: ^{1}H-NMR of curcumin in DMSO-d_6 [158]. 175

Figure 9-20: ^{1}H-NMR of curcumin in methanol-d_4 [158]. 175

Figure 9-21: ^{1}H-NMR of curcumin and choline chloride (1:1 n/n) in DMSO-d_6 [158]. 176

Figure 9-22: ^{1}H-NMR of curcumin and choline chloride saturated in methanol-d_4 [158]. 177

Figure 9-23: ^{1}H-NMR of betaine in DMSO-d_6 [158]. 178

Figure 9-24: ^{1}H-NMR of curcumin and betaine (1:1 n/n) in DMSO-d_6 [158]. 178

Figure 9-25: ^{1}H-NMR of carnitine in DMSO-d_6 [158]. 179

Figure 9-26: ^{1}H-NMR of curcumin and carnitine (1:1 n/n) in DMSO-d_6 [158]. 179

Figure 9-27: ^{1}H-NMR of N_{3333}Br in DMSO-d_6 [158]. 180

Figure 9-28: ^{1}H-NMR of curcumin and tetrapropylammonium bromine (1:1 n/n) in DMSO-d_6 [158]. 180

Figure 9-29: ^{1}H-NMR of levulinic acid in DMSO-d_6 [158]. 181

Figure 9-30: ^{1}H-NMR of curcumin and levulinic acid (1:1 n/n) in DMSO-d_6 [158]. 181

Figure 9-31: ^{1}H-NMR of lactic acid in DMSO-d_6 [158]... 182

Figure 9-32: ^{1}H-NMR of pyruvic acid in DMSO-d_6 [158]. 182

Figure 9-33: Determination of the keto-enol-ratio of curcumin in DMSO-d_6 [158]. 183

Figure 9-34: Determination of the keto-enol-ratio of curcumin in methanol-d_4 [158]. 183

Figure 9-35: Determination of the keto-enol-ratio of curcumin with choline chloride as an additive in DMSO-d_6 [158]. 184

Figure 9-36: Determination of the keto-enol-ratio of curcumin with choline chloride as an additive in methanol-d_4 [158]. 184

Figure 9-37: NOESY spectrum of curcumin and ChCl 1:1 (n/n) (blue/green), curcumin (pink), and ChCl (purple) in DMSO-d_6 [158]... 185

Figure 9-38: NOESY spectrum of curcumin and ChCl 1:1 (n/n) (blue/green) and curcumin (pink/red) in methanol-d_4 [158]. 185

Figure 9-39: NOESY spectrum of curcumin and Bet 1:1 (n/n) (blue/green), curcumin (pink), and Bet (purple) DMSO-d_6 [158]... 186

Figure 9-40: NOESY spectrum of curcumin and Car 1:1 (n/n) (blue/green), curcumin (pink), and Car (purple) DMSO-d_6 [158]. 186

Figure 9-41: NOESY spectrum of curcumin and N_{3333}Br 1:1 (n/n) (blue/green), curcumin (pink), and N_{3333}Br (purple) DMSO-d_6 [158]. 187

Figure 9-42: Solubility of curcumin in ethanolic solutions in mol% of lactic acid (red squares), levulinic acid (blue circles), pyruvic acid (green up-facing triangles), 2-oxobutyric acid (yellow diamonds), 2-oxovaleric acid (turquoise left-facing triangles), and 4-acetylbutyric acid (brown right-facing triangles), with references hexanoic acid (beige hexagons) and triacetin (orange stars). The solubilities in pure TriA, Lac, Lev, and Pyr are depicted as well [158]. 187

Figure 9-43: Hansen space surrounding curcumin in the enol form [158]. 188

Figure 9-44: Chemical potential of the cyclic conformations of levulinic acid (blue triangles) and pyruvic acid (green down-facing triangles) as predicted via COSMO-RS calculations [158]. 189

Figure 9-45: Curcumin solubility in mixtures of a) lactic acid, b) levulinic acid, and c) pyruvic acid-based NADES depending on the acid content in wt% where the grey squares represent the choline chloride NADES, the red dots betaine NADES, and the blue triangles the carnitine NADES [158]. 190

Figure 9-46: UV/Vis examination of the solubility of curcumin in ethanolic solutions of natural flavors (w/w). Cinnamaldehyde is presented by brown squares, benzaldehyde by purple circles, citral by orange triangles, trans-anethole by red down-facing triangles, benzyl benzoate by green diamonds, and limonene by blue left-facing triangles [169]. 191

Figure 9-47: ^{1}H NMR spectrum of curcumin in MeOD [169]. 192

Figure 9-48: ^{1}H NMR of curcumin in cinnamaldehyde and MeOD at a ratio of 30:70 (n/n). The protons of curcumin are assigned at the top and the ones of Cin on the bottom [169]. 193

Figure 9-49: ^{1}H NMR spectrum of curcumin in hydrocinnamaldehyde and MeOD at a ratio of 30:70 (n/n). The protons of curcumin are assigned at the top and the ones of HCi on the bottom [169]. 194

Figure 9-50: NOESY NMR of curcumin in cinnamaldehyde and MeOD at a ratio of 30:70 (n/n) [169]. 195

Figure 9-51: NOESY NMR of curcumin in hydrocinnamaldehyde and MeOD at a ratio of 30:70 (n/n) [169]. 195

Figure 9-52: UV/Vis examination of curcumin in ethanolic solutions of natural flavors (w/w). Cinnamaldehyde is presented by brown squares, cinnamyl acetate by marron circles, 3-phenylpropyl acetate by orange triangles, α-hexyl cinnamaldehyde by golden down-facing triangles, and hydrocinnamaldehyde by yellow diamonds [169]. 196

Figure 9-53: Chromatogram of the pure, synthetic cinnamaldehyde as obtained via GC-FID [169]. 197

Figure 9-54: Chromatogram of Cinnamomum cassia oil by PCW as obtained via GC-FID [169]. 198

Figure 9-55: Chromatogram of Cinnamomum zeylanicum oil by Jean Pütz as obtained via GC-FID [169]........ 199

Figure 9-56: Chromatogram of Cinnamomum verum oil by PCW as obtained via GC-FID [169]. 200

Figure 9-57: Chromatogram of cinnamaldehyde as obtained by GC-MS [169]...... 202

Figure 9-58: Mass spectrum of cinnamaldehyde corresponding to the peak at a retention time of 5.98 min of the chromatogram of pure, synthetic cinnamaldehyde [169]........ 202

Figure 9-59: Chromatogram of the Cinnamomum cassia oil by PCW as obtained by GC-MS [169]. 202

Figure 9-60: Mass spectrum of benzaldehyde corresponding to the peak at a retention time of 3.59 min of the chromatogram of Cinnamomum cassia by PCW [169]. 203

Figure 9-61: Mass spectrum of cinnamaldehyde corresponding to the peak at a retention time of 5.98 min of the chromatogram of Cinnamomum cassia by PCW [169]. 203

Figure 9-62: Mass spectrum of cinnamyl acetate corresponding to the peak at a retention time of 7.11 min of the chromatogram of Cinnamomum cassia by PCW [169]. 203

Figure 9-63: Mass spectrum of coumarin corresponding to the peak at a retention time of 7.1 min of the chromatogram of Cinnamomum cassia by PCW [169]. ... 204

Figure 9-64: Mass spectrum of 2-methoxycinnamaldehyde corresponding to the peak at a retention time of 7.67 min of the chromatogram of Cinnamomum cassia by PCW [169]. 204

Figure 9-65: Chromatogram of the Cinnamomum verum – zeylanicum oil by Jean Pütz as obtained by GC-MS [169]. 204

Figure 9-66: Mass spectrum of o-cymene corresponding to the peak at a retention time of 4.0 min of the chromatogram of Cinnamomum zeylanicum by Jean Pütz [169]. 205

Figure 9-67: Mass spectrum of limonene corresponding to the peak at a retention time of 4.12 min of the chromatogram of Cinnamomum zeylanicum by Jean Pütz [169]. 205

Figure 9-68: Mass spectrum of eucalyptol corresponding to the peak at a retention time of 4.16 min of the chromatogram of Cinnamomum zeylanicum by Jean Pütz [169]. 205

Figure 9-69: Mass spectrum of linalool corresponding to the peak at a retention time of 4.62 min of the chromatogram of Cinnamomum zeylanicum by Jean Pütz [169]. 206

Figure 9-70: Mass spectrum of cinnamaldehyde corresponding to the peak at a retention time of 5.98 min of the chromatogram of Cinnamomum zeylanicum by Jean Pütz [169]. 206

Figure 9-71: Mass spectrum of eugenol corresponding to the peak at a retention time of 6.51 min of the chromatogram of Cinnamomum zeylanicum by Jean Pütz [169]. 206

Figure 9-72: Mass spectrum of caryophyllene corresponding to the peak at a retention time of 7.05 min of the chromatogram of Cinnamomum zeylanicum by Jean Pütz [169]. 207

Figure 9-73: Mass spectrum of cinnamyl acetate corresponding to the peak at a retention time of 7.11 min of the chromatogram of Cinnamomum zeylanicum by Jean Pütz [169]. 207

Figure 9-74: Mass spectrum of benzyl benzoate corresponding to the peak at a retention time of 9.10 min of the chromatogram of Cinnamomum zeylanicum by Jean Pütz [169]. 207

Figure 9-75: Chromatogram of the Cinnamomum verum oil by PCW [169]. 208

Figure 9-76: Mass spectrum of α-pinene corresponding to the peak at a retention time of 3.38 min of the chromatogram of Cinnamomum verum by PCW [169]. 208

Figure 9-77: Mass spectrum of camphene corresponding to the peak at a retention time of 3.52 min of the chromatogram of Cinnamomum verum by PCW [169].. 208

Figure 9-78: Mass spectrum of β-myrcene corresponding to the peak at a retention time of 3.75 min of the chromatogram of Cinnamomum verum by PCW [169]. 209

Figure 9-79: Mass spectrum of α-phellandrene corresponding to the peak at a retention time of 3.94 min of the chromatogram of Cinnamomum verum by PCW [169]. 209

Figure 9-80: Mass spectrum of o-cymene corresponding to the peak at a retention time of 4.07 min of the chromatogram of Cinnamomum verum by PCW [169].. 209

Figure 9-81: Mass spectrum of limonene corresponding to the peak at a retention time of 4.12 min of the chromatogram of Cinnamomum verum by PCW [169].. 210

Figure 9-82: Mass spectrum of β-phellandrene corresponding to the peak at a retention time of 4.15 min of the chromatogram of Cinnamomum verum by PCW [169]. 210

Figure 9-83: Mass spectrum of linalool corresponding to the peak at a retention time of 4.62 min of the chromatogram of Cinnamomum verum by PCW [169].. 210

Figure 9-84: Mass spectrum of cinnamaldehyde corresponding to the peak at a retention time of 5.98 min of the chromatogram of Cinnamomum verum by PCW [169]. 211

Figure 9-85: Mass spectrum of eugenol corresponding to the peak at a retention time of 6.51 min of the chromatogram of Cinnamomum verum by PCW [169].. 211

Figure 9-86: Mass spectrum of caryophyllene corresponding to the peak at a retention time of 7.05 min of the chromatogram of Cinnamomum verum by PCW [169]. 211

Figure 9-87: Mass spectrum of cinnamyl acetate corresponding to the peak at a retention time of 7.11 min of the chromatogram of Cinnamomum verum by PCW [169]. 212

Figure 9-88: Ternary phase diagram of water/ethanol/oil cassia with corresponding correlation curves [169]. 212

Figure 9-89: Calibration curve of curcumin in EtOH [169]. 213

List of Tables

Table 2-1: Overview of various extraction techniques, conventional and nonconventional [2–4,29,36,41–44]. 16

Table 3-1: Chemicals used in Section 3. 44

Table 3-2: Distillation conditions tested for the screening. 46

Table 4-1: Chemicals used in Section 4. 63

Table 4-2: HPLC gradient method. 68

Table 4-3: Comparison of extraction yield and PMI. 81

Table 5-1: Chemicals used in Section 5. 92

Table 5-2: Change of the chemical shift of curcumin depending on the additives. The shift changes of the outer hydroxy groups are marked in red and the shift changes of the enol hydroxy group are in blue. 97

Table 5-3: Examined NADES with their molar ratio and water content in weight percent. 105

Table 6-1: Chemicals used in Section 6. 115

Table 6-2: Chemical shift of curcumin's hydrogen atoms (the assignment of the protons can be seen in Figures 9-47 to 9-49 of the Appendix)in methanol-*d4* mixed with the aroma, either Cin or HCi, in a ratio of 70:30 (*n/n*). An upfield shift of the signals is marked in blue, while a downfield shift is signified in red. 122

Table 9-1: Chemicals of Section 3 with their corresponding abbreviations and structures. 157

Table 9-2: Chemicals of Sections 4 and 5 with their corresponding abbreviations and structures. 157

Table 9-3: Chemicals of Section 6 with their corresponding abbreviations and structures. 159

Table 9-4: Characterizing differences and similarities of ionic liquids and deep eutectic solvents. Inspired by Y. Liu et al. [72,73]. 162

Table 9-5: Assignment of the peaks, found in the chromatogram depicted in Figure 9-1. 163

Table 9-6: Clausius-Clapeyron Calculations of α-ionone, α-irone, and γ-irone at 120 °C, 123 °C, and 126 °C. The bold values corresponding to α-ionone were used as the starting point of the screening and the ones corresponding to γ-irone were used to distillate the real sample in Section 3.3.2. 164

Table 9-7: Relative distilled amount of γ-irone after different distillation steps compared to the respective extraction yield. 164

Table 9-8: Extraction yields of the curcuminoids in mg/g...................................... 169

Table 9-9: Ratio of the enol conformation of curcumin [148]................................ 184

Table 9-10: Hansen Solubility Parameters and corresponding distance to curcumin in the 3D Hansen Space [148]. 188

Table 9-11: Retention time of Cinnamaldehyde and purity as determined via GC-FID. 200

Table 9-12: Retention time of all analyzable ingredients of the different cinnamon oils as assessed via GC-MS. 201

Scientific Contributions

Poster Presentations

May 2021	Huber, V.; Muller, L.; Degot, P.; Touraud, D.; Kunz, W. *NADES-based surfactant-free microemulsions for solubilization and extraction of curcumin from Curcuma Longa*, **Multi-Scale Modelling & Physical Chemistry of Colloids – Bunsen Tagung.** Regensburg 2021.
September 2021	Huber, V.; Muller, L.; Degot, P.; Touraud, D.; Kunz, W. *NADES-based surfactant-free microemulsions for solubilization and extraction of curcumin from Curcuma Longa*, **35th Conference of the European Colloid & Interface Society – ECIS.** Athens 2021.

Oral Presentations

November 2021	Huber, V.; Muller, L.; Degot, P.; Touraud, D.; Kunz, W. *NADES-based surfactant-free microemulsions for solubilization and extraction of curcumin from Curcuma Longa*, **7th International Conference on Food Chemistry & Technology – FCT.** Paris 2021.
May 2022	Huber, V.; Muller, L.; Degot, P.; Touraud, D.; Kunz, W. *NADES-based surfactant-free microemulsions for solubilization and extraction of curcumin from Curcuma Longa*, **Jahrestreffen der ProcessNet-Fachgruppen Extraktion, Phytoextrakte und Membrantechnik.** Frankfurt am Main 2022.

Publications

1. El Maangar, A.; Degot, P.; Huber, V.; Berthault, P.; Diat, O.; Touraud, D.; Zemb, T.; Kunz, W. *Pre-nucleation cluster formation upon ethyl acetate addition to a non-co-solvent anionic hydrotrope.* J Mol Liq. 310 (2020) 113240. https://doi.org/10.1016/j.molliq.2020.113240.
2. Degot, P.; Huber, V.; Hofmann, E.; Touraud, D.; Kunz, W. *Solubilization and Extraction of Curcumin from Curcuma Longa using green, sustainable, and food-approved SFMEs.* J Food Chem. 336 (2021) 127660. https://doi.org/10.1016/j.foodchem.2020.127660.
3. Degot, P.; Huber, V.; Touraud, D.; Kunz, W. *Curcumin extracts from Curcuma Longa – Improvement of concentration, purity, and stability in food-approved and water-soluble surfactant-free microemulsions*. J Food Chem. 339 (2021) 128140. https://doi.org/10.1016/j.foodchem.2020.128140.
4. Huber, V.; Häckl, K.; Touraud, D.; Kunz, W. *Natural Deep Eutectic Solvents: from simple systems to complex colloidal mixtures*. Advances in Botanical Research: Eutectic Solvents and Stress in Plants Volume 97 (2020), p. 17-39. https://doi.org/10.1016/bs.abr.2020.09.001.
5. Degot, P.; Huber, V.; El Maangar, A.; Gramüller, J.; Rohr, L.; Touraud, D.; Gschwind, R. M.; Zemb, T.; Kunz, W. *Triple role of sodium salicylate in solubilization, extraction, and stabilization of curcumin from Curcuma Longa*. J Mol Liq. 329 (2021) 115538. https://doi.org/10.1016/j.molliq.2021.115538.
6. Degot, P.; Funkner, D.; Huber, V.; Köglmaier, M., Touraud, D.; Kunz, W. *Extraction of curcumin from Curcuma Longa using meglumine and pyroglutamic acid, respectively, as solubilizer and hydrotrope*. J Mol Liqu. 334 (2021) 116478. https://doi.org/10.1016/j.molliq.2021.116478.
7. Huber, V.; Muller, L.; Degot, P.; Touraud, D.; Kunz, W. *NADES-based surfactant-free microemulsions for solubilization and extraction of curcumin from Curcuma Longa.* J FoodChem. 355 (2021) 129624. https://doi.org/10.1016/j.foodchem.2021.129624.
8. Huber, V.; Muller, L.; Hioe, J.; Degot, P.; Touraud, D.; Kunz, W. *Improvement of the Solubilization and Extraction of Curcumin 2 in an Edible Ternary Solvent Mixture.* Molecules. Recent Advances in Eco-Friendly Deep Eutectic Solvents Research: Synthesis, Properties and Applications 26 (2021) 7702. https://doi.org/10.3390/molecules26247702.

9. Benkert, C.; Freyburger, A.; Huber, V.; Touraud, D.; Kunz, W. *Development of a Fully Water-Dilutable Mint Concentrate Based on a Food-Approved Microemulsion.* J FoodChem 372 (2022) 131230. https://doi.org/10.1016/j.foodchem.2021.131230.
10. Huber, V.; Degot, P.; Touraud, D.; Kunz, W. *Comment on "Impact of Conventional and Sustainable Solvents on the Yield, Selectivity, and Recovery of Curcuminoids from Turmeric".* ACS Sustain. Chem. Eng. 10 (2022) 2271. https://doi.org/10.1021/acssuschemeng.1c08125.
11. Huber, V.; Hioe, J.; Touraud, D.; Kunz, W. Uncovering the Curcumin *Solubilization Ability of Selected Natural Deep Eutectic Solvents Based on Quaternary Ammonium Compounds*. J Mol Liq 361 (2022) 119661. https://doi.org/10.1016/j.molliq.2022.119661
12. Huber, V.; Schmidt, M.; Touraud, D.; Kunz, W. *Towards a Sustainable and Green Extraction of Curcuminoids Using the Essential Oil of Cinnamomum Cassia*. Submitted to Sust Food Tech.

No licensing was necessary for the reuse of the published work in this dissertation.

Declaration

Eidesstattliche Erklärung

Ich erkläre hiermit an Eides statt, dass ich die vorliegende Arbeit ohne unzulässige Hilfe Dritter und ohne Benutzung anderer als der angegebenen Hilfsmittel angefertigt habe; die aus anderen Quellen direkt oder indirekt übernommenen Daten und Konzepte sind unter Angabe des Literaturzitats gekennzeichnet.

Weitere Personen waren an der inhaltlich-materiellen Herstellung der vorliegenden Arbeit nicht beteiligt. Insbesondere habe ich hierfür nicht die entgeltliche Hilfe eines Promotionsberaters oder anderer Personen in Anspruch genommen. Niemand hat von mir weder unmittelbar noch mittelbar geldwerte Leistungen für Arbeiten erhalten, die im Zusammenhang mit dem Inhalt der vorgelegten Dissertation stehen.

Die Arbeit wurde bisher weder im In- noch im Ausland in gleicher oder ähnlicher Form einer anderen Prüfungsbehörde vorgelegt.

Regensburg, 04.10.2022

Verena Huber

Statutory Declaration

I herewith declare in lieu of oath that I have composed this thesis without any inadmissible help of a third party and without the use of aids other than those listed. The data and concepts that have been taken directly or indirectly from other sources have been acknowledged and referenced.

Other persons have not helped to produce this work as regards its content or making. In particular, I have not used the services of any professional agencies in return for payment or those of other persons. Nobody has received payment in kind – neither directly nor indirectly – from me for any work that is connected with the content of this doctoral dissertation.

The thesis has not been submitted, wholly or substantially, neither in this country nor abroad for another degree or diploma at any university or institute.

Regensburg, 04.10.2022

Verena Huber